Mechanism of action and functional role of the two-pore channels (TPCs) in key vertebrate physiological processes

Lai Hing Chan

Green Templeton College

A thesis submitted for the degree of Doctor of Philosophy

Trinity Term, 2015

Supervisor: Dr. John Parrington

Department of Pharmacology

University of Oxford

Mechanism of action and functional role of the two-pore channels (TPCs) in key vertebrate physiological processes

Lai Hing Chan, Green Templeton College

A thesis submitted for the degree of Doctor of Philosophy, Trinity Term 2015

Abstract

Two-pore channels (TPCs) represent a strong candidate for being pivotal components of the endolysosomal cation channels regulated by nicotinic acid adenine dinucleotide phosphate (NAADP), a novel Ca^{2+}-releasing second messenger. A substantial body of evidence has implicated TPCs functional roles in key physiological processes, such as autophagy, osteoclast formation, neuronal differentiation, etc. Given the importance of Ca^{2+} signals in regulating skeletal muscle development and differentiation, and the rising prominence of NAADP/TPC signalling in regulating different aspects of physiological events, the first part of my research project sought to determine whether this lately-established Ca^{2+} mobilization also plays a role in myogenesis. By using morpholino-based knockdown of TPC2, together with bioluminescence-based Ca^{2+} imaging, a significant disruption of the characteristic Ca^{2+} signalling profiles generated by slow muscle cells of intact zebrafish embryos was noted. In addition, impairment in the gross and fine structure of the trunk of zebrafish embryos was apparent in TPC2 morphants. Thus suggesting involvement of TPC2 in regulating slow muscle cell development. On the other hand, whole-mount *in situ* hybridisation of intact zebrafish embryos revealed an expression of *Tpcn3* mRNA, implicating TPC3 a role in zebrafish embryogenesis.

Previous study showed that TPC2 was transiently upregulated during the early stages of C3H10T1/2 adipocyte differentiation *in vitro*, the second part of my project aimed to investigate whether TPC2 plays a functional role in such process, also to identify the upstream mediators involved in regulating *Tpcn2* expression and potential downstream effectors mediated by TPC2. My findings demonstrated impairment of adipogenesis in TPC2 knockdown cells and in cells depleted of lysosomal stores, indicating an involvement of TPC2 and lysosomal stores in such process. Besides, PKA and Epac were found to be required for the observed *Tpcn2* upregulation, probably via a mechanism involving CREB activity, based on the findings that CREB bound to CRE element of *Tpcn2* promoter. Preliminary results further suggested that calpain might be a potential effector of TPC2 in regulating C3H10T1/2 adipogenesis.

In view of the accumulating evidence showing the participation of NAADP in the nervous system, the third part of my work presented evidence of expression of *Tpcn1* mRNA in several regions of the brain, implicating potential role(s) for TPC1 in those areas.

This thesis is dedicated to my parents. For their endless love, support and encouragement.

Acknowledgements

First and foremost, I have to thank my dearest parents for their endless love, support and encouragement throughout my life, albeit I understand any amount of gratitude shown to them is woefully inadequate. Thank you for all your sacrifices, for all you have given to me, and for always being there for me with such a gigantic love. I am forever indebted to you both. Dad and Mom, you are the best parents in the world and I owe my success to you. I love you! My huge heartfelt thanks go to my lovely and wonderful brothers, Henry and Kevin, as well. Their enormous and unwavering love and support to me never ceases to amaze me. Thank you my beautiful family! I could not have made it without you all! Love you!

I would also like to express my deepest gratitude to my doctoral supervisor, Dr. John Parrington, for his unfailing guidance, insights, support and encouragement over the past five years. This thesis could not have been possible without his impeccable scrutiny and tremendous patience. I am also grateful to Prof. Frances Platt and Dr. Jose Cancela for having served as my examiners. Their thoughtful questions and comments were greatly inspiring and highly valued. Many thanks to Dr. Ruth Tunn, Alaa (Dr to be) and other previous and current members of the Parrington lab who have constantly provided help and supported me all the time.

I am particularly thankful to Prof. Antony Galione for providing a friendly and stimulating environment for scholarly discussion and for offering a cosy working space for part of my experimental work. Special thanks go to members of his lab and the Department for their valuable advice, support and all the happy and relaxing chats. I owe earnest thanks to Dr. Guida Ruas for her professional teaching and assistance; to Dr. Lianne Davis and Dr. Anthony Morgan, for generously sharing their time and expertise; to Clive Garnham, whose impressive technical knowledge has guided me through various experimental work and rescued my failed experiments; and to all of them for their kind tolerance of my ignorance and patient corrections of my mistakes.

I would like to extend my sincerest thanks and appreciation to Dr. Andy Lam, whose encyclopaedic knowledge and inspirational suggestions have hugely enlightened my work and thinking, without his selfishless assistance and immense support this thesis could not have been accomplished. I am also grateful to Dr. Florence Serres, for her *in situ* hybridisation advice and assistance; and Sam and Wendy, for their imaging advice and assistance.

I am extremely thankful to Paula Savin, for her overwhelming support and assistance on numerous issues inside and outside the Department. And I am undoubtedly grateful to the Department of Pharmacology and Oxford University, for providing such marvellous place for scientific/academic pursuits. My sincere thanks also go to University College London, where I had a fantastic time during my three years of undergraduate studies and where my passion for pharmacology research was seeded.

Also, I would like to thank Prof. Andrew Miller, Dr. Sarah Webb, Jeffrey Kelu (Dr to be) and Mandy Chan of HKUST, for their great support and assistance during my time as a visiting scholar at the Calcium Aequorin Imaging Lab at HKUST. And special thanks go

to Jo Aldhouse (Visa and Immigration Office of Oxford University), who helped me several times with my visa applications.

During my DPhil journey at Oxford University, I am lucky enough to have met a lot of good friends. My sincere thanks go to all of them who helped me throughout this academic exploration. In particular, I would like to thank MM-ITC, your boundless capacity for love and patience meant a lot to me. Thank you so much for your incredible understanding and encouragement in my many, many moments of crisis. I could not have made it through this frustrating and tough period without you. Also, SN, PL and TW, thank you wholeheartedly for constantly supporting me for whatever I am doing. QJ, PL, VY, KC, TC, MC, AA, KJ … I am sorry I cannot list all the names here, but you are always on my mind. Your friendship adds colour to my life and makes my life a magnificent experience!

Contents

Abbreviations ……..…….……..……..		xiv
Chapter 1: General Introduction ……..		1
1.1	Introduction: Calcium signals play pivotal roles in cell biology ….	2
1.2	Acidic Ca^{2+} stores …….....	4
1.3	NAADP – a novel Ca^{2+}-mobilising second messenger ……...	4
1.3.1	NAADP mobilizes Ca^{2+} release from endolysosomal Ca^{2+} stores ..	4
1.3.2	"Trigger" hypothesis …….....	5
1.3.3	Bidirectional ER/acidic organelles communication …….....	6
1.4	TPC ……..	7
1.4.1	Introduction …….……	7
1.4.2	Structure …….…….	8
1.4.3	Evolution of TPCs …….……..…	9
1.4.4	Tissue distribution …….……..…	10
1.5	Evidence for TPCs being NAADP-mediated Ca^{2+}-release channels …….……..……	11
1.5.1	Why were TPCs proposed as NAADP receptors? ……..	11
1.5.2	Subcellular localization of TPCs in endolysosomal organelles …..	12
1.5.3	TPCs recapitulate characteristics of NAADP-mediated Ca^{2+} release …….……..……...	14
1.6	Controversies about TPCs as target channels for NAADP …….	17
1.7	What type(s) of channel(s) do TPCs belong to? ……..	19
1.8	Functional regulation of TPCs by different regulators ……	20

1.9 NAADP- and TPC-mediated signalling in physiological and cellular processes ……..….. 22

1.10 Disruption in human pathology …….…….. 25

1.11 Aims of this study …….……..…. 26

Chapter 2: Materials and Methods …….……..… 27

2.1 Construct generation …….…….. 28

2.1.1 Purification of total RNA from zebrafish embryo ……... 28

2.1.2 Reverse transcription polymerase chain reaction (RT-PCR) …….. 28

2.1.3 PCR of cDNA …….……..…….. 29

2.1.4 Purification of PCR products …….……. 30

2.1.5 Vector/Insert ligation …….……. 30

2.1.6 Transformation of *E.coli* XL10 Z-competent cells ……. 31

2.1.7 Construct amplification and purification …….…… 31

2.1.8 Construct verification …….……. 31

2.1.8.1 Restriction digest …….……..….. 31

2.1.8.2 Gel electrophoresis …….……. 32

2.1.8.3 Quantification and sequencing …….……... 32

2.1.9 QuikChange II XL Site-directed mutagenesis ……. 32

2.1.10 Construction of recombinant plasmids with mCherry tag ……... 33

2.2 Antibody purification …….……. 35

2.3 Zebrafish husbandry and embryo collection ……... 35

2.4 Microinjection …….……..…….. 36

2.5 Morpholino design and injection …….…… 36

2.6 *In vivo* reconstitution of aequorin and bioluminescence-based Ca^{2+} imaging …….……..……. 37

2.7	Morphological studies of zebrafish embryos ……..……	38
2.8	Whole-mount immunohistochemistry …….	38
2.9	RNA *in situ* hybridization on whole-mount embryos …….	39
2.9.1	Linearization of plasmid DNA ……..…….……..	39
2.9.2	DIG probe synthesis ……..…….……..……	39
2.9.3	*In situ* hybridisation ……..…….……..……	40
2.10	C3H10T1/2 cell culture ……..…….……..……..	41
2.10.1	Cell line amplification and frozen aliquot preparation ……	41
2.10.2	C3H10T1/2 adipogenic differentiation ……..……..	42
2.10.3	Oil Red O staining ……..…….……..……..	44
2.10.4	AdipoRed Assay – quantification of adipogenic differentiation ….	44
2.10.5	Reverse transcription quantitative PCR (RT-qPCR) ……...	45
2.10.5.1	RNA harvest and isolation ……..…….……..……..	45
2.10.5.2	RNA concentration and integrity verification ……..……	45
2.10.5.3	cDNA reverse transcription ……..…….……..……	46
2.10.5.4	Quantitative PCR (qPCR) ……..…….……..……...	46
2.10.5.5	qPCR data analysis ……..…….……..…….	48
2.10.5.6	qPCR housekeeping gene selection ……..……...	49
2.10.6	Ned-19 treatment ……..…….……..……	49
2.10.7	Bafilomycin A1 treatment ……..……..	50
2.10.7.1	Bafilomycin A1 preparation and incubation ……..……..	50
2.10.7.2	Live cell LysoTracker staining ……..……..	50
2.10.8	BAPTA-AM treatment ……..…….……..……	50
2.10.9	PKI treatment ……..…….……..……..	51
2.10.10	ESI-09 treatment ……..…….……..…….	51

2.10.11 8-pCPT-2-O-Me-cAMP-AM treatment ……..……. 52

2.10.12 Immunofluorescence ……..…….……..……... 52

2.10.13 Chromatin immunoprecipitation (ChIP) ……..…… 53

2.10.13.1 Formaldehyde cross-linking and cell lysis ……..……. 53

2.10.13.2 Sonication ……..…….……..……... 53

2.10.13.3 Immunoprecipitation ……..…….……..……... 54

2.10.13.4 Isolation of ChIP DNA ……..…….……..……... 55

2.10.13.5 Analysis of fragment size ……..…….……..…… 55

2.10.13.6 Passivation of concentrators ……..…….. 55

2.10.13.7 Preparation of protein A beads with salmon sperm DNA ……... 55

2.10.13.8 Data analysis ……..…….……..……... 56

2.11 In situ hybridization (ISH) ……..…….……..…….. 57

2.11.1 Preparation of frozen brain sections ……..…….. 57

2.11.2 Pre-hybridization ……..…….……..……. 57

2.11.3 Hybridization ……..…….……..…….. 57

2.11.4 Image and data analysis ……..…….……..…….. 59

2.11.5 Counter staining ……..…….……..…….. 59

2.12 Statistical analysis ……..…….……..……... 60

Chapter 3: Investigations of roles of TPC2 and TPC3 during zebrafish embryogenesis – a focus on myogenesis ……..…….……..…… 61

3.1 Introduction ……..…….……..……. 62

3.1.1 Skeletal muscle development ……..…….…… 62

3.1.2 Ca^{2+} signalling during skeletal muscle development ……... 63

3.1.3 Involvement of NAADP and TPC during skeletal muscle differentiation ……..…….……..…….. 67

3.1.4	Lysosomes play a role in skeletal muscle development ……..	67
3.1.5	Lysosomal Ca^{2+} signaling in regulation of autophagy …….	68
3.1.6	Aims of this chapter ……..…….……..……	69
3.2	Results ……..…….……..…….……..……..	71
3.2.1	Cloning of zebrafish TPC cDNAs and vectors construction ……....	71
3.2.1.1	Cloning of zebrafish TPC cDNAs and vectors construction ……....	71
3.2.1.2	Site-directed mutagenesis ……..…….……..……...	76
3.2.1.3	Construction of recombinant plasmids with mCherry tag ……...	76
3.2.2	Designing morpholinos for injection into zebrafish ……	79
3.2.3	Characterization of muscle-generated Ca^{2+} signals in MO-based knockdown of TPCs using aequorin-based luminescence detection ……..……..…….……..…….	80
3.2.4	Studies of the gross morphology of zebrafish embryos treated with TPC2- and TPC3-MOs ……..…….……..……...	85
3.2.5	Effects of MO-based TPC2 knockdown on the organisation of the trunk musculature ……..…….……..……	87
3.2.5.1	Immunohistochemistry study ……..…….……..……..	87
3.2.5.2	Statistical analysis of metamorphic parameters ……..…….	90
3.2.6	Effects of MO-based knockdown of TPC2 on the development of the trunk musculature of intact zebrafish embryos at ~48 hpf …….	92
3.2.7	Construction of cDNA mutants for rescue constructs …….	94
3.2.8	Expression of *DrTpcn* genes in zebrafish embryos …….	96
3.2.9	Affinity-purification of antibodies that specifically recognise recombinant DrTPCs ……..…….……..……..	98
3.2.10	Localisation of TPC2 in SMCs *in vitro* and *in vivo* …….	100

3.3 Discussion ……..…….……..…….…….. 105

3.3.1 Investigation of DrTPC2-mediated Ca^{2+} signalling in the development of the SMCs in zebrafish embryos ……..……... 105

3.3.1.1 Effects on the temporal characteristics of Ca^{2+} signals by DrTPC2 knockdown ……..…….……..…….. 105

3.3.1.2 Effects of TPC2 inhibition on the motility of zebrafish embryos … 107

3.3.1.3 Pharmacological studies on the influence of TPC2 inhibition on Ca^{2+} activities in SMCs ……..…….……..…….. 107

3.3.1.4 General review on the effects of TPC2 inhibition ……..……. 108

3.3.1.5 Proposal of functional regulatory role of TPC2 in SMC differentiation in zebrafish ……..…….……..…….. 108

3.3.1.6 Localization of TPC2 in SMCs ……..…….……. 110

3.3.2 *In vivo* study of DrTPC3 in zebrafish ……..…… 112

3.3.2.1 *In situ* hybridization of whole mount embryos ……..…….. 112

3.3.2.2 Investigation of DrTPC3-mediated Ca^{2+} signalling in the development of the SMCs in zebrafish embryos ……..…….. 113

3.3.2.3 Brief conclusion ……..…….……..…….……. 113

3.3.3 Future plan ……..…….……..…….……. 114

3.3.4 Conclusion ……..…….……..…….……. 116

3.4 Appendix ……..…….……..…….…… 118

Chapter 4: TPC2 and Adipogenesis ……..…….……..…….……... 121

4.1 Introduction ……..…….……..……. 122

4.1.1 Adipogenesis – general introduction ……..……. 122

4.1.2 Adipocyte development and transcriptional regulation of adipogenesis ……..…….……..…….. 123

4.1.2.1 Determination phase: MSCs to preadipocytes ……..…….... 124
4.1.2.2 Terminal differentiation phase: Preadipocytes to adipocytes …….. 124
4.1.3 Intracellular cAMP signalling in adipogenesis ……..…….. 128
4.1.3.1 cAMP ……..……..……..……..……...……... 128
4.1.3.2 PKA and Epac ……..……..……..……. 129
4.1.3.3 Functional roles of CREB in adipogenesis ……..…… 133
4.1.4 Ca^{2+} signalling and adipogenesis ……..……..…….. 134
4.1.5 NAADP/TPC signalling in adipogenesis and physiological functions of adipocytes ……..……..……..……... 137
4.1.6 The endolysosomal system plays a role in adipogenesis regulation ……..……..……..……..……. 138
4.1.7 Aims of this chapter ……..……..……..……..……... 139
4.2 Results ……..……..……..……..……..…….. 141
4.2.1 Expression profile of TPCN2 mRNA during adipogenic differentiation ……..……..……..……. 141
4.2.2 Effects of TPC2 downregulation on adipocyte differentiation …… 143
4.2.2.1 Measurement of adipogenesis - lipid droplet accumulation …… 143
4.2.2.2 Measurement of adipogenesis – expression of adipocyte marker PPARγ ……..……..……..……..…….. 146
4.2.3 Effect of BAPTA-AM on adipogenesis ……..……. 149
4.2.4 Effect of inhibiting NAADP signalling on adipogenesis ……. 153
4.2.4.1 Effects of bafilomycin A1 on adipogenic differentiation …… 153
4.2.4.2 Effect of Ned-19 on adipogenic differentiation ……..……. 159
4.2.5 Determination of potential upstream mediators - PKA and EPAC ……..……..…….. 162

4.2.5.1 Effect of PKA inhibitor on *Tpcn2* mRNA expression ……. 162

4.2.5.2 Effect of Epac inhibitor on *Tpcn2* mRNA expression ……. 165

4.2.5.2.1 Epac1 and Epac2 mRNA expressions in C3H10T1/2 cells ……. 165

4.2.5.2.2 Effect of selective Epac activator on *Tpcn2* mRNA expression ….. 167

4.2.5.2.3 Effect of selective Epac inhibitor on *Tpcn2* mRNA expression ….. 169

4.2.5.3 Effect of PKA inhibition and Epac inhibition on adipogenesis of C3H10T1/2 cells ……..…….……..……. 171

4.2.6 CREB ……..…….……..…….……..……... 172

4.2.6.1 Expression of CREB and phosphorylated CREB ……..…….. 172

4.2.6.2 Sonication optimization ……..…….……..…….. 174

4.2.6.3 Identification of CRE in MmTPC2 ……..…… 175

4.2.6.4 Recruitment of pCREB to the Tpcn2 promoter ……..……. 175

4.3 Discussion ……..…….……..…….……..…… 178

4.3.1 TPC2 – a novel regulator of C3H10T1/2 cell adipogenesis *in vitro* ……... 178

4.3.2 Intracellular Ca^{2+} regulation in adipogenesis of C3H10T1/2 cells .. 180

4.3.3 Involvement of cAMP effectors – PKA and Epac in *Tpcn2* upregulation ……..…….……..…….……... 183

4.3.4 CREB ……..…….……..…….……..……... 186

4.3.5 How does TPC2 contribute to adipogenesis? ……..…… 188

4.3.5.1 Downstream effectors ……..…….……..……. 188

4.3.5.2 Upstream mediators ……..…….……..…… 190

4.3.6 Future plan for determining TPC role(s) in adipogenesis ……... 191

4.3.6.1 Summary of potential future studies ……..…….……. 191

4.3.6.2 Preliminary study and future investigation of calpain activity in 193

adipogenesis of C3H10T1/2 cells ……..…….…….

4.3.7 Conclusion ……..…….……..…….……. 195

4.4 Appendix ……..…….……..…….……..……. 197

Chapter 5: Expression pattern of *Tpcn1* mRNA in the brain ……..……. 207

5.1 Introduction ……..…….……..…….……... 208

5.1.1 TPCs and NAADP in the nervous system ……..……. 208

5.1.2 Aims of this chapter ……..…….……..…….……... 211

5.2 Results ……..…….……..…….……..……. 213

5.2.1 Expression of *MmTpcn1* mRNA in male mouse brain ……..... 213

5.2.2 Expression of *MmTpcn1* mRNA in female mice brain ……..... 221

5.3 Discussion ……..…….……..…….…….. 230

5.4 Appendix ……..…….……..…….……... 234

Chapter 6: General Discussion ……..…….……..…….…….. 235

6.1 *Tpcn* expression – other possible regulations ……..…… 236

6.2 Alternative functional roles for TPCs? ……..…….. 238

6.3 Final conclusions ……..…….……..…….……... 238

References …… 240

Abbreviations

A list of abbreviations is given below. For those that occur less frequently, definitions are given in the text where appropriate.

$[Ca^{2+}]_i$	intracellular Ca^{2+} concentration
18S	18S ribosomal RNA
BAT	brown adipose tissue
ANOVA	analysis of variance
c/EBP	CCAAT/enhancer-binding protein
C3H10T1/2	murine mesenchymal stem cell line
Ca^{2+}	calcium
Ca_v	voltage-gated Ca^{2+} channels
cADPR	cyclic adenosine diphosphate ribose
cAMP	cyclic adenosine monophosphate
CD38	cluster of differentiation 38
cDNA	complementary DNA
ChIP	chromatin immunoprecipitation
CICR	Ca^{2+}-induced Ca^{2+} release
CREB	cAMP response element binding protein
DKO	double knockout
DM	differentiation medium
DMEM	Dulbecco's Modified Eagle Medium
DMSO	dimethyl sulfoxide

EC	excitation-contraction
Epac	exchange protein activated by cAMP
ER	endoplasmic reticulum
ET	excitation-transcription
FBS	fetal bovine serum
GM	growth medium
HFD	high-fat diet
hpf	hours post fertilization
HYB	hybridization buffer
Hs	*Homo sapiens* (human)
IBMX	3-isobutyl-1-methylxanthine
ISH	*in situ* hybridization
IP_3	inositol 1,4,5-trisphosphate
IP_3R	IP_3 receptor
K_v	voltage-gated potassium channels
KD	knockdown
KO	knockout
LAMP	lysosomal associated membrane protein
LFD	low-fat diet
MCE	mitotic clonal expansion
MEF	mouse embryonic fibroblast
Mm	*Mus musculus* (mouse)
MO	morpholino
MSC	mesenchymal stem cell
mTOR	mammalian target of rapamycin

mRNA	messenger ribonucleic acid
Na_v	voltage-gated Na^+ channels
NAADP	nicotinic acid adenine dinucleotide phosphate
NCS	new born calf serum
NFAT	nuclear factor of activated T-cells
NPC	Niemann-Pick disease type C
O/N	overnight
PBS	phosphate-buffered saline
PFA	paraformaldehyde
PIP	phosphoinositide
$PI(3,5)P_2$	phosphatidylinositol 3,5-bisphosphate
PCR	polymerase chain reaction
PKA	protein kinase A
PKC	protein kinase C
PPARγ	peroxisome proliferator-activated receptor gamma
QP	quiet period
RT-qPCR	reverse transcription quantitative PCR
RT	room temperature
RyR	ryanodine receptor
SDS	sodium dodecyl sulfate
SERCA	sarcoplasm/endoplasmic reticulum Ca^{2+} ATPase
shRNA	small hairpin RNA
siRNA	small interfering RNA
SMC	slow muscle cell
Sp	*Strongylocentrotus purpuratus* (sea urchin)

SP1	signalling period 1
SP2	signalling period 2
SR	sarcoplasmic reticulum
TBS	Tris-buffered saline
TPC	two-pore channel
TRP	transient receptor potential
TRPML1	transient receptor potential mucolipin 1
WAT	white adipose tissue
WT	wild-type

Chapter 1:

General Introduction

1.1 Introduction: Calcium signals play pivotal roles in cell biology

Calcium (Ca^{2+}) signalling is crucial in controlling multitude of cellular events [1] and dysregulation of Ca^{2+} signalling pathways leads to various kinds of diseases [2]. For instance, egg activation by sperm following fertilization generates a substantial transient rise of intracellular Ca^{2+}, which appears to be a universal aspect in all species studied so far [3]. This versatile signalling system is then used continually throughout the entire life of all the life forms to regulate physiological events during development, differentiation and even cell death [4]. As such, a combination of Ca^{2+} channels, pumps, exchangers and buffering mechanisms are harnessed to precisely control the spatiotemporal changes of Ca^{2+} concentrations generated by different stimuli [5], for the assembly of cell-specific Ca^{2+}-mediated stimuli and therefore modulation of many downstream effects [1, 5].

Ca^{2+} signals are generated from intracellular stores or external medium. The two well-established intracellular stores for Ca^{2+} release are endoplasmic reticulum (ER) or its muscle equivalent, sarcoplasmic reticulum (SR) [1]. Notably, Ca^{2+} release through ER/SR is regulated by Ca^{2+} itself and also by two well-characterized intracellular second messengers, the inositol trisphosphate (IP_3) and cyclic adenosine diphosphate ribose (i.e. cyclic ADP-ribose; cADPR) [1].

Hydrolysis of phosphatidylinositol 4,5-bisphosphate mediated by receptor-induced activation of phospholipase C produces two key mediators, diacylglycerol and IP_3 [6-8]; while cADPR is synthesized by ADP-ribosyl cyclases [9, 10]. Both IP_3 and cADPR mediate Ca^{2+} release from specific Ca^{2+} channels resided on the ER/SR, namely the IP_3 receptors (IP_3Rs) and ryanodine receptors (RyRs) respectively. Both receptors display structural and functional correlations and are also biphasically regulated by cytosolic Ca^{2+}, such that Ca^{2+} at low concentrations triggers the channel and enhances its open probability

while at higher concentrations inhibits the channel [6-8, 10]. This biphasic regulation is now considered to be important for the production of spatiotemporal characteristics of cytosolic Ca^{2+} [4].

Recently, nicotinic acid adenine dinucleotide phosphate (NAADP) has emerged as a new class of Ca^{2+}-mobilizing second messenger [11, 12]. It predominantly targets a distinct type of Ca^{2+} store from those regulated by IP_3/cADPR – the acidic endolysosomal organelles [13-17]. However, there have been controversies about the molecular identity of the NAADP-mediated Ca^{2+} channel. Several candidates like RyRs, endolysosomal transient receptor potential (TRP) channels (e.g. TRPMLs, TRPM2) [15, 17-21] and a novel channel family called two-pore channels (TPCs) have been studied, with a significant amount of evidence relating TPCs to NAADP, hence being the best fit candidate of the elusive NAADP receptors.

In this chapter, topics including acidic Ca^{2+} stores, NAADP-mediated mobilisation, TPC structure, evolution, distribution, subcellular localization, TPC-mediated Ca^{2+} signalling, current controversies, functional regulations, NAADP/TPC-mediated physiological and cellular processes as well as disruption in human pathology are reviewed. Subsequent chapters focus in more detail on the possible roles of TPCs in zebrafish embryogenesis; also the functional roles of TPC2 and the underlying molecular mechanisms regulated by TPC2-mediated Ca^{2+} signalling during adipogenesis; as well as biochemical analysis of the expression of *Tpcn1* in the brain. Finally an overall analysis and conclusion from all the findings in my studies is presented in the last chapter.

1.2 Acidic Ca^{2+} stores

The so-called acidic Ca^{2+} stores comprise a group of organelles which are rich in both H^+ (therefore acidic lumen) and Ca^{2+}. These include acidocalcisomes, vacuoles, endosomes, lysosomes, lysosome-related organelles, secretory vesicles, and the Golgi complex [22, 23]. It is well established that these organelles play pivotal roles in various major cellular functions, and importantly, their involvement (particularly endolysosomes [23-30]) in Ca^{2+} storage and release is becoming increasingly crucial in the Ca^{2+} signalling network. Ca^{2+} sequestration into acidic Ca^{2+} stores is suggested to involve certain form of Ca^{2+} pumps or exchangers. Different Ca^{2+}-permeable channels including TPCs, members of TRP channel superfamily, and the traditional ER Ca^{2+} release channels IP_3Rs and RyRs, are found on acidic Ca^{2+} stores and mobilize Ca^{2+} release from these stores [22, 23].

1.3 NAADP – a novel Ca^{2+}-mobilising second messenger

1.3.1 NAADP mobilizes Ca^{2+} release from endolysosomal Ca^{2+} stores

NAADP is the most potent among all known Ca^{2+}-mobilising messengers, with efficacy at the picomolar or low nanomolar range (Lee, 1997). The characteristic bell-shaped dose response curve distinguishes NAADP from the other messengers, that Ca^{2+} release is maximal at low nanomolar concentration range but without effect at high micromolar concentrations. Lee and colleagues first identified the Ca^{2+}-mobilising properties of NAADP in the lysosome-related organelles of sea urchin eggs [31]. Since then its Ca^{2+}-releasing activity has been shown in an array of cell types and mammalian tissues [32-35]. Unlike IP_3 and cADPR, NAADP primarily mediates Ca^{2+} release from the acidic Ca^{2+} stores, likely the endolysosomal organelles [13-15, 17, 23, 36]. Findings showing NAADP-induced release from the ER (the nuclear envelope) have also been reported [37].

Enhancement of NAADP levels triggered by cell stimulation was initially shown in sea urchin fertilization [38] and was subsequently exemplified in other cell types [34] despite the underlying mechanisms are ambiguous. Agonists such as cholecystokinin CCK (acting on CCK receptor on pancreatic acinar cells) [39-41], endothelin-1 (acting on e.g. pulmonary smooth muscle) [42, 43], glucagon-like peptide 1 GLP1 (acting on GLP1 receptor in pancreatic β cell) [44] etc. have been shown to induce Ca^{2+} signals by promoting NAADP synthesis. Although a number of receptor activations seem to couple to combinations of NAADP and cADPR or IP_3 [41, 45, 46], yet there are some conditions in which NAADP acts as the key or exclusive messenger [47]. ADP-ribosyl cyclases (including CD38), the enzymes involved in cADPR production, are also proposed to mediate NAADP synthesis [48-50]. These enzymes are also identified in or related to acidic stores [44, 51], suggesting a requirement of acidic pH for their functions. Interestingly, coupling between CD38 and the receptor-mediated NAADP synthesis has also been reported but the underlying mechanisms remain to be elucidated [50, 52, 53].

1.3.2 "Trigger" hypothesis

Interactions between NAADP-induced Ca^{2+} release and the Ca^{2+} release channels on the ER/SR are commonly seen and were initially demonstrated in pancreatic acinar cells [39]. That a small, localized Ca^{2+} release from acidic stores induced a larger Ca^{2+} release from the ER was observed. Similar amplification was subsequently reported in sea urchin eggs [54-56] and other mammalian cell types [35]. Such functional coupling is known as the "trigger" hypothesis [55], whereby NAADP responds to cellular stimulation by inducing a "trigger" (localised; first phase) release of Ca^{2+} from acidic stores, which is then amplified (globalized; second phase) by Ca^{2+}-induced Ca^{2+} release (CICR) via recruiting classic Ca^{2+} release channels (IP_3R and RyR) from nearby ER [33].

1.3.3 Bidirectional ER/acidic organelles communication

The conventional cross talk (i.e. "channel chatter" [57]) between the NAADP and IP_3/cADPR pathways has been emphasized on anterograde signalling from acidic organelles to ER via CICR which is crucial for amplification and Ca^{2+} oscillations and waves [55]. Intriguing results from recent work conducted in mammalian cells [58, 59] and sea urchin eggs [60] demonstrated that local communication occur at junctions between ER and acidic stores, where local microdomains of high Ca^{2+} concentration are found, and that acidic stores are favourably stimulated by these microdomains [60]. Findings also revealed that Ca^{2+} released from ER (by IP_3/cADPR) evokes the NAADP pathway through "retrograde" signalling via activation of Ca^{2+}-dependent NAADP production and then NAADP-mediated channels [60]. A computational model of lysosome-ER coupling further demonstrated that functional heterogeneity of these Ca^{2+} microdomains can be created by differential arrangements of Ca^{2+} signalling proteins at membrane-contact sites [61, 62]. Such bidirectional organelle communication suggests for the potential of creating Ca^{2+} oscillations and waves, in addition to broad implications for endolysosomal functions [60].

1.4 TPC

1.4.1 Introduction

TPCs (gene name *Tpcn*) were first cloned from rat kidney (rat TPC1) [64] and from *Arabidopsis* (AtTPC1) [65] based on their sequence similarity with voltage-gated Na^+ and Ca^{2+} channels (Na_v and Ca_v respectively). However, functional data for animal TPCs has been lacking until AtTPC was established as a plant vacuole Ca^{2+} release channel [66] mobilizing long range Ca^{2+} waves [67]. Such discovery was an exciting progression as vacuoles represent the major acidic Ca^{2+} stores in plants [22], prompting significant

amount of proposals that TPCs may be the NAADP-sensitive Ca^{2+} release channels on the endolysosomal system in animal cells, i.e. the elusive "NAADP receptors" [68-73].

1.4.2 Structure

TPCs comprise two repeats, each containing 6 transmembrane regions with a re-entrant pore loop between the fifth and sixth hydrophobic regions (Figure 1.1) [15, 18]. Since voltage-gated potassium channels (K_v) contain only one domain while Na_v and Ca_v have four domains, besides, Na_v is suggested to be evolved from K_v [74], thus TPCs might represent an evolutionary intermediate between the one-repeat K_v and the four-repeat Na_v and Ca_v [16]. Dimerization to form four pore-forming loops is required for TPCs to serve as a functional channel [64]. Indeed, evidence for both homodimers and heterodimers was revealed in co-immunoprecipitation [73] and fluorescence resonance energy transfer studies [75]. Glycosylation is also found on the luminal side of the channel (Figure 1.1) [76, 77]. TPC1 and TPC2 share highest homology in the transmembrane regions, especially in the S5, S6 and the pore loop region [78]. Interestingly, plant TPCs differ structurally from animal TPCs by the presence of two predicted EF hand motifs in the linker region (Figure 1.1) [66]. Such EF hands confer sensitivity of NAADP-mediated signals to cytosolic Ca^{2+} in plant TPCs which is absent in animal TPCs [79], hence plant TPCs augment Ca^{2+} release while animal TPCs tend to be the trigger [16].

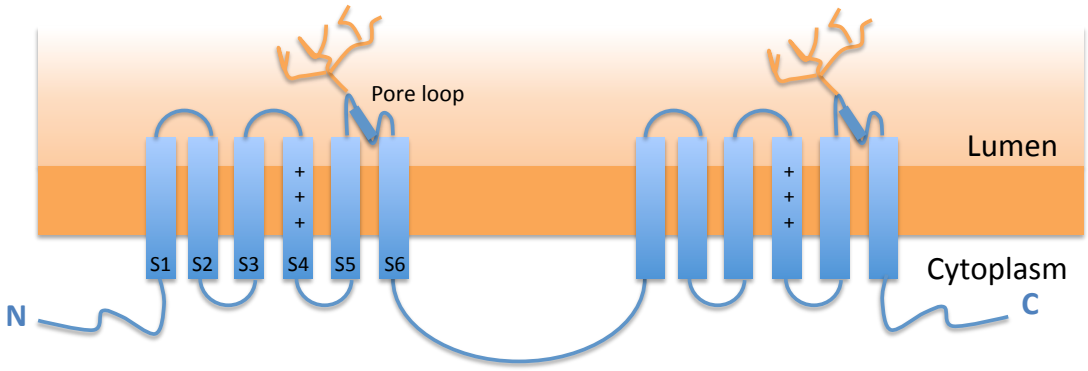

Figure 1.1: Schematic diagram illustrating predicted structure of a monomeric animal TPC subunit, which comprises two homologous domains connected by a cytoplasmic linking section. Each domain comprises six transmembrane α-helics (S1-S6) and a re-entrant pore loop appears between S5 and S6. Glycosylation sites are also found on the luminal side, and positively charged residues are identified in S4. (Adapted from Morgan et al., 2015 [80])

1.4.3 Evolution of TPCs

In plants, angiosperms including *Arabidopsis* [65], rice [81] and wheat [82] express only a single TPC (TPC1) while in tobacco two very homologous genes (NtTPC1A and NtTPC1B) are found [83]. In animals, majority of protostomes (e.g. *Caenorhabditis elegans* and *Drosophila melanogaster*) do not retain any TPC genes [68, 71, 84] apart from some arthropods (e.g. honey bee and jewel wasp) in which a single TPC is expressed [68]. Conversely, all three TPC isoforms are expressed in sea urchins (a basal deuterosostome) and other deuterostomes such as chordates (e.g. fish, birds) [69]. Intriguingly, unlike IP_3Rs and RyRs, TPC isoforms for sea urchins and human only display 30-40% sequence homology which is significantly low [69].

Extraordinarily, TPC3 gene is absent in humans and other primates and some rodent species (e.g. rats and mice) [69], but the full TPC complement is retained in mammals like cows, dogs and horses [69]. Partial TPC3-related sequences were found in chimpanzees and Old World Monkey, suggesting degeneration of TPC3 gene into a pseudogene and functional loss of this gene in humans and other primates [69]. Near full-length TPC3 sequences were identified in New World Monkeys and Prosimians, suggesting the

likelihood of functional TPC3 in these animals [85]. Hence, it is proposed that TPC3 gene degeneration likely started in the common ancestors of Apes and Old World Monkeys [85].

1.4.4 Tissue distribution

Northern blot analysis has discovered a widespread distribution of both *Tpcn1* and *Tpcn2* mRNA in rat, mouse and human tissues. In rat tissues, *Tpcn1* mRNA appears to be most abundant in kidney, followed by liver, lung, and spleen, lower levels were also seen in heart, brain, skeletal muscle and testis [64]. In mouse tissues, both *Tpcn1* and *Tpcn2* were detected in heart, brain, liver, spleen, kidney, embryo, lung, thymus, testis and ovary [73]. *Tpcn1* and *Tpcn2* expression were also evident in multiple areas of the cardiovascular system and the brain as indicated by RT-PCR [73]. *In situ* hybridisation (ISH) of the whole brain (in sagittal section) indicated a higher expression of *Tpcn1* in the cerebellum and dentate gyrus of the hippocampus and lower signals in the remaining parts of the brain, while *Tpcn2* was primarily restricted to the cerebellum, and overlapped modestly with *Tpcn1*; on the other hand, ISH of the kidney (in sagittal section) showed an even distribution of *Tpcn1* throughout the renal cortex and medulla while *Tpcn2* was found primarily in the inner renal medulla, and again overlapped modestly with *Tpcn1* [73]. In human tissues, *Tpcn2* mRNA was detected in human tissues including leukocyte, lung, placenta, small intestine, liver, kidney, spleen, thymus, colon, skeletal muscle, heart and brain, with relatively abundant expression seen in liver and kidney [71].

Exogenous expression of MmTPC1 protein was also explored by western blotting in membrane preparations of mouse tissues [86]; it was most abundant in kidney, and appreciable levels were also seen in liver, spleen and adipose tissue, while moderate expression was found in the lung, heart and brain but very low or almost negligible levels

were observed in the pancreas.

1.5 Evidence for TPCs being NAADP-mediated Ca^{2+}-release channels

1.5.1 Why were TPCs proposed as NAADP receptors?

Early work suggested TPCs as the long-sought-after target channels for NAADP [68, 71, 73] owing to their size [87], subcellular localization to the acidic stores (endolysosomes) and partial pharmacological overlap with NAADP receptors [60, 88-91]. Prompted by these stimulating findings, investigations were conducted to verify for this proposal using genetic (including overexpression, knockdown (KD) and knockout (KO)) and pharmacological approaches, together with evidence obtained from electrophysiological studies, TPCs are established to play an essential role in NAADP signalling. And importantly a number of properties and characteristics of NAADP receptors were reiterated in the expression studies which will be discussed in more detail in section 1.5.3.

1.5.2 Subcellular localization of TPCs in endolysosomal organelles

One of the main reasons for proposing TPCs as NAADP receptors is their endolysosomal localization. Vertebrate TPCs express the conserved lysosomal dileucine-targeting motifs [70]. In particular, interfering with the dileucine motif resulted in HsTPC2 being transported to the plasma membrane but not for HsTPC1, indicating a distinct way of targeting TPC1 from TPC2, which likely occurs via tyrosine-based motifs [70]. A remarkable experiment performed by Brailoiu et al. looking at the NAADP trigger event independently through manipulating the dileucine motif, i.e. the subcellular localization, of TPC2 [70] showed that the plasma membrane-targeted TPC2 mobilised Ca^{2+} influx, but

without any significant amplification, indicating that NAADP did not act directly on ER Ca^{2+} channels which is required for amplifying the initial modest Ca^{2+} signals during the trigger event. Moreover in these cells Ca^{2+} signals with reduced magnitude was revealed, comparable to the endogenous NAADP responses recorded after inhibition of ER Ca^{2+} release in sea urchin eggs [54]. The peaking time of these Ca^{2+} signals was also longer than that found in WT TPC2-expressed cells. These observations could be attributed to the loss of amplification or distinct membrane lipid composition or the luminal environments where TPC2 being in contact with. [16].

For animal TPCs, a number of findings have pointed to their localization within the endolysosomal system, which is consistent with the localization of plant TPCs on vacuoles (an equivalent organelle to the animal endolysosomal system) [66]. Heterologous expression of SpTPCs [69, 92] and HsTPCs [68] showed punctate intracellular distributions in *Xenopus* oocytes and mammalian cells. Remarkable colocalization of HsTPC2 with vesicles labelled with Lysotracker red (a fluorescent weak base) was also demonstrated [84], suggesting the localization of HsTPC2 in acidic organelle. Partial colocalization of TPC1 with endosomes (labelled with rhoB) and lysosomes (labelled with LAMP1) was found [68], while consistent expression on lysosomes was displayed by TPC2 [68, 70]. Intriguingly, when heterologously expressed in starfish oocytes, all SpTPCs exhibited a punctate cortical distribution pattern [92], that was also seen with endogenous SpTCP3 in sea urchin eggs [76], and was also in line with the cortex displaying highest NAADP sensitivity in sea urchin eggs [38] and starfish oocytes [93]. However endogenous NAADP receptors are found in reserve granules expressed throughout the egg [13], suggesting the possibility of dynamic regulation of SpTPC localization during development, which awaits to be verified [16]. Similarly in HEK cells, heterologous expression findings revealed localization to the endolysosomal system for all

mammalian TPCs tested. That co-localization with endolysosomal and other unidentified compartments was found for TPC1 and TPC3, while TPC2 was primarily expressed on lysosomes. The lysosomal localization of endogenous TPC2 in HEK cells was also supported by anti-TPC2 antibody [71]. Collectively, all these findings indicate the endolysosomal localization of animal TPCs. That TPC1 mainly resides in less acidic, early endosomes while TPC2 primarily localizes on more acidic, late endolysosomes [15, 18].

1.5.3 TPCs recapitulate characteristics of NAADP-mediated Ca^{2+} release

Research on the responsiveness of TPCs to NAADP has been demonstrated by different groups. Brailoiu et al. conducted calcium imaging studies in SKBR3 cells and significant increase in NAADP-induced Ca^{2+} signals was shown in cells overexpressing each isoform of sea urchin (*Strongylocentrotus purpuratus*) (SpTPC1-3) and human (HsTPC1 and 2) TPCs, befitting their role as NAADP-sensitive Ca^{2+}-permeable channels [68-70]. Also, inhibition of NAADP-induced signals was seen after addition of selective NAADP antagonist, *trans*-Ned 19 [94], to the SKBR3 cells overexpressed with TPC2 [70]. Besides, blockade of NAADP-mediated TPC-induced Ca^{2+} signals was evident after bafilomycin A1 pretreatment, further supporting the localization of TPCs in acidic organelles [68-70]. Moreover, the marked attenuation of HsTPC1-induced Ca^{2+} signals by inhibition of RyRs implied functional coupling between TPC1 and these ER Ca^{2+} channels [68, 70], in line with that observed with endogenous NAADP receptors in SKBR3 cells [72]. siRNA KD of endogenous TPC1 in SKBR3 cells also significantly suppressed NAADP-induced Ca^{2+} signals, additionally indicating a role of TPCs in NAADP action. Calcraft et al. revealed that heterologous expression of HsTPC1 in SKBR3 cells and HsTPC2 in HEK cells produced augmented NAADP-induced Ca^{2+} signals [71]. Such Ca^{2+} release was shown to occur at nanomolar and low micromolar concentrations of NAADP.

Both TPC1- and TPC2-mobilised signals were blocked by inhibition of ER Ca^{2+} stores and acidic Ca^{2+} stores, indicating functional coupling of these Ca^{2+} channels [71]. Besides, an abrogation of NAADP responses in pancreatic β-cells isolated from *Tpcn2* KO mice and attenuation of endogenous NAADP-evoked responses in TPC2-deficient cells were reported, indicating a role of TPC2 in mediating NAADP-induced Ca^{2+} signals in these cells [71]. In the radioligand binding experiments, increased NAADP binding to membranes was resulted from overexpression of TPC2, suggesting TPCs being direct targets of NAADP [71]. Interestingly, the enhancement was only moderate, indicating the binding of NAADP might require additional binding factors [84].

Given majority of early findings about NAADP mobilisation were discovered in sea urchin egg systems, Ruas et al. performed a comprehensive study on SpTPC characterisation, supporting TPCs as endogenous NAADP targets. In this study, remarkable NAADP binding with nanomolar binding affinity was seen with SpTPC immunocomplexes, suggesting TPCs are part of the endogenous NAADP receptors. Additionally, K^+-dependent irreversible binding of NAADP in these immunocomplexes was demonstrated [76], which is a hallmark characteristics of NAADP binding in the egg system [95]. However, since the purity of immunocomplexes was not mentioned, hence the involvement of other co-factors is possible.

Photoaffinity labelling studies in sea urchin egg membranes revealed labelling of low molecular weight proteins significantly lower than that predicted for direct labelling of TPCs [96]; more intriguingly is that co-immunoprecipitation of these proteins and TPCs was demonstrated [96]. Similar findings were also found in mammalian preparations, that binding proteins of lower molecular weight were labelled [97, 98]. These findings indicate that NAADP binding to small accessory components forming complex with TPCs is more preferable than binding to TPCs directly. In Ruas et al.'s study, NAADP-induced Ca^{2+}

release in HEK cells overexpressing SpTPC1 and 2 was disrupted by bafilomycin A1 pretreatment, as well as NAADP and Ned-19 of desensitising concentrations [76], which is consistent with Brailoiu et al.'s findings in SKBR3 cells [70]. Intriguingly, inhibition of NAADP-triggered Ca^{2+} release was evident in SpTPC3-transfected HEK cells [76], but enhancement was revealed in SKBR3 cells [70]. It remains unclear about the inconsistencies regarding SpTPC3's role in NAADP-triggered Ca^{2+}-release.

It is noteworthy that in HEK cells overexpressed with HsTPC2, substantial biphasic NAADP-induced Ca^{2+} signals were observed: an initial slow pacemaker-like rise of Ca^{2+} responses followed by a larger, more abrupt and global Ca^{2+} release [71]. Inhibition of Ca^{2+} signals of both phases was seen after bafilomycin A1 treatment, while abolishment of the second phase only occurred by thapsigargin addition [71]. This could be explained by the "trigger" hypothesis [55] (section 1.3.2). Intriguingly, the TPC2-mediated Ca^{2+} release in HEK cells peaked in several minutes, whereas endogenous NAADP responses only peaked in seconds [99]. Intriguingly, no functional activity was reported in HEK cells transfected with SpTPC3 [76], contradicting the observations in SKBR3 cells [69].

Distinct NAADP sensitivity of TPC isoforms has been demonstrated in overexpression studies. For instance, HEK cells transfected with MmTPC2 showed the typical bell-shape dose response curve for NAADP response, suggesting some basic properties of NAADP receptors; whereas no NAADP response was observed in MmTPC1-transfected cells [73]. A greater responsiveness to NAADP was also indicated in rat astrocytes overexpressing HsTPC2 than HsTPC1-transfected astrocytes, given their similar transcript levels [100]. Overexpression of TPC2 in HeLa cells [101] and reconstitution of HsTPC2 in a lipid bilayer [102] also demonstrated the typical bell-shaped dose response curve to NAADP. The latter study additionally showed the selective NAADP inhibition by Ned-19; and importantly, the authors suggested the requirement of two NAADP binding sites on TPC2

for the observed specific gating mechanisms, high affinity activation and low affinity inactivation sites [102], which is consistent with the evidence showing two binding sites on NAADP receptors [103].

1.6 Controversies about TPCs as target channels for NAADP

Recently, the status of TPCs as NAADP-mediated Ca^{2+} channels has been confronted with challenging studies conducted by Wang et al. [104] and Cang et al. [105], that TPCs are NAADP-independent channels modulated by other signals were proposed. And that they are not Ca^{2+} channels as originally suggested. By direct patch clamp recordings of TPCs in vacuolin-1 enlarged ensolysosomes and whole cell patch recordings of cell surface-expressed hTPC2 channels, Wang et al. demonstrated currents in WT and TPC-transfected cells, but not in cells isolated from their TPC1/TPC2 double knockout (DKO) mice. They also discovered a high Na^+ permeability in TPCs; and these highly Na^+-selective currents were activated by phosphatidylinositol 3,5-bisphosphate ($PI(3,5)P_2$, an endolysosome-specific phosphoinositide (PIP) which also mediates TRPML1 [106]), but were entirely nonresponsive to NAADP [104], which is in substantial contrast to the existing findings from other groups. On the other hand, Cang et al. proposed that TPCs are modulated by cellular metabolic state. That high ATP levels in nutrient replete cells maintain TPCs in the closed state, and low ATP levels during cell starvation open TPCs, leading to delocalization of mammalian target of rapamycin (mTOR) off the lysosomal membranes and hence regulation of endolysosomal membrane potential, pH stability and amino acid homeostasis [105].

Despite apparent Ca^{2+} release from acidic stores was recorded upon NAADP stimulation, it should be noted that no detection of NAADP-mobilised Ca^{2+} currents was demonstrated in the patch-clamp recordings [104, 105], indicating there could be a loss or inactivation

of important factors that are required for NAADP sensitivity. Hence it remains questionable to conclude that TPCs are nonresponsive to NAADP in this circumstance. On the other hand, the N-terminally tagged TPCs used in Wang et al.'s study may retain TPCs' responsiveness to NAADP [107, 108], as suggested by other findings showing the insensitivity of the N-terminally tagged HsTPC1 [107] and MmTPC1 [73]. Moreover, despite the first 69 and 49 amino acids were deleted respectively from TPC1 and TPC2 at the N terminus of their transgenic mice [104], expression of TPC protein sequences with >90% is expected to be highly likely. And importantly, hTPC1 with first 85 amino acids deleted is retargeted to the ER [107]; whilst hTPC2 with the first 24 amino acids deleted is retargeted to plasma membrane [70, 104], and evidence has been accumulated for NAADP-mediated Ca^{2+} influx and TPC2 channel activity [20, 70]. Hence it remains doubtful whether the transgenic mice generated by Wang et al. were complete TPC "knockouts", as retargeting of physiologically active TPCs to non-endolysosomal locations is likely to occur.

Recently, TPC2 has been shown to be significantly blocked by cytoplasmic Mg^{2+} with an affinity of 60-130 μM, regardless of whether the stimulus is NAADP or lipid [109]. Notably, this powerful inhibitor tends to inhibit TPC currents going from the cytosol to the lumen [109]. Compared with the 2 mM cytoplasmic Mg^{2+} used by Wang et al. and Cang et al., [104, 105] an entire suppression of TPCs is anticipated. Importantly, most findings regarding observation of NAADP-induced responses occurred without the presence of Mg^{2+}, [70, 73, 102, 109-113]. However, when $PI(3,5)P_2$ was included, significant TPC currents were still demonstrable in Wang et al.'s and Cang et al.'s studies, suggesting that either TPCs are not suppressed by Mg^{2+} or only NAADP-stimulated TPCs can be blocked by Mg^{2+} under their conditions [80]. Again, future work is required to elucidate if Mg^{2+} gives rise to the existing puzzlement.

1.7 What type(s) of channel(s) do TPCs belong to?

Another big challenge regarding TPC signalling is the role(s) of TPCs: are they solely Ca^{2+} channels? or do they actually belong to other types of ion channels? Recently, some groups have suggested that TPCs act as Na^{+}-selective channels [104, 105, 114, 115], but not Ca^{2+} channels as initially suggested [70, 102, 112, 113]. For groups that previously looked into Ca^{2+} permeability only, significant Na^{+} currents were revealed after re-examining the ion permeability [92, 109-111]; yet selectively between the two ions was relatively low [92, 110, 111]. Given the Na^{+} currents were activated by $PI(3,5)P_2$ [104, 105, 114], one may speculate that the lipid could be switching the originally Ca^{2+}-selective TPCs to a more Na^{+}-selective channel, just like that seen with TPC1 . However, this explanation is sceptical as both NAADP- and $PI(3,5)P_2$-induced TPC currents resulted in comparable biophysical characteristics [110]. Also, even TPCs are Na^{+}-permeant channels does not imply that they are conflicting the Ca^{2+} hypothesis. It is not uncommon for channels to have permeability to other cations, IP_3R and RyR, for example, are also well-known for their high conductivity of K^{+} [102, 116, 117]. And perhaps TPCs would functionally behave like a “non-selective” channel, just like NMDA glutamate receptors which are both Na^{+}- and Ca^{2+}-permeant [118]. In fact, if TPCs are Na^{+} channels (but not Ca^{2+} channels) that regulates NAADP-mediated Ca^{2+} release, a more complicating ionic circuit model than previously suggested is undeniably required, as proposed by Morgan and Galione in their recent review about the influences of Na^{+} on Ca^{2+} release [63]. A number of factors including TPC biophysical properties and acidic store electrochemical gradients are needed to be taken into considerations in the first instance [63].

Notably, another recent paper has demonstrated that TPC1 exhibited a substantially higher permeability for H^{+} (~500 folds) than Na^{+} or Ca^{2+} [111]. This is particularly tempting as earlier findings showed that NAADP signalling triggered alkalinisation of endolysosomal

compartments in sea urchin eggs [60, 119], pancreatic acinar cells [49], atrial myocytes [120] and HeLa cells overexpressed with TPC2 [101], the findings of TPC1's remarkable permeability to H^+ could thus provides an interpretation for such observations.

1.8 Functional regulation of TPCs by different regulators

Accumulating findings from both direct (with reconstitution of TPCs in bilayers) [102, 111, 112] and indirect [60, 121] evidence has shed light on TPCs (and NAADP receptors) regulation by Ca^{2+}. This is in stark contrary to earlier findings in which nonresponsiveness to Ca^{2+} feedback was demonstrated [15]. And importantly, Ca^{2+} has been shown to exert their regulatory effects on the luminal [102, 112] and cytosolic side [111], suggesting new routes for dynamic regulation of Ca^{2+} signalling between acidic stores and other organelles [60].

Mg^{2+} is another cation that has been showed to modulate TPCs lately [109]. The blocking effect of cytosolic Mg^{2+} on TPC1, as discussed previously, is independent of the type of stimulus. Since only TPC1 is susceptible to Mg^{2+}, whether this powerful inhibitor can also suppress TPC2 (and probably TPC3) and whether it has the same inhibiting effects in other species await further elucidations.

Apart from regulation by Ca^{2+} and Mg^{2+}, several findings have suggested stimulation of TPCs [111-113] and channel opening [102, 114] by acidic luminal pH whilst insignificant influence was also reported [104, 109]. It is not impossible that luminal pH might have an effect on TPCs given their endolysosomal localization. However discrepancies appear between groups and no clear conclusion can be drawn at the moment.

$PI(3,5)P_2$, as discussed in previous sections, has recently been shown to regulate TPC channel activities [104, 105, 109-111, 114, 122] and it should be noted that $PI(3,5)P_2$ exerts its regulatory effects by changing the ion permeability instead of direct stimulation

of TPCs [111].

Intriguingly, membrane potential has lately been revealed to modulate TPC1 and TPC3 [111, 112, 114, 115] but not TPC2 [70, 102, 113], besides its regulation on ion movement across endolysosomal membrane [15]. Cang et al. suggested that endolysosomes might be electrically excitable organelles, and that TPC1 can respond to pH changes which confers endolysosomes with voltage sensing ability, thus it explains how Ca^{2+} release may be affected by membrane potential [105, 114].

Leaving aside the Na^{+} channel proposals, mounting evidence has indicated that NAADP activation of TPCs is not simply direct binding to TPC channels (like the direct binding of IP_3 to IP_3Rs), instead a separate NAADP-binding protein which forms complexes with TPCs is required. Additional details regarding evidence of NAADP binding to accessory proteins have already been discussed in section 1.5.3 A number of kinases have been proposed to interact with TPCs – mTOR [105, 109, 123], p38 [109], small GTPases (Rabs) [110, 123], Hax-1 [124] to name a few. And intriguingly some of them have been shown to modulate TPC function. Identifying these binding proteins has become one of the important issues in NAADP research. Certainly, it gives deeper insight into how TPC and NAADP are interacted in the signalling system and also provides explanation to the many discrepancies arisen between groups.

The discovery of eight putative PKC phosphorylation sites in rat TPC1 implicates they may play a role in regulating TPC functions [64], which awaits to be investigated. On the other hand, the findings of putative *N*-glycosylation sites mapping to the region between S5 and the pore loop [64, 73, 77] and enhanced NAADP-induced Ca^{2+} release resulted from mutation of these *N*-glycosylation sites [77] implicate *N*-glycosylation in TPC functional regulation.

Apart from the well-described CICR and the newly established bidirectional

ER/endolysosomes communication, recent evidence has proposed a new, regulatory role of TPC2 in modulating store-operated Ca^{2+} entry (SOCE) [125]. That TPC2 KD resulted in suppression of thapsigargin-induced SOCE was apparent in human cells without interfering Ca^{2+} accumulation in the ER, which was likely modulated by interaction with STIM1 and Orai1 as suggested by the co-immunoprecipitation studies. Further investigations are required to clarify the possible functional role of TPC2 in such regulation. Nevertheless this further highlights the significance of dynamic regulation between different Ca^{2+} signalling pathways.

Collectively, significant amount of findings support the notion that TPCs are indispensable for NAADP-mediated signalling, however the increasing number of conflicting results between groups suggests that further examinations are crucial to clarify the discrepancies. Equally important is the search for the accessory factors that NAADP bind to, as well as the regulators that mediate the interaction between NAADP/TPC signalling and downstream effectors.

1.9 NAADP- and TPC-mediated signalling in physiological and cellular processes

Research of the roles of NAADP and TPCs in physiological and cellular processes is still at the beginning, however several lines of findings have recently indicated their involvement in major developmental stages *in vivo* and cellular differentiation *in vitro*. NAADP and TPCs also contribute to regulation of autophagy, endolysosomal trafficking and functions, as exemplified in an array of studies employing different pharmacological (Ned-19, bafilomycin A1, NAADP-AM etc.) and genetic (KD, KO, overexpression) techniques. A list highlighting their physiological relevance is displayed below (Table 1). Given ample evidence implicating their significance in these physiological and cellular

functions, future studies are required to clarify the underlying mechanisms of NAADP and TPC signalling pathways, as well as their interactions with other Ca^{2+} signalling pathways, in mediating these processes.

Table 1 Functional roles of NAADP/TPC in different physiological and cellular processes

Fertilization and embryogenesis		
- Animal model/cell type - Physiological/cellular event	*Major findings of studies*	*References*
Fertilization of sea urchins and starfish	During fertilization, a significant increase in NAADP triggers a cortical flash, generating Ca^{2+} wave required for egg activation, and leads to embryogenesis.	[38]
Starfish oocytes and embryos	TPC2 and TPC3 KD impairs fertilization envelop formation and also leads to embryo lethality at the gastrula stage; moreover, a combined perturbation but not individual disruption of all three TPCs results in significantly aberrant Ca^{2+} wave.	[126]
Acrosome reaction	NAADP triggers acrosome reaction at physiological concentrations in the absence of extracellular Ca^{2+}.	[127]
Embryonic development in zebrafish	Detailed description refers to Chapter 3.	[128, 129]
Mammalian fertilization and embryonic development	Transgenic mice with TPC single or double KO are fertile and viable and capable to develop into adulthood, likely due to Ca^{2+} signalling pathway remodelling [1].	[71, 86, 92]
Muscle contraction		
Pulmonary artery smooth muscle cells	Endothelin-1 enhances NAADP level and the subsequent amplification of NAADP-mediated Ca^{2+} signals by RyRs results in contraction.	[43]
Detrusor and taenia cascum smooth muscle	TPC2-deficient mice are lack of NAADP-induced contractions of detrusor and taenia cascum muscle; while compensation of Ca^{2+} signalling might exist to sustain carbachol-induced contractions.	[130]
Muscle contraction in zebrafish	Detailed description refers to Chapter 3.	[128, 129]
Differentiation		
- Animal model/cell type - Physiological/cellular event	*Major findings of studies*	*References*
Neuronal differentiation in PC12 cell line	Liposome-mediated delivery of NAADP and cADPR but not IP_3 induces Ca^{2+} release and neuronal morphology development.	[131]
Commitment and differentiation of mouse embryonic stem (ES) cells	TPC2 signalling blocks ES cell differentiation into early neural progenitors but is needed for the later stage of neural differentiation.	[132]
Skeletal muscle	NAADP-AM stimulates myogenic differentiation in	[133]

differentiation in primary skeletal muscle precursor cells and C2C12 myogenic cell line	both cell types; whereas in C2C12 cells deficient of TPC1 or TPC2, such process is absent. Impairment of myogenesis also occurs when NAADP signalling is inhibited pharmacologically.	
Osteoclast differentiation	TPC2 expression is elevated in osteoclast precursor cells upon induction of osteoclastogenesis and TPC2 mediates such process likely via regulating intracellular Ca^{2+} signalling and NFAT translocation in osteoclastic precursors.	[134]
Osteoclast formation	Extracellular application of NAADP at high concentrations reduces osteoclast formation and resorption, implicating involvement in such process.	[135]
Keratinocyte differentiation	Extracellular application of NAADP not only promotes human epidermal keratinocyte differentiation into terminally differentiated cells but also enhances their migration and proliferation.	[136]
Angiogenesis	Disruption of NAADP signalling pharmacologically and genetically leads to inhibition of 1. Ca^{2+} release induced by vascular endothelial growth factor (VEGF); 2. *in vitro* and *in vivo* angiogenic responses to VEGF; 3. *in vivo* VEGF-induced vessel formation in matrigel plugs.	[137]
Thermogenesis in brown adipose tissue (BAT)	Disruption of BAT thermogenesis occurs in TPC1/2 DKO mice, owing to reduction of lipid availability and use and also impairment of β-adrenergic receptor signalling.	[138]
Autophagy, endolysosomal trafficking and functions		
- Animal model/cell type *- Physiological/cellular event*	*Major findings of studies*	*References*
Autophagy in rat astrocytes	NAADP-induced Ca^{2+} release from acidic stores and NAADP-mediated upregulation of LC3II and beclin-1levels suggest a regulatory role of NAADP/TPC2 signalling in autophagy.	[100]
Autophagosome-lysosomal fusion in HeLa and mouse ES cells	NAADP/TPC2 signalling suppresses autophagosomal-lysosomal fusion through alkalinisation of lysosomal pH, resulting in accumulation of autophagosomes.	[101]
Autophagic flux in coronary arterial myocytes	NAADP signalling mediates autophagosome trafficking and fusion with lysosomes through regulating dynein ATPase activity.	[139, 140]
Cholera toxin B transport	Overexpression of HsTPC1 and TPC2 in HEK cells disturbs the trafficking of cholera toxin B from endosomes to the Golgi complex, which in turn impedes lysosome biogenesis.	[76]
Endolysosomal trafficking in mouse embryonic fibroblasts (MEFs)	MEFs from TPC1- or TPC2-deficient mice display normal endolysosomal pH or morphology; TPC1 KO MEFs upset cholera toxin transport from the plasma membrane to the Golgi complex while TPC2 KO MEFs delay ligand-induced platelet-derived growth factor receptor β degradation, which relies on transport to lysosomes, suggesting different roles of TPC1 and	[86]

	TPC2 in the endolysosomal pathway.	
Endolysosomal degradation in embryonic mouse fibroblasts and hepatocytes	Substantial trafficking impairment in the endolysosomal degradation pathway occurs in TPC2-deficient cells; also TPC2-deficient mice exhibit defects in hepatic cholesterol reserve and utilization.	[110]
Lysosome proliferation	Pharmacologically-induced lysosomal dysfunction in primary cultures of rat hippocampal neurons and PC12 cells results in deregulation (exaggeration) of NAADP signalling which results in neuronal dysfunction.	[141]
Lysosomal function	Deviant lysosomal Ca^{2+} release and altered TPC expression resulted from absence of presenilins, a protein needed for effective proteolysis in autophagy, possibly lead to impairment of autophagy.	[142]
Apoptosis	Physical association between HsTPC2 and Hax-1, an anti-apoptotic protein, has been identified.	[124]
Skeletal muscle autophagic signalling	Alterations in autophagic flux occur in skeletal muscle of TPC2 KO mice; and association with the nutrient sensor mTOR allows TPC2 to regulate muscle homeostasis.	[123, 143]
Nutrient sensing	Significant reduction in muscle endurance after fasting occurs in TPC1/2 DKO mice; and interaction between TPCs and mTOR might couple metabolism to endolysosomal functions.	[105]

1.10 Disruption in human pathology

Given their impact on diverse functional regulations of physiological and cellular process, it is not astonishing that NAADP and TPC signalling are involved in human diseases, however NAADP or TPC mutations with disease-causing potential have not been recognised in studies so far. Some indirect evidence for potential risk factors has been arisen from a genome-wide study in which two single polymorphisms in HsTPC2 gene have been identified to be linked with hair pigmentation phenotypes (blond versus brown) in northern Europeans [144]. Whether the NAADP and TPC signalling are involved in other human diseases and whether alterations of these pathways are a cause or consequence of diseases are intriguing research topics which await further elucidations.

1.11 Aims of this study

This study aims to explore the mechanism of action and possible functional roles of TPCs in vertebrate physiology, so as to provide deeper insights about our understanding of NAADP/TPC mobilisation, which has gained rising prominence in the Ca^{2+} signalling field. The main objectives of this research project are:

1. To investigate the expression patterns and the role(s) of TPCs during zebrafish embryogenesis, with a focus on muscle development;
2. To investigate the roles of TPC2-mediated signalling during adipogenesis
3. To investigate the mechanisms underlying the regulation of TPC2 expression during adipogenesis, including potential upstream mediators and downstream effectors;
4. To investigate *Tpcn1* mRNA expression in different regions of the mouse brain

A more detailed explanation for each objective is presented in each experimental chapter.

Chapter 2:

Materials and Methods

All chemical reagents were purchased from Sigma-Aldrich UK unless otherwise specified. All experiments were carried out at room temperature (RT) unless otherwise specified. All washes and elutions were conducted and all solutions and dilutions and media were prepared using 18MΩ water double-deionised (ddH_2O) by reverse osmosis unless otherwise specified. Also, all media were either autoclaved or filter-sterilised before use.

2.1 Construct generation

2.1.1 Purification of total RNA from zebrafish embryo

Frozen zebrafish embryos were kindly provided by Prof. Roger Patient's lab at the Weatherall Institute of Molecular Medicine, Oxford. Total RNA was extracted and purified using QIAGEN RNeasy mini kit according to manufacturer's instructions. Embryos were harvested by centrifugation (10,000 xg, 15 minutes, 4°C). Lysis buffer (buffer RLT) was added to disrupt the cell pellet. Homogenization of the lysate was performed with a syringe and needle. Homogenized lysate was mixed with one volume of 70% ethanol and transferred to RNeasy spin column and centrifuged (8,000 xg, 15 seconds) to bind RNA to the column filter. The bound RNA was washed and treated with DNase I (approximately 30 Kunitz units per column), followed by further washes. The RNA was eluted with RNase-free H_2O and concentration and integrity was checked.

2.1.2 Reverse transcription polymerase chain reaction (RT-PCR)

One step RT-PCR was performed using the SuperScript™ III One-Step RT-PCR System with Platinum® Taq High Fidelity according to manufacturer's instructions, whereby cDNA synthesis and PCR amplification were performed in a single tube. See Table 2.1 for reaction mix details. Sequence-specific primers (Invitrogen) were designed. The reaction mix was incubated in a preheated thermal cycler using the cycling conditions outlined in

Table 2.2.

Table 2.1 Reaction Mixture

Component	Volume per reaction (µl)
Nuclease-free H_2O	9
2x Reaction Mix	12.5
Forward primer (5 µM)	1
Reverse primer (5 µM)	1
SuperScript™ III RT/Platinum® Taq High Fidelity Enzyme Mix	0.5
Template RNA (~300 ng/µl)	1
Total per reaction	**25**

Table 2.2 Cycling conditions of one-step RT-PCR

Step	Temperature	Time	Number of cycles
1. cDNA synthesis and pre-denaturation	50°C 94°C	30 minutes 2 minutes	1
2. PCR amplification	94°C (Denaturation) 54°C (Annealing) 68°C (Extension)	15 seconds 30 seconds 4 minutes	40
3. Final extension	68°C	10 minutes	1

2.1.3 PCR of cDNA

PCR of cDNA was performed using the *PfuUltra* II Hotstart PCR Master Mix according to manufacturer's instructions. Reaction mixture details are listed in Table 2.3. Sequence-specific primers (Invitrogen) were designed. The reaction mix was incubated in a preheated thermal cycler using the cycling conditions outlined in Table 2.4.

Table 2.3 Reaction Mixture for PCR

Component	Amount per reaction (µl)
PfuUltra II Hotstart 2x Master Mix	25
Forward primer (10 µM)	1
Reverse primer (10 µM)	1
DNA template (100 ng/µl)	1
Nuclease-free ddH_2O	22
Total reaction volume	**50**

Table 2.4 Cycling conditions for *PfuUltra* II Hotstart PCR Master Mix

Step	Temperature	Time	Number of cycles
1.	95°C	1 minute	1
2.	95°C (Denaturation)	20 seconds	40
	54°C (Annealing)	20 seconds	
	72°C (Extension)	1.5 minutes	
3.	72°C	3 minutes	1

2.1.4 Purification of PCR products

PCR products were purified using QIAquick Spin method (QIAGEN). Briefly, PCR samples were mixed with binding buffer and then centrifuged (17,900 xg, 1 minute) to bind the DNA to the silica membrane of a spin column. The bound DNA was washed and then eluted with TE buffer.

2.1.5 Vector/Insert ligation

Purified PCR samples were cloned into the pCRII-TOPO vector (Dr TPC1 and DrTPC2) using the TOPO TA Cloning Kit (Lifetechnologies) and the reaction mixture was incubated for 30 minutes. For ligation of PCR samples with the pGEM-T easy vector (Promega) (DrTPC3), the reaction mixture was incubated for 1 hour. The cloning reactions were set up as follows (Table 2.5 and 2.6):

Table 2.5 Reaction mixture for pCRII-TOPO vector/insert ligation

Component	Amount per reaction (µl)
PCR product	4
pCRII-TOPO vector	1
6x salt solution	1
Total reaction volume	**6**

Table 2.6 Reaction mixture for pGEM-T Easy Vector/insert ligation

Component	Amount per reaction (µl)
2x Rapid Ligation Buffer	5
pGEM®-T Easy Vector (50 ng/µl)	1
PCR product (vector:insert in 1:1 molar ratio)	For DrTPC3, 38 ng was needed
T4 DNA Ligase	1
Nuclease-free ddH_2O	Added to a final volume of 10
Total reaction volume	**10**

2.1.6 Transformation of E.coli XL10 Z-competent cells

E.coli XL10 Z-competent cells were thrawed on ice and the ligation product was added to cells on ice and mixed by gently stirring. The reaction mixture was incubated on ice for 5 minutes. Then the cells were spread onto a pre-warmed 3.5% (w/v) LB-agar plate with 100 µg/ml ampicillin and incubated at 37°C overnight (O/N).

2.1.7 Construct amplification and purification

A few single antibiotic-resistant colonies were selected and added into LB medium with 100 µg/ml ampicillin and incubated at 37°C for 12-18 hours in a shaking incubator. Plasmid DNA was isolated from the bacterial cultures by miniprep (QIAGEN) in accordance with manufacturer's protocols. Concisely, cells were harvested by centrifugation (6,800 xg, 3 minutes) followed by resuspension in lysis buffer, precipitation of DNA and removal of genomic DNA by centrifugation (17,900 xg, 10 minutes). The precipitated DNA was then bound to the spin column, washed, and eluted by buffer TE.

2.1.8 Construct verification

2.1.8.1 Restriction digest

Plasmid DNA (pCRII-TOPO.DrTPC1, pCRII-TOPO.DrTPC2 and pGEM-T easy vector.DrTPC3) up to 20 µg were digested by incubating with restriction enzyme EcoRI (2 U/µg) in 10x Tango buffer (all from Fermentas) for 2 hours.

2.1.8.2 Gel electrophoresis

Digested products were run on 1% agarose gel to determine the presence of ligated vector and insert:

Gels containing 1% or 1.5% (w/v) agarose in 1x Tris acetate-EDTA (TAE) buffer (40 mM Tris acetate, 1 mM EDTA; pH 8.0) were used, with ethidium bromide (Fisher) added to final concentration of 0.5 μg/ml. Prior to loading, samples were mixed with 1/5 volume of 6x Orange DNA Loading dye (Fermentas) and loaded beside a molecular weight standard (O'GeneRuler 1kb or 1kb Plus DNA ladder, Fermentas). Electrophoresis was conducted in 1x TAE buffer at 120V. DNA was visualised under UV transilluminator and images were taken by Syngene imaging system and GeneSnap software.

2.1.8.3 Quantification and sequencing

Concentrations of the miniprep products were determined using NanoDrop spectrophotometer (ThermoScientific). They were then sent for sequencing (GATC Biotech or Source BioScience) using specific sequencing primers and cDNA sequences generated were checked by the CAP3 sequence assembly programme[1] [145].

2.1.9 QuikChange II XL Site-directed mutagenesis

Site-directed mutagenesis was performed to correct the point mutations that occurred in each DrTPC using the QuikChange II XL Site-directed mutagenesis kit (Agilent Technologies) according to manufacturer's protocols. Briefly, PCR reaction mixture was set up as indicated in Table 2.7 and cycling conditions are given in Table 2.8. After amplification of the mutated products, *Dpn* I digestion of the amplification products was performed to digest the parental supercoiled dsDNA. 1 μl of *Dpn* I restriction enzyme (10

[1] http://pbil.univ-lyon1.fr/cap3.php

U/µl) was added to each amplification reaction. The reaction mixture was incubated at 37°C for 1 hour. After mutagenesis, transformation and miniprep were performed and the products were sent for sequencing and correct sequence was verified.

Table 2.7 Reaction Mixture for QuikChange II XL method

Component	Amount per reaction (µl)
PfuUltra II Hotstart 2x Master Mix	10
Forward primer (10 µM)	1
Reverse primer (10 µM)	1
DNA template (100 ng/µl)	1
Nuclease-free ddH_2O	7
Total reaction volume	**20**

Table 2.8 Cycling conditions for QuikChange II XL method

Step	Temperature	Time	Number of cycles
1.	95°C	2 minutes	1
2.	95°C	30 seconds	18
	55°C	1 minute	
	68°C	1 minute/kb	
3.	68°C	7 minutes	1

2.1.10 Construction of recombinant plasmids with mCherry tag

To generate constructs with mCherry tag, pcDNA5/TO.MmTPC1.mCherry provided by Dr Guida Ruas was cut with restriction digestion enzymes to generate mCherry tag which was then introduced to the three DrTPC plasmids by ligation.

Firstly, the recombinant plasmids with mutations corrected were used as templates for amplification by PCR using specific primers for each DrTPC. Then the PCR products and pcDNA5/TO.MmTPC1.mCherry plasmid were digested by incubation for 2 hours with KpnI (2 U/µg) and then NotI (2 U/µg) in 10x Tango buffer (all from Fermentas).

The digested products were run on a 1% agarose gel and the desired band was excised and DNA was extracted and purified from the gel using the QIAquick Gel Extraction Kit (QIAGEN) according to manufacturer's instructions. Briefly, binding buffer was added to

dissolve the gel and bind the plasmid DNA, followed by precipitation with isopropanol and centrifugation (17,900 xg, 1 minute). The plasmid DNA that was bound to the silica membrane of a spin column was washed with washing buffer before eluted with elution buffer.

After purification, the mCherry tag was inserted into the linearized vectors containing DrTPC by ligation. In brief, vector and insert DNA were taken in a molar ratio of 1:3 and incubated with T4 DNA ligase (NEB) and ligation buffer (NEB) for 2 hours followed by heat inactivation at 65°C for 10 minutes. Details of reaction mixture are listed in Table 2.9.

Table 2.9 Reaction mixture for vector/insert ligation with T4 DNA Ligase

Component	**Amount per reaction (µl)**
10x T4 DNA Ligase Buffer	2
Vector DNA (50 ng/µl)	1
Insert DNA	Insert:Vector in a molar ratio of 1:3 (i.e. 37.5 ng of insert DNA per 50 ng of vector)
T4 DNA Ligase	1
Nuclease-free ddH_2O	Added to give a final volume of 20
Total reaction volume	**20**

After ligation, plasmid DNA was isolated form *E.coli* cells grown O/N in LB with ampicillin (see section 2.1.6). Construct amplification and purification (see section 2.1.7) was performed and the purified constructs were double-digested firstly with HindIII and then NotI, and gel electrophoresis was performed to verify the presence of ligated vector and insert. Finally miniprep concentration was determined and sent for sequencing to get the correct cDNA sequence (see section 2.1.8).

2.2 Antibody purification

Anti-DrTPC1, anti-DrTPC2 and anti-DrTPC3 immune sera were produced by Covalab (Table 2.10).

Table 2.10 Antigenic peptide sequences used for preparation of immune sera

	Peptide A	Peptide B
DrTPC1	IGLKWKARRSGEHWC	YSRKNREPLDDPEDC
DrTPC2	LTYTSDIRVKPKPWC	KSDDPKQNGEWQTYC
DrTPC3	MSEGKTEKTSHTLTC	VYNNYKKYLKEEVRC

Sera for each DrTPC were generated from two rabbits (labelled 2100 and 2167 for DrTPC1, 2137 and 2162 for DrTPC2, 025001and 025029 for DrTPC3). Purification of these sera against individual peptides (all of them contain an addition of N-terminal cysteine residue) was performed by SulfoLink coupling resin (Pierce) according to manufacturer's protocols. Affinity-purified antibodies are labelled according to the serum from which they were purified and the purifying antigenic peptide (e.g. 2100A).

2.3 Zebrafish husbandry and embryo collection

Wild type (AB strain; obtained from the Zebrafish International Resource Centre, University of Oregon, Eugene, OR, USA) zebrafish (*Danrio* rerio) and the α-actin-apoaequorin-IRES-EGFP (α-actin-aeq) transgenic line generated by Cheung et al., 2011 [128] were kept in system water maintained at ~28°C and pH ~7.0 in the zebrafish facility of Hong Kong University of Science and Technology (HKUST). The zebrafish were kept in a 14 hours light/10 hours dark cycle to encourage spawning [146]. Fertilized eggs were collected and immediately transferred to 30% Danieau's solution (17.4mM NaCl, 0.21mM KCl, 0.12mM $MgSO_4$, 0.18mM $Ca(NO_3)_2$ and 1.5mM HEPES, pH7.2). Embryos were maintained at ~28°C throughout development and all experiments.

2.4 Microinjection

Injection chambers were made with 1% agarose (Invitrogen) with a groove of ~1 mm width and ~25 mm length in the agarose to fit the size of intact zebrafish embryos. Injection pipettes were pulled from borosilicate glass capillaries (1B100F-4; World Precision Instruments) using a horizontal puller (Narishige PN-3). Tip of micropipette was wrecked and bevelled at 30° to produce a diameter of ~10 μm. A microinjection system comprising a micromanipulator (Zeiss) and either a Nikon SMZ-745T (Nikon) or a Zeiss Stemi SV 6 (Zeiss) bottom-illuminated stereomicroscope, along with a PLI-100 pressure-injection system (Medical Systems Corp., USA), were used for zebrafish embryo microinjection. For all experiments, the injection pressure was kept at 15 PSI (i.e., 105 kPa).

2.5 Morpholinos design and injection

Morpholinos (MO) were obtained from Gene Tools, LLC (Philomath, Oregon, USA). The type of morpholinos used in this study work through an RNase-H independent process that blocks translational initiation. Consequently, all morpholinos were arbitrarily designed to bind to the 5' UTR and coding sequence flanking and including the initiating methionine. Sequences were selected based on design parameters according to the manufacturer's recommendations, namely 21-25mer antisense oligonucleotides of ~50% G/C and A/T content with no predicted internal hairpins. Four consecutive G nucleotides were also avoided. Sequences were as follows (sequence complimentary to the predicted start codon is underlined):

anti-DrTPCN2 MO: CAGCCAGCAGCGGTTCTTCTTCCAT

anti-DrTPCN3 MO: TTTTCTCAGTCTTCCCCTCAGACAT

p53-MO was co-injected with the anti-DrTPC-MO (~1.5:1 ratio) to prevent any off-target

effects [147, 148]. Standard control-MO was used as a specificity control. All oligos were prepared at a stock concentration of 1mM in ddH_2O after which ~1.5 nl of the diluted oligos were injected into embryos at the 1- to 4-cell stage to reach a dose of ~2.5 ng.

2.6 *In vivo* reconstitution of aequorin and bioluminescence-based Ca^{2+} imaging

A 10 mM stock solution of *f*-coelenterazine (NanoLight® Technologies) was kindly provided by Prof. Andrew Miller of HKUST. For *in vivo* reconstitution of active aequorin, α-actin-aeq transgenic embryos were incubated with 50 μM *f*-coelenterazine in Danieau's solution at ~28°C in the dark. Incubation began at the ~8-cell to 64-cell stage (i.e. 1.25 to 2 hours post fertilization (hpf)) and stopped at the ~16-somite stage (~17 hpf). Due to high background photon count, residual *f*-coelenterazine was eliminated by gently washing the embryos after incubation. Embryos were then dechorionated manually. Dechorionated embryos were placed in custom-made imaging chambers (similar to injection chambers except that the agarose was coated on glass coverslip) for optimal photon acquisition and covered with lids wrapped with Parafilm ® (American National Can) for minimal moisture loss. Embryos were occasionally immobilized by adding 2-3% methylcellulose (w/v) in Danieau's solution. Luminescence-based Ca^{2+} imaging was performed in the custom-built Photon Imaging Microscope Systems (Science Wares) and photomultiplier tube-based luminescence detection systems (Science Wares). After data acquisition, 1% triton X-100 (v/v) in Danieau's solution was administered to lyse the embryo and "burn-out" (i.e. expose) the residual aequorin to extracellular Ca^{2+}.

2.7 Morphological studies of zebrafish embryos

Bright-field imaging of the morphology of embryos was acquired using a Zeiss Axioskop microscope and the "Nikon ACT-1 Version 2.63" system. Embryos were dechorionated before experiment and mounted in the custom-made injection chamber (section 2.4). Embryos were then immobilized with 2-3% methylcellulose (w/v) in Danieau's solution, or sometimes anaesthetized by 0.0168% MS-222 (i.e. tricane) (w/v).

2.8 Whole-mount immunohistochemistry

For whole-mount immunolabelling of the myosin heavy chain and F-actin, embryos at ~24 hpf were dechorionated either manually or by pronase (1 mg/ml in Danieau's solution) for 3-5 minutes followed by a few gentle washes in Danieau's solution. Embryos were fixed with 4% (w/v) paraformaldehyde (w/v) (PFA; Electron Microscopy Sciences) in phosphate-buffered saline (PBS; 137 nM NaCl, 2.68 mM KCl, 16 mM Na_2HPO_4, 4 mM $NaH_2PO_4 \bullet 2H_2O$, pH 7.3) containing 4% sucrose (VWR International) O/N at 4°C, followed by three 10-minute PBS washes and were stored at 4°C (maximum for 4 weeks) prior to immunolabelling. While for long term storage, embryos were kept in 0.05% (w/v) sodium azide (VWR International) in PBS.

Dual labeling of myosin heavy chain and F-actin with F59 anti-myosin heavy chain primary antibody (Developmental Studies Hybridoma Bank, University of Iowa) and fluorescent phalloidin respectively was performed. Firstly, fixed embryos were washed three times (10 minutes each) with 0.1% (v/v) Triton X-100 in PBS (PBST). Then they were permeabilised by incubation with 1% (v/v) dimethyl sulphoxide (DMSO) in PBST (PBDT) for 1 hour, followed by incubation with blocking buffer (10% (v/v) goat serum/1% (v/v) bovine serum albumin/PBDT) for 2 hours. Next they were incubated with

the mouse F59 anti-myosin heavy chain primary antibody (diluted at 1:5 or 1:10 in blocking buffer) O/N at 4°C, followed by five 10-minute blocking buffer washes, and then incubated for 2-3 hours in the dark with Alexa Fluor® 488 goat anti-mouse IgG (H+L) secondary antibody and Alexa Fluor® 546 phalloidin (Molecular Probes) (diluted to 1:200 and 1:50 in blocking buffer respectively). Lastly, embryos were rinsed extensively with wash buffer in the order of PBDT, PBST and PBS. Gentle agitation was applied to facilitate incubation and washing steps throughout the experiment.

2.9 RNA *in situ* hybridization on whole-mount embryos

2.9.1 Linearization of plasmid DNA

pCRIITOPO.DrTPC1, pCRIITOPO.DrTPC2 and pGEM T easy.DrTPC3 plasmid DNAs were used as templates for linearization. In order to synthesize probes that are about 1-2 kb, the plasmids were linearized using appropriate restriction enzyme which cut at a restriction site 1-2 kb upstream or downstream from the sp6 or T7 promoters. Linearization was confirmed by running a small amount of digested product on a gel. Linearized DNA was then purified by the QIAquick Spin method (QIAGEN) before proceeding to probe synthesis.

2.9.2 DIG probe synthesis

DIG probes were synthesized to provide an average length of 1-2 kb nucleotides using the DIG RNA Labeling kit (SP6/T7) (Roche) according to manufacturer's protocols. Briefly, to 1 μg of template, RNase-free and DNase-free ddH_2O was added to a final volume of 13 μl, and then the following was added in order for a total volume of 20 μl:

Table 2.11: Reaction mixture for DIG probe synthesis

Reagent	Volume
10x NTP labelling mixture	2 µl
10x Transcription buffer	2 µl
Protector RNase inhibitor	1 µl
RNA Polymerase SP6 or T7	2 µl

The mixture was incubated for 2 hours at 40°C, followed by DNaseI treatment to remove the template DNA with a further 30 minutes incubation at 37°C. 80 µl ddH_2O was added and probe was passed through prepared spin column. The probe labelling reaction was added into a mixture of 10 µl LiCl and 250 µl 100% ethanol and the whole mixture were incubated at -20°C O/N. The probe was pelleted by centrifugation (13200 rpm, 30 minutes, 4°C) and washed gently with ethanol and centrifuged again (13200 rpm, 20 minutes, 4°C). The pellet was allowed to air dry and subsequently resuspended in RNase-free ddH_2O and stored at -20°C.

2.9.3 In situ hybridisation (ISH)

Embryos at 24 hpf stage were fixed with 4% (w/v) PFA in PBS O/N at 4°C, dechorionated manually and dehydrated O/N in methanol at -20°C. The embryos were then rehydrated stepwise in methonal/PBS and finally put back in 100% PBT (1x PBS/0.1% Tween 20), followed by proteinase K treatment for 10 minutes and reaction was stopped by washing with PBS twice 5 minutes each. Embryos were postfixed in 4% (w/v) PFA/PBS for 20 minutes and then washed with PBT 5 times 5 minutes each. Fixed embryos were prehybridized for at least 2 hours at 65°C in hybridization buffer (HYB) (50% formamide, 5x SSC, 50 µg/ml heparin, 500 µg/ml tRNA, 0.1% Tween 20, 9 mM citric acid), followed by hybridization using the same HYB containing 30-50 ng of probe O/N at 65°C. The embryos were then washed in the following order at 65°C: HYB for 5 minutes, 50% HYB/2x SSC for 30 minutes, 2x SSC for 20 minutes, 0.2x SSC for 20 minutes. Further

washes were performed at RT in PBS for 15 minutes and two times 5 minutes each. The embryos were incubated in 2% blocking agent (Roche) in MAB (100 nM maleic acid pH 7.5, 150 mM NaCl) for at least 3 hours before incubation O/N at 4°C with anti-DIG-AP (anti-DIG antibody from sheep, conjugated with alkaline phosphatase AP) in 2% blocking agent in MAB. Finally the embryos were washed in PBS 4 times 30 minutes each and then equilibrated with BM staining buffer for 3 times 5 minutes each. Detection was performed in BM Purple AP substrate (Roche) in the dark. When the colour developed, reaction was stopped by several washes in PBS. The embryos were then refixed in 4% (w/v) PFA/PBS O/N at 4°C and subsequently rinsed with PBS for 2 times and then transferred to 75% glycerol in PBS and stored at 4°C.

2.10 C3H10T1/2 cell culture

All cell cultures were maintained in a humidified 5% CO_2/air atmosphere at 37°C.

2.10.1 Cell line amplification and frozen aliquot preparation

A frozen aliquot of C3H10T1/2 cells (clone 9, passage 16) was kindly provided by Dr Costa Christodoulides of the Oxford Centre for Diabetes, Endocrinology and Metabolism. Amplification of the cells and more frozen aliquots were prepared from this initial aliquot. After being thawed quickly in a 37°C water bath with gentle swirling, the cells were diluted slowly in prewarmed growth medium (GM) (see Table 2.12 for details) in a T25 flask (Cellstar). After 7 hours of incubation, the medium was changed to fresh GM to remove cryopreservatives, dead cells and cell debris. The medium was then changed every two days and the cells were passaged when ~70-80% confluency was reached. The medium was discarded and the cells were washed with sterile PBS, followed by 5 minutes trypsin-EDTA incubation at 37°C. When detachment of cells from surface was complete,

additional GM was added to inactivate the trypsin, then the cells were added to a falcon tube (BD) for centrifugation (1000 rpm for 5 minutes). The supernatant was aspirated and fresh GM was added to resuspend the cell pellet. The cells were transferred to a T75 flask and incubated at 37°C. When they grew to ~ 70-80% confluence again, the above steps were repeated except that resuspension was performed in freezing medium (FBS/10% dimethyl sulfoxide (DMSO)) and the cells were aliquoted, stored and cooled slowly in a -80°C freezer O/N. Frozen aliquots were transferred to liquid nitrogen tank for long term storage. Cells were at passage 19-23 for all experiments.

2.10.2 C3H10T1/2 adipogenic differentiation

C3H10T1/2 cells were thrawed, amplified and passaged at ~70-80% confluence. They were grown in GM and refreshed every two days.

For differentiation experiments, GM was used for resuspension and the cells were split at an appropriate split ratio according to the plate size and the experimental conditions. The cells were kept in GM and refreshed every two days. At 1-2 days post-confluence, differentiation was induced, termed as ‘day 0’, and the cells were cultured according to the standard adipogenic differentiation protocols (Table 2.12 and Figure 2.1). At day 0, GM was replaced by DM (which included base DM plus 3-isobutyl-1-methylxanthine (IBMX), dexamethasone and insulin, thereafter termed “MDI"). At day 2, DM was changed to post-DM. Then from day 4 onwards, the cells were maintained in base-DM and refreshed every second day. Differentiation continued for a total of 8-10 days when they became differentiated adipocytes. For untreated controls, cells were grown in GM and refreshed every second day throughout the experimental period.

Experiments that involved pharmacological treatments for evaluating the influence on mRNA expressions or degree of differentiation were performed using the same protocols

but different media were used to culture the cells and time of harvesting was also modified in accordance with experimental conditions (details are explained in figure legends).

Table 2.12 Standard media used for adipogenesis of C3H10T1/2 cells (modified from Dr Ruth Tunn's thesis)

Medium		Composition	Use
Growth medium	Growth medium (GM)	DMEM (Sigma D6546) 10% newborn calf serum (NCS) 100U/ml penicillin 100µg/ml streptomycin 2mM L-glutamine	Growth of cells prior to differentiation experiments, and maintenance of control cells
Induction medium	Base differentiation medium (base-DM)	DMEM (Sigma D6546) 10% FBS 100U/ml penicillin 100µg/ml streptomycin 2mM L-glutamine	Adipogenic differentiation of cells, day 4 onwards
	Complete differentiation medium (DM)	Base-DM 1µM insulin 0.5mM 3-isobutyl-1-methylxanthine (IBMX) 1µM dexamethasone	Adipogenic differentiation of cells, day 0-2
	Post differentiation medium (post-DM)	Base-DM 1µM insulin	Adipogenic differentiation of cells, day 2-4

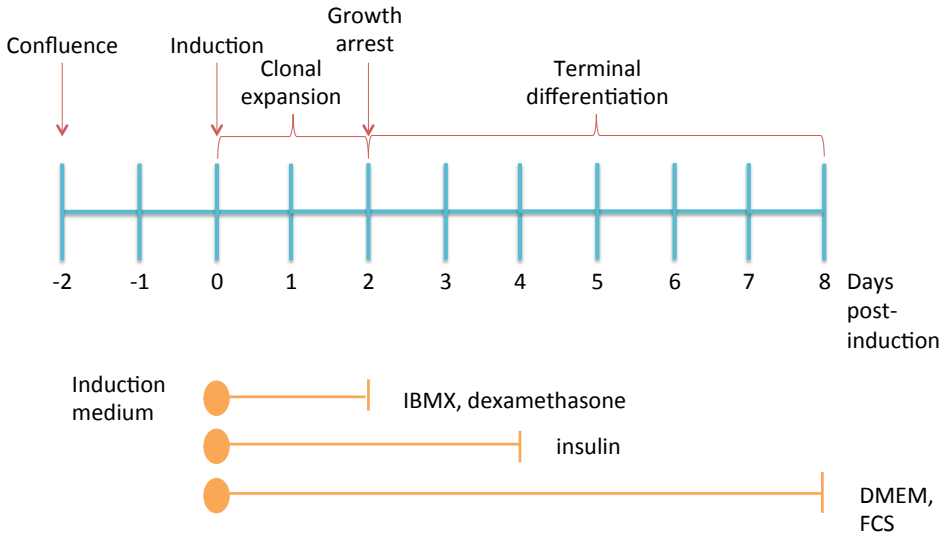

Figure 2.1 Diagram illustrating the adipogenic differentiation medium components used at each stage of adipogenesis. (modified from Dr Ruth Tunn; in preparation)

2.10.3 Oil Red O staining

Adipogenic differentiation of C3H10T1/2 cells was detected by Oil red O staining of the lipid droplets. Cells were counterstained with hematoxylin (Harris Sigma) to visualise the nuclei. 0.3% (w/v) Oil Red O in 99% isopropanol was prepared as stock solution. A working solution was prepared by 3:2 dilution of the stock solution and then filtered through a 0.44μm filer paper (Whatman Puradisc). C3H10T1/2 cells were grown on 25mm coverslips in 6 wells plates. On the day of experiment, the cells were rinsed with sterile PBS and fixed with 4% (w/v) PFA/PBS for 45 minutes. The fixed cells were then washed with sterile PBS and incubated with 60% isopropanol for 5 minutes, followed by a further 5-minute incubation with the Oil Red O working solution. 60% isopropanol was added to remove excess Oil Red O solution and cells were washed again with PBS before being counterstained with hematoxylin for 1 minute. The cells were given two final washes with ddH_2O and kept wet in ddH_2O until being imaged using a Leica DM 500B microscope.

2.10.4 AdipoRed Assay – quantification of adipogenic differentiation

C3H10T1/2 cells were grown in 96 well plates and subjected to the standard adipocyte differentiation protocols and appropriate drug treatment depending on the purpose of the experiment. On 8-10 days post-induction, media were aspirated and cells were washed once with 200 μl PBS per well. 200 μl fresh PBS + 5 μg/ml of Hoechst was added to each well (for detection of nuclei, used as an indication of cell number) and cells were incubated for 15 minutes at 37°C, followed by addition of 5 μl of AdipoRed Reagent (Lonza) per well, then cells were incubated for another 15 minutes at 37°C. Fluorescence of AdipoRed and Hoechst was measured in a plate reader at excitation/emission of 485/572 nm and 350/461 nm respectively. A blank well without cells was used as

background. Cells subjected to adipocyte differentiation protocols but no drug treatment were used as a positive control while cells grown in GM was used as a negative control. In some cases, DMSO control was included with addition of DMSO (1/1000) into the DM. Ratio of AdipoRed signal to Hoechst signal was calculated and the background signal was subtracted. Average mean from several wells was calculated and used as an indication of the degree of differentiation.

2.10.5 Reverse transcription quantitative PCR (RT-qPCR)

2.10.5.1 RNA harvest and isolation

C3H10T1/2 cells were grown in 3.5cm dishes. At particular time points, total RNA was extracted and purified using QIAGEN RNeasy mini kit according to manufacturer's protocolss. The medium was removed and cells washed twice with sterile PBS. To each dish 350µl cell lysis buffer RLT (with 1% β-mercaptoethanol to denature RNase) was added and the cells were scraped off with a Corning® cell scraper and transferred to a QIAshredder column for centrifugation (14,500 rpm, 2 minutes). The homogenised cell lysate was stored at -80°C before RNA isolation. The frozen lysate was thrawed quickly at RT and mixed with one volume of 70% ethanol, transferred to an RNeasy spin column for centrifugation (10,000 rpm, 15 seconds). The filter-bound RNA was washed before DNase I treatment (~30 Kunitz units per column) and washed again afterwards. Subsequent to elution with RNase-free H_2O, RNA was verified for concentration and integrity.

2.10.5.2 RNA concentration and integrity verification

RNA concentration and protein purity were determined using a NanoDrop spectrophotometer. All samples displayed A_{260}/A_{280} ratio between 2.1 and 2.4, suggesting protein contamination of low level [149]. RNA integrity (500 ng RNA/sample) was

verified using gel electrophoresis (1.2% gel). Two sharp and clear 28S and 18S ribosomal RNA bands were displayed with a ratio of ~ 2:1 in all samples, suggesting RNA of decent quality [149].

2.10.5.3 cDNA reverse transcription

High Capacity cDNA Reverse Transcription Kit (Applied Biosystems) was used to synthesize cDNA from RNA, in accordance with manufacturer's protocolss. Concisely, a reaction mix containing 2µg of RNA (in 10µl of nuclease-free H_2O) and 2X RT master mix (see Table 2.13 for 2X master mix components) was prepared. The reaction mix was incubated in a thermal cycler using the following cycling conditions: 25°C for 10 minutes, then 37°C for 120 minutes, then 85°C for 5 minutes.

The cDNA synthesised was stored at -80°C for later quantitative PCR. Two sets of control reactions (from randomly picked samples) were also prepared: no RNA control, to check for RNA contamination from external sources during preparations; no reverse transcriptase control, to test for genomic DNA contamination. No significant PCR amplification was seen for both reactions.

Table 2.13 2X RT Master Mix

Component	Volume per reaction (µl)
10x RT Buffer	2.0
25x dNTP Mix (100mM)	0.8
10x RT Random Primers	2.0
MultiScribe™ Reverse Transcriptase	1.0
RNase Inhibitor	1.0
Nuclease-free H_2O	3.2
Total per reaction	**10.0**

2.10.5.4 Quantitative PCR (qPCR)

qPCR was performed using Roche LightCycler 480 System. Primers were generously provided by Dr Ruth Tunn and were designed based on the Roche Universal ProbeLibrary

Assay Design Center[2]. Target genes analysed were *Tpcn2*, peroxisome proliferator-activated receptor gamma 2 (PPARγ2) and c-fos (see Table 2.14 for details of primers used). During qPCR, the fluorescence emission (generated from fluorescent SYBR® green dye by cDNA amplification) is proportional to the amount of synthesised DNA and an amplification curve is generated.

Preliminary qPCR experiments were conducted to check for appropriate cDNA concentrations for each primer pair that generated a C_T value lying in the 10-30 working range. 5ng/µl was selected as the most appropriate concentration. Master mixes for each primer pair were prepared according to Table 2.15. cDNA was diluted to 5ng/µl. 15µl of the master mix was pipetted into each well of LightCycler 480 multiwell plate 384, then 5µl of cDNA was added. Each sample was conducted in duplicate and average result was obtained. Cycling conditions are given in Table 2.16. Data acquisition was performed by LightCycler 480 SW 1.5 software. All experiments were performed in triplicate or unless otherwise stated.

Table 2.14 qPCR primer sequences

Gene	Forward primer sequence	Reverse primer sequence
Tpcn2	CCCTGGCTGTATACCGATTG	GTCCCAGAGCGACAGTGG
PPARγ2	GAAAGACAACGGACAAATCACC	GGGGGTGATATGTTTGAACTTG
β-Act	CTAAGGCCAACCGTGAAAAG	ACCAGAGGCATACAGGGACA

Table 2.15 qPCR master mix

Components	Volume per reaction (µl)
PrecisionPLUS (Primerdesign) Forward primer (6pmols of 5µM) Reverse primer (6pmols of 5µM) RNase/DNase free H_2O (Primerdesign)	10 1.2 1.2 Up to final volume
Template (25ng of 5ng/µl) (added into well)	5
Final volume	**20**

[2] http://www.roche-applied-science.com/sis/rtpcr/upl/index.jsp?id=UP030000

Table 2.16 qPCR cycling conditions

	Step	Temp (°C)	Time
	1. Enzyme activation	95	2 min
50x cycle	2. Denaturation	95	15 sec
	3. Data collection	60	1 min

2.10.5.5 qPCR data analysis

Data acquisition and graph generation were performed by LightCycler 480 SW 1.5 software. During PCR, the fluorescence emission (generated from fluorescent SYBR® green dye by cDNA amplification) is proportional to the amount of synthesised DNA and an amplification curve is generated. Amplification graphs quantifying the fluorescence of each template sample were plotted against cycle number, and C_T value for each sample was calculated. C_T value was used for data analysis. It represents the threshold cycle of which fluorescence reaches a defined threshold value and must be set in the exponential phase of the curve. Thus the more abundant the template sample, the lower the C_T value. Data was analysed using the $2^{-\Delta\Delta C_T}$ algorithm method (also known as the delta-delta-C_T or ddC_T algorithm). Results were normalised against a housekeeping gene (see section 2.8.5.6), the normalised values of target templates were then compared to that of the reference template (zero hour time point for differentiation time course experiments) and the resulting values gave an indication of the relative fold changes in gene expression. Details of calculations are given below:

$\mathbf{\Delta C_T = \Delta C_{TT} - \Delta C_{TH}}$

$\mathbf{\Delta\Delta C_T = \Delta C_T - \Delta C_{TR}}$

Relative gene expression fold change of target template = $2^{-\Delta\Delta C_T}$

where C_{TT} = value of target template, C_{TH} = value of housekeeping gene, C_{TR} = value of reference template (i.e. control sample).

2.10.5.6 qPCR housekeeping gene selection

Housekeeping genes are used for normalisation to ensure that variations among samples are not artefactual. Normalisation of differences (arising from variations in amounts or quality of starting material, variations in RNA preparation and cDNA synthesis etc) is calculated by normalising the expression level of sample to that of a stably expressed housekeeping gene. Three potential candidates were assessed for expression stability: 18S ribosomal RNA (18S), glyceraldehyde-3-phosphate dehydrogenase (GAPDH) and β-actin (β-Act). They are commonly used in adipogenesis research as reported in published literatures, also they have been checked for suitability before in Dr John Parrington's lab. Additionally they are personally recommended by Inês Sá Pereira of Dr Daniel Anthony's lab (Department of Pharmacology, University of Oxford). Quantification of RNA expression of these genes was conducted in 6 samples via the ddC_T algorithm method. β-Act was found to be the most stably expressed genes among all samples and was chosen as housekeeping gene for subsequent analyses.

2.10.6 Ned-19 treatment

A stock solution of Ned-19 (Tocris) (1000x the highest final concentration) was prepared in DMSO. Working doses of Ned-19 were freshly prepared from the stock by serial dilutions in DM. C3H10T1/2 cells were grown in 96-well plates following the standard adipogenic differentiation protocols. On day 0 and 1, cells were treated with Ned-19. From day 2 onwards, cells were cultured following the standard differentiation protocols (Ned-19 was not included in the medium). On day 8, AdipoRed assay was performed to quantify lipid droplets (section 2.10.4). Minimum of 8 wells were assayed per experimental condition.

2.10.7 Bafilomycin A1 treatment

2.10.7.1 Bafilomycin A1 preparation and incubation

A 1mM stock of bafilomycin A1 (in DMSO) was generously provided by Dr Lianne Davis. Working doses of bafilomycin were freshly prepared from the stock by serial dilutions in DM.

C3H10T1/2 cells in 96-well plates were induced to differentiate on day 0 and treated with bafilomycin A1 for certain specific periods respectively. After incubation with bafilomycin, medium was replaced with fresh DM (without bafilomycin) and the cells were cultured according to the standard differentiation protocols. A DMSO control was included with DMSO diluted 1:1000 in DM. On day 10, AdipoRed assay was performed to quantify lipid droplets. Minimum of 8 wells were assayed per experimental condition.

2.10.7.2 Live cell LysoTracker staining

C3H10T1/2 cells were grown on 25mm coverslips coated with 0.2% gelatin. Where indicated, cells were incubated with 1μM bafilomycin for 4 hours or 8 hours prior to staining with LysoTracker Green DND-25 (Invitrogen). Cells were washed twice in imaging buffer (composition in mM: 121 NaCl, 5.4 KCl, 0.8 $MgCl_2$, 2 $CaCl_2$, 6 $NaHCo_3$, 5.5 D-Glucose, 25 Hepes, pH 7.4), then loaded with 50 nM LysoTracker Green for 15 minutes in imaging buffer, followed by three washes. Cells were viewed with a 10x objective on an Olympus microscope, using the FITC scope excitation/emission parameters (nm): 490/525.

2.10.8 BAPTA-AM treatment

BAPTA-AM (Life technologies) of 100mM stock was prepared in DMSO. Working doses of BAPTA-AM were freshly prepared from the stock by serial dilutions in DM.

C3H10T1/2 cells in 96-well plates were induced to differentiate on day 0 and treated with BAPTA-AM for 45 minutes. After 45 minutes incubation, medium was replaced with fresh DM (without BAPTA-AM) and the cells were cultured according to the standard differentiation protocols. On day 10, AdipoRed assay was performed to quantify lipid droplets. Minimum of 8 wells were assayed per experimental condition.

2.10.9 PKI treatment

PKI 14-22 amide (myristoylated) (Tocris) of 800μM was prepared in ddH_2O. On the day of treatment, C3H10T1/2 cells grown in 6-well plates were incubated with PKI diluted from the stock for 2 hours. Then complete DM was added to the cells without removing GM (final concentration of PKI = 10 μM) to induce differentiation. The cells were cultured following the standard differentiation protocols with induction medium refreshed with new drug (10 μM PKI). The cells were harvested at several particular time points and total RNA was isolated and gene expressions were assessed by RT-qPCR (section 2.10.5).

2.10.10 ESI-09 treatment

ESI-09 (Biolog) of 50mM was prepared in DMSO. On the day of treatment, the stock was diluted 1:10 in DMSO to give a 5mM solution. This was further diluted down to the final concentration in GM (1% DMSO) and added to cells.

C3H10T1/2 cells grown in 6-well plates were incubated with ESI-09 for 30 min and complete DM was added without removing GM (final concentration of ESI-09 = 25μM) to induce differentiation. The cells were cultured following the standard differentiation protocols with induction medium refreshed with new drug (25μM). The cells were harvested at several particular time points and total RNA was isolated and gene expressions were assessed by RT-qPCR.

2.10.11 8-pCPT-2-O-Me-cAMP-AM treatment

8-pCPT-2-O-Me-cAMP-AM (Tocris) of 25mM was prepared in DMSO. On the day of treatment, the drug was diluted from the stock in GM and added into the cells. C3H10T1/2 cells grown in 6-well plates were treated with the drug for 2 hours. Then complete DM was added to the cells to induce differentiation without removing GM (final concentration of drug = 10 μM). The cells were cultured following the standard differentiation protocols with induction medium refreshed with new drug (10 μM). The cells were harvested at several particular time points and total RNA was isolated and gene expressions were assessed by RT-PCR.

2.10.12 Immunofluorescence

C3H10T1/2 cells were grown to confluence on 3.5 mm coverslip coated with gelatin and were subjected to the standard differentiation protocols. At each time point, the cells were fixed with 4% (w/v) PFA in 0.1 M TBS at 4°C for 10 minutes. Fixation was quenched by washing in 0.1 M glycine in PBS for 5 minutes and then in TBS, followed by permeabilisation in TBS + 0.4% (v/v) Triton X-100 for 5 minutes. Permeabilised cells were washed twice for 1 minute with TBS. Non-specific binding sites were blocked in 10% BSA in TBS for 30 minutes. Then the cells were transferred to 800 μl primary antibody (anti-CREB rabbit polyclonal (sc-186X, SantaCruz) and anti-pCREB rabbit polyclonal (Upstate)) prepared in 3% BSA and incubated for 1 hour. The cells were washed 4x with 3% (w/v) BSA in TBS for 5 minutes each and then incubated for 45 minutes with 400 μl secondary antibody (Alexa Fluor 488 anti rabbit Fab, Invitrogen) prepared in 3% TSA, followed by four washes in TBS for 5 minutes each and a quick dip in ddH_2O. The cells were mounted in ProLong Diamond Antifade mounting medium (Invitrogen) and allowed to dry in the dark O/N and then stored in the dark at 4°C. Images

were captured using a Zeiss Meta 510 LSM confocal microscope. For the control experiment, cells were grown in GM throughout the entire time course and the same protocols was followed.

2.10.13 Chromatin immunoprecipitation (ChIP)

Details of all buffers mentioned in the following paragraphs are listed in Table 2.17

2.10.13.1 Formaldehyde cross-linking and cell lysis

C3H10T1/2 cells were grown to confluent in 10cm dishes. Two sets of cells were prepared: control (quiescent) and stimulated. The latter one was stimulated with 50 μM forskolin and DM for 2 hours before fixation. Cells were formaldehyde cross-linked by adding 1% formaldehyde/PBS for 10 minutes in dark. Formaldehyde was removed and 125 mM glycine was added to quench formaldehyde for 5 minutes, followed by two washes with ice cold PBS. Cells were then scraped in ice cold PBS and three plates of cells from the same treatment were pooled together for centrifugation (1000 xg, 7 minutes, 4°C). The cell pellet was then resuspended in ice cold lysis buffer and left on ice for 10 minutes, then centrifuged as above and the pellet was resuspended in ice cold wash buffer, centrifuged again and the pellet was resuspended in sonication buffer with 1% (w/v) SDS, before proceeding to the sonication step.

2.10.13.2 Sonication

Samples resuspended in sonication buffer were rotated for one hour, followed by dilution with an equal volume of sonication buffer (no SDS). Sonication was performed on ice with a Sonics and Materials Vibracell VC 130 sonicator (Jenson PLS suppliers) and a 3mm probe. Cross-linked lysates were sonicated over a time course and amplitude range

to identify the optimal conditions so that chromatin was sheared to an average fragment size of 100-1000 bp. Subsequent experiments followed this condition for sonication. After sonication, cell debris was pelleted by centrifugation (12000 xg, 15 minutes) and supernatant chromatin was kept at -80°C until further processed.

2.10.13.3 Immunoprecipitation

An aliquot of sonicated supernatant chromatin was kept as an 'input' control while the remaining portion was diluted to 0.1% SDS with dilution buffer and transferred to passivated concentrator (see section 2.10.13.6) to concentrate the sample by centrifugation (2000 xg, 15-30 minutes) to a final volume of <0.5 ml and adjusted to 0.5 ml with flow through. Flow through was kept at -80°C. Concentrated sample (~25 µg) was pre-cleared by incubating with pre-equilibrated slurry for 1 hour at 4°C with gentle rotation, then centrifuged (2000 xg, 2 minutes, 4°C) to pellet the sepharose beads. Antibody was added to the supernatant and incubated O/N at 4°C with gentle rotation. No antibody was added for the negative control aliquot. Pre-equilibrated slurry (freshly prepared) was added to the sample the next day and incubation was continued for a further 2 hours at 4°C. Samples were centrifuged as above to collect beads and chromatin. The beads were washed for 3 minutes each time with gentle rotation at 4°C with 1ml of each of the following buffers and pelleted as above: two times with low salt buffer, two times with high salt buffer, one time with LiCl buffer and two times with TE buffer. After the TE wash and centrifugation, elution buffer (freshly prepared) was added to elute the immune-complexes from the beads and incubated for 15 minutes with gentle rotation. The samples were centrifuged as above and supernatant was collected. The elution step was repeated and the two eluates were combined together. At the same time, elution buffer was also added to the 'input control' aliquot.

2.10.13.4 Isolation of ChIP DNA

5 M NaCl was added to each tube of eluate (final [Na^+] = ~0.3 M) and incubated at 65°C O/N to reverse cross-linking, followed by incubation with 40 mM Tris-HCl/10 mM EDTA/100 µg/ml proteinase K for 1.5 hours at 45°C to digest the proteins. DNA was then purified using a ChIP DNA Clean & Concentrator (Zymo Research) according to manufacturer's protocolss and stored at -20°C. DNA levels were quantified by RT qPCR.

2.10.13.5 Analysis of fragment size

An aliquot ($1/10^{th}$) of sonicated sample (supernatant chromatin) was removed, diluted with ddH_2O and treated with 50 µg/ml RNase A for 1 hour at 37°C, followed by O/N incubation with 100 µg/ml proteinase K (to digest the proteins) at 65°C to reverse cross-linking. DNA was purified using Qiagen PCR purification kit and fragment sizes were analysed by agarose gel electrophoresis (1.5%).

2.10.13.6 Passivation of concentrators

Vivaspin 6 concentrators (10000 MWCO PES membrane, Sartorius) was washed once with ddH_2O and centrifuged (2000 xg for 3 minutes). Flow-through was discarded and residual water was removed carefully by pipetting. The membrane and plastic of the concentrators were passivated with passivation solution (0.02% BSA, 0.05 mg/ml salmon sperm DNA, dilution buffer, 0.1% SDS) for 2 hours with gentle rotation. The blocking solution was poured out and the device rinsed with ddH_2O three times. The device was filled with ddH_2O and stored at 4°C until ready to use.

2.10.13.7 Preparation of protein A beads with salmon sperm DNA

Protein A Sepharose 4 Fast Flow suspension (50% slurry; GE Healthcare) was centrifuged

(2000 xg, 1 minute, 4°C). Beads (pellet) were washed three times in dilution buffer (0.1% SDS), with 2 minutes incubation at 4°C per wash and centrifuged as above between each wash. After the final wash, salmon sperm DNA and BSA was added to the beads to a final concentration of 0.05 mg/ml and 0.2% respectively, and the suspension was incubated for 30 minutes at 4°C. Subsequently, it was washed once with dilution buffer and an equal volume of dilution buffer was added to make a 50% slurry which was then kept at 4°C until use.

2.10.13.8 Data analysis

Data was presented as percent input of each IP sample relative to input chromatin for each amplicon and ChIP sample as indicated.

Table 2.17 List of buffers used in ChIP

Buffer	Composition
Lysis buffer	10mM Tris-HCl pH 8.0, 0.25% Triton-X-100, 10mM EDTA, 1X protease inhibitor cocktail (Roche), 50mM NaF
Wash buffer	10mM Tris-HCl pH 8.0, 200mM NaCl, 1mM EDTA, 1X protease inhibitor cocktail (Roche), 50mM NaF
Sonication buffer + 1% SDS	10mM Tris-HCl, 100mM NaCl, 1mM EDTA, 1% SDS, 1X protease inhibitor cocktail (Roche)
Sonication buffer without SDS	10mM Tris-HCl, 100mM NaCl, 1mM EDTA, 1X protease inhibitor cocktail (Roche)
Dilution buffer	22.5mM Tris-HCL pH 8.0, 1.25% Triton-X-100, 2.25mM EDTA, 162.5mM NaCl, 1X protease inhibitor cocktail (Roche), 50mM NaF
Low salt buffer	20mM Tris-HCl pH 8.0, 1% Triton-X-100, 2mM EDTA, 150mM NaCl, 0.1% SDS
High salt buffer	20mM Tris-HCl pH 8.0, 1% Triton-X-100, 2mM EDTA, 500mM NaCl, 0.1% SDS
LiCl buffer	0.25M LiCl, 10mM Tris-HCl pH 8.0, 1% Triton-X-100, 1mM EDTA, 1% sodium deoxycholate
TE buffer	10mM Tris-HCl pH 8.0, 1mM EDTA
Elution buffer	1% SDS, 100mM $NaHCO_3$

2.11 *In situ* hybridization (ISH)

2.11.1 Preparation of frozen brain sections

Brains were removed and snap-frozen in isopentane (-40°C) before being processed for *in situ* hybridization. After warming to -14°C in a cryostat (Bright), brains were mounted onto a specimen holder and sectioned in the coronal plane. Cryostat-cut tissue sections of 12 µm were thaw-mounted onto gelatin-coated microscope slides and were stored at -80°C until use.

2.11.2 Pre-hybridization

On the day of pretreatment, sections were taken out of the -80°C freezer and left to thaw at RT. The slides were then fixed in 4% PFA for 10 minutes, then rinsed in PBS twice (just by dipping), followed by TEA/AA incubation for 10 minutes, then dehydrated in 70% (v/v) ethanol (for 1 minute,) 80% ethanol (for 1 minute), 95% ethanol (for 2 minutes), 100% ethanol (for 1 minute), delipidated in chloroform (for 10 minutes), 100% ethanol (for 1 minute) and finally 95% ethanol (for 1 minute). Pre-treated sections were allowed to drain and to air dry O/N stored at -20°C until ready for ISH use.

2.11.3 Hybridization

Sense and antisense (i.e. oligo complementary to mRNA coding for *Tpcn1*) probes for the *Tpcn1* gene were ordered (Table 2.18).

A 40-base antisense oligonucleotide probe to the *Tpcn1* mRNA was designed using the BLAST database to ensure the sequence of the probe was specific to *Tpcn1*. The secondary structure of the oligonucleotide probe was checked using the DNA calculator tool from Sigma Genosys to ensure that the sequence contained no potential hairpin and

dimer. The sequence was ordered from Sigma Genosys. A sense sequence presenting the same biophysical characteristics was ordered to be used as a negative control.

Table 2.18 Sequence of sense and antisense probe

Sense probe:	ACAAGTTCAAGTCTTTGCTGCTGCACAAACGGACCGCCAT
Antisense probe:	ATGGCGGTCCGTTTGTGCAGCAGCAAAGACTTGAACTTGT

The oligonucleotide was then resuspended in DEPC-water at a concentration of 2 pm/µl. For the *in situ* hybridisation procedure, the oligonucleotide was labelled using the 3' tail labelling reaction using terminal transferase and 35-S deoxynucleotide triphosphate . Briefly the oligonucleotide was prepared as followed: mixture was made up for ^{35}S labelling later and was prepared in the following order (Table 2.19):

Table 2.19 Oligonucleotide preparation

Components	**Volume per reaction (µl)**
DEPC ddH2O	17
TdT 5X forward buffer	7
Oligo 2pm/ul	3
Terminal transferase	2

The oligo mixture was incubated at 37°C water bath for 30 minutes. The labelled probe was separated from the unlabelled probe and the free label using a Sephadex column. 3 µl of the eluate containing the labelled oligo was then counted in a scintillation counter. Hybridization (HYB) buffer was made by mixing formamide (50%), 4X SSC, Herring sperm DNA (1 mg/ml), Heparin (100 µg/ml), PolyA (1 mg/ml), Denhardt's (5X), and Dextran Sulfate (10% w/v). The hybridisation mixture was prepared by adding the labelled oligonucleotide to the HYB buffer containing DTT (50 mM) in an appropriate ratio calculated based on the radioactivity counts. The mixture was mixed well and 200 µl of hybridisation solution containing 10^6 cpm was applied onto each slide and coverslipped. The slides were hybridized O/N (16-18 hours) at 35°C in a humidified hybridization chamber containing 4 layers of Whatman filter paper soaked in formamide

(50%) and 4X SSC. After O/N hybridization, coverslips were washed in 1X SSC. Slides were washed in 1X SSC at 55°C for 20 minutes three times, followed by two 60 minutes washes with 1X SSC at RT. Slides were finally dipped in ddH_2O to rinse off the 1X SSC. The slides were then left to air dry O/N in the fume hood. They were organised in empty photographic cassettes according to treatment and brain region, and a 'known' ^{14}C microscale was included. The slides were exposed to Biomax film (Amersham, UK) for 10 days and the film was developed. Negative Controls included hybridisation of sections using the sense probe.

2.11.4 Image and data analysis

Images of different sections were captured using a monochromatic camera (Olympus). The relative abundance of *Tpcn1* in selected areas was determined by densitometric quantification of autoradiograms (MCID, Canada). Optical density values were calibrated to ^{35}S tissue equivalents using ^{14}C microscales (Amersham, UK). Densitometric values measured from the three sections of each animal were averaged and calculated as nCi/g tissue. Areas of interest were outlined according to the Franklin and Paxinos Mouse Brain Atlas.

2.11.5 Counter staining

Slides were incubated in Toludine Blue (Fisher) for 10 minutes to stain cell bodies and help the identification of brain structures. They were then dipped in multiple changes of ddH_2O until the remaining ddH_2O was nearly clear, followed by dehydration in increasing concentrations of ethanol and clearing in Xylene for 20 minutes. Slides were mounted using DPX mouting agent and coverslipped. After drying O/N, pictures of the sections were taken on a colour camera (Olympus). Images were taken for the counter stained

slides the next day.

2.12 Statistical analysis

All data are presented as +/- standard error of the mean (SEM). Majority of data comparisons were analysed by an unpaired two-tailed student's *t-test* (*p<0.05; **p<0.01; ***p<0.001); while one-way analysis of variance (ANOVA) with a *post-hoc* Turkey test (#p<0.05; ##p<0.01; ###p<0.001) was employed to compare 3 or more data sets. When examining gene expression during adipogenesis time course, one-way ANOVA with a *post-hoc* Dunnett test was performed to compare expression at all time points to expression at time zero (§p<0.05; §§p<0.01; §§§p<0.001). Statistical analyses were performed using Prism software.

Chapter 3:

Investigations of roles of TPC2 and TPC3 during zebrafish embryogenesis – a focus on myogenesis

3.1 Introduction

3.1.1 Skeletal muscle development

Skeletal muscle comprises the largest organ of the body. It serves an array of functions in the organism and is primarily characterized by its motor control via muscle fiber contractions. The process of muscle generation, also known as myogenesis, is divided into different stages. Muscles arise originally from somites during embryonic myogenesis, with a number of inductive (including myogenic regulatory factors such as *MyoD* and *Myf5*) and repressive signals (such as bone morphogenetic protein) from tissues surrounding the somites (including neural tube, notochord etc.) trigger the formation of muscle precursor cells [150, 151]. These precursor cells then undergo commitment to the myogenic fate and migrate to target muscle groups. Postnatal muscle development depends upon myoblast fusion and increases of muscle fiber size [152] (Figure 3.1). Adult skeletal muscle is capable of regeneration after injury. This type of myogenesis requires activation of satellite cells which can differentiate into new fibers [153]. Importantly, expression of same transcription factors and signalling molecules has been revealed in both embryonic myogenesis and regeneration in adult musculature [154].

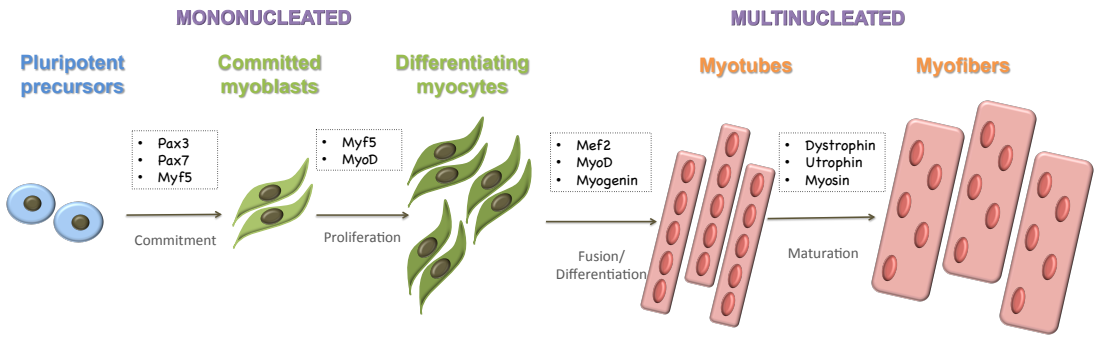

Figure 3.1: Schematic diagram illustrating the process of myogenesis and the key regulatory factors in each stage of myogenesis.

3.1.2 Ca^{2+} signalling during skeletal muscle development

It is well-established that Ca^{2+} signalling is crucial for regulating mature muscle contraction [155], mounting evidence has also indicated the involvement of Ca^{2+}-dependent pathways in different myogenic processes, as exemplified by a number of *in vitro* studies using isolated muscle cells or explants in culture [156-163] and also a few *in vivo* findings [128] [164, 165] which are discussed as follows.

In isolated chick skeletal myoblasts, it has been shown that a net movement of Ca^{2+} is crucial for myoblast fusion [166, 167]. Later in cultured *Xenopus* embryonic myoctyes, spontaneous Ca^{2+} transients which arisen from intracellular stores have been reported during early myocyte differentiation, which were suppressed by inhibiting the caffeine-sensitive Ca^{2+} stores. A disruption in cytoskeletal organization was also observed with BAPTA treatment, further indicated the involvement of Ca^{2+} signals during myofibrillogenesis [156]. Subsequent studies identified RyRs and Ca^{2+}/calmodulin-dependent myosin light chain kinase (MLCK), both of which play obligatory Ca^{2+} signalling roles in muscle contraction, to be associated with the Ca^{2+} transient mediated-myofibrillogenesis described above [157]. In addition, reports have suggested that RyR-mediated Ca^{2+} transients were essential for the incorporation of actin and titin, two of the most abundant sarcomeric proteins, into the sarcomere [161, 162]. Notably, both intact *Xenopus* paraxial mesoderm and cultured *Xenopus* myocytes were shown to display Ca^{2+} transients with comparable characteristics, and an association of these Ca^{2+} signals with somite development and myocyte maturation was suggested [164]. While the Ca^{2+} transients described above were characterised by their long duration (namely LDTs), another type of Ca^{2+} transients, which were also RyR-sensitive but with a short duration (namely SDTs), were demonstrated in embryonic myocytes prepared from neural plate of *Xenopus* embryos [156, 157, 164]. Remarkably in C2C12 cells, three spatiotemporally

distinct Ca^{2+} signals were identified, namely Ca^{2+} oscillations, localized Ca^{2+} spikes and global Ca^{2+} spikes [158]. Findings indicated that the spontaneous and repetitive Ca^{2+} transients occurred during early myogenesis were correlated with cytosolic oscillatory mechanisms while the global intracellular Ca^{2+} spikes noted in late myogenesis were generated by a membrane oscillatory mechanism as a result of the coupling between Ca_v and RyRs. Moreover, the temporal pattern of global intracellular Ca^{2+} spikes in mature myotubes was found to be based on spontaneous membrane depolarizations. Later, suggestions on functional differences of the spatiotemporally distinct Ca^{2+} transients have been proposed, that they might be required for controlling distinct cytosolic signalling pathways and nuclear gene transcription events, as well as triggering localized formation events at the sarcolemma [168]. In addition to the spatiotemporal patterns, evidence has also highlighted the significance of Ca^{2+} oscillation frequency, as exemplified by the induction of *de novo* functional sarcomere assembly and its subsequent development, likely via activation of calpain-mediated proteolysis by the Ca^{2+} oscillatory signals [163]. Apart from RyRs, functional roles of IP_3Rs have also been reported in several *in vitro* findings [159, 169], indicating a recruitment of distinct Ca^{2+} signalling systems in myogenesis. For example, in cultured rodent myotubes, RyR and IP_3R were shown to be associated with fast and slow Ca^{2+} wave production respectively and IP_3Rs were revealed to reside on the nuclear envelop and the SR [159]. The RyR-mediated Ca^{2+} release was suggested to be correlated with excitation-contraction (EC) coupling whereas the IP_3R-meidated Ca^{2+} signals were implicated in controlling gene transcription in the nucleus [159], as evidenced by phosphorylation of kinases ERK1/2 and the transcription factor called cAMP-responsive element-binding protein (CREB) [160]. Besides, it was shown that in cultured rat skeletal myotubes, nuclear IP_3R-regulated Ca^{2+} signals were produced during excitation-transcription (ET) coupling through activation of transcriptional

activators including CREB [170].

Further to these, experiments using intact zebrafish embryos as *in vivo* models provided striking evidence for the functional importance of Ca^{2+} signalling in myogenesis. Elegant work performed by Brennan et al. discovered acetylcholine (ACh)-induced RyR-mediated intracellular Ca^{2+} release between ~17 to ~22 hpf from the stimulated primary motor neuron. Such Ca^{2+} signals were found to elicit spontaneous contractions of slow muscle cells (SMCs) responsible for embryonic movements, thus suggesting involvement in formation of physiologically functional muscle unit. Besides, both pharmacological and genetic studies revealed an impairment in myofibril and sarcomere organisation, indicating a role in regulation of myofibrillogenesis by Ca^{2+} signals [165]. Later, Cheung et al. performed another remarkable research employing both intact zebrafish embryos and transgenic zebrafish with α-actin promoter targeting apoaequorin expression specifically to muscle cells [128]. In this study, two Ca^{2+} signalling periods between ~17.5 to ~24 hpf with distinct spatiotemporal properties were identified during differentiation of SMCs: signalling period 1 (SP1) comprised Ca^{2+} signals between ~17.5 to ~ 19.5 hpf and signalling period 2 (SP2) which started after ~23 hpf (Figure 3.2). Initial phase of SP1 was characterised by low frequency Ca^{2+} signals while higher frequency Ca^{2+} signals were detected in the late phase. SP2 showed a similar frequency to that of the late phase of SP1. In between SP1 and SP2 was a quiet period (QP) where negligible Ca^{2+} signals were observed. Nuclear Ca^{2+} signals predominated in the early SP1 which were regulated by IP_3Rs and correlated with ET coupling; whereas cytoplasmic, RyR-mediated Ca^{2+} signals predominated the late SP1 and the entire SP2, and were associated with the early and late developmental stages that regulate SMC differentiation and subsequent myotome patterning, in addition to EC coupling. Therefore the zebrafish results further confirmed the earlier research utilizing *Xenopus* embryos, in which RyRs were the major Ca^{2+}

releasing system and were associated with skeletal muscle differentiation [156, 157, 164, 168]. Importantly, it was also suggested that the SP1 Ca^{2+} signals were produced solely by SMCs, as evidenced by both pharmacological and genetic studies.

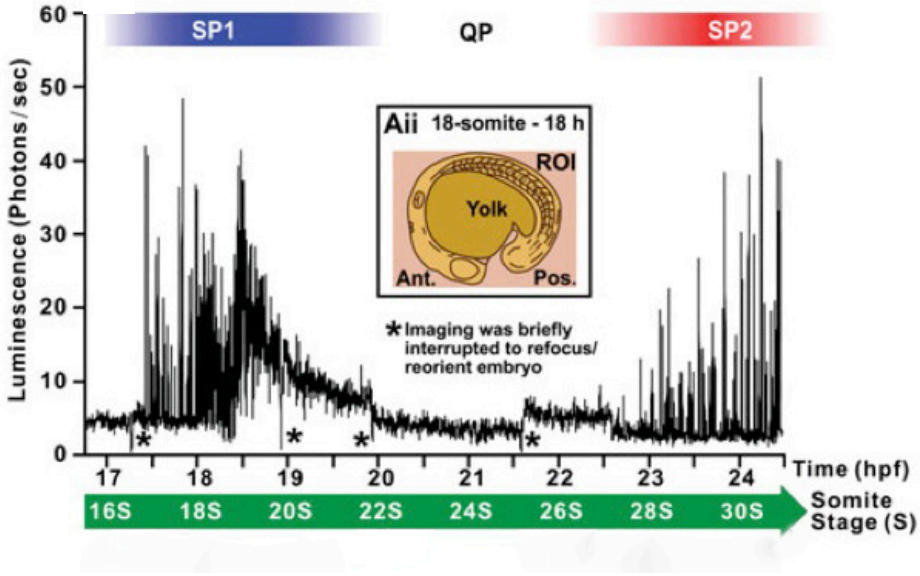

Figure 3.2: Ca^{2+} signaling profile of SMC characterized by Cheung et al. Two Ca^{2+} signaling periods, namely SP1 and SP2, with different frequencies and durations are noted during SMC differentiation. SP1 and SP2 are separated by QP, a period with negligible Ca^{2+} signals. (Adapted from Cheung et al., 2011 [128])

Taken together these studies, an important message is that Ca^{2+} release, mediated through IP_3Rs and RyRs, is critical in regulating a multitude of processes during myogenesis. Different Ca^{2+} signaling patterns generated by distinct duration, frequency and amplitude of Ca^{2+} release and interplay between these Ca^{2+} signals allow for functional diversity in such regulation in muscle cells.

3.1.3 Involvement of NAADP and TPC during skeletal muscle differentiation

With its rising prominence in different aspects of cellular and physiological functions, the NAADP/TPC pathway has recently been demonstrated to play a role in myogenesis as well. Thus using skeletal muscle precursor cells and C2C12 cells, NAADP, through inducing Ca^{2+} release from TPCs on acidic organelles, was shown to promote skeletal muscle differentiation, resulting in formation of new skeletal muscle cells from precursors [133]. Another study also suggested that NAADP could be involved in mature skeletal muscle contraction, likely via mobilizing Ca^{2+} release from RyR type 1 on the SR [171]. Results from these studies added new clues to the regulation of myogenesis and muscle contraction, highlighting the complex Ca^{2+} signalling network in muscle cells.

3.1.4 Lysosomes play a role in skeletal muscle development

Skeletal muscle contains a substantial reserve of primary amino acids and thus represents a crucial component in controlling electrolyte balance, nutrient availability and pH homeostasis [172]. Major mechanisms that regulate protein turnover in skeletal muscle are ubiquitin/proteasome-dependent and autophagy/lysosome-dependent proteolytic pathways [173]. Impairments in these cell proteolytic systems result in muscle atrophy and sarcopenia during aging. Autophagy refers to catabolic pathways involving sequestration of targeted cytoplasmic components and whole organelles in double-membrane vesicles called autophagosomes, which then translocate to lysosomes for fusion and degradation or recycling [174]. The cytoprotective properties of autophagy protect the cells against a variety of stresses, be it metabolic, inflammatory, neurodegenerative or therapeutic [175, 176]. Importantly, basal autophagic activity is indispensable for tissue homeostasis due to its partial regulation in protein turnover and selective degradation of intracellular damaged

proteins and organelles. The significance of autophagy in skeletal muscle physiology is exemplified by lysosomal myopathies lately reported [177]. Two disorders in the skeletal muscle called Pompe disease and Danon disease, in which autophagic vacuoles are detected, have been linked to impairment of lysosomal proteins.

3.1.5 Lysosomal Ca^{2+} signaling in regulation of autophagy

Recent study has identified that autophagy can be regulated by lysosomal Ca^{2+} signaling via stimulating the activity of Ca^{2+}-dependent phosphatase calcineurin and the transcription factor EB (TFEB) [178]. This newly discovered pathway is independent of mTOR, a kinase well known to negatively regulate autophagy [179]. Previously TPCs have been demonstrated to play a role in controlling cellular metabolic state, in a way that they were physically associated and functionally coupled to mTOR [105]. It is noteworthy that in this study TPC1 and TPC2 were suggested to be ATP-sensitive Na^{+} channels rather than Ca^{2+} channels proposed by other groups. Later another group suggested the participation of TPC2 in maintaining muscle homeostasis (protein turnover) through controlling autophagy signalling in skeletal muscle, likely by mediating mTOR reactivation via the PI3K/AKT/mTOR pathway and autophagy termination [143]. Several lines of evidence further points to the involvement of NAADP/TPC pathway in autophagy. Thus autophagosome accumulation is increased when TPC2 or NAADP-AM are overexpressed, as evidenced by increased expression of lipidated microtubule-associated protein 1A/1B light chain 3A (LC3-II) [100, 101]; whereas attenuated LC3-II expression is apparent with TPC1 or TPC2 KD or Ned-19 treatment [100, 101, 142].

3.1.6 Aims of this chapter

Mounting evidence has indicated that skeletal muscle development, both during embryonic myogenesis and adult myogenesis, is linked to Ca^{2+} signalling. In particular, the lysosomal Ca^{2+} signalling has recently been demonstrated an association with autophagy regulation, a mechanism identified to be significant for skeletal muscle physiology. Given TPCs are potential Ca^{2+} channels located on acidic endolysosomes, researchers also revealed that the NAADP/TPC pathway was involved in adult myogenesis as well as regulation of autophagy and maintenence of skeletal muscle homeostasis. With the rising prominence of lysosomes and NAADP/TPC in the field of skeletal muscle development, my study therefore aimed at looking into the role(s) of NAADP/TPC pathway in embryonic myogenesis.

In my research, I used zebrafish as an animal model because zebrafish embryos are particularly well suited to the study of muscle development. Firstly, fertilization and subsequent developmental stages are *ex vivo*. Besides, its embryos are relatively large and optically transparent during the first 24 hours post fertilisation. Thus one can easily manipulate the embryos during experiments, which also favours the use of optical microscopy to monitor their growth. In addition, somatic muscles form a big ratio of the body, and huge success has been obtained using zebrafish for the investigations of early stages of muscle development in both embryological and genetic fields. Throughout my entire study, I employed an α-actin-aequorin transgenic zebrafish line, in which apoaequorin was expressed specifically in the trunk skeletal musculature [128].

I also confirmed the zebrafish TPC genes by screening the zebrafish genome and cDNA sequence databases. Three TPC isoforms (DrTPC1-3) were identified which made it possible to now investigate the role(s), if any, of NAADP and TPCs in Ca^{2+} signalling events during embryonic myogenesis. To do this, a combination of techniques were

utilized. First of all, the three zebrafish cDNA were cloned. These were then used as a template for designing anti-TPC morpholinos which were injected into fertilized zebrafish eggs to determine their effects on myogenesis. The influence on Ca^{2+} signalling events during myogenesis by knockdown of TPCs was investigated, by using the Ca^{2+} sensitive bioluminescent probe aequorin in conjunction with sophisticated Ca^{2+} imaging methods. Morphological changes were also compared by different types of imaging and immunostaining of specific muscle marker proteins. Finally, the expression pattern of TPCs in zebrafish embryos was studied by *in situ* hybridization.

3.2 Results

3.2.1 Cloning of zebrafish TPC cDNAs and vectors construction

All primers used in construct generation are listed in Materials and Methods.

3.2.1.1 Cloning of zebrafish TPC cDNAs and vectors construction

The pCRII-TOPO.DrTPC1 plasmid, pCRII-TOPO.DrTPC2 plasmid and pGEM-T Easy.DrTPC3 plasmid encoding *DrTPC1*, *DrTPC2* and *DrTPC3* respectively were constructed.

Firstly, total RNA from zebrafish embryos was extracted and purified and the RNA integrity was checked and confirmed to be intact and of good quality, as indicated by the appearance of two clear bands in the gel in a 2:1 ratio around 3 kb and 1.5 kb, which corresponds to 28S rRNA and 18S rRNA respectively (Figure 3.4A). RT-qPCR was then performed to amplify the cDNAs encoding DrTPC1 and DrTPC3 from a cDNA library derived from zebrafish embryos. The cDNA products were checked on a gel. The fragments around 2500 bp which correspond to DrTPC1 (size: 2418 bp) (Figure 3.4B) and DrTPC3 (size: 2322 bp) (Figure 3.4C) were extracted and the gel purified products served as templates for subsequent PCR. For DrTPC2, an IMAGE cDNA clone encoding DrTPC2 was obtained (Geneservice) (Image clone 3816064).

PCR was performed to amplify the cDNA sequences encoding the three DrTPCs using the gel purified products (DrTPC1 and DrTPC3) and IMAGE clone (DrTPC2) as templates. The appearance of a prominent band on the gel observed between 2 and 2.5 kb (Figure 3.4D, E and F) confirmed successful amplification of DrTPC sequences. The PCR products obtained were then purified. Purified DrTPC1 and DrTPC2 were subcloned by ligation into pCRII-TOPO vector (Lifetechnologies) while DrTPC3 was ligated with the pGEM-T Easy vector (Promega). E. coli XL10 Z-competent cells were transformed with the ligation products. Miniprep was performed on picked colonies to extract the

recombinant plasmids. Restriction digest of the eluted recombinant plasmids was performed using EcoRI enzyme. EcoRI cuts the constructs at 2 different sites, resulting in two fragments of different sizes. Almost all samples showed two clear bands in the gel, with the larger sized fragments corresponding to the vector (~4 kb for pCRII-TOPO-vector and 3 kb for pGEM-T Easy vector) and the smaller sized fragments at around 2.5 kb corresponding to DrTPCs, suggesting successful insertion of DrTPCs into the plasmids (Figure 3.4G, H and I). The minipreped samples with correctly formed constructs were sent for sequencing.

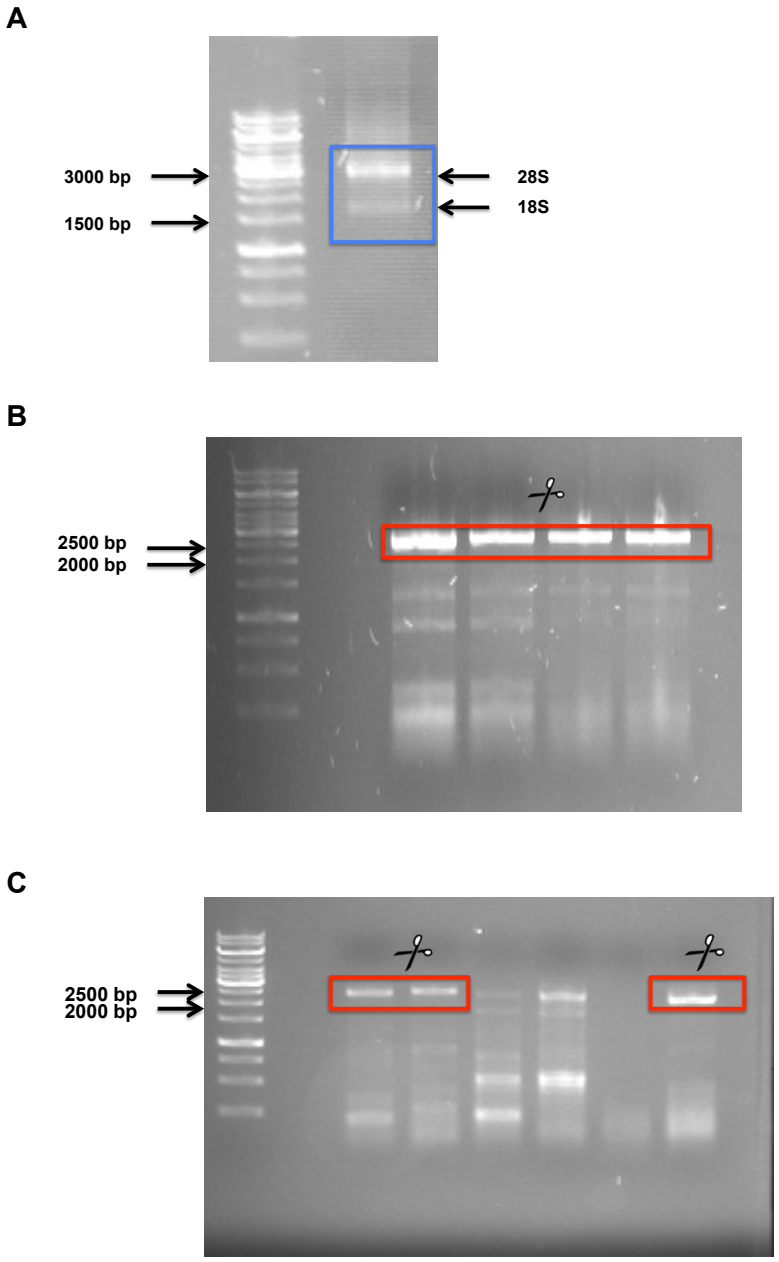

Figure 3.4: (A) Quality of RNA was analysed on gel electrophoresis. Two distinct bands in a 2:1 ratios which correspond to 28S and 18S respectively indicating RNA was intact and of good quality. **(B)** A gel was run to check the cDNA product from RT-PCR, a prominent band of size between 2 and 2.5 kb indicated DrTPC1 cDNA was successfully generated. **(C)** A gel was run to check the cDNA product from RT-PCR, a prominent band of size between 2 and 2.5 kb indicated DrTPC3 cDNA was successfully generated.

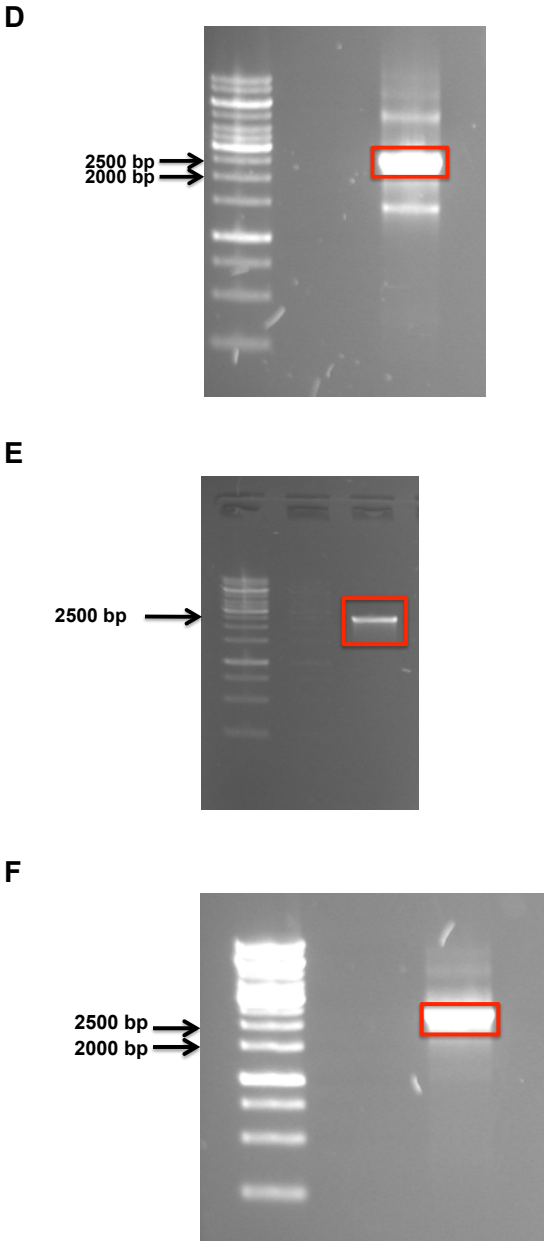

Figure 3.4: Gels were run to check the PCR products. Prominent and single band with size between 2 and 2.5 kb was observed in each gel which suggested that cDNA sequences were successfully amplified from the templates. **(D)** PCR product of DrTPC1 sequence amplified from the purified cDNA generated by RT-PCR; **(E)** PCR products of DrTPC2 sequence amplified from the Image clone; **(F)** PCR product of DrTPC3 cDNA amplified from the purified cDNA generated by RT-PCR.

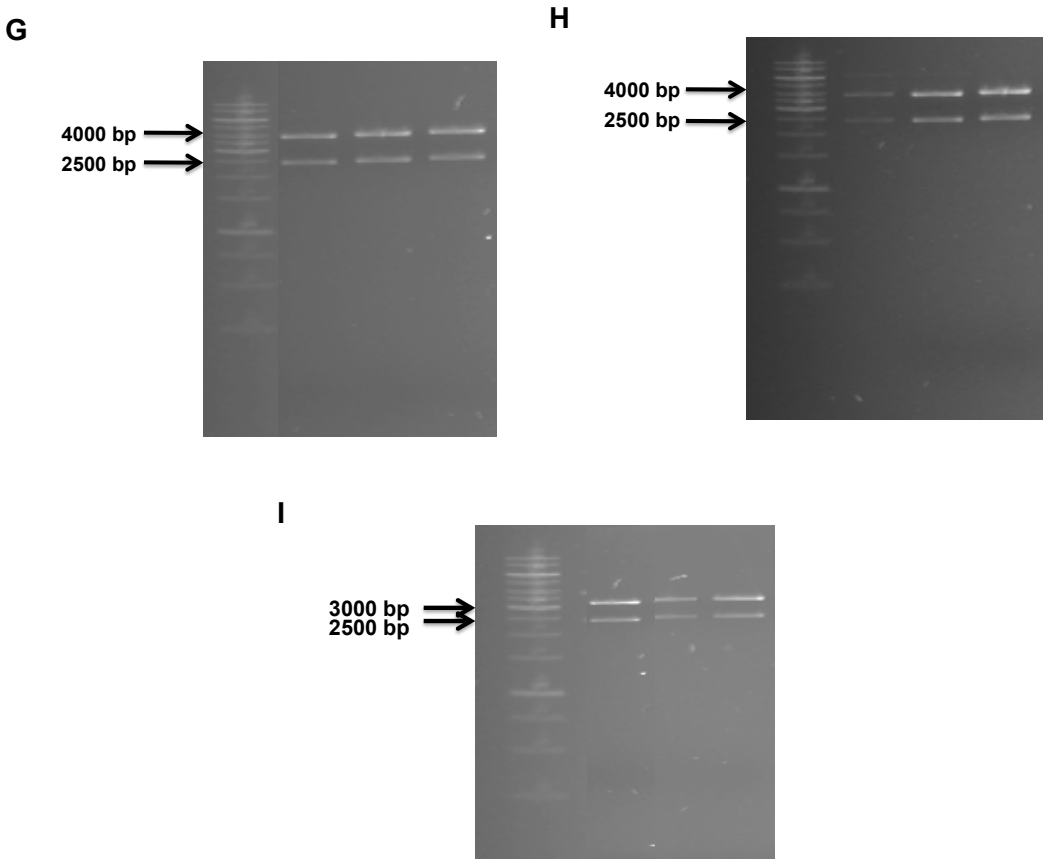

Figure 3.4: Gels were run to assess the digested products generated from restriction digestion using EcoRI restriction enzyme. Two clear bands with correct sizes were observed in each gel, indicating the plasmids were successful digested. **(G, H)** The band with size of ~4 kb corresponds to the pCRII-TOPO vector, while the lower bands located between 2 and 2.5 kb correspond to DrTPC1 and DrTPC2; **(I)** The band with size of ~3 kb corresponds to the pGEM-T Easy vector, while the lower band which is located between 2 and 2.5 kb correspond to DrTPC3.

3.2.1.2 Site-directed mutagenesis

Sequencing revealed point mutation for all three DrTPCs. For DrTPC1 and DrTPC2, a point mutation occurred at 1805th and 782th base respectively, G was substituted for A in both cases, and the mutated codon resulted in a change of the 602th and 261th amino acid respectively from Asn to Ser. Whereas in DrTPC3, two point mutations were observed, one at the 1853th base where C was replaced for T and the other at the 2084th base where G was substituted for A, leading to mutation of the 618th and 695th codon, encoding amino acids for Pro instead of Leu and Arg instead of Gln respectively. Therefore, to correct the point mutation(s) in these DrTPCs, Stratagene QuickchangeTM site-directed mutagenesis was performed followed by DpnI digestion of the template plasmids (i.e. the plasmids with point mutation), resulting in PCR product (i.e. the plasmid with mutation corrected) only. Transformation and subsequent miniprep were conducted to produce the corrected recombinant plasmids. Successful correction was achieved for all three DrTPCs as determined by the sequencing check.

3.2.1.3 Construction of recombinant plasmids with mCherry tag

Three pcDNA5/TO.DrTPC.mCherry plasmids encoding *DrTPC1*, *DrTPC2* and *DrTPC3* respectively were constructed by inserting cDNA fragment that encodes corresponding *DrTPC* into the pcDNA5/TO.mCherry plasmid. Firstly, PCR was performed to amplify the region encoding *DrTPC* with HindIII and NotI flanking the 5' and 3' region respectively, using pCRII-TOPO vector (DrTPC1 and DrTPC2) and pGEM-T Easy vector (DrTPC3) as templates. The PCR products were checked on a gel and then purified for subsequent restriction enzyme digestion with KpnI and NotI restriction enzymes. A pcDNA5/TO.MmTPC1.mCherry plasmid was kindly provided by Guida Ruas. Restriction enzyme digestion was performed on this plasmid using the same restriction enzymes and

the double digested products were run on agarose gel, then the larger sized band (~6.4 kb) which corresponded to the pcDNA5TO.mCherry vector was excised and purified. Ligation was performed to ligate the purified DrTPCs with the gel purified pcDNA5TO.mCherry vector using PfuUltra. E. coli XL10 Z-competent cells were transformed with the ligation products. Miniprep was performed on picked colonies to extract the recombinant plasmids. Double restriction digest of the eluted recombinant plasmids were performed using HindIII and NotI enzymes. As shown in figure 3.4J, K and L, fragments of around 6 kb and 2.5 kb were observed, confirming that all three pcDNA5TO.DrTPC.mCherry constructs were correctly formed. Constructs were also verified by sequencing.

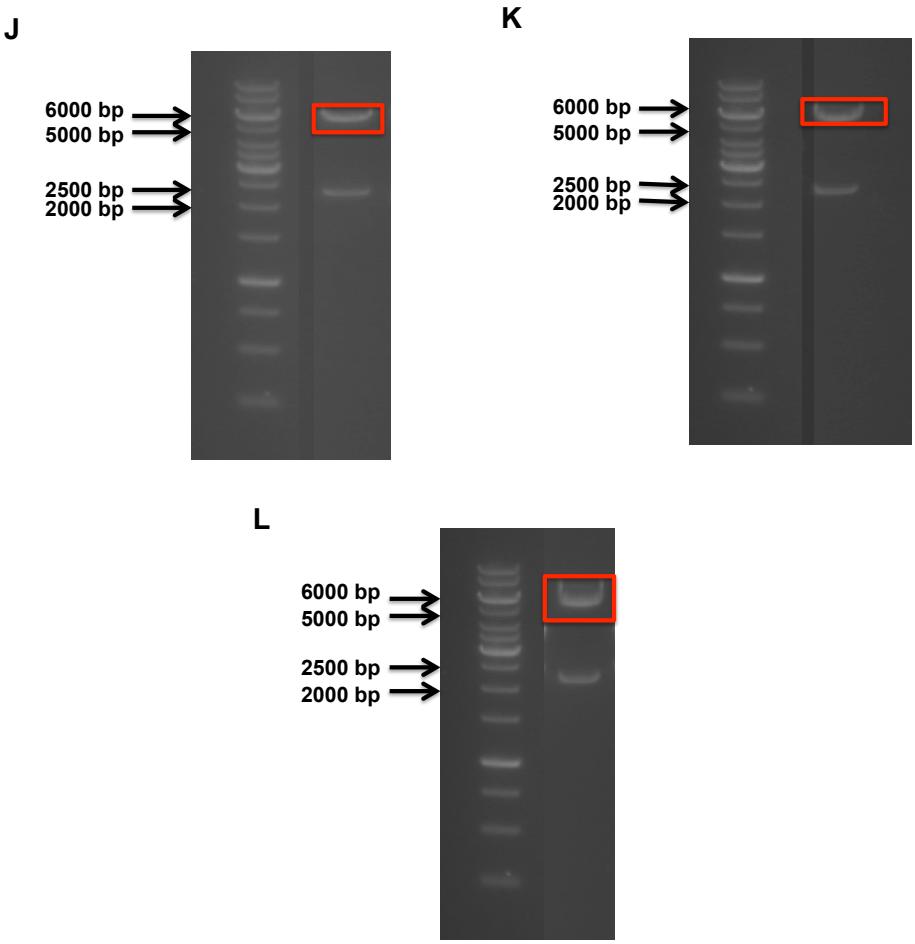

Figure 3.4J, K and L: Gels were run to assess the restriction digestion using HindIII and NotI restriction enzymes. Two separate bands with correct sizes were observed in each gel, indicating successful restriction digestion of the plasmids. The larger sized band which is located around 6 kb corresponds to the pcDNA5TO.mCherry vector while the lower band with size between 2 and 2.5 kb corresponds to DrTPC.

3.2.2 Designing morpholinos for injection into zebrafish

Morpholinos (MOs) were obtained from Gene Tools, LLC (Philomath, Oregon, USA). The type of MO we used works through an RNase-H independent process that blocks translational initiation. Consequently, all MOs were arbitrarily designed to bind to the 5' UTR and coding sequence flanking and including the initiating methionine. We selected sequences based on design parameters according to the manufacturer's recommendations, namely 21-25 mer antisense oligonucleotides of ~50% G/C and A/T content with no predicted internal hairpins. Four consecutive G nucleotides were also avoided. Sequences were as follows (sequence complimentary to the predicted start codon is underlined):

DrTPCN1 MO: TCCGCCATCCCGCAGAACCAAGACT

DrTPCN2 MO: CAGCCAGCAGCGGTTCTTCTTCCAT

DrTPCN3 MO: TTTTCTCAGTCTTCCCCTCAGACAT

3.2.3 Characterization of muscle-generated Ca^{2+} signals in MO-based knockdown of TPCs using aequorin-based luminescence detection

Characterization of the muscle-generated Ca^{2+} signals in zebrafish has recently been reported by Cheung et al. [128]. Two distinct phases of Ca^{2+} signals (SP1 from ~17.5 to 19.5 hpf and SP2 from 23 hpf onwards) are detected in transgenic fish expressing apoaequorin solely in the trunk musculature which are separated by a period with limited Ca^{2+} signals (QP from ~19.5 to 23 hpf) (detailed description refers to section 3.1.2 and Figure 3.2). Further to their characteristic frequencies and durations, it is found that IP_3R-mediated Ca^{2+} signals are predominant during early SP1 whereas RyRs are responsible for the Ca^{2+} signals in late SP1 and generally the entire SP2 period.

Here, the same α-actin-aeq transgenic line was used to investigate the effects of TPC2 KD and TPC3 KD on muscle-generated Ca^{2+} signals in zebrafish. A reverse genetic approach by means of MO KD was employed. Using this transgenic line allows investigations of Ca^{2+} signaling events specifically in the muscle cells. Transgenic fish embryos were injected with ~2.5 ng standard control MO, anti-*Tpcn2* MO or anti-*Tpcn3* MO (hereafter control-MO, TPC2-MO and TPC3-MO respectively) at the 1- to 4-cell stage and muscle-generated Ca^{2+} signals between 17-24 hpf were acquired using an aequorin-based luminescence detection technique. The pattern of the Ca^{2+} signals produced by the control-MO resembled that of the untreated control generated in previous studies [128]; the onset and duration of SP1, QP and SP2 (Figure 3.5A) were comparable to those previously described, i.e. SP1 Ca^{2+} activities began and ended around 17.5 and 19.5 hpf respectively, which was followed by QP and then SP2 Ca^{2+} activities began around 23.5 hpf.

The average spike frequency of Ca^{2+} signals was also calculated on a 30 minutes interval basis and a peak is defined as any value higher than the values immediately before and after it, and also higher than the background value determined from the pre-SP1 level

subjected to evaluation in each experiment. As shown in Figure 3.5D, the average frequencies of the SP1 and SP2 phases in control-MO injected embryos are not the same as those previously characterized in the uninjected embryos but the general Ca^{2+} signaling pattern is comparable to that of the uninjected control [128]. The presence of a small discrepancy in the frequency between those recorded here and those by Cheung et al. [128], i.e. from ~17.5 to ~24.5 hpf, might be explained by the different generations of the α-actin-aeq transgenic embryos being used and expected experimental variation [180, 181].

Intriguingly, TPC2-MO treated embryos displayed a distinct temporal Ca^{2+} pattern (Figure 3.5B). It appears that no significant Ca^{2+} signals were detected until 20.5 hpf, and the Ca^{2+} signal activity occurring during ~20.5-23 hpf exhibited a distinct spike frequency pattern to the SP1 and SP2 of both uninjected control and control-MO injected embryos (Figure 3.5D). Since recording was only obtained until 24.5 hpf, any differences in QP and SP2 Ca^{2+} signals of TPC2-MO treated embryos remain to be identified.

A delay in SP1 period was also observed with TPC3-MO treated embryos, with onset beginning at ~19 hpf, i.e. a roughly 1.5 hours-delay. Unlike TPC2-MO treated embryos, however, the delay seen with TPC3-MO treated embryos was shorter and the duration of the Ca^{2+} activity was comparable to the control-MO treated and untreated embryos (Figure 3.5C). Also, a dramatic attenuation in the spike frequencies was noted with these delayed Ca^{2+} activities in TPC3-MO treated embryos (Figure 3.5D).

The addition of triton X-100 at the end of each experiment suggests that the decline of luminescence seen during the last couple of hours in TPC2-MO and TPC3-MO treated embryos was a result of TPC2 KD and TPC3 KD but not a lack of active aequorin in the embryo (results were not shown here).

MO injection may generate ‘off-target’ effects and the most common and well-described

phenotype is p53 dependent neural toxicity [148] [182, 183]. Coinjection of p53-MO was not performed here, instead embryos without necrosis (i.e. embryos with transparent heads) were chosen for Ca^{2+} signaling recording and other MO KD experiments described later. My collaborator Mr Kelu J.J. in Prof. Andrew Miller's lab at the HKUST performed a control experiment using p53-MO injection into the same transgenic zebrafish line and a comparable Ca^{2+} signaling pattern as those described in my control-MO experiment and the untreated control previously characterized by Cheung et al. was observed with this p53-MO control experiment (Appendix section 3.4.1).

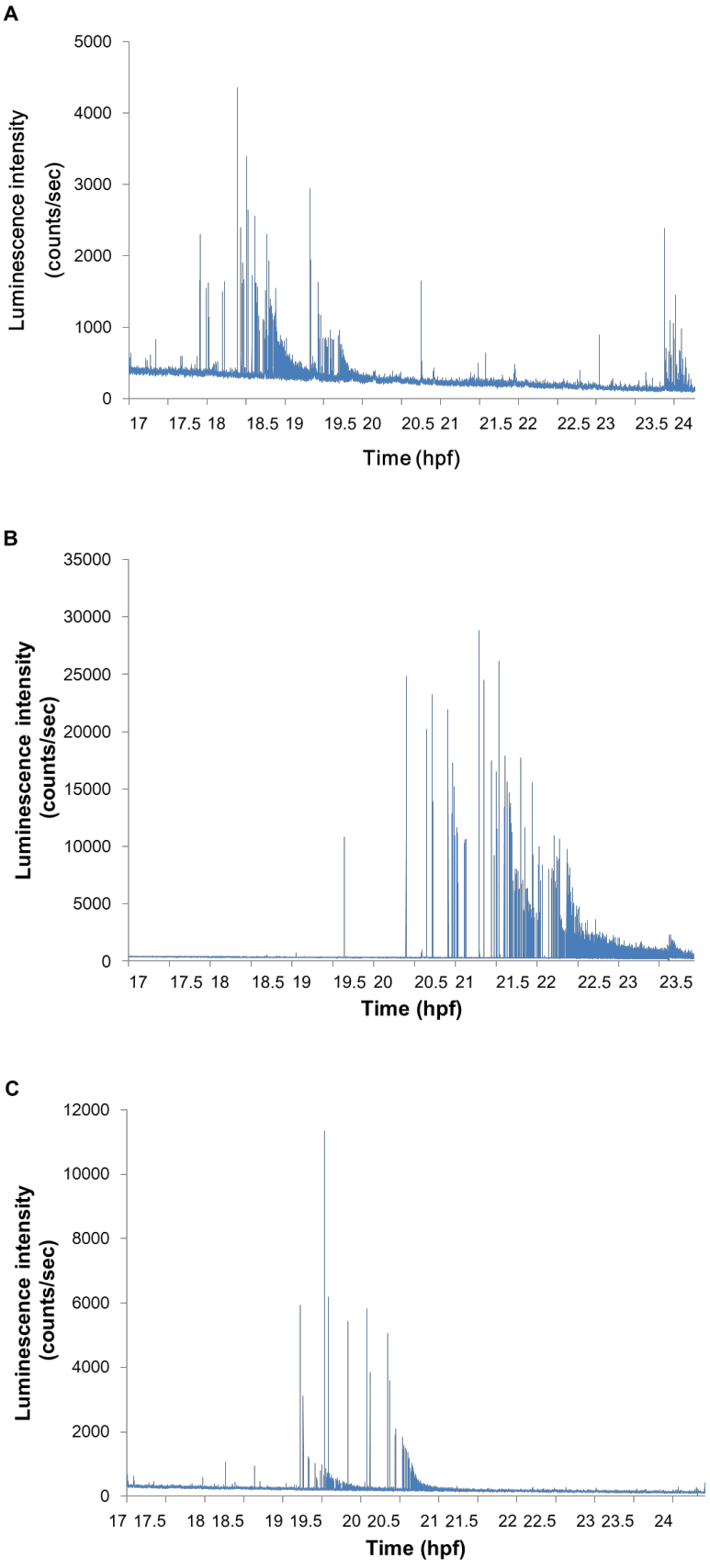
A
Luminescence intensity (counts/sec)
5000
4000
3000
2000
1000
0
17 17.5 18 18.5 19 19.5 20 20.5 21 21.5 22 22.5 23 23.5 24
Time (hpf)
B
Luminescence intensity (counts/sec)
35000
30000
25000
20000
15000
10000
5000
0
17 17.5 18 18.5 19 19.5 20 20.5 21 21.5 22 22.5 23 23.5
Time (hpf)
C
Luminescence intensity (counts/sec)
12000
10000
8000
6000
4000
2000
0
17 17.5 18 18.5 19 19.5 20 20.5 21 21.5 22 22.5 23 23.5 24
Time (hpf)

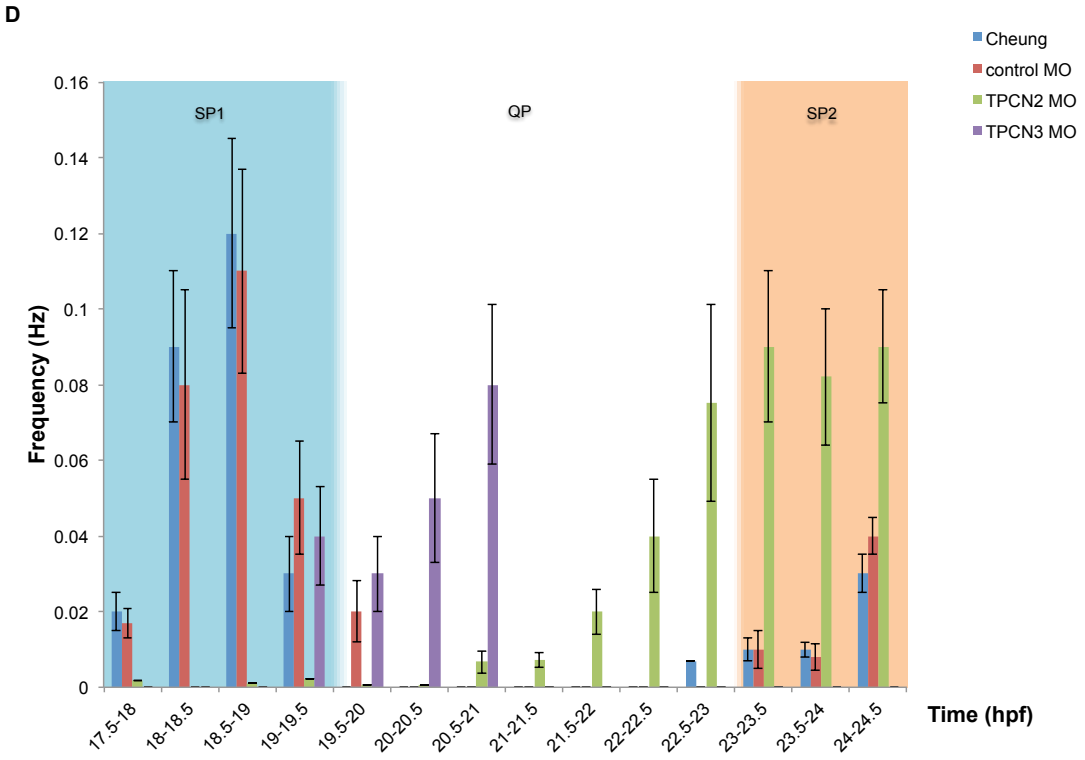

Figure 3.5: (A, B, C) Ca^{2+} signaling profile generated by SMC from ~17 to ~24 hpf, visualized using aequorin-based luminescence detection. Representative temporal profiles of the luminescence generated by the α-actin-aeq transgenic embryos that were injected with **(A)** control-MO (~2.5 ng); **(B)** TPC2-MO (~2.5 ng); **(C)** TPC3-MO (~2.5 ng) at the 1- to 4-cell stage. Data were plotted every 1 second, with each data point representing luminescence collected in 1 second for an imaging field covering the entire embryo from ~17 to ~24 hpf. n=10 for **(A, B)**, n=3 for **(C)**. **(D)** Bar chart showing the frequency of the Ca^{2+} signals generated in the trunk musculature from ~17 to ~ 24 hpf in uninjected control, control-MO injected, TPC2-MO injected and TPC3-MO injected embryos respectively. The distinct Ca2+ signaling periods, namely SP1 (from ~17.5 to ~19.5 hfp) and the SP2 (from ~23 to ~24.5 hpf), as well as the QP (from ~19.5 to ~ 23 hfp) are highlighted for reference. n=10 for all except TPC3-MO treatment in which n=3. Data presented ± SEM.

3.2.4 Studies of the gross morphology of zebrafish embryos treated with TPC2- and TPC3-MOs

Having established that TPC2 KD and TPC3 KD perturb the muscle-generated Ca^{2+} signaling in zebrafish embryos, an investigation was conducted to determine whether such disruption in Ca^{2+} signaling would influence the development of trunk musculature. The gross morphology of TPC2 KD and TPC3 KD embryos were first compared with untreated and control-MO treated embryos. Representative bright field (BF) images of whole embryos showed that both untreated and control MO-treated embryos displayed straight and normal tails (Figure 3.6) whilst a distinct and reproducible phenotype of a downward trunk curvature was observed with TPC2 KD (TPC2-MO + p53-MO) embryos (Figure 3.6) at ~24-26 hpf. For TPC3 (TPC3-MO + p53-MO) morphants, it was noted that the tip of the tail kinked out of the plane ("hooked" tail) when looking under the microscope, however the "hooked" tail was hardly captured by the camera so that it appeared as a straight tail as shown in the BF image (Figure 3.6). The "hooked" tail noticed with TPC3 morphants is phenotypically different from the curved tail observed with TPC2 morphants, suggesting that TPC2 and TPC3 may play a different role during zebrafish embryogenesis.

While a distinct phenotype was identified with control and KD embryos, BF images of higher magnification (40x) revealed normal chevron-shaped somites in the anterior trunk (i.e. somites 6-8) for control embryos and TPC3 KD embryos as indicated by the dotted lines in figure 3.4, but a slight bending of the "V" angle was seen with the TPC2 morphants such that a U shape rather than V shape was observed, indicating the shape of somites was affected to a slight extent after TPC2 KD.

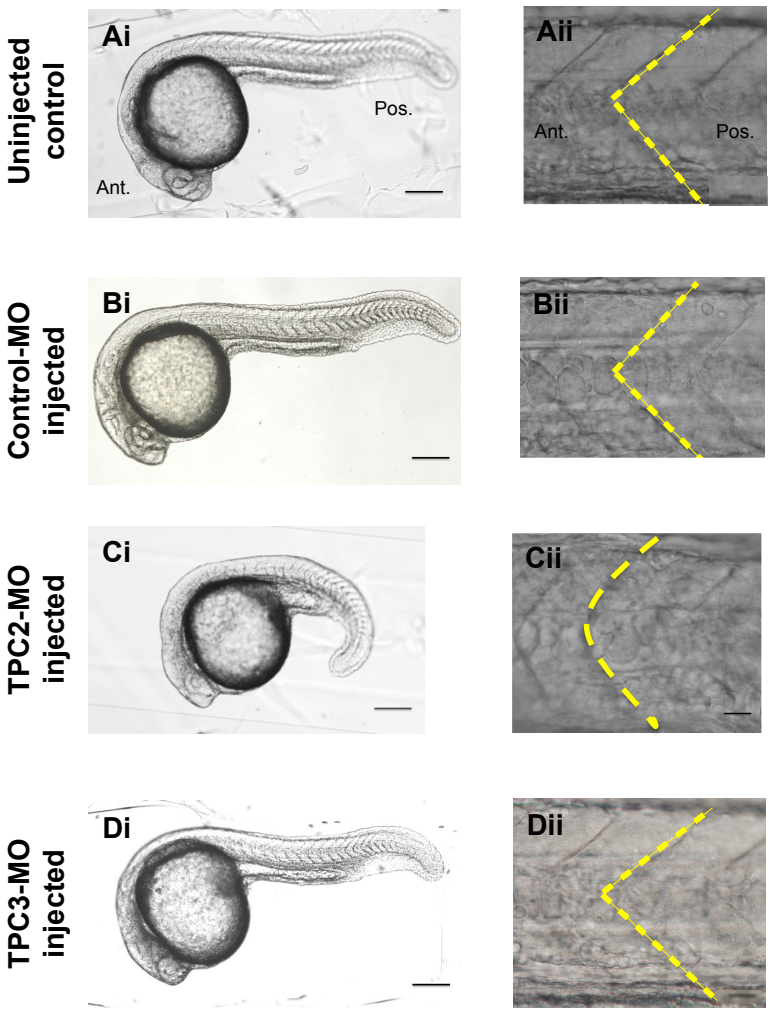

Figure 3.6: Effects of MO-based TPC2 KD and TPC3 KD on the gross trunk musculature of zebrafish embryos. Embryos were **(A)** untreated or **(B)** control-MO treated or **(C)** TPC2-MO treated or **(D)** TPC3-MO treated. Bright field images were taken at ~24-25 hpf, displaying the gross morphology of representative embryos. Magnification at 5x for **(i)** and 40x for **(ii)**. Scale bar is 200 μm for **(i)** and 20 μm for **(ii)**.

3.2.5 Effects of MO-based TPC2 knockdown on the organisation of the trunk musculature

3.2.5.1 Immunohistochemistry study

Since TPC2 KD produced a curved tail with downward bending in zebrafish embryos, further studies were performed to look into the effects on the organisation of trunk musculature, particularly in SMCs during muscle development. The fine morphology of TPC2 morphants was examined to characterise the muscle defects in more details. Dual labelling of F-actin and myosin heavy chain with phalloidin and F59 primary antibody respectively was performed using embryos fixed at ~24 hpf. Embryos of 24 hpf were chosen because sarcomeres are well organised in the SMCs from 20 hpf to 24 hpf [128]. In the controls (Figure 3.7A-C, A*-C*and 3.8A-C, A*-C*), characteristic chevron shaped somites were clearly observed and the myofibrils displayed a normal striated pattern; whereas a slight deformation of the shape of somites was revealed with TPC2 (TPC2-MO + p53-MO) morphants (Figure 3.7D-F, D*-F*and 3.8D-F, D*-F*), and the slow muscle fibers looked less straight spanning the myotome than those of the controls. Furthermore, abnormalies in myofibers were apparent after TPC2 KD as disruption in the normal sarcomeric pattern in certain myofibrils was noticeable; both actin and myosin were less well-organised as a clear degree of bending was seen with actins and myosins. Collectively, the current data indicate that TPC2 KD produces a perturbation in the organisation of trunk musculature, and that the formation of SMCs and sarcomeres was disrupted as well.

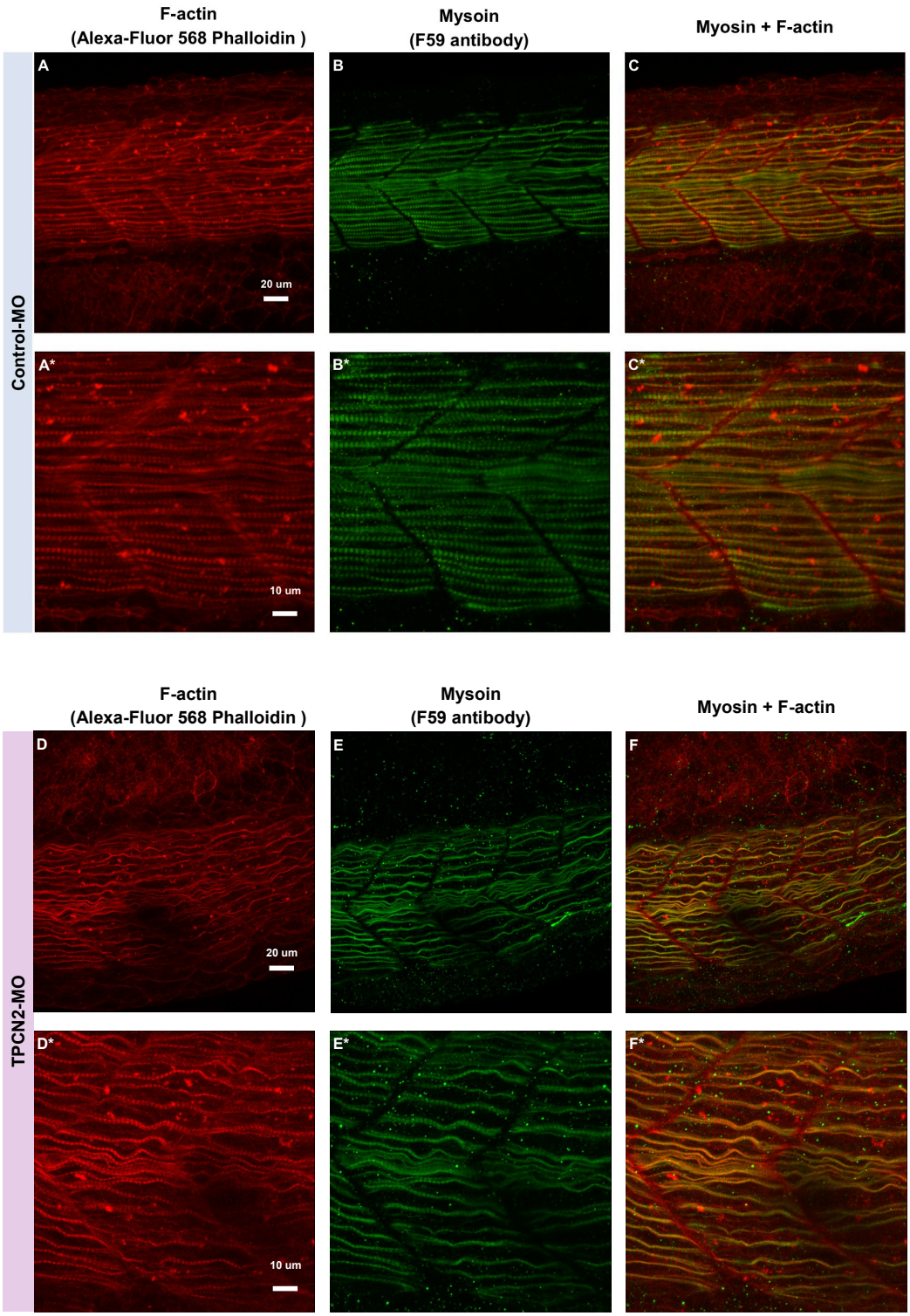

Figure 3.7: Effect of MO-based TPC2-KD on SMC development. (A-C and A*-C*) Control-MO treated embryos; **(D-F and D*-F*)** TPC2-MO treated embryos. **(A*-F*)** represent images of higher magnification; **(F and F*)** represent images when the two channels were merged. Dual labelling with F-actin and myosin using phalloidin and F59 primary antibody respectively was conducted on embryos fixed at ~24 hpf for visualisation of the fine structure of the trunk musculature. Each fluorescence image is a stack of confocal optical sections obtained through the anterior trunk. Anterior to the left and posterior to the right. The first somite on the left represents somite 7. Scale bars were 20 μm and 10 μm for **(A-F)** and **(A*-F*)** respectively.

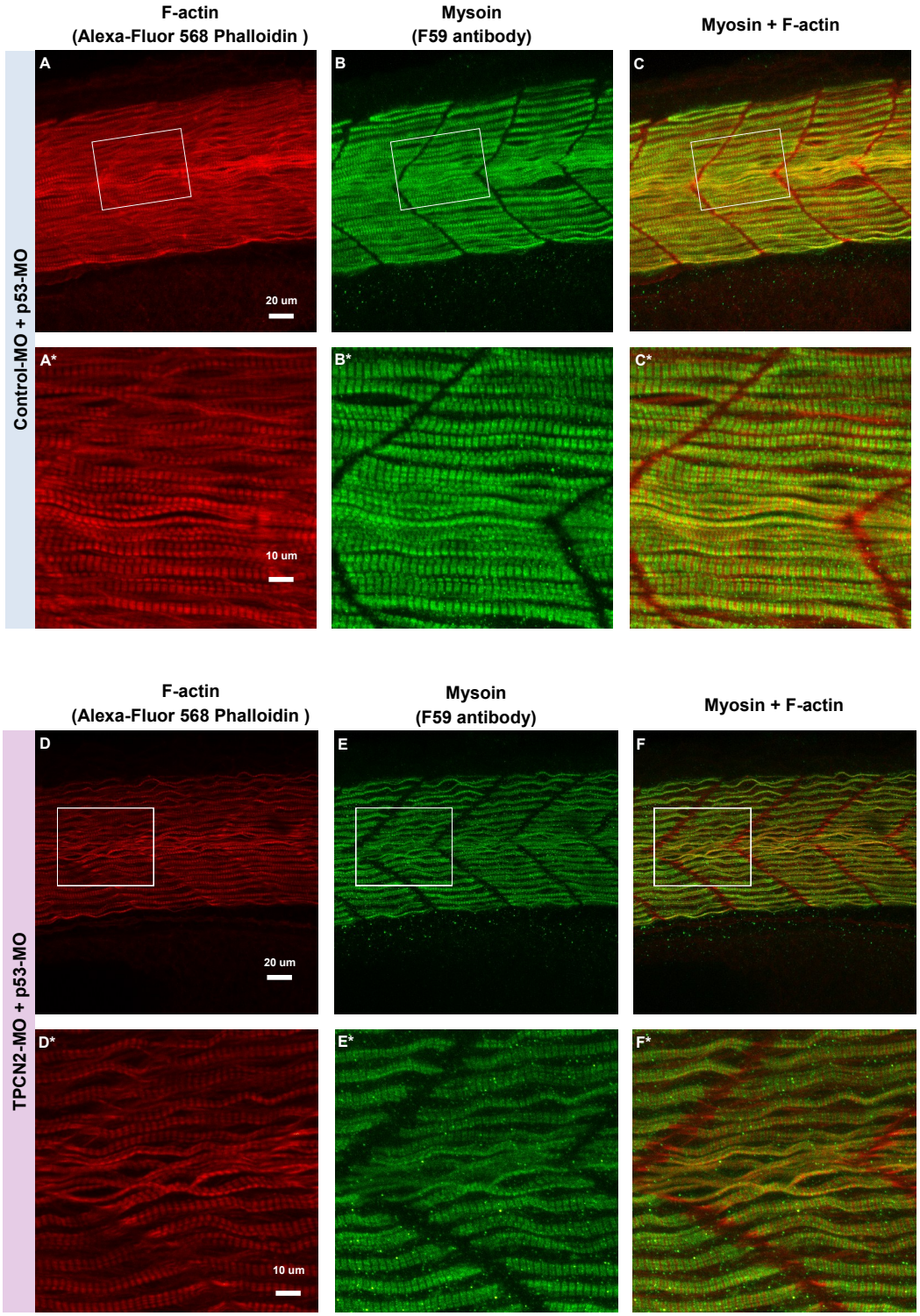

Figure 3.8: Effect of MO-based TPC2-KD on SMC development. (A-C and A*-C*) Control-MO + p53-MO treated embryos; **(D-F and D*-F*)** TPC2-MO + p53-MO treated embryos; **(A*-F*)** represent images of higher magnification; **(F and F*)** represent images when the two channels were merged. Dual labelling with F-actin and myosin using phalloidin and F59 primary antibody respectively was conducted on embryos fixed at ~24 hpf for visualisation of the fine structure of the trunk musculature. Each fluorescence image is a stack of confocal optical sections obtained through the anterior trunk. Anterior to the left and posterior to the right. The first somite on the left represent somite 7. Scale bars were 20 µm and 10 µm for **(A-F)** and **(A*-F*)** respectively.

3.2.5.2 Statistical analysis of metamorphic parameters

In order to quantify the influence of TPC2 KD (TPC2-MO + p53-MO) on the development of the trunk musculature, statistical analysis of metamorphic parameters derived from the trunk musculature, somites and the SMCs located in somites 6-10 was performed on the control and TPC2 morphants (Figure 3.9).

Firstly, the ratio of myofiber length/somite length was calculated to assess the degree of straightness of the slow muscle fibers; TPC2 morphants were characterised to be not straight according to the above criteria as explained in the figure legend, further supporting the above observation that slow muscle fibers were less straight in TPC2 morphants. A significant reduction was also noted for somite length and myofiber length in TPC2 morphants. In addition, the myofiber width was found to be significantly shorter in TPC2 morphants than in controls. The somite angle was also measured to evaluate the influence on somite shape resulted from TPC2 KD. No significant difference was found between the TPC2 morphant and the control. The myotome width was demonstrated to be significantly smaller in TPC2 morphant than the control. In addition, a significantly smaller number of slow muscle myofibers in the anterior somites were found in the TPC2 morphant than in the control.

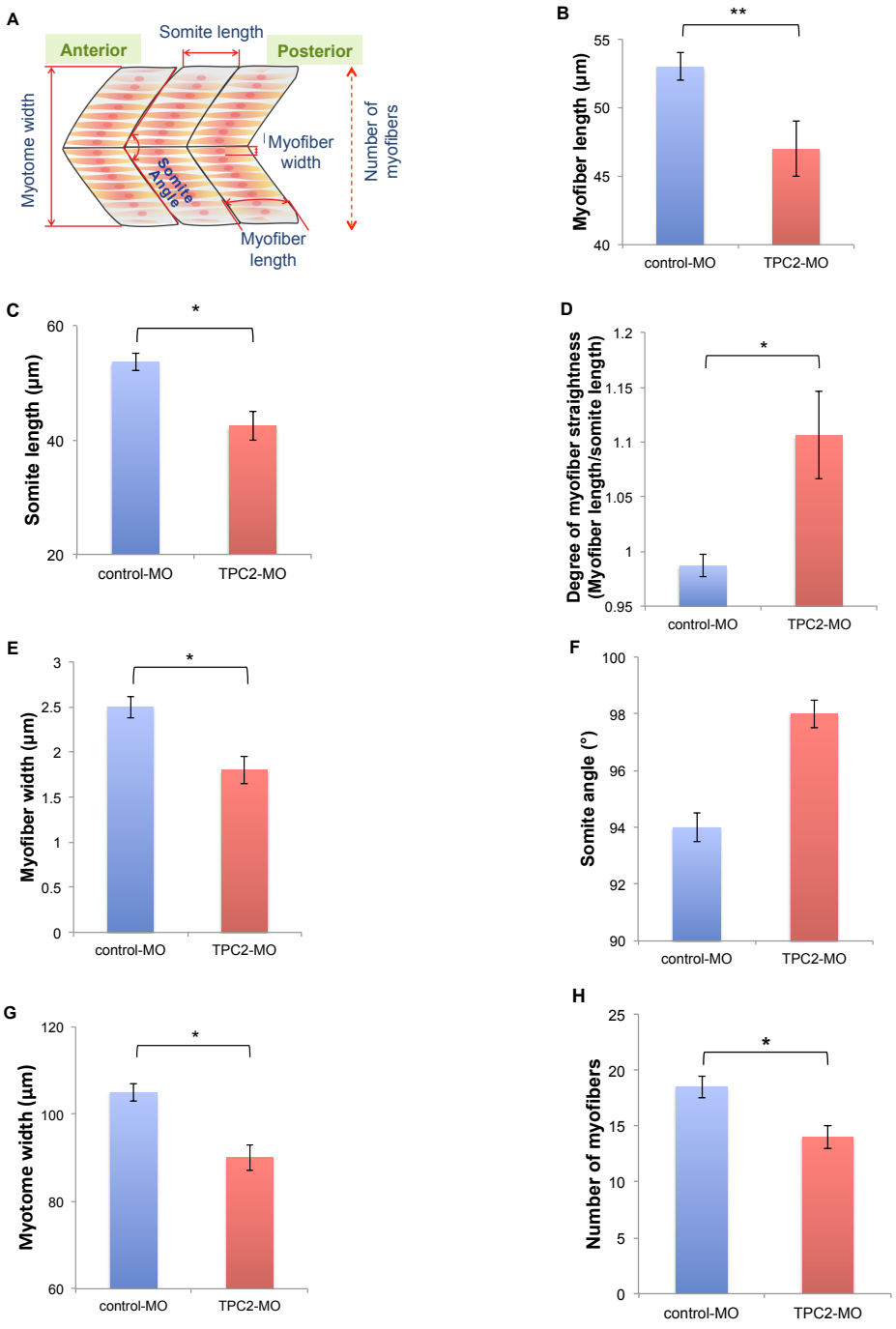

Figure 3.9: Quantification of the effect of MO-based TPC2-KD on the development of the SMCs. (A) A diagram depicting the seven parameters of the trunk musculature and the SMCs that were measured; measurement was based on the confocal images taken from whole-mount immunolabelled embryos at ~24 hpf through the anterior somites 6-10. **(B)** Myofiber length **(C)** Somite length; **(D)** Degree of myofiber straightness; **(E)** Myofiber width; **(F)** Somite angle; **(G)** Myotome width; **(H)** Number of myofibers. For **(B,C,D)**, three measurements were taken from the dorsal, medial and ventral regions within one somite and two somites were assessed per embryo. **(D)** Slow muscle fiber was regarded as not straight (or wavy) when ratio of myofiber length/somite length was greater than 1. **(E)** For myofiber width, 10 myofibers were picked randomly from 3 somites per embryo and the average value represented the myofiber width of that embryo. For **(F, G)** measurements were taken from 3 somites per embryo. **(H)** The number of myofibers was counted in 3 somites per embryo. n=10. *p<0.05, **p<0.01 (student's *t-test*). Data presented ± SEM.

3.2.6 Effects of MO-based knockdown of TPC2 on the development of the trunk musculature of intact zebrafish embryos at ~48 hpf

The zebrafish trunk curls around the vegetal pole initially during the segmentation period (10-24 hpf). With the formation of new somites progressing in an anterior-to-posterior manner and extension of the tail, the whole body length elongates. Ultimately the trunk straightens and by 24 hpf the embryo no longer adopts a curled appearance [184]. In an attempt to confirm that the significant trunk curvature of the TPC2 morphants shown at ~24 hpf is not merely an effect of a general delay in development, the development of the TPC2 morphants continued to be monitored and BF images of the untreated embryos and the TPC2-MO (+ p53-MO) treated embryos were taken at ~48 hpf (Figure 3.10). Intriguingly, the characteristic phenotype of distinctive trunk curvature with downward bending tail was still noticeable at ~48 hpf with the TPC2 morphant. The U shaped somites were noticeable as well, albeit the bending of "V" angle was only to a minor extent. Additionally, a small edema was seen in the heart cavity of the TPC2 morphant, which was not noted at ~24 hpf. At higher magnification, both the untreated control and the TPC2 morphant displayed the chevron-shaped somites in the anterior trunk (somites 6-8).

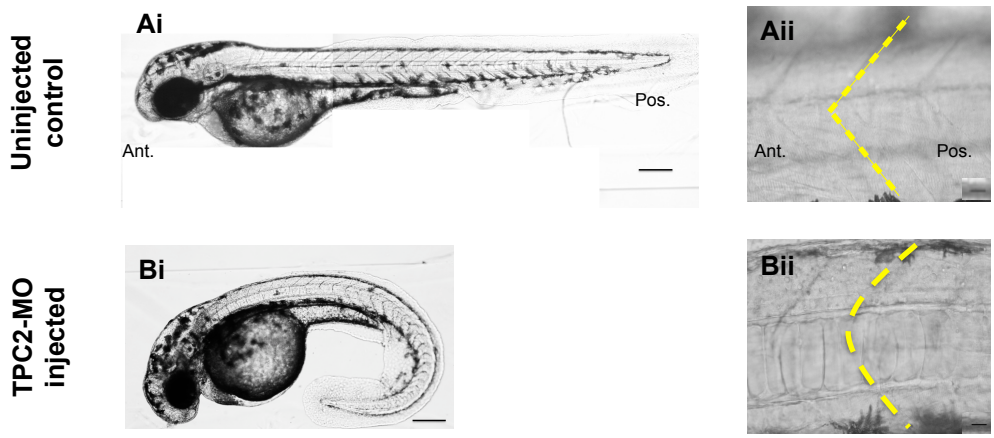

Figure 3.10: Effects of MO-based TPC2 KD on the gross trunk musculature of zebrafish embryos. Embryos were **(A)** untreated or **(B)** TPC2-MO treated. Bright field images were taken at ~48 hpf, displaying the gross morphology of representative embryos. Magnification at 5x for **(i)** and 40x for **(ii)** and scale bar is 200 µm and 20 µm respectively.

3.2.7 Construction of cDNA mutants for rescue constructs

In order to address the MO specificity and to confirm the effects observed with TPC2 KD and TPC3 KD generated by the specific MO, it is important and necessary to perform an mRNA rescue experiment to investigate whether those noted effects can be reversed, i.e. "rescued". This is done by co-injection of a synthetic mRNA encoding the proteins from the targeted locus but not recognised by the experimental MO target sequence [185, 186]. For translation-blocking MOs, rescue constructs can be engineered to alter the nucleotide sequences without changing the encoded protein through degeneracy of the genetic code [147], which can be achieved by introduction of one or more silent point mutations in the mRNA sequence.

The construction of DrTPC cDNA clones with silent mutation(s) introduced in the MO-targeted sequences was first demonstrated. These modified, mutated cDNA clones subsequently served as templates for *in vitro* transcription to generate the mRNA rescue constructs.

For the TPC1 MO-targeted sequence, a nucleic acid of the last codon encoding Ala was mutated silently; for TPC2 MO-targeted sequence, two silent point mutations were made at the second and third codons both encoding Glu; for TPC3 MO-targeted sequence, one nucleic acid in each of the second and third codons encoding Ser and Glu respectively were silently mutated. pGEM-T easy.DrTPC1, pCRIITOPO.DrTPC2 and pGEM-T easy.DrTPC3 plasmids were used as templates for silent mutant cloning. Mutation was performed using the Stratagene QuickchangeTM site-directed mutagenesis method, followed by DpnI digestion of the template plasmids (i.e. original plasmids without point mutation(s)), resulting in PCR products (i.e. the plasmids with silent mutation(s) introduced) only. Transformation of *E. coli* with the mutated plasmids and subsequent isolation of the mutated plasmids by miniprep were conducted. Successful silent point

mutations were achieved as determined by the sequencing check. The plasmids with successful introduction of silent mutations were sent to Prof. Andy Miller's lab for subsequent *in vitro* transcription for generation of the final mRNA rescue constructs and rescue experiments using these rescue constructs were carried out by Prof. Andy Miller and his colleagues. This showed that a partial rescue was observed when the rescue construct was injected in conjunction with the TPC2-MO and p53-MO (Appendix section 3.4.2).

3.2.8 Expression of DrTpcn genes in zebrafish embryos

To study the expression pattern of the three *DrTpcn* genes during zebrafish development, RNA *in situ* hybridization on whole zebrafish embryos at the 24 hpf stage was performed. DIG-labelled sense and antisense RNA probes were hybridized to embryos and the expression pattern of *DrTpcns* described below was acquired by a *DrTpcn*-specific RNA probe which corresponds to the 5' region of the *DrTpcn* cDNA (a fragment containing the 5'untranslated region and coding region up to the restriction site). Labelling of antisense RNA probe revealed expression of *DrTpcn3* near the tail of the embryos. The signals seemed to be associated with the blood cells in the tail, associated with the region where intermediate cell mass (ICM) and posterior blood island (PBI) are located. A less intense signal was also observed in the lower trunk (Figure 3.11).

No labelling was seen with the sense RNA probe and the control embryo in the absence of any probes. However no labelling was detected for the *DrTpcn1* and *DrTpcn2* sense and antisence probes at the same developmental stage. This could be due to insufficient incubation time. Yet the possibility that absence of these two genes at this stage cannot be ruled out if they are only transiently expressed at particular developmental stages. Further studies are required to examine the expression pattern of these two genes in more details. Due to time limitations, only the 24 hpf embryos were assessed.

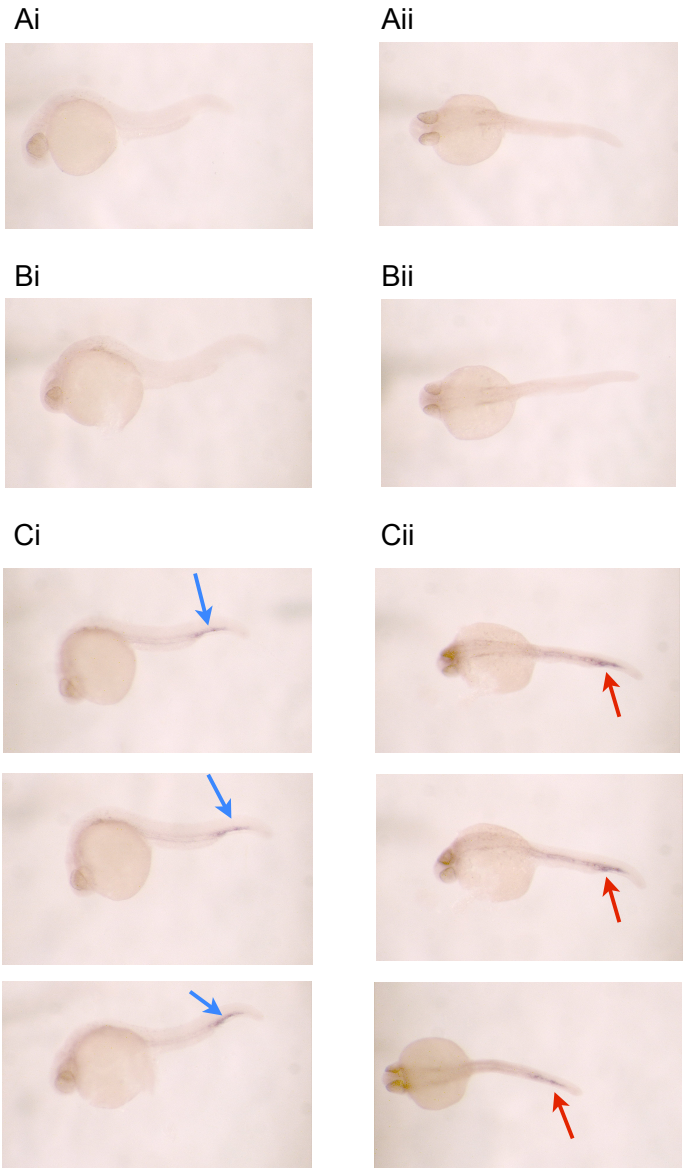

Figure 3.11: RNA in situ hybridization of **(A)** control, **(B)** *DrTpcn3* sense probe, and **(C)** *DrTpcn3* antisense probe on whole-mount zebrafish embryos at 24 hpf. A fairly intense labelling by *DrTpcn3* antisense probe is detected in the cells near the tail as indicated by the blue and red arrows panel **C**. Panels **Ai**, **Bi** and **Ci** show lateral views with anterior to the left; panels **Aii**, **Bii** and **Cii** show dorsal views.

3.2.9 Affinity-purification of antibodies that specifically recognise recombinant DrTPCs

In order to generate antibodies that specifically recognise and detect endogenous DrTPCs (sequences of antibody are listed in Materials and Methods), the antibodies in the immune sera were concentrated and other IgGs that contribute to nonspecific background binding were removed. This was achieved by affinity purification of the immune sera generated from the two rabbits (DrTPC1: 2100, 2167; DrTPC2: 2137, 2162; DrTPC3: 025001, 025029) against the individual antigenic peptides A and B. Therefore, four affinity-purified antibodies were produced for each TPC. To ascertain the capability and specificity of each antibody, dot blot analysis of anti-DrTPCs antibodies were tested on these antigenic peptides A and B. Figure 3.10 shows clearly that for anti-DrTPC1 antibody, purified antibody 2100 coupled with A (i.e. 2100A) and purified serum 2167 coupled with A (i.e. 2167A) recognised peptide A but not peptide B, whereas 2100B and 2167B failed to recognise either peptide. For anti-DrTPC2 antibody, both 2137A and 2162A recognised peptide A but not peptide B, while 2167B and 2162B recognised both peptide A and peptide B. For anti-DrTPC3 antibody, both 025001B and 025029B recognised peptide B but not peptide A, whereas neither peptide A nor peptide B was recognised by 025001A and 025029A.

Due to the unavailability of zebrafish cell lines, detection of exogenous TPCs (overexpression of cells with DrTPCs) by purified antibodies could not be verified in the present study.

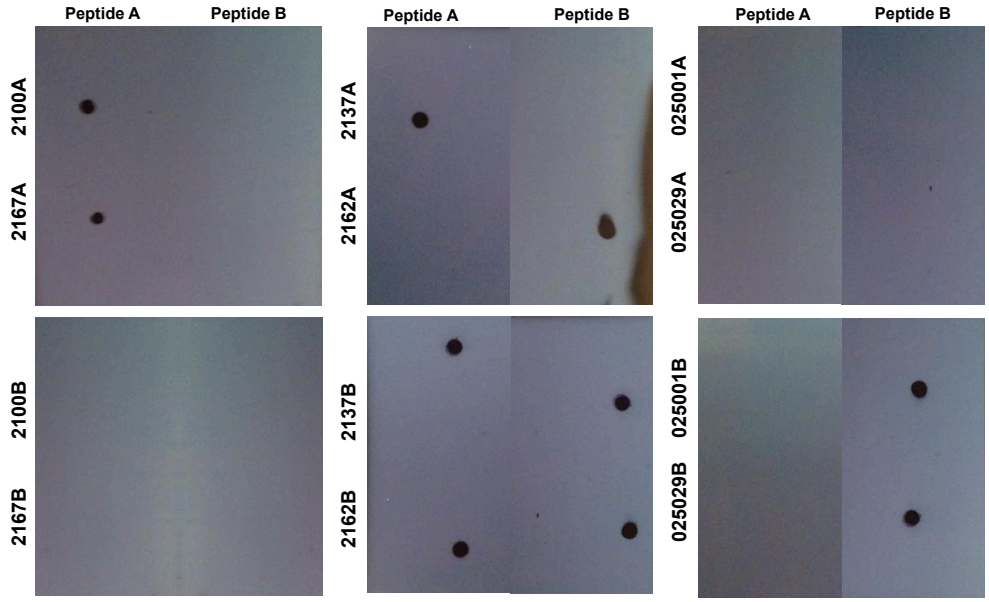

Figure 3.12: Dot blot analysis of anti-DrTPCs antibodies raised against peptide A and peptide B were tested on these antigen peptides. A nitrocellulose membrane was spotted with peptide A and peptide B, and then blotted with affinity-purified anti-DrTPC1 antibody, anti-DrTPC2 antibody, and anti-DrTPC3 antibody respectively. A dark dot appeared when the antibody recognised the antigen peptide.

The following localisation study was conducted by my collaborator Mr JJ Kelu using the purified anti-DrTPC2 antibody provided by Dr Parrington's lab (as described in section 3.2.9).

3.2.10 Localisation of TPC2 in SMCs in vitro and in vivo

Using the custom-made anti-DrTPC2 antibody, a temporal expression profile of TPC2 in SMCs in intact embryos (Figure 3.13A-E) was established by Mr JJ Kelu. Between ~16 to 24 hpf, (i.e., the period when the adaxial cells (SMC progenitors) migrate and differentiate [187]); there was a gradual increase in the level of TPC2 expression in SMCs. In addition, over time there was a transition in the pattern of expression of TPC2; such that between ~16 to 18 hpf, it was expressed in a homogeneous punctate pattern, and then between ~20 and 24 hpf a distinct banding pattern developed (Figure 3.13Civ-3Eiv).

The subcellular localization of TPC2 was also revealed using primary zebrafish muscle cells (Figure 3.14 and 3.15). In this system, a transition from a homogeneous and punctate TPC2 labeling pattern in the forming myofibers after ~24 h in culture to a far more organized pattern of localization characterized by distinct sarcomeric banding after ~48 h in culture (Figure 3.15Bb and Be) was also demonstrated. Thus it was estimated that the stage of myogenesis following ~24 h and ~48 h of primary culture is approximately equivalent to the early (i.e., ~18 to 20 hpf) and late (i.e., ~20 to 24 hpf) stages of SMC myogenesis *in vivo*, respectively. Such an *in vitro* to *in vivo* developmental stage comparison is also supported by the localization patterns of IP_3R and RyR in SMCs (compare Figure 3.15D-E, with Figure 3.2). Taken together, Kelu's immunolabeling studies suggested a changing pattern of TPC2 localization as the SMCs differentiate.

In muscle cell cultures, TPC2 labeling was localized adjacent to the sarcomeric I-band region, which contains the Z-disc (Figure 3.15B). Also, nuclear and peri-nuclear

localization of TPC2 and LAMP1 was observed in ~24 h primary cultures, i.e., equivalent to SMCs *in vivo* at ~18 hpf (Figure 3.14Aa-Ac, Ca-Cc). This indicates that lysosomes containing TPC2 were in close proximity to the nuclear region at the time of SMC differentiation. Furthermore, IP_3R type III and RyR were both localized in the peri-nuclear regions in SMC primary cultures at around the same time (Figure 3.14Ea-Ed).

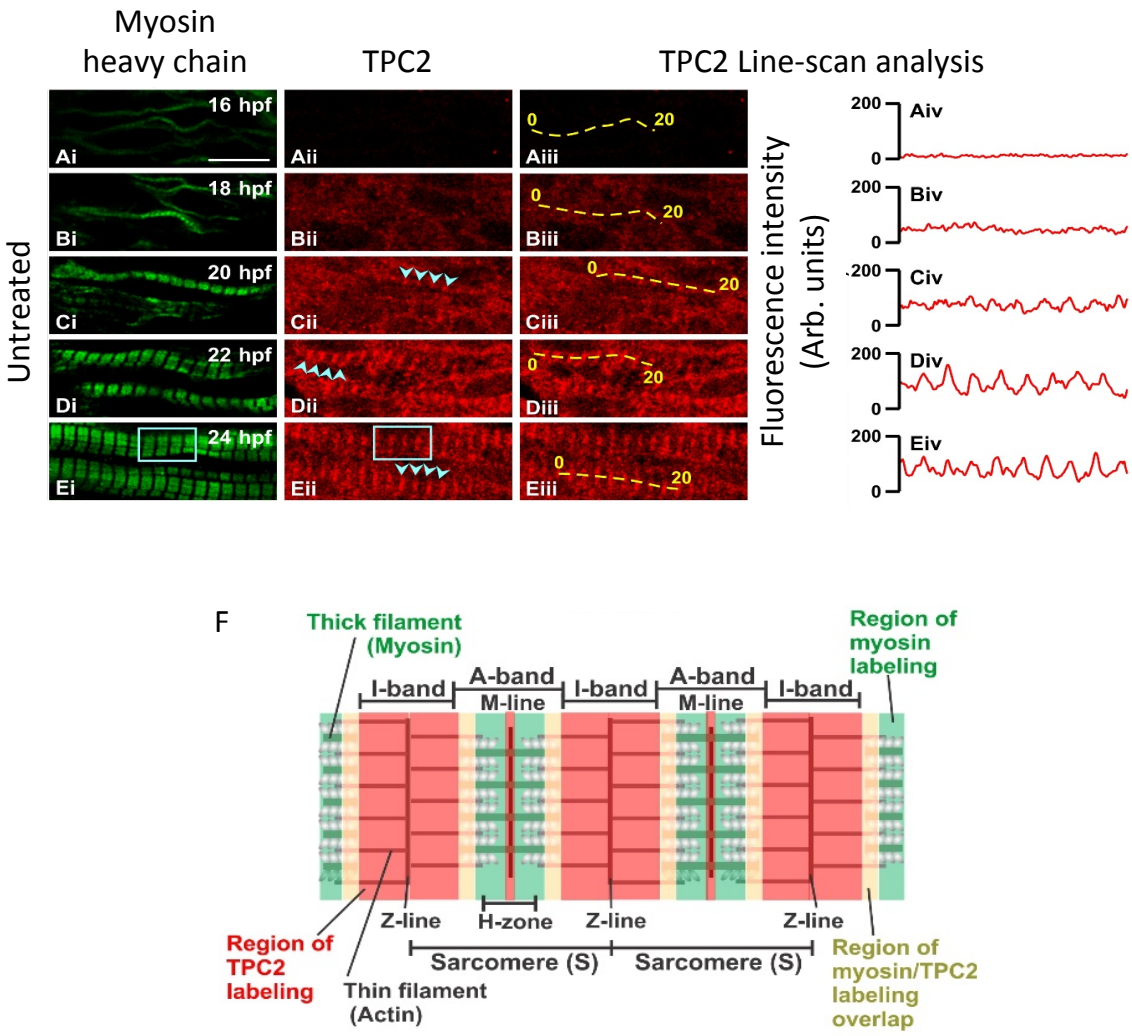

Figure 3.13: TPC2 expression in the SMCs of intact zebrafish embryos. Fixation of embryos were performed between 16 hpf and 24 hpf, followed by dual immunolabelling with **(A to E)** myosin heavy chain and TPC2 antibody. **(F)** A schematic diagram of two sarcomeres. Scale bar is 10 µm. **(Aiii to Eiii)** Line-scan analyses. (Adapted from Kelu et al., 2015 [129])

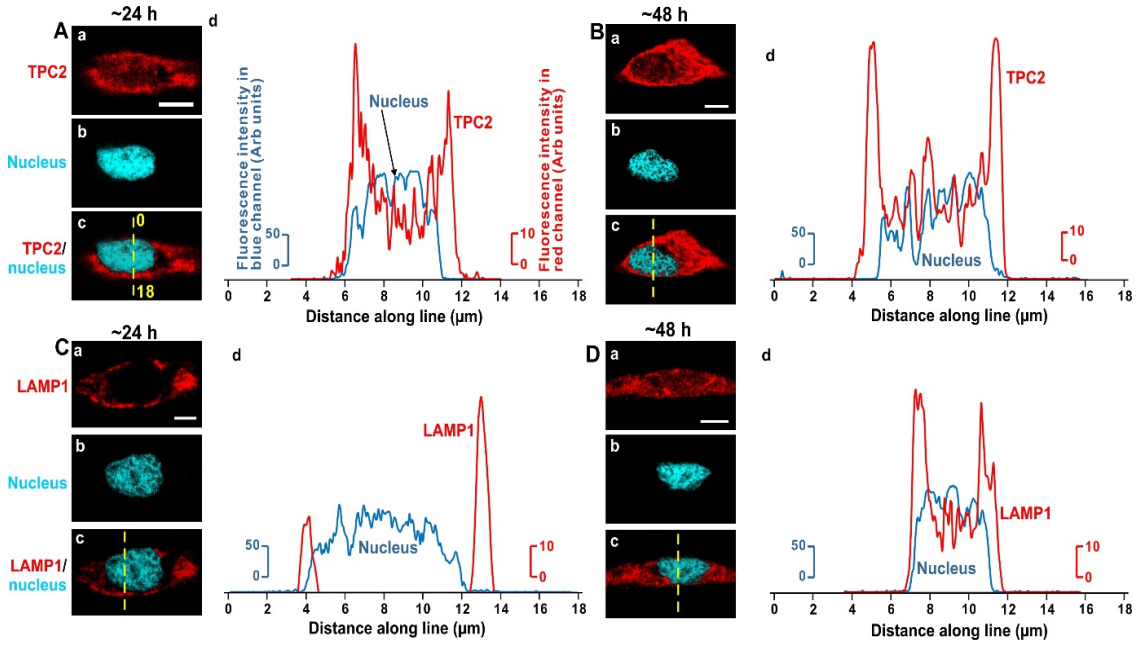

Figure 3.14: Subcellular localization of TPC2 and other proteins in the nuclear region of SMCs. Dual-immunolabelling of the cells with **(A,B)** myosin heavy chain and TPC2 antibodies; **(C,D)** myosin heavy chain and LAMP1 antibodies. Images were captured at the widest part of the nucleus. In panel **(A-D),** the myosin heavy chain antibody was used to recognize SMCs and thus is not displayed. **(a)** shows localization of TPC2 and LAMP1 alone; **(b)** shows localization of nucleus alone; and **(c)** shows the superimposed images (TPC2 or LAMP1 superimposed with nucleus). Scale bar is 5 µm. **(Ad-Dd)** Line-scan analyses. The 0 and 18 in **(Ac)** show the start and end point of the line-scan respectively and is correlated to the x-axis in **(Ad)**. (Adapted from Kelu et al., 2015 [129])

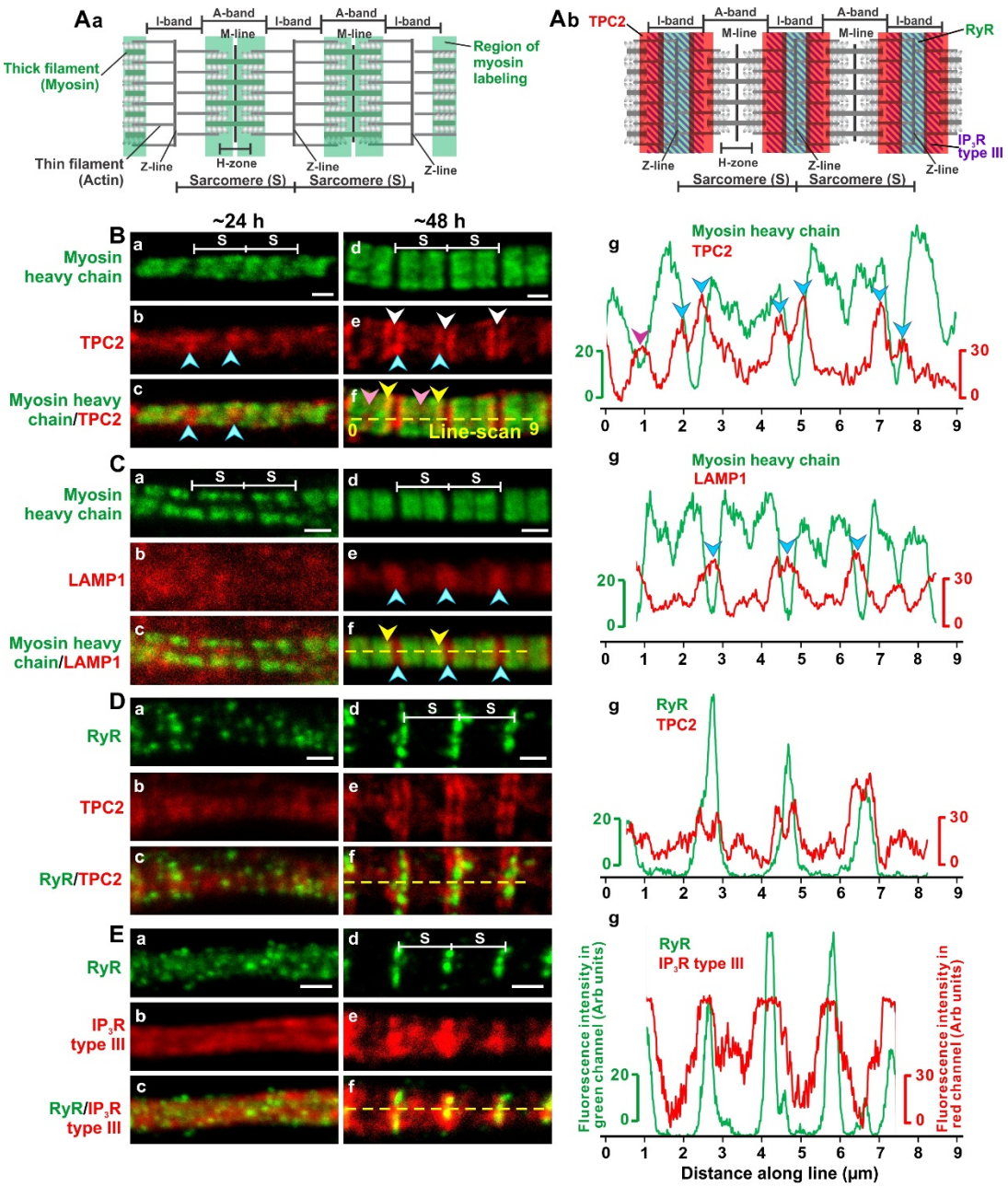

Figure 3.15: TPC2 localization in the myofibers of SMCs primary cultures. (**A**) Schematic diagrams of two sarcomeres demonstrating the localization of (**Aa**) myosin (green) and (**Ab**) TPC2 (red), RyR (green) and IP_3R (diagonal shading). (**B-E, panels a-f**) Localization of TPC2 and other proteins in the myofibrils or SR. Dual-immunolabelling of cells with: (**B**) myosin heavy chain and TPC2 antibodies; (**C**) myosin heavy chain and LAMP1 antibodies; (**D**) RyR and TPC2 antibodies; and (**E**) RyR and IP_3R type III antibodies. In (**B-E, panels a-c**), cells were cultured for ~24 hours while in (**B-E, panels d-f**) for ~48 hours. **(a, d and b, e)** shows localization pattern of individual protein alone and **(c, f)** shows the superimposed images. Scale bar is 1 µm. (**B-E, panel g**) Line-scan analyses. Blue arrowheads show TPC2 banding at I-band; pink arrowheads show less obvious TPC2 banding at M-line; white arrowheads show regions where TPC2 is excluded around the z-line; yellow arrowheads show areas where TPC2 and myosin heavy chain overlap; yellow dashlines show locations of line-scans. (Adapted from Kelu et al., 2015 [129])

3.3 Discussion

3.3.1 Investigation of DrTPC2-mediated Ca^{2+} signalling in the development of the SMCs in zebrafish embryos

My research on this topic has been published in a recent paper:

"Two-pore channel 2 activity is required for SMC-generated Ca^{2+} signaling during myogenesis in intact zebrafish" [129]

3.3.1.1 Effects on the temporal characteristics of Ca^{2+} signals by DrTPC2 knockdown

In the present study, the temporal characteristics of Ca^{2+} signals were assessed by aequorin-based Ca^{2+} imaging using transgenic zebrafish embryos. TPC2 KD was achieved by MO approach and its effects on the muscle-generated Ca^{2+} signals were demonstrated [129].

A disruption of Ca^{2+} signals in the SP1 and SP2 phases was apparent (Figure 3.5B), so negligible Ca^{2+} signals were detected between 17-19.5 hpf when SP1 Ca^{2+} signals occurred in normal control (uninjected) embryos [128] and control-MO injected embryos (Figure 3.5A); whereas Ca^{2+} signals that are not supposed to appear during the QP phase between 19.5-23 hpf were noted between 20.5-24 hpf. Since SP2 lasts from 23 hpf onwards and the current recording was stopped at 24 hpf, no information can be obtained regarding Ca^{2+} signals after 24 hpf. This TPC2 KD-mediated disruption of Ca^{2+} signals was further confirmed by the average spike frequency of which a remarkably different pattern was exhibited by TPC2 morphants (Figure 3.5D), compared with control-MO injected and uninjected embryos. Taken together, these data provide preliminary evidence that the lysosomal TPC2 could be involved in regulating Ca^{2+} activity in SP1 and at least the very early phase of SP2. As characterized previously, IP_3Rs are responsible for Ca^{2+} release in early SP1 while RyRs contribute to Ca^{2+} release in late SP1 and whole SP2

[128]; the disruption elicited by TPC2 KD thus implicates TPC2 in a regulatory role in IP_3R- and/or RyR-mediated Ca^{2+} signaling that give rise to the distinct patterns seen in SP1 and SP2, with the former being associated with ET coupling while the latter with SMC differentiation and EC coupling.

A continuation study [129] based on my findings was carried out by my collaborator Mr Kelu JJ in Miller AL's lab. In his study, recording of Ca^{2+} signals was extended from 24 hpf to 30 hpf. It was shown that Ca^{2+} spikes were still detectable after 24 hpf, thus the Ca^{2+} signals arising after 24 hpf was also called SP2 as they are Ca^{2+} activities that continued from the initial SP2 signals characterized previously [128]. Also, application of higher concentrations of TPC2-MO (5 ng; double of the dose used in my experiments) with p53-MO led to complete inhibition of both SP1 and SP2 Ca^{2+} signals (from 17 to 30 hpf) (Appendix section 3.4.3) and negligible spike frequency throughout the entire period. Together with my results which showed a disruption to a less extent in the Ca^{2+} activities and the spike frequency pattern due to application of a lower dosage of MO, it is therefore suggested that inhibition of both SP1 and SP2 signals mediated by MO-based KD of TPC2 follows a dose-dependent manner. A rescue experiment was also performed to rescue the attenuation brought by TPC2 KD. Thus co-injection of TPC2-MO and p53-MO was followed by injection of the rescue construct *Tpcn2*-mRNA which is not recognized by the TPC2-MO (details of construct design see section 3.2.7). A partial rescue of the Ca^{2+} signals in both SP1 and SP2 was demonstrated (Appendix section 3.4.2), indicating the specificity of action of the TPC2-MO.

As discussed earlier, SMCs were solely responsible for the SP1 Ca^{2+} activities [128]. Hence perturbation of Ca^{2+} activities by TPC2 inhibition indicated that TPC2 play a role in regulation of SMC-mediated Ca^{2+} activities. On the other hand, Ca^{2+} signals occurring between ~23 to ~30 hpf were suggested to be generated by both SMCs and fast muscle

cells (FMCs) [188]. Thus, the attenuation of Ca^{2+} activities during SP2 period implicated that TPC2 might also be involved in FMC-mediated Ca^{2+} activities.

3.3.1.2 Effects of TPC2 inhibition on the motility of zebrafish embryos

Kelu's continuation studies included an investigation on the spontaneous and touch-evoked coiling activity of zebrafish embryos. Substantial impairment in motility was noted for TPC2 morphants compared with the normal activity seen with WT embryos. Previously, Cheung et al. have suggested that the cytoplasmic component of the SP1 Ca^{2+} signals, as well as the early phase of SP2 Ca^{2+} activities (~23 to ~24 hpf) which was entirely cytoplasmic, could contribute to the spontaneous trunk coiling activity in zebrafish embryos [128]. Given TPC2 morphants displayed a disruption in this early trunk movement, an association between TPC2-mediated Ca^{2+} signals in the SMC during that period (i.e. from ~17 to ~24 hpf) and the spontaneous coiling activity is proposed, which awaits to be ascertained. Conversely, the burst swimming of zebrafish larvae which occurs after ~27 hpf [189] was not mediated by SMCs but facilitated mainly by the FMCs [190], which only started to develop after ~20 hpf [191]. Since TPC2 morphants showed a disruption in their evoked coiling activity, implicating that TPC2-mediated Ca^{2+} signals in the FMCs play a role in mediating such motility.

3.3.1.3 Pharmacological studies on the influence of TPC2 inhibition on Ca^{2+} activities in SMCs

Complementary evidence from pharmacological treatments with bafilomycin A1 and Ned-19 further supported the findings acquired via TPC2-MO treatment [129] (Appendix section 3.4.4 and 3.4.5). Thus Ca^{2+} signals of both late SP1 and the entire SP2 were abolished following bafilomycin A1 treatment after the start of SP1.

3.3.1.4 General review on the effects of TPC2 inhibition

As presented by the current data here in my study and those results in Kelu's study, TPC2 KD mediated via genetic or pharmacological methods resulted in a disruption of the SP1 and SP2 Ca^{2+} signaling profiles, which led to significant impairment of embryo motility. Thus it is proposed that TPC2 may play a role in mediating the SMC-exclusive SP1 signals that are associated with SMC differentiation and the spontaneous trunk coiling activity. Furthermore, TPC2 may participate in the early phase of SP2 (from ~23 to ~27 hpf) which could be responsible for the continued spontaneous coiling activity and the touch-evoked coiling activity. Its involvement in mediating the late SP2 signals (from ~27 to ~30 hpf), which contribute to the FMC-induced burst swimming activity, cannot be ruled out either. Together, these results indicate the importance of TPC2 in regulation of the ET coupling during SP1 and regulation of SMC and FMC contraction [129]. Future studies are required to clarify whether an interplay between TPC2 and IP_3Rs/RyRs occurs in these regulatory events.

3.3.1.5 Proposal of functional regulatory role of TPC2 in SMC differentiation in zebrafish

Zebrafish embryos injected with TPC2 MO displayed significant trunk curvature (downward bending of the trunk), indicating abnormalies in the development of the trunk musculature (Figure 3.6, 3.7 and 3.8). The impairment produced by TPC2 KD was not merely an effect of general developmental delay, as the characteristic phenotype was still apparent until at least ~48 hpf (Figure 3.10). Apart from a decrease in SMC number i.e. myofiber number (Figure 3.9), the myofibril morphology of the SMCs was also significantly altered in the TPC2 morphants (Figure 3.9), as evidenced by the wavy myofibers, shorter myofiber length and width, shorter somite length and shorter myotome

width. All these indicated a disruption of myofibrillogenesis by TPC2 KD and once again supporting the speculation that TPC2 is crucial for the SMC differentiation.

Complementary results from Kelu's study indicated that application of higher dosage of TPC2-MO led to more severe perturbation of the trunk musculature development and myofibril morphology, indicating the inhibitory effects mediated by TPC2 KD on trunk and myofibril development occurred in a dose-dependent manner. Notably, somites were only modestly affected (i.e. slightly U-shaped) when a lower MO concentration was used, but the effect was more significant (i.e. U-shaped) with higher TPC2-MO concentration application, suggesting a dose-dependent inhibition on somite development. And similarly, the characteristic trunk curvature was still apparent until at least ~48 hpf (Appendix section 3.4.6), confirming the idea that factors other than general developmental delay was involved in the impairment. Importantly, pharmacological treatment using bafilomycin A1 and Ned-19 resulted in a dose-dependent perturbation of the trunk development similar to that seen with TPC2 morphants.

Taken together, it is suggested that disruption of TPC2-mediated Ca^{2+} signals via genetic or pharmacological approach is associated with the developmental impairment of the SMC. And given the evidence described previously, TPC2 is thus implicated in a functional role in regulating SMC differentiation in zebrafish embryos, likely via a mechanism that involves lysosomal Ca^{2+} release modulated by TPC(s). In fact, recent studies have already indicated the influence of impaired SMC-mediated Ca^{2+} activities on myofibril development [128][165]. Hence, the identification of TPC2's involvement suggested a new pathway in regulation of SMC differentiation.

3.3.1.6 Localization of TPC2 in SMCs

A temporal expression profile of TPC2 in SMCs in intact zebrafish embryos and muscle cell cultures was revealed using the anti-TPC2 antibody [129]. Thus a shift in TPC2 expression pattern was observed: from homogeneous, punctate pattern (~16-18 hpf *in vivo*; after ~24 hours *in vitro*) to more organized, distinct banding pattern (~20-24 hpf *in vivo*; after ~48 hours *in vitro*). The observed switches in expression pattern indicated that TPC2 might be involved in diverse roles during SMC differentiation. Localisation study identified TPC2 labelling adjacent to the sarcomeric I-band. In the centre of I-band is Z-disc, a region abundant with a multitude of proteins, hence a close association with intracellular signalling (mainly for mechanosensation and mechanotransduction) [192]. Notably, certain Ca^{2+}-sensitive proteins such as calcineurin [193] and muscle lim protein [194] have been identified in the Z disc, implying that they may participate in TPC2-mobilised Ca^{2+} activities during myogenesis, hence mediating the ET coupling [128]. Localisation of TPC2 and LAMP1 labelling near the I-band also indicated that TPC2 might be associated with the EC coupling. Briefly, EC coupling starts with a neuronal stimulation, generating an action potential which travels along the sarcolemma, giving rise to Ca^{2+} release from the SR, followed by Ca^{2+} binding to troponin, thus exposing the myosin-binding sites on actin which allows for subsequent binding of myosin, resulting in muscle contraction. Since I-band contains thin filaments composed of actin proteins, and given the adjacent localisation of TPC2 and LAMP1 to I-band, hence it is likely that TPC2 might involve in EC coupling, possibly via lysosomal Ca^{2+} release.

The finding of co-localisation of LAMP1 with myosin bands juxtaposed to I-band in SMCs of intact zebrafish embryos [129] is in agreement with that revealed previously [195]. Thus a juxtaposition of lysosomes and related organelles with the transverse tubules (t-tubules; which are found in the Z line [196]) at the level of I-band was revealed in frog

skeletal muscle fibres.

On the other hand, a juxtaposition of both RyR and IP_3R type III with the I-band in SMCs was also identified. The close association between these three Ca^{2+} releasing channels as revealed in the localisation studies thus leads to the speculation that TPC2-mobilised Ca^{2+} release from lysosomal stores may trigger the RyR/IP_3R-mobilised Ca^{2+} release from the SR, likely via the CICR mechanism [35], which gives rise to the EC coupling.

Subcellular localisation study using muscle cell cultures demonstrated nuclear and peri-nuclear localization of TPC2 and LAMP1 occurring ~24 hours [129]. This corresponds to ~18 hpf *in vivo*, when SMC differentiation is happening. Interestingly a peri-nuclear localisation was also revealed for RyR and IP_3R type III during the same period. Thus it is likely that TPC2 may regulate the RyR- and/or IP_3R-mediated Ca^{2+} signals owing to their co-localization at around the same time. Given IP_3Rs are suggested to be responsible for the nuclear Ca^{2+} signals in early SP1 [128] which contributes to ET coupling [170], one may speculate that TPC2 may participate in the IP_3R-mediated nuclear Ca^{2+} signalling, possibly by serving as an upstream trigger, and hence a role in ET coupling as proposed earlier in my study. Nuclear and peri-nuclear localisation of TPC is not atypical as previous report has shown NAADP-mediated Ca^{2+} release from the nucleus in isolated neurons of *Aplysia* [197], also TPCs-mediated Ca^{2+} release near the peri-nuclear region in mouse spermaids has been demonstrated [127].

3.3.2 In vivo study of DrTPC3 in zebrafish

3.3.2.1 *In situ* hybridization of whole mount embryos

In situ hybridization of zebrafish embryos at 24 hpf stage was performed using DIG-labelled antisense probes which hybridized to *DrTpcn1*, *DrTpcn2* and *DrTpcn3* mRNA respectively. Findings revealed the presence of *Tpcn3* in the blood cells near the tail, in the region where intermediate cell mass (ICM) and posterior blood island (PBI) are located (Figure 3.11).

ICM is the site where primitive hematopoiesis, more precisely primitive erythropoiesis, takes place [198-200]. One of the major transcription factors for this process is the zinc-finger transcription factor *gata1*, which is expressed very early during zebrafish embryo development, around 4-5 somites stage (~12 hpf) and eventually gives rise to the first circulating blood cells [198, 201]. Primitive erythropoiesis stops around 24 hpf as indicated by diminishing levels of hematopoietic transcription factors in the ICM [202]. It is followed by a transient wave of hematopoiesis in the PBI, also known as caudal hematopoietic tissue (CHT). After circulation begins around 24 hpf, *gata1* expression decreases in the ICM but not in the PBI, indicating a shift in the site of blood development. This transient wave only happens for a brief period, and is also known as the first wave of definitive hematopoiesis, representing a transient wave between primitive and definitie hematopoiesis [203]. Expression of *Tpcn3* gene in these regions thus implicated it a role in hematopoiesis. Therefore future studies on identifying the functional role(s) of TPC3 in such process(es) would definitely provide deeper understanding of the NAADP/TPC-mediated mechanisms in similar processes, particularly that zebrafish share a lot of similarities in hematopoiesis with other vertebrates which confer it an excellent model to study human diseases related to hematopoiesis.

Since expression was only investigated at 24 hpf, the spatial pattern of TPC3 at different

zebrafish developmental stages cannot be assessed here. Further studies are definitely required to look into the expression pattern and also temporal profile of expression using *in situ* hybridization, RT-qPCR, western blotting as well as immunofluorescence studies with the custom-made and purified anti-DrTPC3 antibody.

3.3.2.2 Investigation of DrTPC3-mediated Ca^{2+} signalling in the development of the SMCs in zebrafish embryos

The effects of TPC3 KD by MO approach on the muscle-generated Ca^{2+} signals were also demonstrated. Ca^{2+} signals were not detected until ~19 hpf, and negligible signals were observed after ~21 hpf (Figure 3.5C), such delay in Ca^{2+} signals leads to a speculation that it may be resulted from general developmental delay. However, data obtained from the average spike frequency revealed a distinct pattern from that seen with the SP1 of the controls (Figure 3.5D), indicating that TPC3 KD produced an impairment of the Ca^{2+} signaling in both SP1 and SP2 and that general developmental delay is not the major cause of such disruption. Importantly, distinct patterns in average spike frequency were recorded for TPC2 ad TPC3 morphants, suggesting that the impairment appears to come from different sources.

3.3.2.3 Brief conclusion

Little is known concerning TPC3 compared with the other two TPC isoforms TPC1 and TPC2. It has been shown that TPC3 is broadly present in deuterostomes, but it evolved into a pseudogene in humans and other primates [69]. And interestingly, this pseudogene is richly expressed in a sequence tag cluster found in the reproductive organs. Therefore characterization of TPC3 functions would definitely provide better insights into the evolution of the TPC family.

3.3.3 Future plan

The findings presented here were based on MO KD as well as pharmacological treatment, since some off-target effects generated by MO cannot be avoided even they are lowered to a minimum with the inclusion of p53 MO, making it difficult to distinguish between specific and non-specific effects. Interruption of other signalling pathways and transcription factors could happen with pharmacological agents, therefore it is vitally important to validate the findings with robust controls. The Crispr/Cas9 system has been increasingly implemented in zebrafish and other animal models. This system has been proved to provide better alternatives to other gene KD approaches due to its high efficiency at generating mutations, which has been extensively reviewed [204]. Therefore it would be very useful indeed to compare the phenotypes and effects on Ca^{2+} signalling etc. between TPC2 mutants generated by different means of gene KD/KO. Although the partial rescue produced by the rescue construct has already provided preliminary evidence that the MO-generated effects were TPC2-specific, it would definitely be better and more compelling if consistent results can be obtained from the Cripsr/Cas9 KD.

A suggestion has been raised on the multiple functional roles of TPC2 in zebrafish embryogenesis (see previous discussion). Recall that a slight edema was observed with TPC2 morphants at ~48 hpf, this suggests that TPC2 may in addition play a role in cardiac function. Interestingly, a recent study demonstrated an essential role of NAADP-mediated modulation of couplon activity in eliciting spontaneous diastolic Ca^{2+} transients in isolated mice cardiac myocytes and arrhythmias in the intact animal [205]. Thus, it would be useful to explore how TPC2 KD is related to the abnormalies seen with the heart during zebrafish embryogenesis.

An impairment in spontaneous coiling and touch-evoked responses after TPC2 KD was demonstrated, indicating an interruption in both the motility and behaviour, which may be

arisen from the severity of the muscle deformities observed in TPC2 morphants; it is also possible that TPC2 KD may alter the development of the primary neurons and the formation of neuromuscular junctions with the SMC. Previous evidence has in fact implicated NAADP signalling in an essential role in neuronal development [131]. Thus, it would be useful to investigate the influence of TPC2 KD on the development and functions of heart, development of primary motor neurons and the formation of AChRs in the trunk of zebrafish.

On the other hand, future studies exploring the roles of TPC3 in zebrafish embryogenesis is equally important, particularly since preliminary evidence in the current study has shown its presence during the developmental stage of zebrafish embryos. TPC1, however, was not inspected in my zebrafish study except in the failed attempt to determine its localisation by *in situ* hybridization; still one cannot rule out its role in zebrafish embryogenesis. Previous findings have shown its importance for NAADP action in addition to the more well-characterised TPC2 [68], and more intriguing are its distinct effects in endolysosomal trafficking shown by the removal of TPC1 or TPC2 which suggested differential roles in endo-lysosomal trafficking [86]. Does this imply that TPC1 will also play a dissimilar role to TPC2 in other key physiological processes? Such speculation needs to be ascertained by future investigations.

3.3.4 Conclusion

My research presents the first *in vivo* evidence that TPC2-mediated Ca^{2+} signalling is both essential and necessary for the development of SMCs in intact zebrafish embryos. By using a reverse genetic approach through anti-TPC2 MO treatment to knockdown TPC2, together with the aequorin-based luminescence detection, the characteristic SP1 and SP2 SMC-generated Ca^{2+} signalling signatures [128] were significantly interrupted after TPC2 KD. In addition, such MO-based TPC2 KD resulted in a characteristic phenotype with a downward bending of the trunk, whereas somites were affected to a lesser extent as the chevron shape was still apparent. Such downward bending of the trunk was still observed at ~48 hpf, indicating the impairment was not a result of general developmental delay. Moreover, whole-mount immunohistochemistry revealed a disruption in the formation and organization of the myofibers as well as the sarcomeric patterning in SMCs of TPC2 morphants. Together, these data implicated TPC2 in an essential role during the development of SMCs in intact zebrafish embryos. On the other hand, a continuation study performed by my collaborator Mr Kelu JJ showed that Ca^{2+} signals in both SP1 and SP2 phases were completely abolished when higher doses of MO was used to knockdown TPC2, which also led to more severe effects in the gross and fine structures of the trunk, suggesting that the inhibition elicited by MO-based TPC2 KD followed a dose-dependent manner. Furthermore, the aforementioned disruption produced by genetic KD was supported, to a certain extent, by the pharmacological treatment with bafilomycin A1 and Ned-19. Regarding the spatial characteristics, both TPC2 and lysosome were shown to be expressed adjacent to the I-band region of sarcomeres with a striated pattern *in vivo* and *in vitro*. Similar to TPC2, IP_3Rs and RyRs were also shown to be co-localized in a region near the I-band *in vitro*, suggesting that an interplay among these three Ca^{2+} release channels may occur which mediates Ca^{2+} signalling during muscle development, perhaps

through the "trigger" hypothesis, whereby a small local Ca^{2+} release from the acidic stores via TPC2 triggers additional Ca^{2+} release from either RyRs and/or I_3Rs through CICR mechanism.

In conclusion, these findings provide exciting and convincing evidence which implicates a novel role for TPC2 during myogenesis of intact zebrafish embryos, in that TPC2 may contribute to the triggering of muscle-generated Ca^{2+} signals, which are crucial for the development and function of SMCs, thus adding new insights into the complex Ca^{2+} signalling system responsible for skeletal muscle differentiation and function in vertebrates. On the other hand, the preliminary evidence also provides interesting clues about the involvement of TPC3 during embryogenesis in zebrafish and future investigations will be crucial for understanding its definite role(s), thereby additionally expanding our understanding on the scope of the TPC family evolution.

3.4 Appendix

3.4.1 Ca^{2+} signalling profile of SMC with p53-MO injection (Adapted from Kelu et al., 2015 [129])

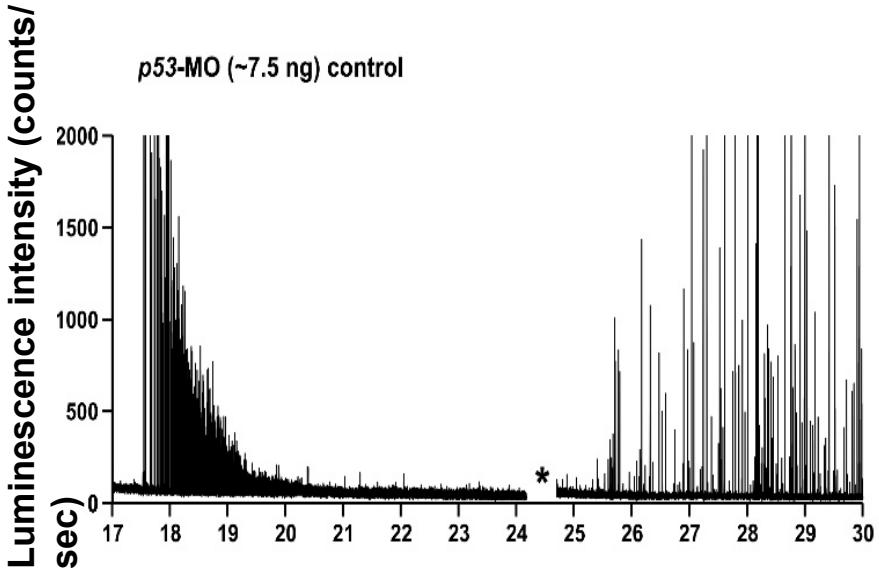

3.4.2 Ca^{2+} signalling profile of SMC with TPC2-MO + p53-MO co-injection followed by rescue construct injection (Adapted from Kelu et al., 2015 [129])

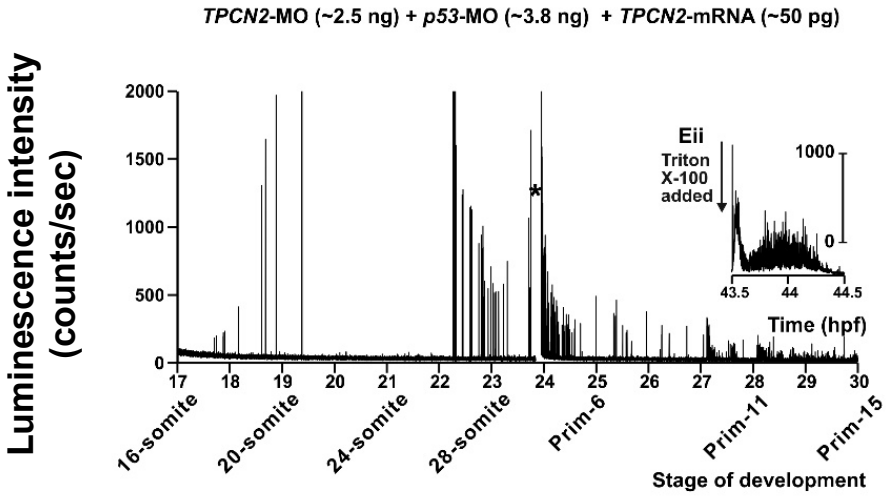

3.4.3 Ca^{2+} signalling profile of SMC with TPC2-MO (5 ng) + p53-MO co-injection (Adapted from Kelu et al., 2015 [129])

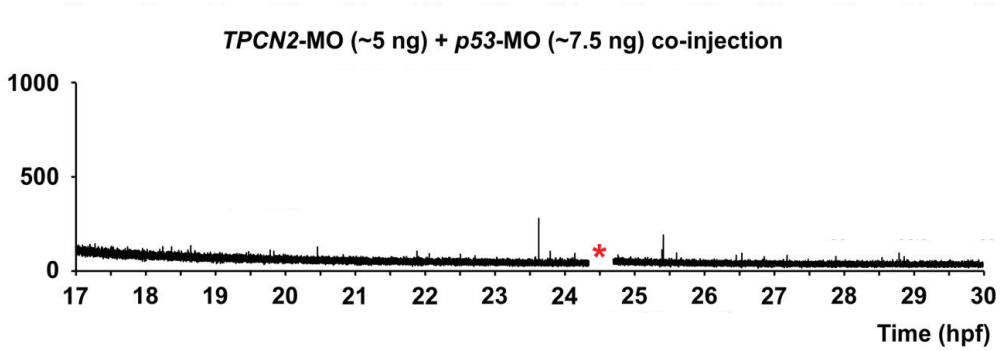

3.4.4 Ca^{2+} signalling profile of SMC with 1 µM bafilomycin A1 treatment (Adapted from Kelu et al., 2015 [129])

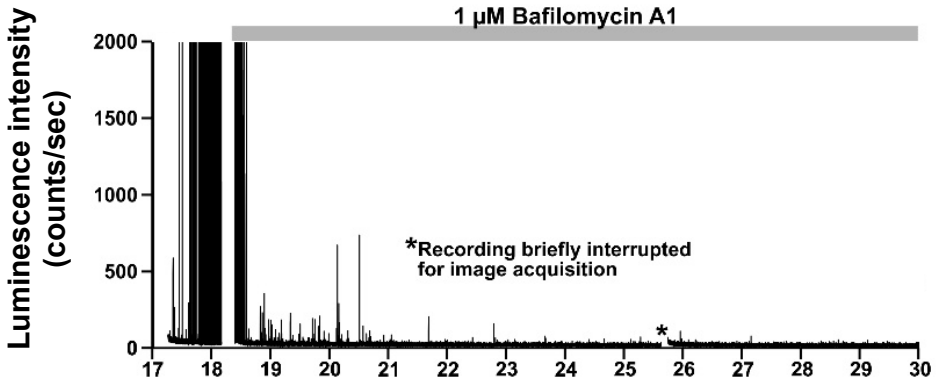

3.4.5 Ca^{2+} signalling profile of SMC with 250 µM Ned-19 treatment (Adapted from Kelu et al., 2015 [129])

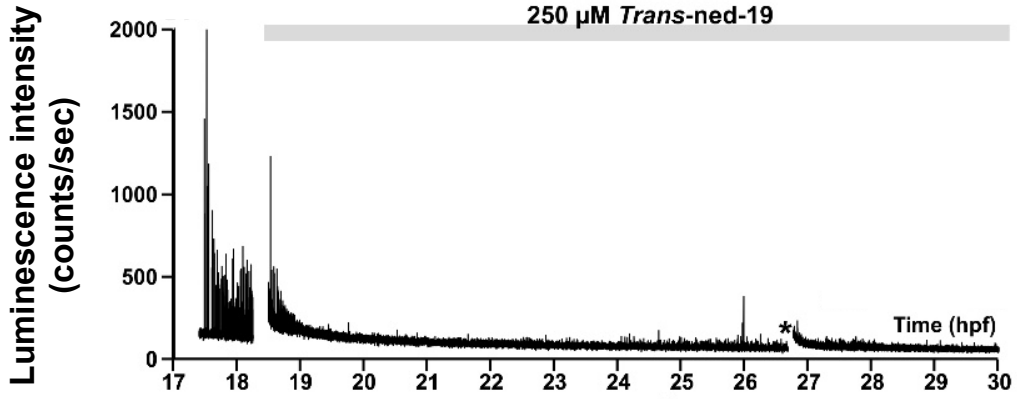

3.4.6 Gross and fine structure of the trunk musculature in zebrafish embryo injected with 5 ng TPC2-MO (+ p53-MO) (Ei-Rv: 24 hpf; Di-Dii: 48 hpf) (adapted from Kelu et al., 2015 [129])

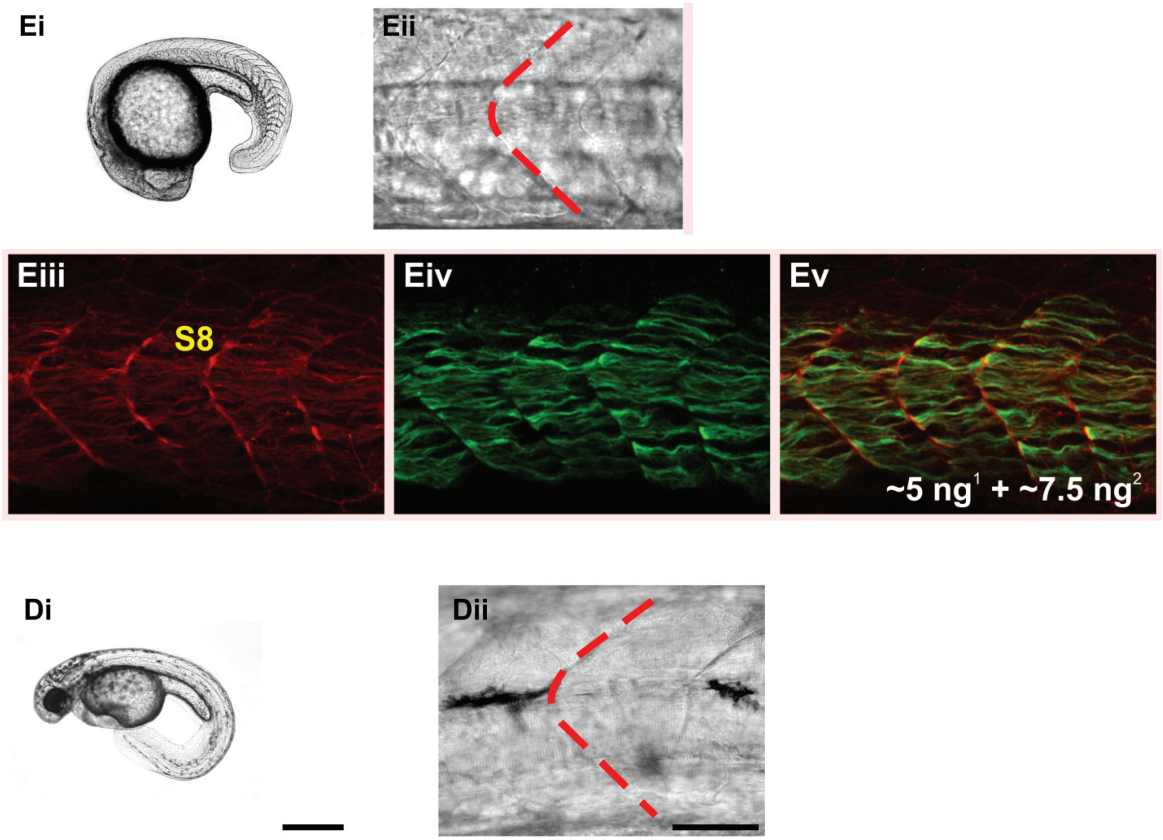

Chapter 4:

TPC2 and Adipogenesis

4.1 Introduction

4.1.1 Adipogenesis – general introduction

Adipocytes are derived from pluripotent mesenchymal stem cells (MSC) in a process known as adipogenesis [206-208]. They have the capacity to differentiate into different lineages including adipocytes, myocytes, osteoblasts, chondroblasts and neurocytes [209-211]. White adipose tissue (WAT) which comprises primarily white adipocytes is a major type of fat present in adult humans. In addition to its tradition role in lipid storage and insulin signalling, recent studies have recognised paracrine and endocrine function of WAT, suggesting a crucial role in regulation of whole body metabolism and homeostasis [212]. Thus, excess of WAT which is caused by increased adipocyte size and number is correlated with obesity and related metabolic diseases, indicating that an understanding of the complexities of adipogenesis and also adipocyte dysfunction is of vital significance to human diseases [213].

Adipogenesis is a complex and highly coordinated yet not fully elucidated process characterised by a sequence of gene activation events strictly regulated by a multitude of distinct factors [206, 207, 214]. Cell culture studies have been crucial for identifying and characterising the pivotal steps of adipogenesis. Two commonly used *in vitro* cell models including the pluripotent C3H10T1/2 cells and the committed preadipocyte cell line 3T3-L1, have faithfully recapitulated the processes of adipogenesis *in vivo* [208, 215, 216].

4.1.2 Adipocyte development and transcriptional regulation of adipogenesis

Adipogenesis occurs in two main stages: determination (also known as 'commitment') phase and terminal differentiation phase.

4.1.2.1 Determination phase: MSCs to preadipocytes

The initial step of adipogenesis involves the conversion of MSCs to preadipocytes (Figure 4.1). The molecular mechanism underlying the early stages of differentiation are poorly elucidated [206, 215]. Pivotal mediators identified to promote or block the commitment step include the BMP family members BMP2 and BMP4 [218, 219], Wnt [220-222] and Hh (hedgehog) [223-225].

4.1.2.2 Terminal differentiation phase: Preadipocytes to adipocytes

Following commitment, preadipocytes go through several rounds of proliferation to reach confluence (Figure 4.1) [206]. Cells at post-confluence stage are induced to differentiate to adipocytes by addition of differentiation inducers, a hormonal cocktail consisting of high concentrations of insulin or physiological levels of insulin-like growth factor 1 (IGF1), glucocorticoids such as dexamethasone, and an intracellular cyclic AMP (cAMP)-elevating agent such as 3-isobutyl-1-methylxanthine (IBMX) or forskolin [206]. Cells enter a transient growth arrest state [208, 215] followed by mitotic clonal expansion (MCE) [207, 216, 226] and elevated expression of 'immediate early' genes such as CCAAT/enhancer binding protein (C/EBP) β and δ during the first couple of hours post-induction (Figure 4.1). Subsequent to these early events is the activation of master transcription factors C/EBPα and peroxisome proliferator-activated receptor γ (PPARγ), which is characterised by a second growth arrest followed by terminal differentiation (Figure 4.1) [206, 207, 216, 226-228]. C/EBPα and PPARγ activate adipocyte-specific

genes responsible for inducing the synthesis of enzymes, transporters, receptors as well as structural proteins, all of which are essential for acquisition of adipocyte phenotype [206, 208].

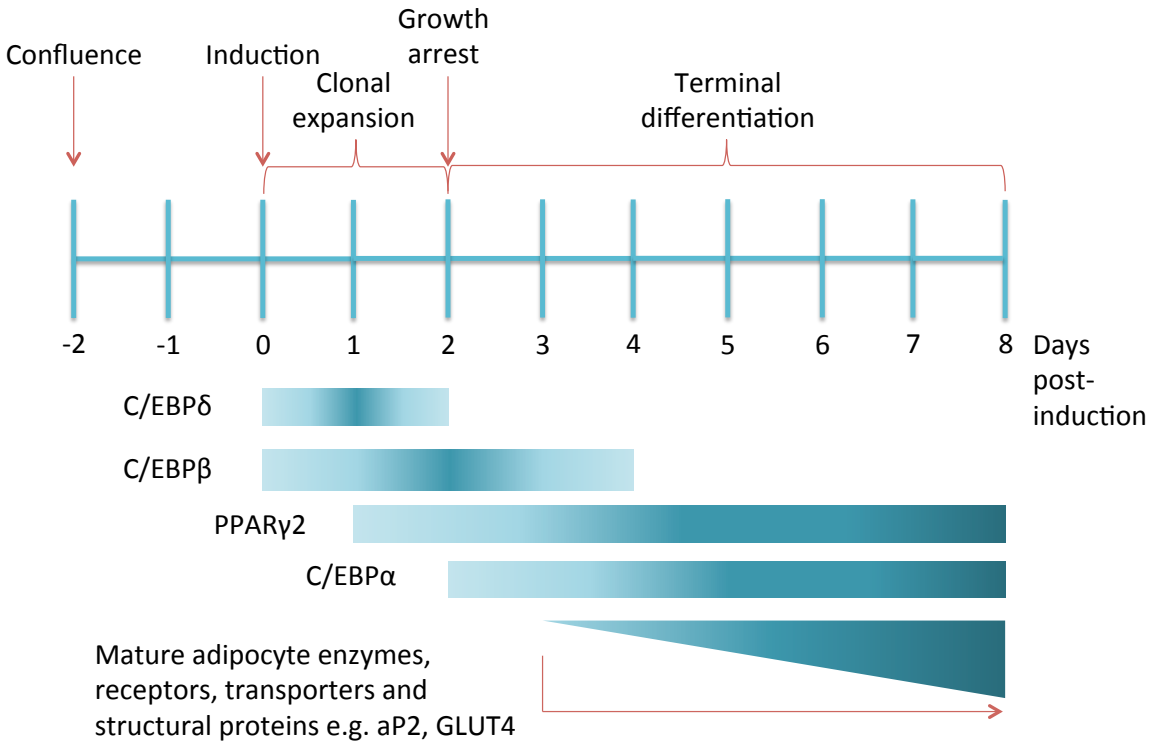

Figure 4.1: Expression of major molecular regulators of adipogenesis during differentiation (Modified from Dr Ruth Tunn; in preparation)

C/EBPs and PPARγ are regarded as integral members of the genetic cascade in adipogenesis and their roles have been extensively reviewed in different literatures [206-208, 215, 216, 226-228, 230-236]. Albeit debatable [232], it seems that C/EBPβ does not require PPARγ to induce C/EBPα expression [237]. Also, C/EBPα and PPARγ can feed back to stimulate their own expression as well as that of the other. Besides, forced expression of either C/EBPα or PPARγ (and its ligand) induces adipogenesis without addition of exogenous inducing agents. While PPARγ is necessary and sufficient to transactivate many adipocyte-specific genes, C/EBPα is needed for the acquisition of insulin sensitivity in adipocytes [238].

4.1.3 Intracellular cAMP signalling in adipogenesis

4.1.3.1 cAMP

During terminal differentiation, factors that elevate intracellular cAMP such as IBMX or forskolin significantly enhance the induction of the adipogenesis program [206].

IBMX is a non-specific phosphodiesterase (PDE) inhibitor which also enhances adenylyl cyclase activity through blockade of inhibitory G protein G_i (precisely, it inhibits basal G_i function) [239]. The resulting enhanced intracellular cAMP level is correlated with critical events during early differentiation which include inhibition of Wnt10b [240] and Sp1 [241] and induction of C/EBPβ [242-244]. Besides, cAMP acts synergistically with PPARγ ligands to regulate the transcriptional activity of PPARγ [245]. Furthermore, implications of cAMP in the production of endogenous PPARγ ligand during the initial differentiation stages have been reported [246-250]. To note, elevated cAMP levels also induce the activity of CREB, an essential transcriptional activator for adipogenesis [251, 252] (detailed description of CREB see section 4.1.3.3).

The mechanisms underlying the cAMP-mediated effects in adipogenesis have been attributed to two intracellular cAMP receptors, the classic cAMP-dependent protein kinase (PKA) (Figure 4.2) and the lately revealed exchange protein activated by cAMP (Epac), a family of GTP exchanging factors for the small GTP-binding proteins Rap1 and Rap2 [253]. The coexistence of these two pathways has been significantly demonstrated in different cell types and they are found to converge on same molecular targets via independent operating systems [254-257]. In adipogenesis of preadipocytes, however, the definitive roles and underlying mechanisms of PKA and Epac are only partially revealed, with the cAMP/PKA pathway seems more perplexing as both stimulatory and inhibitory effects have been reported while Epac looks to be more proadipogenic.

4.1.3.2 PKA and Epac

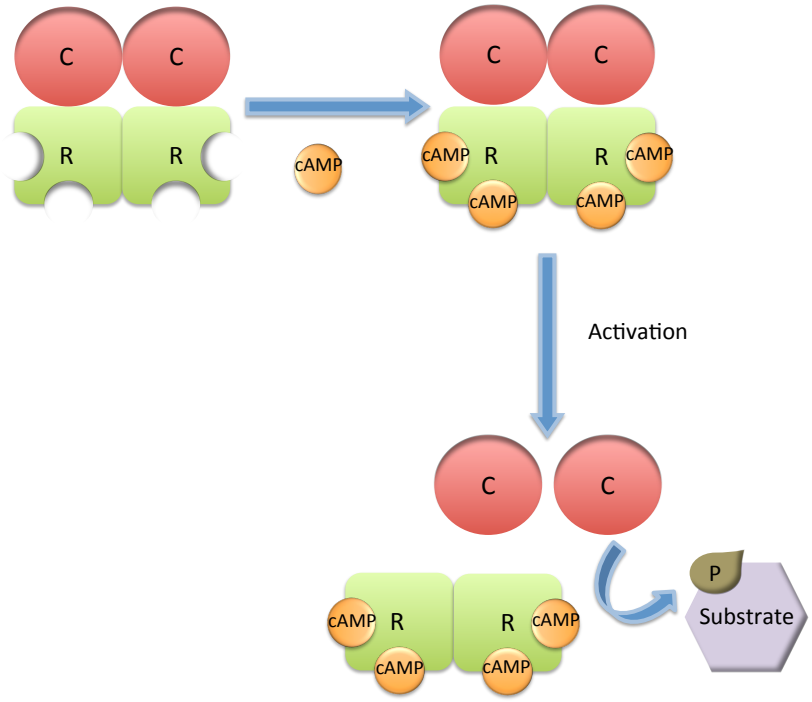

Figure 4.2: PKA structure and its activation. In its inactive state, PKA exists as a heterotetramer comprising two regulatory subunits (R) and two catalytic subunits (C). Activation of PKA involves binding of cAMP to R (2 cAMP molecules per R) of the kinase which induces a conformational change, releasing C from the holoenzyme complex. The free C displays catalytic activity and interacts with proteins to phosphorylate their target substrates.

PKA is a serine-threonine kinase which regulates cAMP-mediated effects via phosphorylation of downstream targets [259]. It exists either as an inactive holoenzyme comprising two catalytic (C) subunits and two regulatory (R) subunits, or as dissociated subunits. Four different forms of R subunits exist (RIα, RIβ, RIIα and RIIβ) which contribute to different PKA isoforms and play essential role in controlling PKA activity (Figure 4.2). It has been well documented that different PKA isoenzymes are involved in different and cell-specific functions in controlling cell growth and differentiation [260-266].

In adipogenesis, the use of PKA C subunit inhibitors H89 and mPKI showed that PKA's kinase activity was not required for cAMP's proadipogenic effect in 3T3-L1 preadipocytes

[249, 267-269]. Also, PKA activation was involved in EGF-mediated inhibition of adipogenesis, implicating Pref-1, a well-described inhibitor of adipogenesis, might act through PKA activation to inhibit differentiation. Besides, expression studies have demonstrated a shift in balance of PKA C and R subunits during adipogenesis [267]: PKA activity was shown to increase during the first 24 hours post-induction and decline subsequently, accompanied by a corresponding upregulation of R subunits expression. Such shift was later suggested to be crucial for the differentiation events and that activation of R subunits as well as Epac was needed for 3T3-L1 preadipocyte adipogenesis [268].

Among all R subunits, RIIb subunit was shown to be abundantly expressed during mouse and human adipose tissue development [270-273] and also adipogenesis in 3T3-L1 preadipocytes and primary human preadipocytes [273], suggesting its pro-adipogenic effect during differentiation.

Epac KD expression study revealed that activation of Epac is necessary but not sufficient for 3T3-L1 adipogenesis [268] while another study reported successful adipogenesis by replacing selective Epac analog with IBMX in 3T3-L1 preadipocytes [274]. Interestingly, the latter study also indicated a requirement of cAMP/PKA signalling for MCE, albeit MCE is not essential for 3T3-L1 adipogenesis [274]. On the other hand, earlier findings revealed that activation of PKA or Epac alone with selective PKA or Epac analog failed to induce adipogenesis in both 3T3-L1 preadipocytes and human mesenchymal stem cells (hMSCs) [275, 276]; by contrast a synergistic effect by PKA and Epac has been suggested to promote adipogenesis by another group: downregulation of Rho and Rho-kinase activity by PKA impaired the proadipogenic insulin/IGF1 signalling which was restored by Epac activation in 3T3-L1 cells [275]. Similarly, in human mesenchymal stem cells derived from adipose tissue (hMADS), activation of both cAMP/PKA and cAMP/Epac

signalling pathways was required to promote adipogenesis [276]. In isolated hMSCs, Epac was demonstrated to act via the Rap/PI3K/PKB/CREB signalling pathway, activating CREB and hence upregulation of PPARγ expression which ultimately enhancing adipogenesis [277]. The same study also indicated a proadipogenic effect of PKA, which possibly converges at the level of CREB, but acts via a distinct mechanism of action from Epac due to its inability to activate PI3K and PKB [277]. The discrepancies between these studies could be due to the different concentrations of drugs used, which were not clearly mentioned in the reports. Collectively, the precise mechanism for cAMP-mediated adipogenesis is still elusive.

4.1.3.3 Functional roles of CREB in adipogenesis

Transcriptional activation of CREB is induced by phosphorylation from various kinases, such as PKA and Ca^{2+}/calmodulin-dependent protein kinases, on serine 133 (Ser133) residue [278]. Such phosphorylation is obligatory for CREB-stimulated gene transcription [279]. In addition to its role as an essential transcriptional activator of adipogenesis, CREB has also been implicated as an intermediate in the cAMP signalling pathway during adipocyte differentiation.

Activated CREB stimulates C/EBPβ expression which in turn triggers expression of C/EBPα and PPARγ, the master adipogenic transcription factors [216, 219, 244, 252, 277, 280]. Importantly, forced expression of constitutively active CREB initiates adipocyte differentiation in 3T3-L1 preadipocytes while dominant-negative CREB inhibits differentiation [251]. The significance of CREB is further highlighted by the impairment of adipogenic capacity in CREB-deficient mouse embryo fibroblast [252]. Similarly, *in vivo* and *in vitro* findings demonstrate that small interfering RNA-mediated depletion of CREB and the closely related factor ATF1 inhibited adipogenesis [281]. Interestingly it

has been found that in 3T3-L1 preadipocytes, not only cAMP mimetics (acting via PKA) but also insulin signalling could phosphorylate (at Ser 133) and activate CREB; the insulin catalysed transcriptional activation occurs via a distinct mechanism though: the extracellular signal-regulated kinase 1/2 (ERK1/2) signalling pathway [282]. In addition, Epac may act through PI3K/PKB/PKD pathway to phosphorylate and activate CREB, leading to upregulation of PPARγ [277]. To note, cAMP-mediated activation of CREB also regulates gene expression of other key factors participated in the early adipogenesis e.g. stearoyl-CoA desaturase gene 1 [283], Wnt10b [240], cyclic nucleotide phosphodiesterase 3B [284], cyclin D1 [285] etc. Therefore, all these data suggested that CREB not only functions in early adipogenesis but also leads a pivotal role during later stage of differentiation.

4.1.4 Ca^{2+} signalling and adipogenesis

The role of Ca^{2+} signalling during adipogenesis is less well established and seems to be complex, as both pro-adipogenic and anti-adipogenic effects have been reported. Ca^{2+} signalling appears to regulate adipogenesis at the MCE stage and its effect on the cell cycle is mostly positive. Ca^{2+} transients are evident preceding DNA synthesis and during mitosis [286-290], a rise in CaM protein levels is also observed before DNA synthesis. Depletion of ER IP_3-sensitive Ca^{2+} pools with thapsigargin blocks DNA synthesis, protein synthesis and nuclear transport, which eventually leads to cessation of cell division [287, 291-293]. Ca^{2+}/CaM is necessary for regulating cell proliferation: proliferation is accelerated by overexpression of CaM [287, 294, 295]; by contrast, both proliferation and DNA synthesis are prevented by CaM antagonists or anti-CaM antibodies [287, 296-302]. Moreover, calcineurin and CaMKII, the two downstream targets of Ca^{2+}/CaM known to be involved in cell cycle regulation, interact with cell cycle-modulating proteins to

accelerate proliferation [287].

On the other hand, when treated with thapsigargin or a calcium ionophore A23187 during the early stage of differentiation (24-48 hours post induction), the resulting elevated intracellular Ca^{2+} concentration ($[Ca^{2+}]_i$) suppresses adipogenesis in both 3T3-L1 preadipocytes [303] and human preadipocytes [304]; by contrast, adipogenesis is promoted during the late stage (48-72 hours post induction) in human preadipocytes [304]. A similar biphasic regulatory pattern was also observed when treated with more physiological Ca^{2+} agonists including KCl and agouti protein in human preadipocytes [304]. Since thapsigargin and A23187 treatment will also cause intracellular Ca^{2+} store depletion, thus endogenous Ca^{2+} signalling will be disrupted, disguising highly specific signalling. Suppression of adipogenesis seen after Ca^{2+} chelator addition suggested that instead of elevated $[Ca^{2+}]_i$, it was store depletion that generated the inhibitory effect during the early stage. Such suppression was caused by a blockade of post-confluent mitosis [303], which was in agreement with the effects seen in cell cycle by Ca^{2+} signalling perturbation reviewed above. That the observed stimulatory effects at the later phase of differentiation may suggest a pro-adipogenic capacity for Ca^{2+} during terminal differentiation is rather controversial because the increased $[Ca^{2+}]_i$ triggered by pharmacological agents are less likely to mimic the physiological Ca^{2+} events happening during differentiation.

Effector proteins provide Ca^{2+} alternative means to regulate adipogenesis as they are recruited by Ca^{2+} to transduce the Ca^{2+} signals to affect transcription and thus mediating differentiation.

CaMKII has been shown to undergo a biphasic increase in its autonomous activity in 3T3-L1 preadipocyte differentiation: an initial increase during the first 15 hours post-induction, then a sharp decline at 24 hours, followed by a sustained increase from 24-48 hours [305].

By contrast, adipogenesis was effectively repressed with the inclusion of CaMKII inhibitors during 6-12 hours or 12-48 hours post-induction [305].

Another Ca^{2+} signal transducer, the phosphatase calcineurin, has also been implicated in adipogenesis. Activation of calcineurin by Ca^{2+}/CaM induces dephosphorylation of NFAT transcription factor, resulting in NFAT translocation to the nucleus and thus mediating transcription [306]. NFAT is present in differentiated but not undifferentiated adipocytes. It activates an aP2 reporter during 3T3-L1 preadipocyte adipogenesis and acts at a critical time point of 1-2 days post-induction [307]. Intriguingly, calcineurin inhibition by specific inhibitors overcomes the inhibitory effect of calcium ionophore-stimulated elevation of $[Ca^{2+}]_i$ on adipogenesis of 3T3-L1 preadipocytes, while constitutively active calcineurin impeded differentiation capacity [308].

Activity of a Ca^{2+}-activated protease, calpain, has been shown in adipogenesis of both 3T3-L1 preadipocytes [309, 310] and ST-13 preadipocytes established from adult primitive mesenchymal cells [311]. Calpain mRNA and protein are abundantly expressed in 3T3-L1 preadipocytes and levels decline during differentiation. Pharmacological inhibition of calpain represses adipogenesis by precluding the binding of c/EBPβ to the c/EBPα promoter [309]. Calpain is also involved in suppression of turnover of CHOP-10 [312] and CUP/AP-2α [313]. The former is a dominant-negative isoform of C/EBPβ present in growth-arrested preadipocytes while the latter is a transcriptional repressor of the C/EBPα gene [314]. Moreover, calpain degrades the cyclin-dependent kinase inhibitor p27 during the MCE phase of adipogenesis in 3T3-L1 cells, allowing growth-arrested preadipocytes to re-enter the cell cycle and undergo MCE [310]. Furthermore, calpain may be involved in degradation of mature ADD1/SREBP1, thereby inhibiting the production of endogenous PPARγ ligand. Collectively, calpain functions both positively and negatively during 3T3-L1 cell adipogenesis: stimulatory on the sequential events of

MCE while inhibitory as seen in degradation of ADD1/SREBP1 [315]. Intriguingly, calpain behaves differently in ST-13 preadipocytes, of which MCE is not obligatory for differentiation [311]. Thus pharmacological inhibition of calpain induces PPARγ and C/EBPα expression but impedes insulin-stimulated glucose uptake in these cells and expression of a dominant-negative μ-calpain also enhanced adipogenesis [311].

4.1.5 NAADP/TPC signalling in adipogenesis and physiological functions of adipocytes

Preliminary evidence suggesting a role for TPC2 in adipogenesis has been reported by Dr Ruth Tunn (in preparation). Thus *Tpcn2* mRNA level was shown to be transiently upregulated during early adipogenesis in C3H10T1/2 cells, due to the effects of IBMX-induced upregulation of cAMP levels. The same report also pointed to a transient reduction in *Tpcn1* mRNA level and an IBMX-induced downregulation of CD38 level during adipocyte differentiation. In addition, western blotting experiments demonstrated an expression of TPCs in C3H10T1/2 cells and immunofluorescence findings indicated a punctate distribution for mCherry-tagged TPCs and some co-localisation with a lysosomal marker. Together, TPC2 was implicated in a role in adipogenesis. A recent study has also indicated the participation of NAADP-mediated Ca^{2+} signalling pathway in insulin-stimulated glucose uptake and PPARγ-induced insulin sensitization in adipocytes [316]. Thus insulin-stimulated NAADP production occurred through CD38-dependent (by activation of both IR/IRS-1/PI3K/AKT and PKG signalling pathways) and CD38-independent (by activation of IR/IRS-1/PI3K/AKT pathway only) pathways, and NAADP induced $[Ca^{2+}]_i$ rises which mediated GLUT4 and GLUT1 trafficking to the plasma membrane, resulting in glucose uptake in adipocytes. Furthermore, it was demonstrated that PPARγ promoted NAADP production by upregulation of CD38, thereby enhancing

insulin-stimulated glucose uptake. Inhibition of the NAADP signalling pathway inhibited both insulin-stimulated and PPARγ-mediated GLUT4 and GLUT1 translocation, consequently blocking glucose uptake. CD38 KO resulted in a partial inhibition of insulin-stimulated glucose uptake but a complete inhibition of both PPARγ-mediated glucose uptake in adipocytes, as well as PPARγ-induced alleviation of glucose tolerance in diabetic mice. Hence it was indicated that NAADP signalling pathway is essential in mobilising PPARγ-induced insulin sensitization. In a recent study investigating NAADP transport, findings related to adipocytes were also reported [317]. Thus substantial NAADP uptake was found in adipocytes and pancreatic β-cells but not acinar cells when induced by high glucose. Additionally, external administration of NAADP was shown to promote insulin secretion in β-cells and glucose uptake in adipocytes through the NAADP-mediated Ca^{2+} signalling in the cells. That NAADP uptake was only seen in glucose-metabolizing cells indicated a selective role for NAADP in glucose homeostasis, operating via an auto-/paracrine manner, and thus implicating it a therapeutic potential as an antidiabetic agent.

4.1.6 The endolysosomal system plays a role in adipogenesis regulation

Recently the lysosomal degradative pathway of macroautophagy has been shown to modulate adipocyte differentiation [318]. Thus genetic inhibition of an essential macroautophagy gene autophagy-related 7 (*Atg7*) decreased lipid accumulation and protein levels of adipogenesis markers in 3T3-L1 cells. Atg5 KD or inhibition of autophagy or lysosomal function pharmacologically produced comparable results. Besides, adipocyte-selective mice KO of Atg7 demonstrated a switch from white adipocytes to brown adipocytes, resulting in decreased WAT mass but increased BAT mass, thereby an enhanced insulin sensitivity, fatty acid β-oxidation and lean body mass.

The findings were indicative of an important functional role of autophagy in regulating adipocyte development and differentiation which in turn controls the balance between white and brown adipocytes.

Recent genome-wide association study and genetic studies has suggested a correlation between the single nucleotide polymorphisms within the Niemann-Pick C1 gene (*NPC1*) and early-onset and morbid adult obesity as well as insulin resistance (independent of obesity) in human [319-322]. NPC1 protein mediates the trafficking of lipoprotein-derived lipids including cholesterol and fatty acids from late endolysomes to other cellular compartments, thus a role in regulating intracellular cholesterol homeostasis [323-325]. Disruption of this transport system results in accumulation of cholesterol and sphingolipids within the late endolysosomal compartment, known as Niemann-Pick disease type C (NPC), a rare lysosomal storage disease [326]. Later it was shown that in NPC1 heterozygous ($NPC1^{+/-}$) male mice, a substantial increase in weight gain was resulted from high-fat diet (HFD) but not low-fat diet (LFD) [327] and adipocyte hypertrophy was developed in those mice, implying a link to insulin resistance and glucose intolerance [328]. In human WAT adipocytes, a high NPC1 expression was detected [329, 330] which was upregulated in obesity, again implicating NPC1 in regulating adipocyte functions associated with obesity [330]. Subsequent study demonstrated that NPC1 is a critical regulator in maintaining insulin action at distinct levels in adipocytes [331]. Thus, pharmacological and genetic inhibition of NPC1 disrupted in the short term, the insulin signalling (decreased IRS1 expression with reduced Akt activation) and insulin-mediated GLUT4 translocation, and in the long term, downregulation of GLUT4 transcription. Taken together, evidence is accumulating to indicate the significance of NPC1 in modulation of insulin sensitivity in adipocytes.

4.1.7 Aims of this chapter

With the accumulating evidence showing the functional roles of the endolysosomal system in adipogenesis and also preliminary evidence demonstrating the participation of TPC2-mediated signalling in this process, this chapter therefore aims at exploring in more detail how the NAADP/TPC pathway regulates adipogenesis. Firstly, the effects of Ca^{2+} signalling on adipogenesis in C3H10T1/2 cells were investigated using specific pharmacological agents. The study was followed by examining the influence of blocking TPC2 pharmacologically, as well as the mechanisms underlying the regulation of TPC2 expression during adipocyte differentiation through investigations of potential upstream mediators. Finally, potential downstream effectors were studied to identify possible pathways mediated by TPC2 in regulating adipogenesis in C3H10T1/2 cells.

4.2 Results

4.2.1 Expression profile of TPCN2 mRNA during adipogenic differentiation

TPC2 mRNA levels in differentiating C3H10T1/2 cells subjected to standard adipogenic differentiation induction protocol involving treatment with MDI were determined using RT-qPCR (Figure 4.9). The TPC2 mRNA expression profile has been characterised previously by Dr Ruth Tunn (in preparation) but since a new batch of C3H10T1/2 cells (clone 10, passage 16; kindly provided by Dr Christodoulides of the Oxford Centre for Diabetes, Endocrinology and Metabolism) were used in my studies, it was important to check for any significant variations in mRNA expression pattern that arose from batch effects. As shown in Figure 4.9, TPC2 mRNA levels displayed a significant and transient increase early in differentiation at 4-8 hours post-induction. The level peaked at 8 hours with a more than 6 fold increase, and decreased after 24 hours to a level approximately 2.5 fold higher than the starting value, and remained approximately the same at 48 hours. The expression profile is similar to that seen in Dr Ruth Tunn's studies (Appendix 4.4.1), namely that a significant increase occurred at 4-8 hours, except that the peak occurred at 4 hours instead of 8 hours. Overall, both sets of data suggested a significant transient rise in TPC2 mRNA expression at 4-8 hours, followed by a significant decline at 24 hours with levels remaining about the same thereafter.

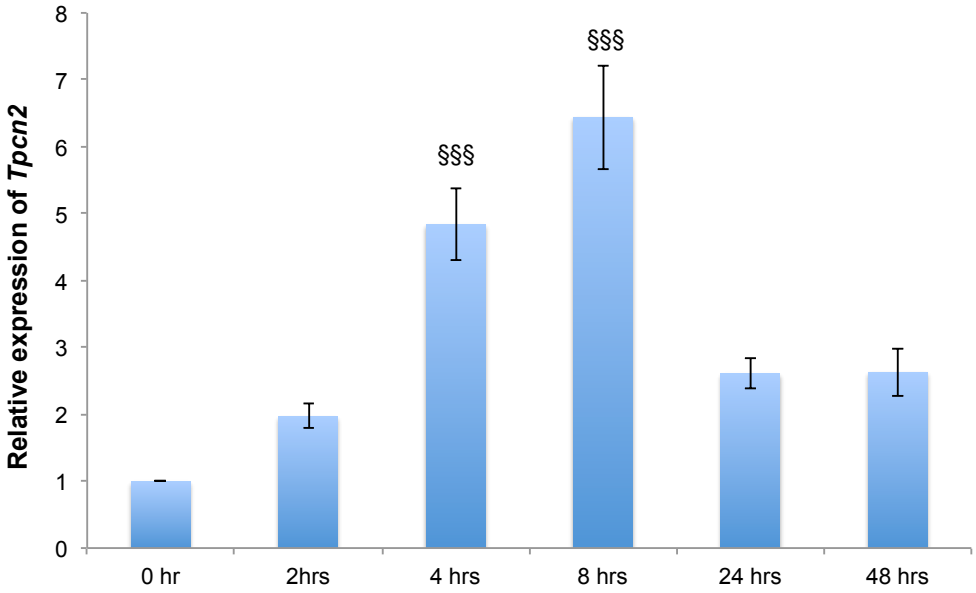

Figure 4.9: Expression profile of *Tpcn2* mRNA levels in differentiating C3H10T1/2 cells (hr(s)= hour(s)). Cells were subjected to standard adipogenic differentiation protocol at 2 days post-confluence. Values were normalised to the geometric mean of β-Actin mRNA expression and are presented as fold-change relative to 0 hr value. n=8. §§§p<0.01 (ANOVA, *post-hoc* Dunnet test vs 0 hr). Data presented as ± standard error of mean (SEM).

4.2.2 Effects of TPC2 downregulation on adipocyte differentiation

4.2.2.1 Measurement of adipogenesis - lipid droplet accumulation

The expression profile of TPC2 mRNA in differentiating C3H10T1/2 cells demonstrated a significant transient upregulation during early differentiation *in vitro*, suggesting a potential functional role for the TPC2 protein in that period. To examine whether TPC2 plays a part in adipogenesis, three stably transfected C3H10T1/2 cell lines (generated by David Gay) were employed, which contained either an empty vector (pLK0.1), a scrambled non-specific shRNA construct, or an anti-TPC2 shRNA construct. The inclusion of an independent TPC2-specific shRNA and a non-targeting control (pLK0.1) were used to eliminate potential off-target effects. Transfected cells were exposed to the standard adipogenic protocol and at 8 days post-induction, they were quantified for lipid accumulation using the AdipoRed staining protocol to determine the degree of differentiation. As shown in Figure 4.10A, very low levels of lipid accumulation were found in all cell lines without MDI induction. Maximal lipid accumulation was noted with untransfected (WT) cells stimulated with MDI induction. Both pLK0.1 and scrambled shRNA transfected cell lines showed comparable differentiation with the WT cells as indicated by high levels of lipid accumulation (Figure 4.10A) and Oil Red O staining after MDI induction (Figure 4.10C). In contrast, cells stably transfected with anti-TPC2 shRNA displayed a marked attenuation in differentiation, lipid accumulation was reduced by 50% compared with the WT cells (Figure 4.10C), and Oil Red O staining was similar to that of confluent preadipocytes maintained in GM without differentiation inducers throughout the entire time course (Figure 4.10C), suggesting a significant inhibition in the adipogenesis capacity of the TPC2KD cells.

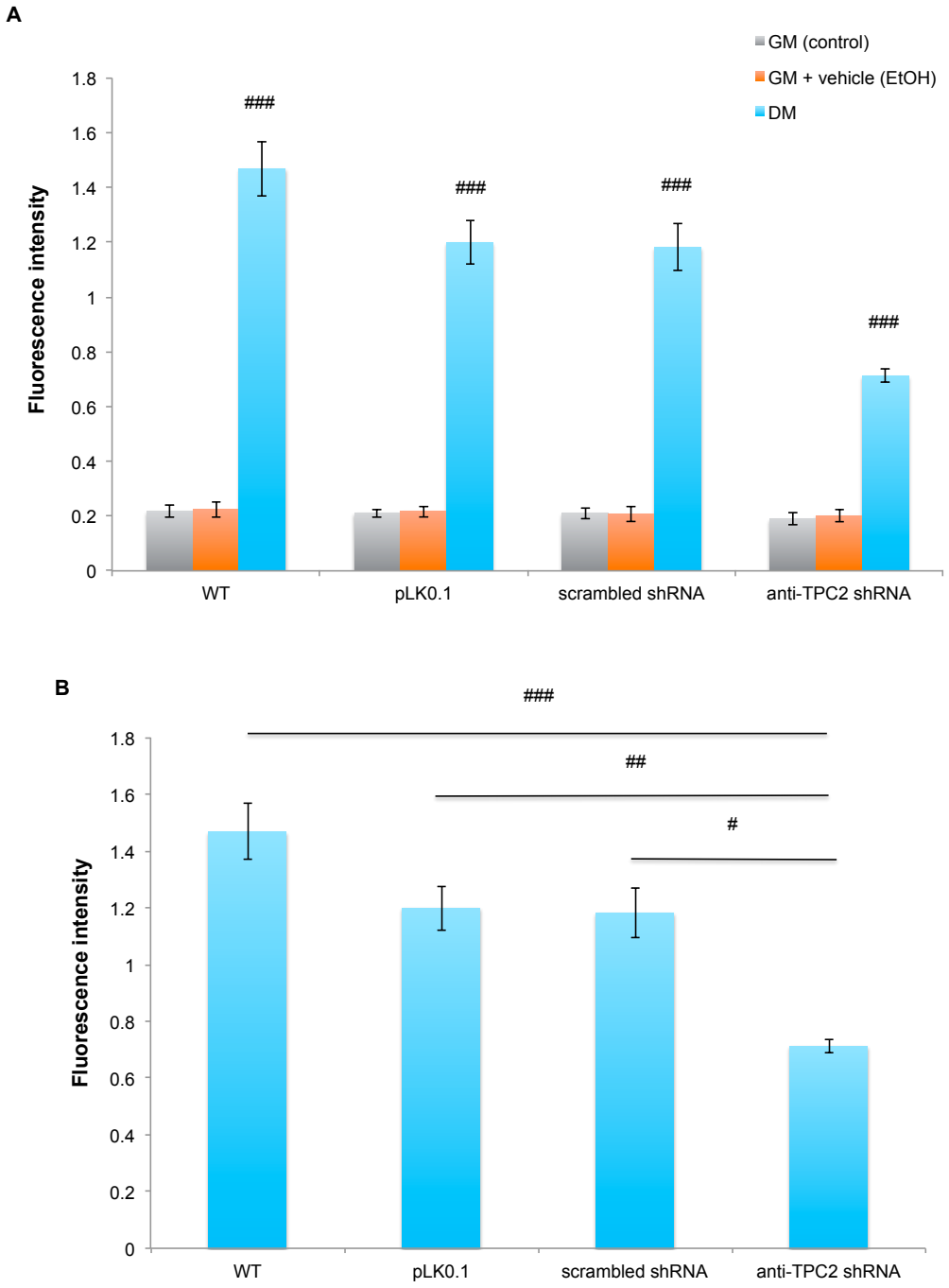

Figure 4.10: Quantification of AdipoRed assay of adipogenesis in non-transfected (WT), empty vector (pLK0.1)-transfected, non-specific scrambled shRNA-transfected and anti-TPC2 shRNA construct-transfected C3H10T1/2 cells. **(A)** At 2 days post-confluence, cells were either maintained in GM (control), GM + vehicle (ethanol (EtOH)), or exposed to standard adipogenic differentiation protocol (DM) as described in Materials and Methods, and assayed 8 days post-induction. **(B)** Collated results of the cells treated with DM. n = 5. #p<0.05; ##p<0.01; ###p<0.001 (ANOVA, *post-hoc* Turkey test). Data presented ± SEM.

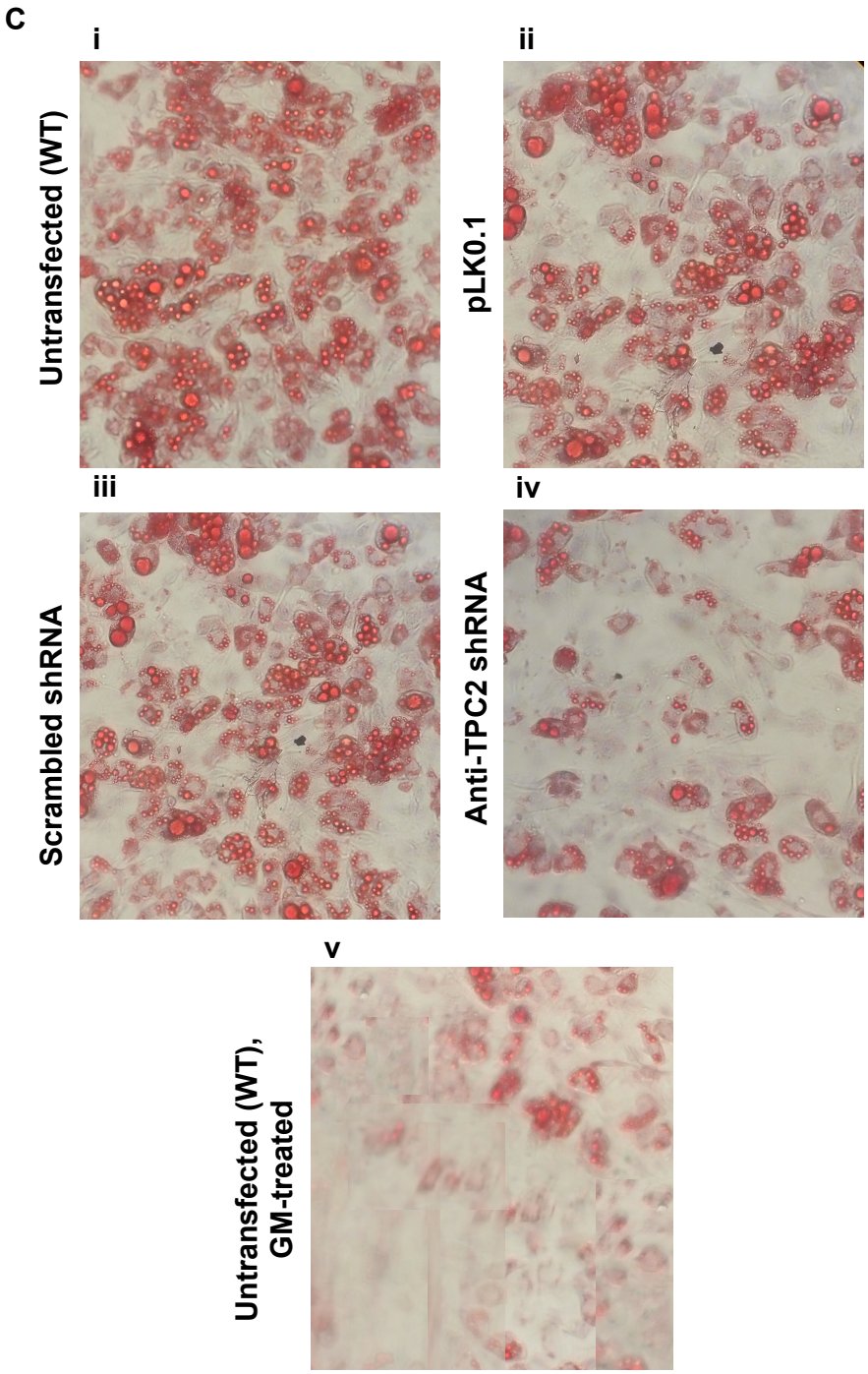

Figure 4.10C: Oil Red O staining of triglycerides at 8 days post-induction in **(i, v)** untransfected or **(ii)** empty vector pLK0.1 expressing or **(iii)** scrambled shRNA expressing or **(iv)** anti-TPC2 shRNA expressing C3H10T1/2 cells induced to undergo adipogenesis according to the standard adipogenic differentiation protocol except for **(v)** in which cells were treated with GM only. Cells were counterstained with hematoxylin to visualize the nuclei.

4.2.2.2 Measurement of adipogenesis – expression of adipocyte marker PPARγ

PPARγ is a well-known adipocyte marker which has been commonly used for assaying differentiation. It is expressed at significant levels during early adipogenesis. Previous studies by Dr Ruth Tunn have shown that sustained PPARγ mRNA expression occurs at 24 hours post-induction onwards in C3H10T1/2 cells (in preparation; Appendix 4.4.2) and in 3T3-L1 cells [242]. Here, the influence of TPC2 downregulation on the expression of PPARγ for adipogenic conversion was investigated. Relative PPARγ mRNA expression levels at 24 and 48 hours post-induction were determined in WT, pLK0.1, scrambled shRNA, and anti-TPC2 shRNA transfected C3H10T1/2 cells using RT-qPCR (Figures 4.11 and 4.12). For both time points, maximal PPARγ mRNA expression was seen with WT cells induced to differentiate with DM. Both pLK0.1 and scrambled shRNA transfected cells, when stimulated with DM induction, displayed a comparable level of PPARγ expression as WT cells. In contrast, a significant reduction was seen with the anti-TPC2 shRNA transfected cells: PPARγ expression fell by 35% and 25% at 24 and 48 hours respectively compared with the other three cell lines. This not only reconfirmed the inhibition of adipogenic capacity induced by TPC2 downregulation, but the marked repression in PPARγ expression also suggested that TPC2 acts upstream of this master adipogenesis regulator.

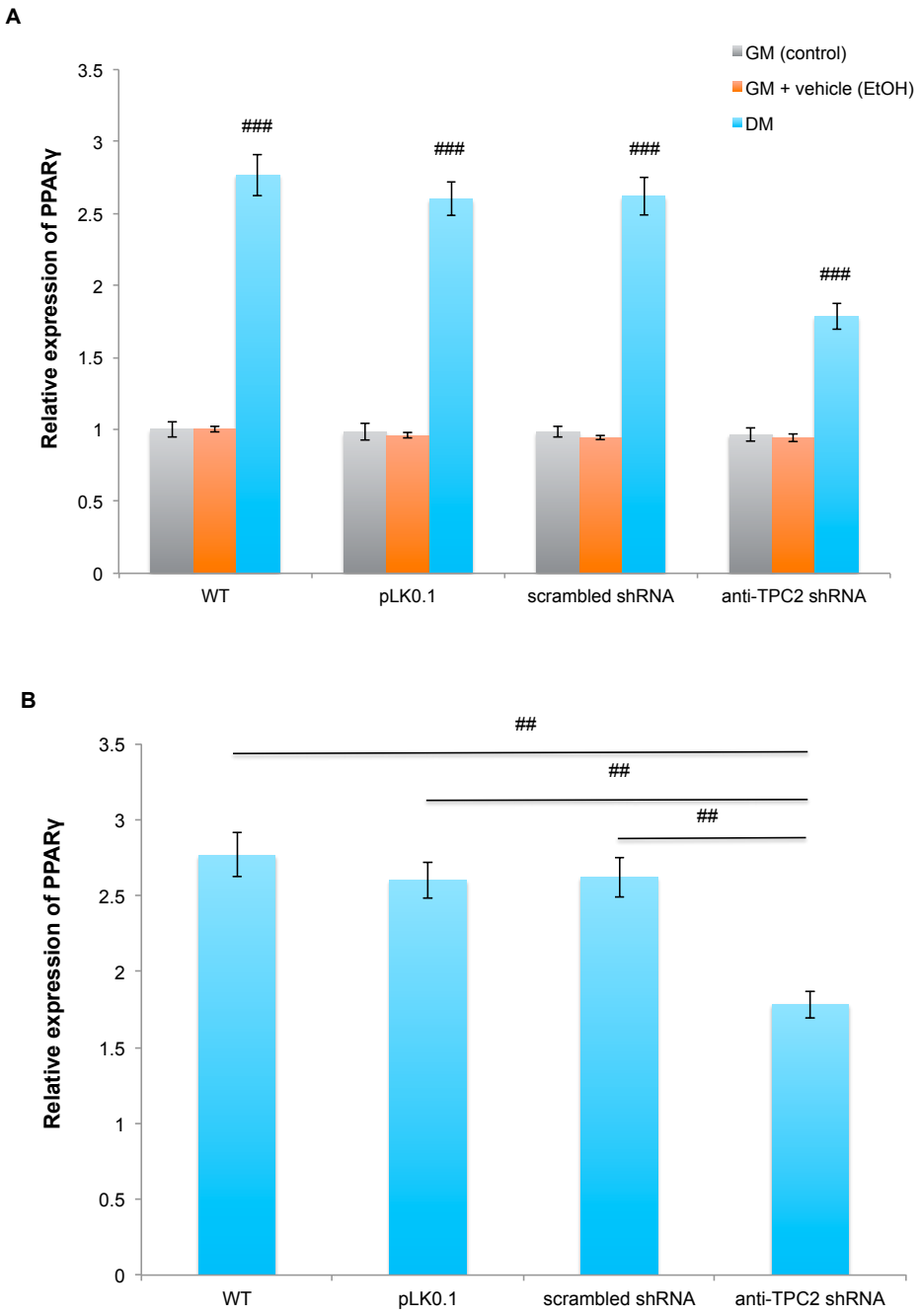

Figure 4.11: Expression of *PPARγ* mRNA levels at 24 hours post-induction in non-transfected (WT), empty vector (pLK0.1)-transfected, non-specific scrambled shRNA-transfected and anti-TPC2 shRNA construct-transfected C3H10T1/2 cells. **(A)** Cells were either treated with GM (control), GM + vehicle (ethanol (EtOH)), or subjected to standard differentiation protocol. PPARγ mRNA levels were determined at 2 days post-induction by RT-qPCR. Values were normalised to the geometric mean of β-Actin mRNA expression and are presented as fold-change relative to WT cells treated with GM. **(B)** Collated results of the cells treated with DM. n = 5. ###$p<0.001$ (ANOVA, *post-hoc* Turkey test vs GM control). Data presented ± SEM.

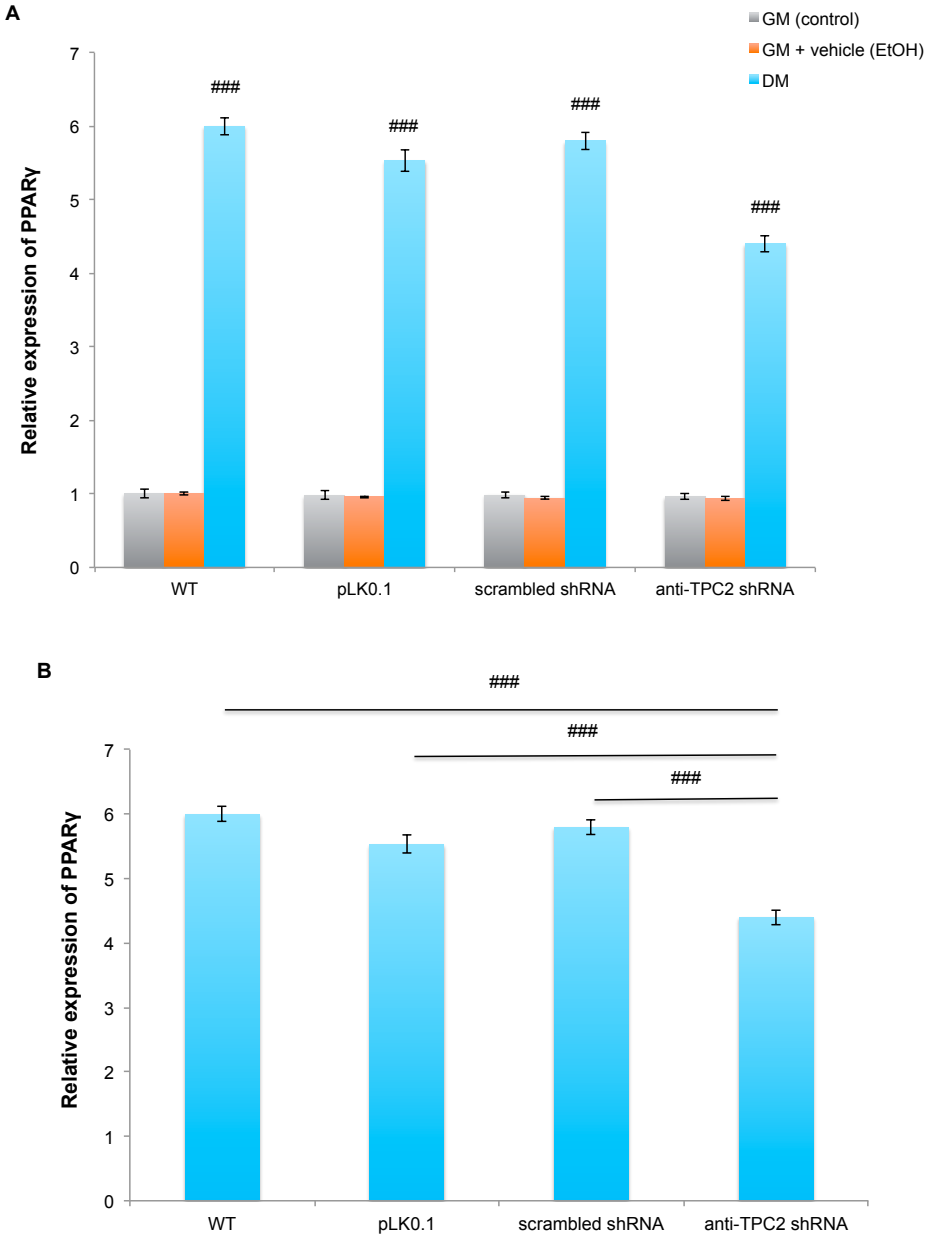

Figure 4.12: Expression of *PPARγ* mRNA levels at 48 hours post-induction in non-transfected (WT), empty vector (pLK0.1)-transfected, non-specific scrambled shRNA-transfected and anti-TPC2 shRNA construct-transfected C3H10T1/2 cells. **(A)** Cells were either treated with GM (control), GM + vehicle (ethanol (EtOH)), or subjected to standard differentiation protocol. PPARγ mRNA levels were determined at 2 days post-induction by RT-qPCR. Values were normalised to the geometric mean of β-Actin mRNA expression and are presented as fold-change relative to WT cells treated with GM. **(B)** Collated results of the cells treated with DM. n = 5. ###$p<0.001$ (ANOVA, *post-hoc* Turkey test vs GM control). Data presented ± SEM.

4.2.3 Effect of BAPTA-AM on adipogenesis

To investigate the effects of $[Ca^{2+}]_i$ on adipogenic differentiation of C3H10T1/2 cells, BAPTA-AM which is a membrane-permeable Ca^{2+} chelator [332], was used to lower cytosolic concentration. The ability of BAPTA-AM to alter adipocyte differentiation was assessed by treating C3H10T1/2 cells with MDI and increasing concentrations of BAPTA-AM. Lipid accumulation (Figure 4.13A) and cell morphology (Figure 4.13C) at 10 days post-induction were measured by AdipoRed staining. As shown in Figure 4.13A, the inhibition of lipid accumulation in BATPA-AM treated C3H10T1/2 cells was discovered to occur in a dose-dependent manner. Maximal triacylglycerol levels were noted with 1 μM and 3 μM BAPTA-AM treatment, with values comparable to non-treated cells induced to differentiate with DM, in other words, no obvious inhibition was seen at low concentrations of BAPTA-AM. When BAPTA-AM concentration was further increased to 10 μM, a slight yet insignificant drop in triacylglycerol levels was noticed. A profound and significant reduction in lipid accumulation was observed at BAPTA-AM concentrations of 30μM or higher, with triacylglycerol levels decreased by more than 70% to a level similar to that of non-treated cells maintained in GM throughout the entire time course (Figure 4.13B), indicating a severe disruption of adipogenesis by BAPTA-AM at high concentrations. C3H10T1/2 cells treated with increasing doses of BAPTA-AM compared with untreated cells as visualised by AdipoRed staining of triglycerides (Figure 4.13C). Taken together, BAPTA-AM was shown to exert a dose-dependent inhibitory effect on adipogenesis in C3H10T1/2 cells with an IC_{50} calculated to be 14.12μM. Cell number and viability were not measured, but there was no obvious cell death in any of the conditions tested.

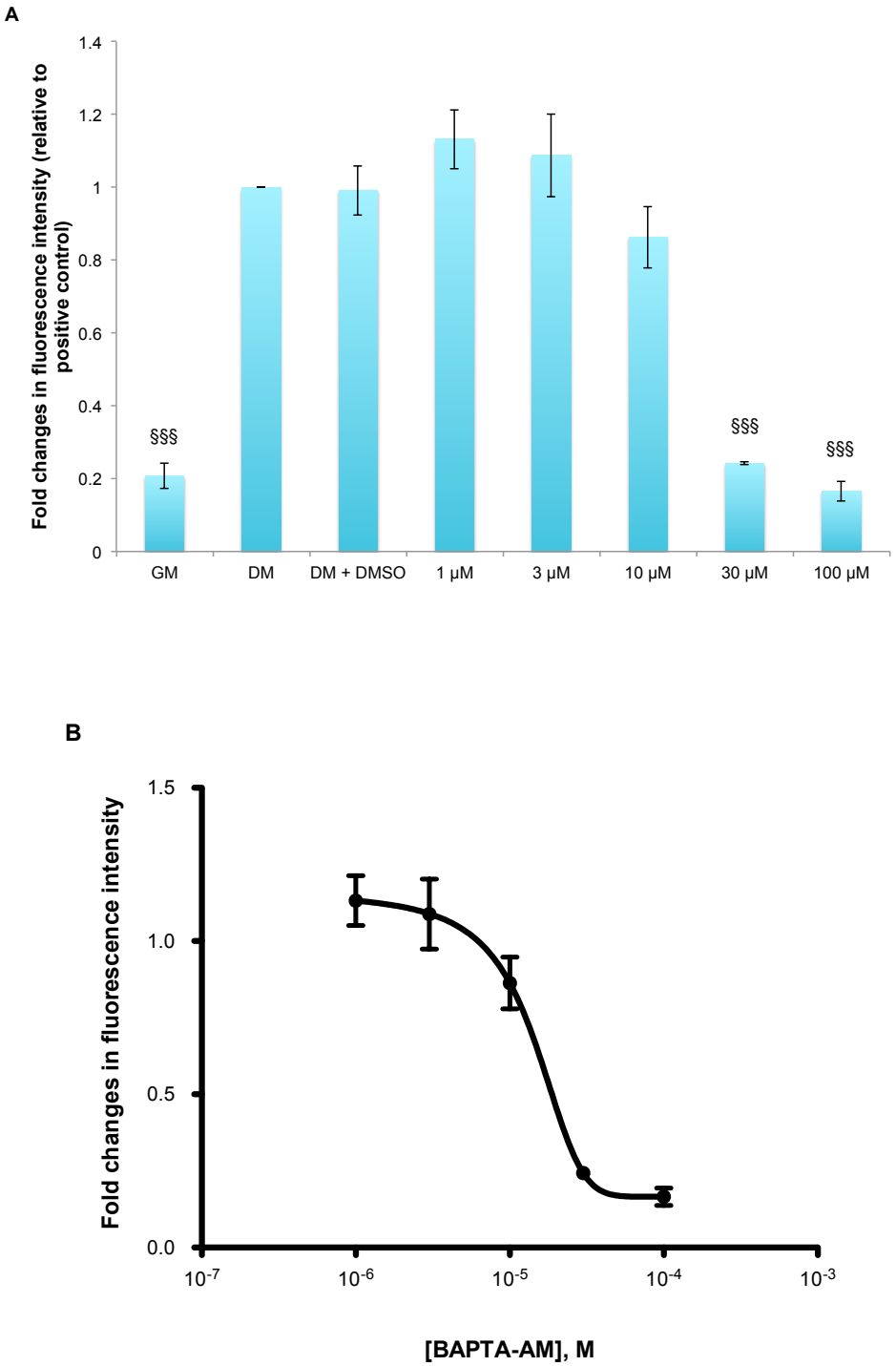

Figure 4.13: (A) Effect of BAPTA-AM on adipogenesis of C3H10T1/2 cells, quantified via AdipoRed fluorescence. At 2 days post confluence, cells were treated with DM containing various concentrations of BAPTA-AM for 45 minutes, and then subjected to the standard differentiation protocol. No pretreatment with drug was performed for non-treated cells, i.e. positive control (DM only) and DMSO control (inclusion of DMSO). Negative control was maintained in GM. Cells were assayed 10 days post-induction. Results expressed relative to fluorescence intensity of positive control. **(B)** Dose-inhibition curve was generated based on the results shown in figure 4.13A and IC_{50} was calculated from this curve. n = 4. §§§p<0.001 (ANOVA, *post-hoc* Dunnett test vs positive control). Data presented ± SEM.

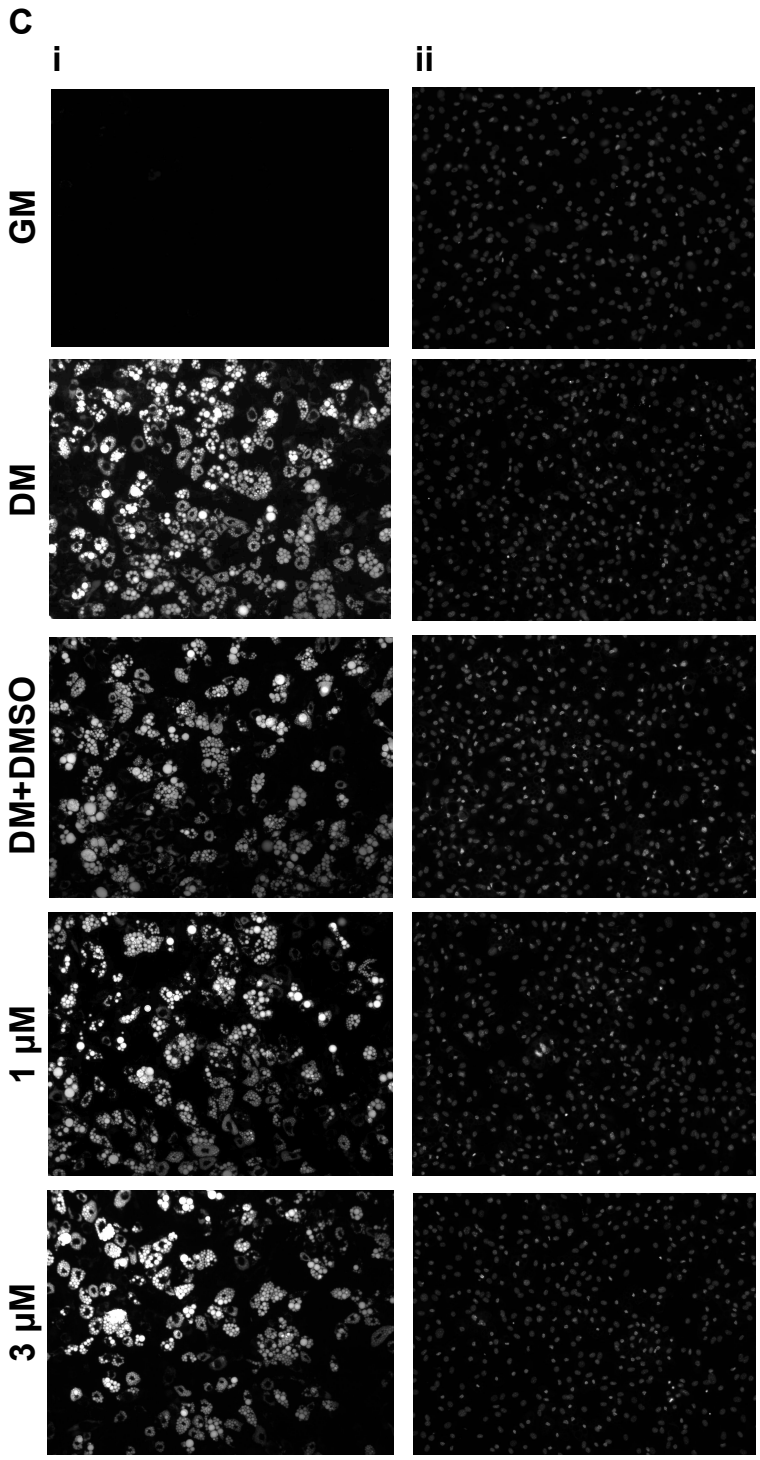
C
i
ii
GM
DM
DM+DMSO
1 µM
3 µM

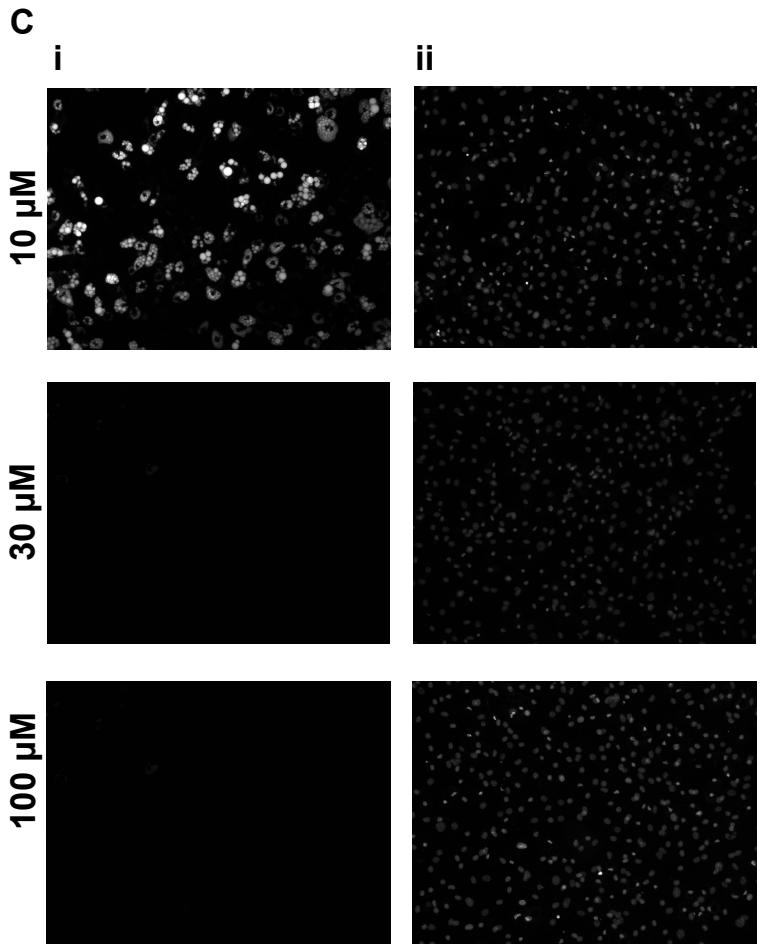

Figure 4.13C: AdipoRed staining of triglycerides in differentiating C3H10T1/2 cells with pre-treatment of a range of BAPTA-AM concentrations for 45 minutes. Cells were counterstained with Hoechst to visualize the nuclei.

4.2.4 Effect of inhibiting NAADP signalling on adipogenesis

The transient upregulation of TPC2 mRNA expression during early adipogenesis and the impairment in adipogenic capacity of anti-TPC2 shRNA treated cells implicates involvement of this novel Ca^{2+} channel in adipogenesis. Given that TPC2 has been implicated as a key component of NAADP-induced Ca^{2+} signalling, pharmacological agents that block this signalling pathway were used to evaluate the impact of such inhibition on adipocyte differentiation in C3H10T1/2 cells.

The sea urchin egg homogenate radioligand competition binding assay was not employed in my study as this assay was deemed impractical as judged by previous studies of NAADP levels in C3H10T1/2 cells by Dr Ruth Tunn.

4.2.4.1 Effects of bafilomycin A1 on adipogenic differentiation

Bafilomycin, a well-known lysosomal H^+-ATPase inhibitor which blocks NAADP-mediated Ca^{2+} release in a number of cell types [40, 43][333], was initially used to determine if Ca^{2+} stored in acidic organelles was required. Ca^{2+} loading of these stores is dependent on the proton gradient and, as such, bafilomycin is able to deplete lysosomal stores of Ca^{2+} content [334]. C3H10T1/2 cells were treated with various concentrations of bafilomycin during 0-4 hours and 0-8 hours respectively after induction of differentiation by DM. Dose dependence inhibition and similar inhibitory effect were observed in both time frames (IC_{50} for 0-4 hours and 0-8 hours: ~33.39 nM, 31.80 nM) (Figures 4.14A-D). At low bafilomycin concentrations (1 nM to 10 nM), lipid accumulations in these drug-treated cells were found comparable to that of non-treated cells induced to differentiate by DM. When the bafilomycin concentration was increased to 30 nM, lipid accumulation was significantly abolished. Maximal suppression occurred at 100 nM and 300 nM, an 80% reduction in the lipid accumulation was observed and the level was comparable to that of

non-treated cells maintained in GM throughout the entire time course. C3H10T1/2 cells treated with increasing doses of bafilomycin were compared with untreated cells as visualised by AdipoRed staining of triglycerides (Figure 4.14E). Collectively, bafilomycin exerted a similar dose-dependent inhibitory effect on adipogenesis of C3H10T1/2 cells during both time windows (Figures 4.14C and D). Cell number and viability were not measured, but there was no obvious cell death in any of the conditions.

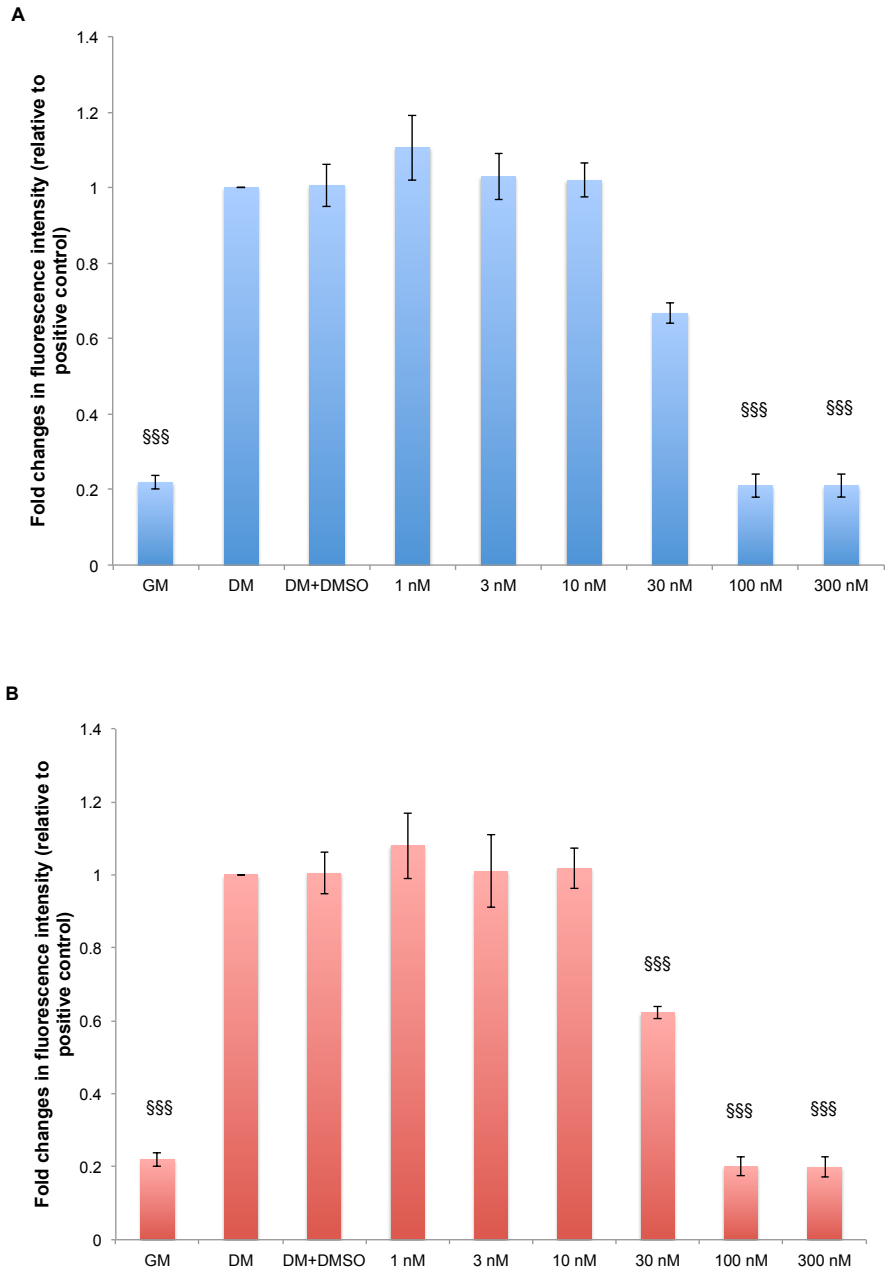

Figure 4.14: Effect of bafilomycin A1 on adipogenesis in C3H10T1/2 cells, quantified via AdipoRed fluorescence. At 2 days post-confluence, cells were treated with DM containing various concentrations of bafilomycin for **(A)** 4 hours or **(B)** 8 hours and then subjected to the standard differentiation protocol. No pretreatment with drug was performed for non-treated cells, i.e. the positive control (DM only) and DMSO control (inclusion of DMSO). The negative control was maintained in GM. Cells were assayed 10 days post-induction. Results are expressed relative to fluorescence intensity of positive control (i.e. no bafilomycin treatment). n = 4. ***p<0.001 (ANOVA, *post-hoc* Dunnett test vs positive control). Data presented ± SEM.

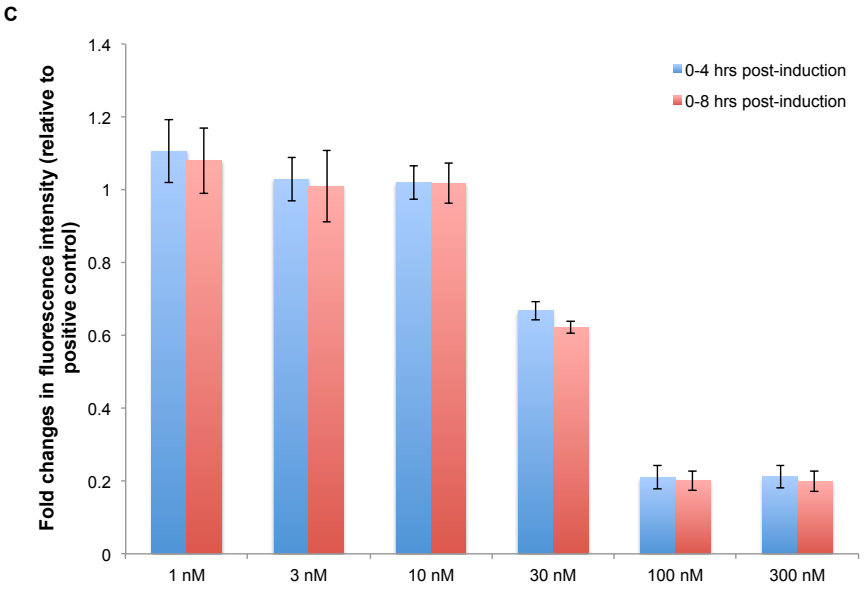

Figure 4.14C: Comparison of effect of bafilomycin pretreatment during two different time windows.

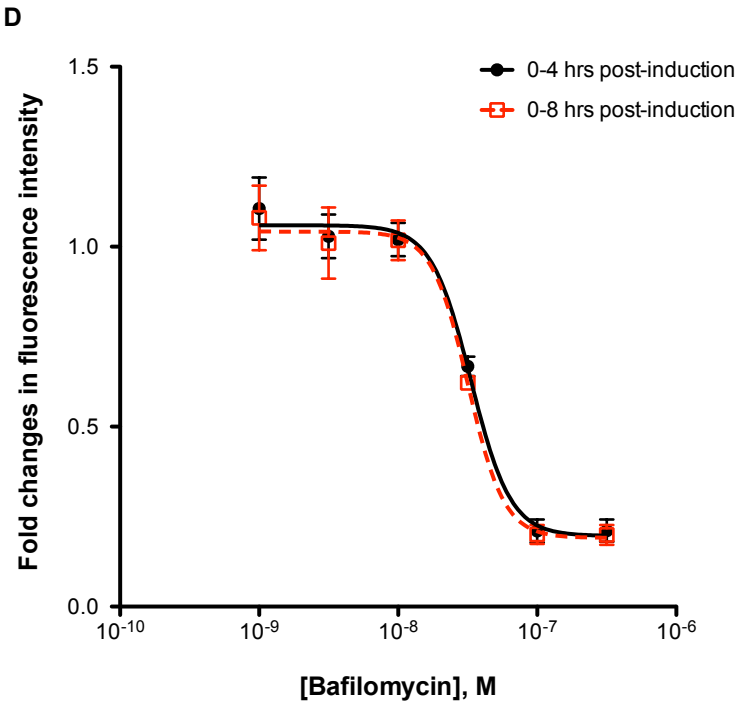

Figure 4.14D: Dose-inhibition curves were generated based on the results shown in figure 4.14A and B. Corresponding IC_{50} value was calculated from these curves. n = 4. Data presented ± SEM

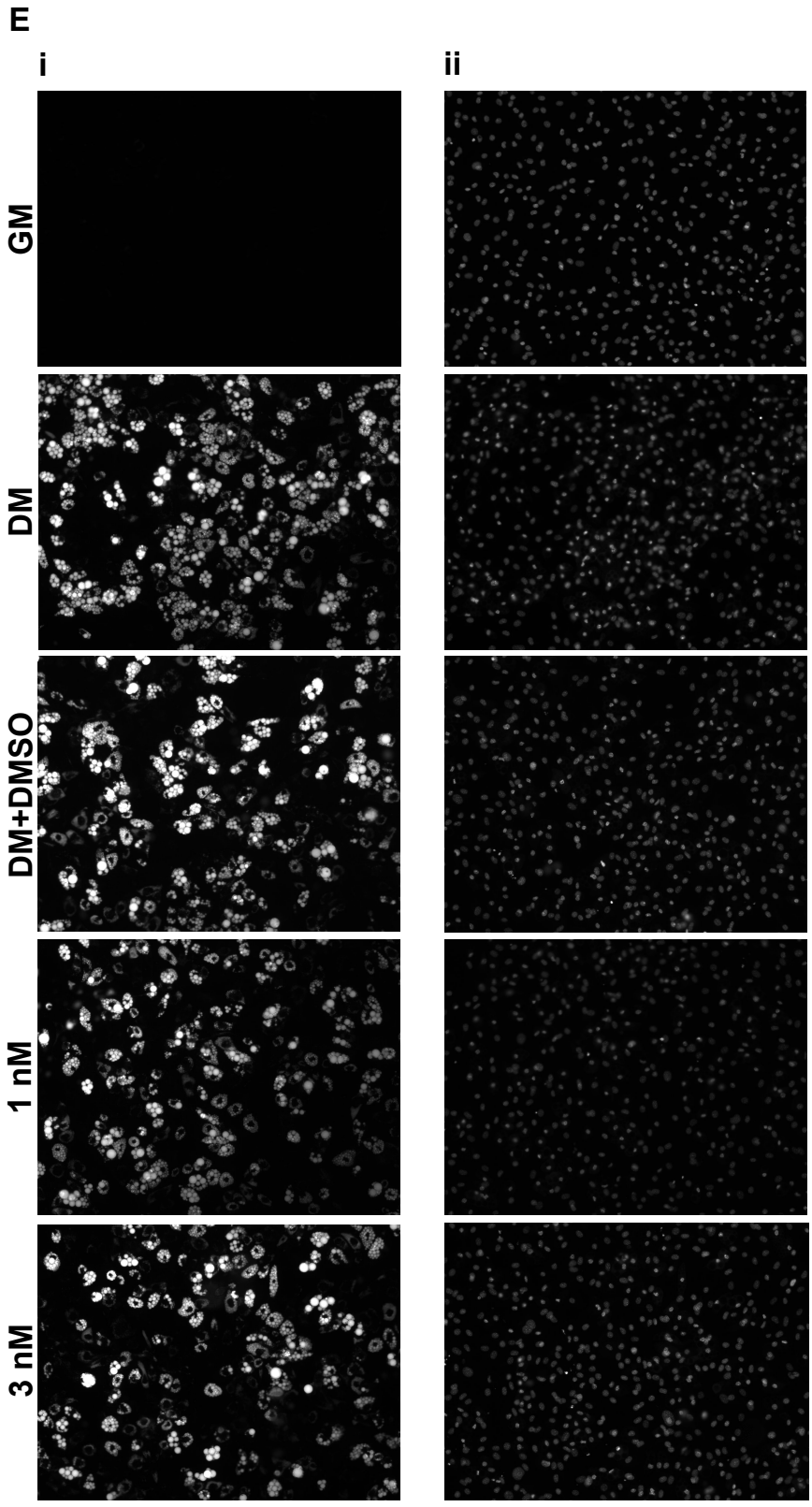
E
i
ii
GM
DM
DM+DMSO
1 nM
3 nM

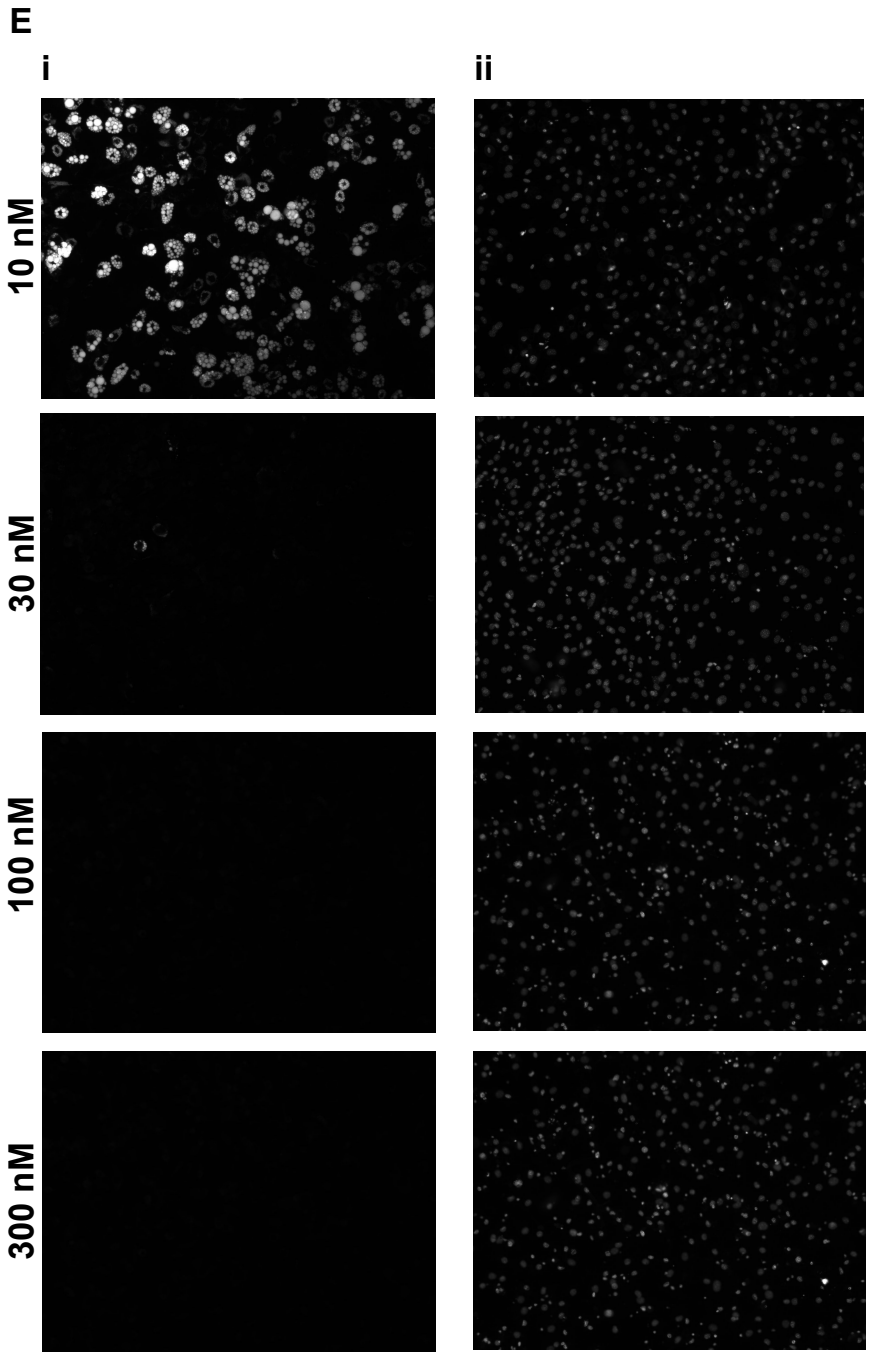

Figure 4.14E: AdipoRed staining of triglycerides in differentiating C3H10T1/2 cells with pre-treatment of a range of bafilomycin concentrations during 0-4 hours post-induction. Cells were counterstained with Hoechst to visualize the nuclei.

4.2.4.2 Effect of Ned-19 on adipogenic differentiation

Next, a specific NAADP antagonist Ned-19 was used to block NAADP signalling selectively [94][335, 336]. C3H10T1/2 cells were treated with a range of concentrations of Ned-19 during the first 48 hours after induction of differentiation by DM. For all concentrations tested, no significant difference in lipid accumulation was observed between the Ned-19 treated cells and non-treated cells stimulated by DM as determined by lipid accumulation (Figures 4.15A and B), although a slight yet insignificant decrease was seen at 30 μM and 100 μM though (Figure 4.15A). An even higher concentration (300 μM) was also included in the studies, but severe cell death occurred 2 days post-induction in every experiment due to the cytotoxic effects of high dosage, thus evaluation of influence of Ned-19 at concentrations higher than 100 μM was deemed impossible. These data suggest that unlike BAPTA-AM and bafilomycin, no significant inhibitory effect on adipogenesis in C3H10T1/2 cells was identified for Ned-19 treatment in the range of concentrations examined here, although a slight suppression was seen at higher doses; also effects of Ned-19 on adipogenic conversion at doses higher than 100 μM were inconclusive due to the severe cell death that occurred.

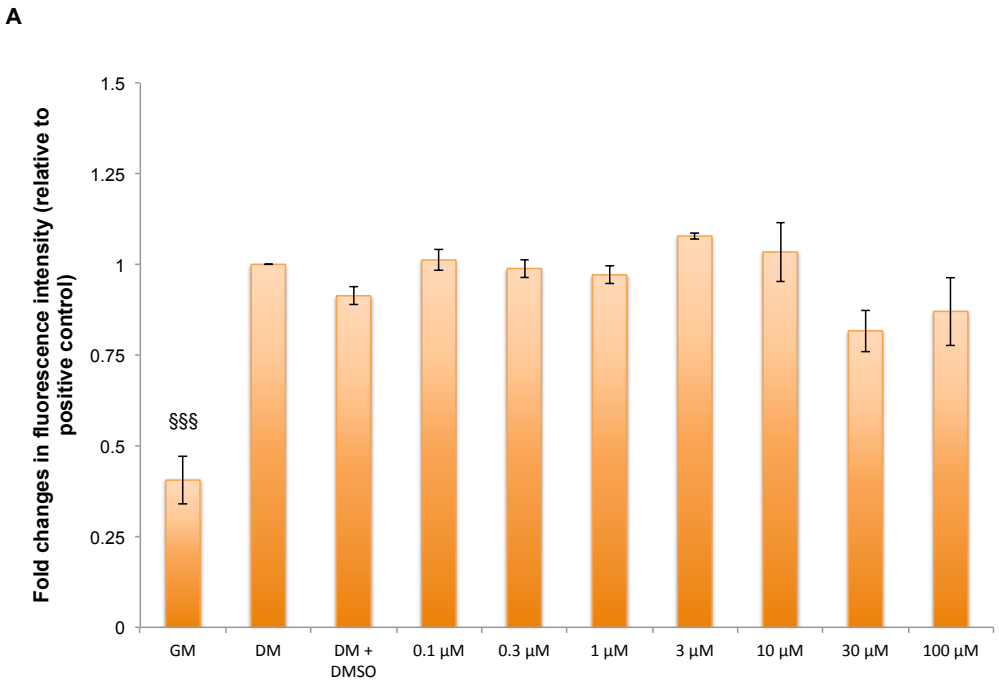

Figure 4.15A: Effect of Ned-19 on adipogenesis in C3H10T1/2 cells, quantified via AdipoRed fluorescence. At 2 days post-confluence, cells were subjected to the standard differentiation protocol with the inclusion of Ned-19 in the medium during the first 48 hours of differentiation. No drug treatment was performed for non-treated cells, i.e. positive control (DM treatment only), DMSO control (inclusion of DMSO) and negative control (maintained in GM). Cells were assayed 8 days post-induction. Results expressed relative to fluorescence intensity of positive control. n = 4. (ANOVA, *post-hoc* Dunnett test vs positive control). Data presented ± SEM.

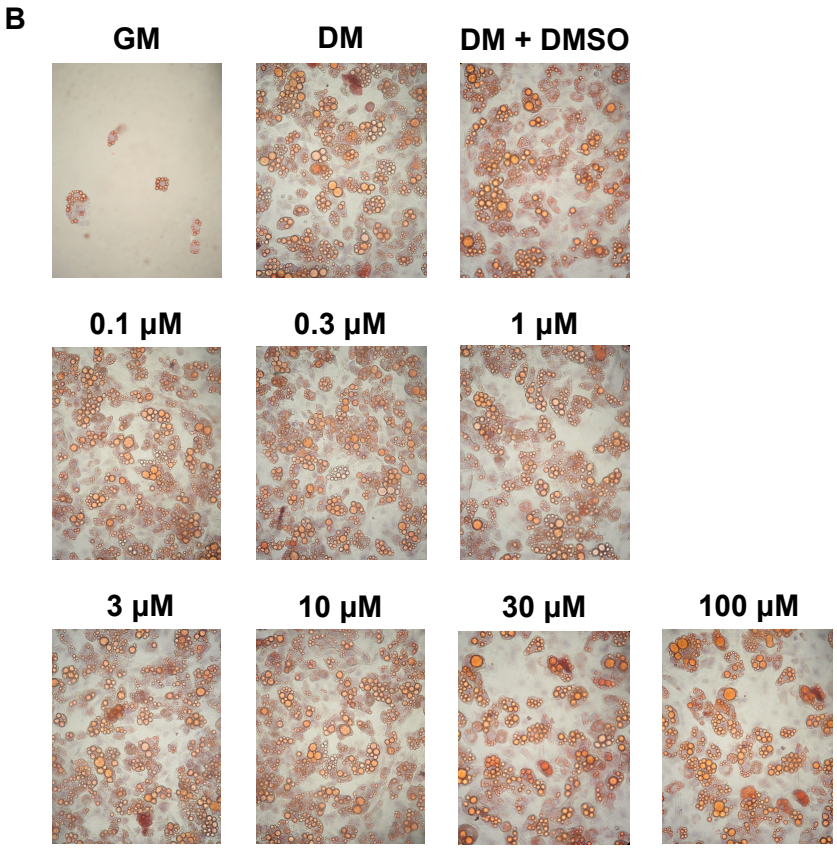

Figure 4.15B: Oil Red O staining of triglycerides in differentiating C3H10T1/2 cells with inclusion of Ned-19 in DM during the first 48 hours of differentiation. Cells were counterstained with hematoxylin to visualize the nuclei.

4.2.5 Determination of potential upstream mediators - PKA and EPAC

Previous studies by Dr Ruth Tunn and David Gay (in preparation) have shown an upregulation of TPC2 mRNA expression mediated by cAMP in C3H10T1/2 cells induced to differentiate into adipocytes at 4 hours post-induction. Thus, addition of IBMX alone was necessary and sufficient to upregulate TPC2 mRNA levels (Appendix 4.4.5). Both rolipram (a specific PDE IV inhibitor that increases cAMP levels) and forskolin (this increases cAMP levels via activation of adenylyl cyclase [337]) treatment also upregulated TPC2 mRNA levels at the same time point, albeit to a slightly lower extent than IBMX (Appendix 4.4.6). To further elucidate the underlying mechanisms of cAMP-induction of TPC2 expression, the roles played by PKA and Epac, regarded as the two main effectors of cAMP signalling [253, 338], were investigated here. Pharmacological agents including a specific PKA inhibitor, a specific Epac inhibitor, and an Epac agonist were used for the following studies: Time course experiments to assess TPC2, Epac1, Epac2 and PPARγ mRNA expression up to 2 days post-induction were carried out, expression levels being evaluated using RT-qPCR. Specific primer sets were used, the same TPC2 and PPARγ primer set from Dr Ruth Tunn's studies being employed. Expression after 2 days post-induction were not examined in my studies because upregulation of *Tpcn2* expression has been shown to occur during early adipogenesis (section 4.2.1), so studies focusing on the early differentiation period were the prime goal.

4.2.5.1 Effect of PKA inhibitor on *Tpcn2* mRNA expression

To determine whether PKA kinase activity is necessary for cAMP-mediated upregulation of *Tpcn2* mRNA expression in DM-induced differentiating C3H10T1/2 cells, a highly specific PKA inhibitor PKI 14-22 (PKI) was employed. PKI is a myristoylated and membrane permeable form of heat-stable protein kinase inhibitor which works by

inhibiting the catalytic subunit of PKA [339]. Two other common PKA inhibitors, namely H89 and KT 5720, were avoided due to their lack of specificity; thus, they inhibit several other kinases with similar potency [340].

Both PKI-treated and non-treated (control) cells displayed a similar *Tpcn2* mRNA expression pattern throughout the entire time course (Fig. 4.16A and B): expression increased significantly during 2-4 hours post-induction with a peak at 8 hours, then dropping after 24 hours and remaining about the same at 48 hours. One striking finding is that blockade of the catalytic activity of PKA resulted in upregulation of *Tpcn2* expression at 24 and 48 hours with levels comparable to that seen at 4 hours (Fig. 4.16B). When comparing *Tpcn2* mRNA expression between PKI-treated and non-treated cells at each time point (Fig. 4.16C), a significant decrease was noted for PKI-treated cells at 2 hours post-induction, with an approximately 50% reduction compared with the control cells. However, no significant alteration was seen at 4 and 8 hours post-induction when *Tpcn2* expression was substantially upregulated. Moreover, the PKI-mediated upregulation seen at 24 and 48 hours became insignificant when compared with the non-treated cells. The data here suggested an inhibitory effect on *Tpcn2* mRNA expression by PKI-induced inhibition of PKA catalytic activity at 2 hours after differentiation induction, which occurred earlier than the significant upregulation mediated by cAMP-elevating agents.

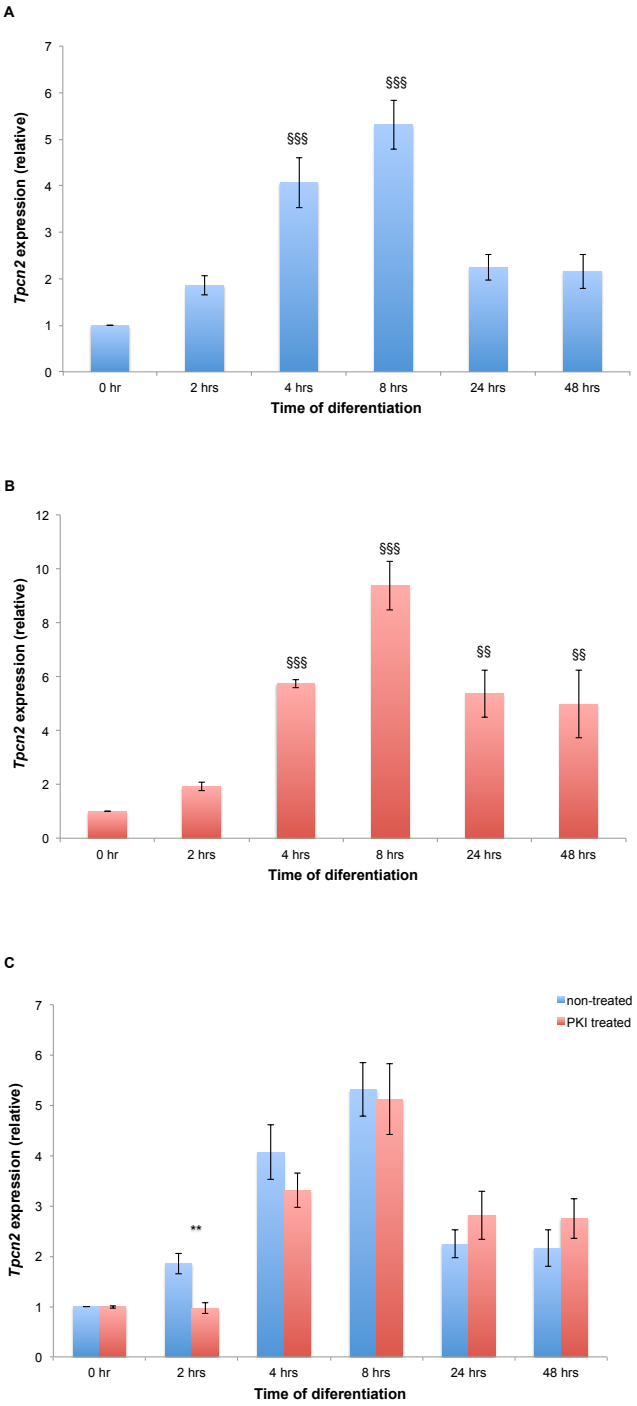

Figure 4.16: Expression of *Tpcn2* mRNA in **(A)** non-treated and **(B)** PKI-treated C3H10T1/2 cells. **(C)** Comparison of *Tpcn2* mRNA in non-treated and PKI-treated C3H10T1/2 cells. At 2 days post-confluence, both non-treated and PKI-treated cells were subjected to the standard differentiation protocol with the inclusion of 10 μM PKI in the medium during the entire time course for PKI treated cells. RNA was isolated at 0 hr, 2 hrs, 4 hrs, 8 hrs, 24 hrs and 48 hrs from cells after differentiation induction and drug treatment. Expression levels were determined by RT-qPCR. Values were normalised to the geometric mean of β-Actin mRNA expression and are presented as expression relative to 0 hr. For **(C)**, expressions were relative to 0 hr of non-treated cells. n = 5. §§p<0.05, §§§p<0.01 (ANOVA *post-hoc* Dunnett test vs 0 hr). **p<0.01 (student's *t-test*). Data presented ± SEM.

4.2.5.2 Effect of Epac inhibitor on *Tpcn2* mRNA expression

Having determined the effects of PKA inhibition on *Tpcn2* mRNA expression in DM-induced C3H10T1/2 cells, the effects on *Tpcn2* expression of another well-known cAMP signalling effector, Epac, were also studied to understand whether cAMP-mediated activation of Epac is required for such expression.

4.2.5.2.1 Epac1 and Epac2 mRNA expressions in C3H10T1/2 cells

Firstly, the expressions of Epac1 and Epac2 were evaluated by RT-qPCR in order to determine whether Epac1 and/or Epac2 was differentially expressed during adipocyte differentiation in C3H10T1/2 cells. While Epac2 mRNA was nearly undetectable, Epac1 mRNA was expressed in 2 days post-confluent preadipocytes (Figure 4.17C). At 2 hours post-induction, Epac1expression rose to and peaked at a level about four fold higher than the starting level, and then dropped by half at 4 hours and declined further at 8 hours to a level even lower than the starting value; it then stabilised at that level for 2 days. At 6 days post-induction, however, expression increased back to the same level seen with 4 hours post-induction, that is about two fold higher than the starting value (Figure 4.17A). In contrast, Epac2 mRNA expression was so low that it was hardly detectable in both undifferentiated and differentiated C3H10T1/2 cells. When expression values were normalised to the starting level, Epac2 mRNA expression did not show any changes throughout the entire time course (Figure 4.17B). The expression profiles of both Epac1 and Epac2 demonstrated here were in agreement with those observed in 3T3-L1 cells induced to differentiate using the same hormonal cocktail (MDI) [275].

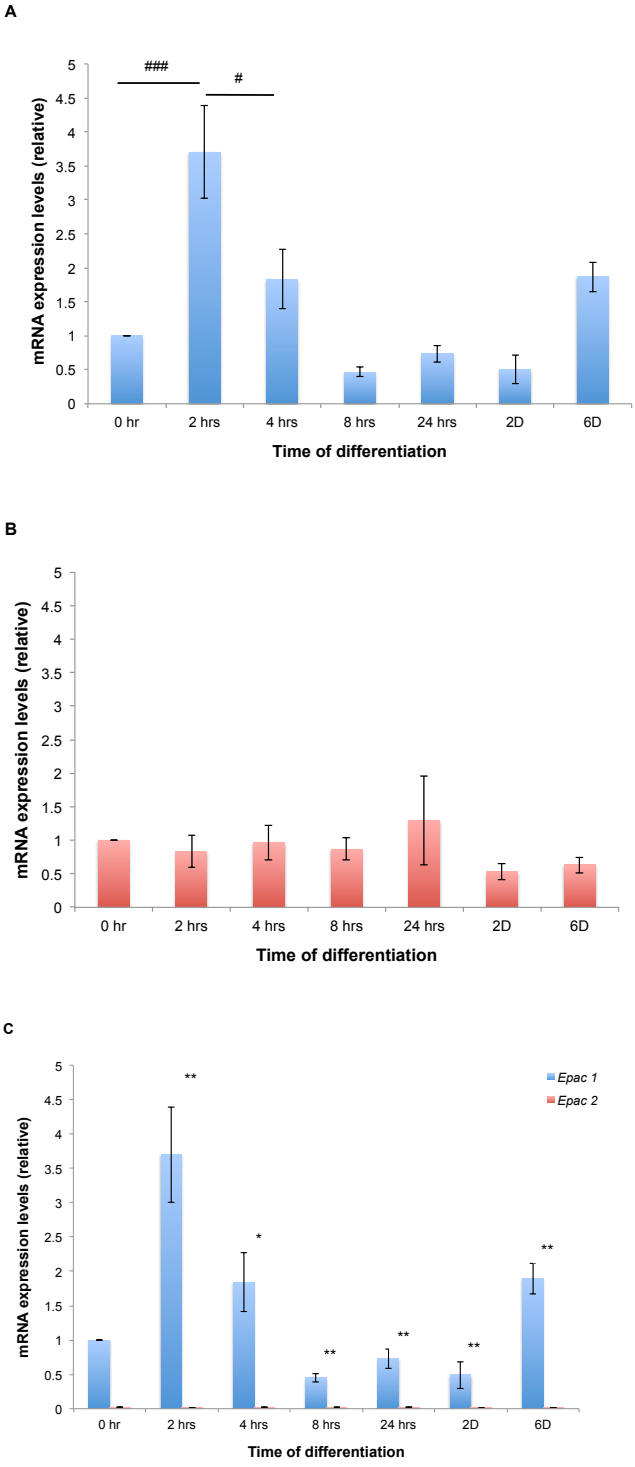

Figure 4.17: mRNA expression of **(A)** Epac1 and **(B)** Epac2 during adipogenesis in C3H10T1/2 cells. At 2 days post-confluence, cells were subjected to the standard differentiation protocol. RNA was isolated at 0 hr, 2 hrs, 4 hrs, 8 hrs, 24 hrs, 2D and 6D from cells after differentiation induction. Expression levels were determined by RT-qPCR. **(C)** Comparison of Epac1 and Epac2 mRNA expression. Values were normalised to the geometric mean of β-Actin mRNA expression and are presented as expression relative to 0 hr. For **(C)**, expression of both Epacs was relative to 0 hr of Epac1. n = 3. ###p<0.001; #p<0.05 (ANOVA, *post-hoc* Turkey test; only significant difference between consecutive time points are noted). *p<0.05; **p<0.01 (Student's *t-test*). Data presented ± SEM.

4.2.5.2.2 Effect of selective Epac activator on Tpcn2 mRNA expression

Having established that Epac1 but not Epac2 is abundantly expressed in C3H10T1/2 cells, investigation of the effects of this mediator on *Tpcn2* expression was conducted. A selective Epac-activating cAMP analog 8-pCPT-2'-*O*-Me-cAMP (8pCPT) [341, 342] was used to substitute for IBMX in the differentiation assay, to check whether activation of Epac1 alone was sufficient to mimic the effect of cAMP-mediated upregulation of *Tpcn2* expression in C3H10T1/2 cells. This was found not to be the case, as an Epac specific agonist did not stimulate significant *Tpcn2* mRNA upregulation throughout the whole time course, nor did the ins/dex treatment (i.e. DM without IBMX) produce any significant upregulation (Figure 4.18). Thus, it appears that activation of Epac *per se* is not sufficient to elicit such remarkable upregulation seen with cAMP-elevating agents. Alternatively, this could be due to the concentration used being not enough to elicit an effect. It would be interesting to investigate the effects using a range of concentrations and see if any effects would occur at higher or lower concentrations.

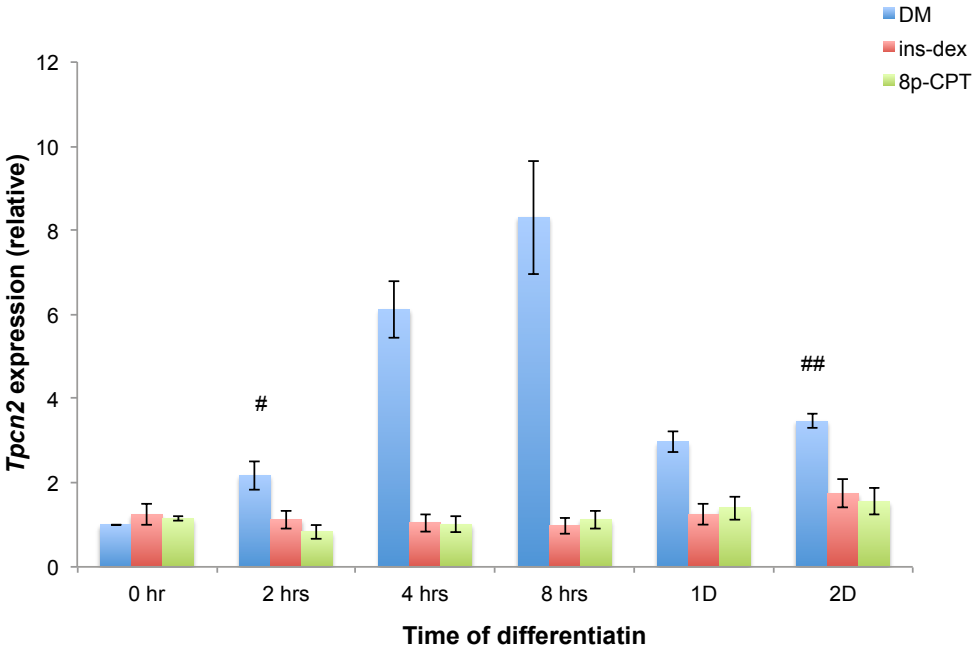

Figure 4.18: Effect of Epac analog (8p-CPT) on *Tpcn2* mRNA expression in C3H10T1/2 cells. At 2 days post-confluence, cells were treated for two days with complete DM (DM), DM lacking IBMX (ins-dex) or DM lacking IBMX but with 10 µM 8p-CPT (8p-CPT). RNA was isolated at 0 hr, 2 hrs, 4 hrs, 8 hrs, 24 hrs and 48 hrs from cells after differentiation induction and drug treatment. Expression levels were determined by RT-qPCR. Values were normalised to the geometric mean of β-Actin mRNA expression and are presented as expression relative to 0 hr of DM treated cells. n = 5. §p<0.05; §p<0.01; §§§p<0.001 (ANOVA, *post-hoc* Turkey test). Data presented ± SEM.

4.2.5.2.3 Effect of selective Epac inhibitor on Tpcn2 mRNA expression

To determine whether Epac1 activation was necessary for cAMP-mediated upregulation of *Tpcn2* mRNA expression in C3H10T1/2 cells, the effects of a specific Epac inhibitor ESI-09 was evaluated. As shown in figure 4.19, both ESI-09-treated and non-treated (control) cells exhibited similar *Tpcn2* mRNA expression patterns throughout the whole time course. When comparing the expression level at each time point, significant attenuation was noted at 2 and 4 hours post-induction in ESI-09-treated cells, with more than two fold reduction compared with the non-treated cells. However, no significant alteration was seen at 8 hours post-induction during which maximal upregulation of *Tpcn2* was recorded. This is not unpredictable as Epac1 expression was shown to be downregulated at 8 hours to a level below the starting value (Figure 4.17A). Thus results here indicated that Epac activation is essential for cAMP-mediated upregulation of *Tpcn2* mRNA expression at 2 and 4 hours but not at 8 hours in differentiating C3H10T1/2 cells. Since only one concentration has been tested here, it would be informative to determine whether the influence of Epac activation on *Tpcn2* expression follows a dose-response profile; this could be evaluated by using a range of ESI-09 concentrations.

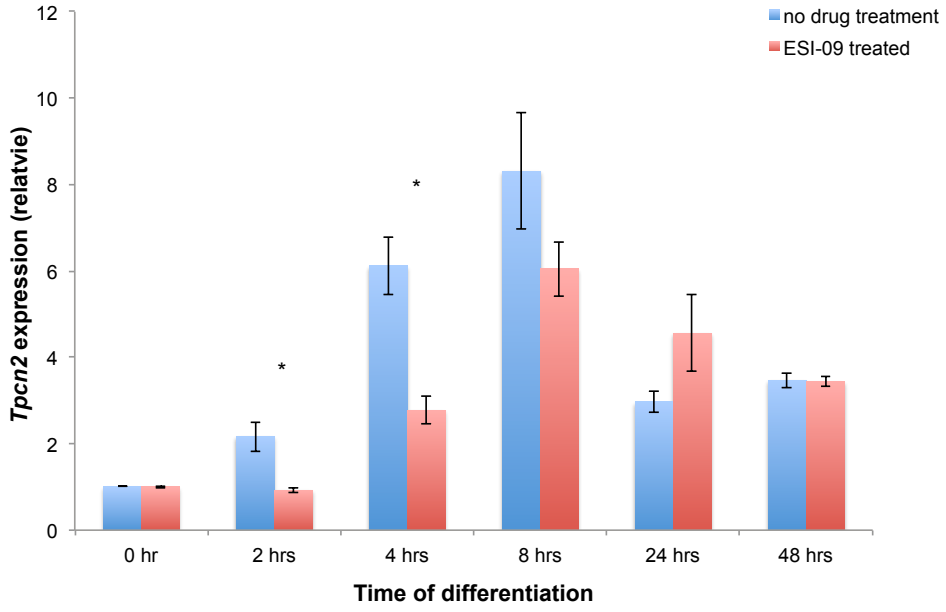

Figure 4.19: Expression of *Tpcn2* mRNA in C3H10T1/2 cells in response to ESI-09 (Epac inhibitor) treatment. At 2 days post-confluence, cells were subjected to the standard differentiation protocol with the inclusion of 25 µM ESI-09 in the medium throughout the whole time course. RNA was isolated at 0 hr, 2 hrs, 4 hrs, 8 hrs, 24 hrs and 48 hrs from cells after differentiation induction and drug treatment. Expression levels were determined by RT-qPCR. Values were normalised to the geometic mean of β-Actin mRNA expression and are presented as expression relative to 0 hr of non-treated cells. n=3. * $p<0.05$ (student's *t-test*). Data presented ± SEM.

4.2.5.3 Effect of PKA inhibition and Epac inhibition on adipogenesis of C3H10T1/2 cells

An investigation was also carried out to determine whether PKI and ESI-09 inhibition has an effect on MDI-induced adipogenesis in C3H10T1/2 cells. Here, the degree of adipogenesis was monitored by measuring mRNA expression levels of an adipocyte marker gene PPARγ in PKI-treated, ESI-09-treated and non-treated (control) C3H10T1/2 cells respectively. Suppression of Epac by ESI-09 led to an abridged basal PPARγ level, about 50% reduction was observed compared with the control, indicating a significant inhibitory effect on this process; while an insignificant suppression of PPARγ expression was seen in PKI treatment, indicating that adipogenesis was only insignificantly inhibited (Figure 4.20).

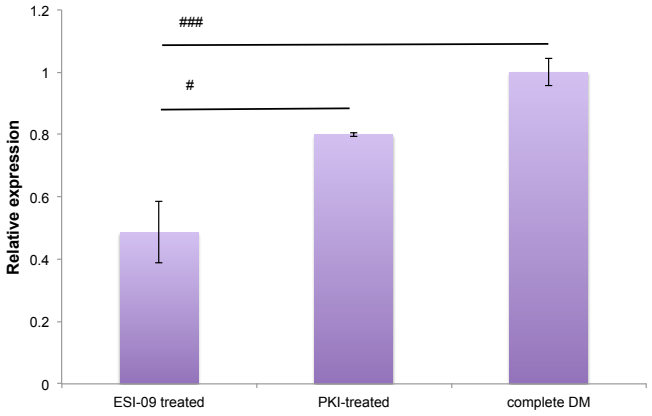

Figure 4.20: Expression of *PPARγ* mRNA levels at 6D post-induction in C3H10T1/2 cells. At 2 days post-confluence, cells were subjected to standard differentiation protocol. RNA was isolated from cells at day 6 after differentiation induction. Expression levels were determined by RT-qPCR. Values were normalised to the geometric mean of β-Actin mRNA expression and are presented as expression relative to the positive control (complete DM treated cells). n = 3. #$p<0.05$; ###$p<0.001$ (ANOVA, *post-hoc* Turkey test). Data presented ± SEM.

4.2.6 CREB

The intriguing observation of cAMP-mediated upregulation of *Tpcn2* expression and the downregulation resulting from selective PKA or Epac inhibition prompted the investigation of the role of CREB protein, a well characterised transcription factor that binds to the CRE site, as a potential mediator of *Tpcn2* expression.

Involvement of CREB in adipogenesis induction has been established in previous studies [251] and such adipogenic effects may be mediated by phosphorylation of CREB either through direct PKA or indirect Epac-mediated PI3/Akt activation [277]. Given the cAMP-mediated upregulation of *Tpcn2* expression and downregulation stimulated by selective PKA or Epac inhibition during early adipogenesis, an investigation of CREB's involvement in *Tpcn2* expression regulation was conducted. Attempts have been made to knockdown CREB expression by transfecting a dominant-negative CREB (kindly made by David Gay) into C3H10T1/2 cells using a range of transfection reagents but no success has been reported as determined by measurement of protein levels using immunofluorescence. Otherwise it would provide a useful model to test whether CREB is functionally important for *Tpcn2* expression. In view of this issue, another method was employed here to assess the role of CREB in *Tpcn2* expression.

4.2.6.1 Expression of CREB and phosphorylated CREB

Expression of CREB and phosphorylated CREB (pCREB) in C3H10T1/2 cells were analysed following differentiation induction. Cells at 0, 2, 4 and 8 hours post-induction were fixed for immunofluorescence using anti-CREB and anti-pCREB antibody to detect the proteins. As shown in figure 4.21, CREB was expressed constitutively over the entire time course even prior to exposure to DM (0 hr). pCREB was not detected before differentiation induction, but was expressed after induction at all time points tested.

Quantitative comparison of the expression levels however cannot be concluded by the findings here. Future experiments determining their expression levels quantitatively would be informative which can be achieved by western blotting with appropriate specific antibodies.

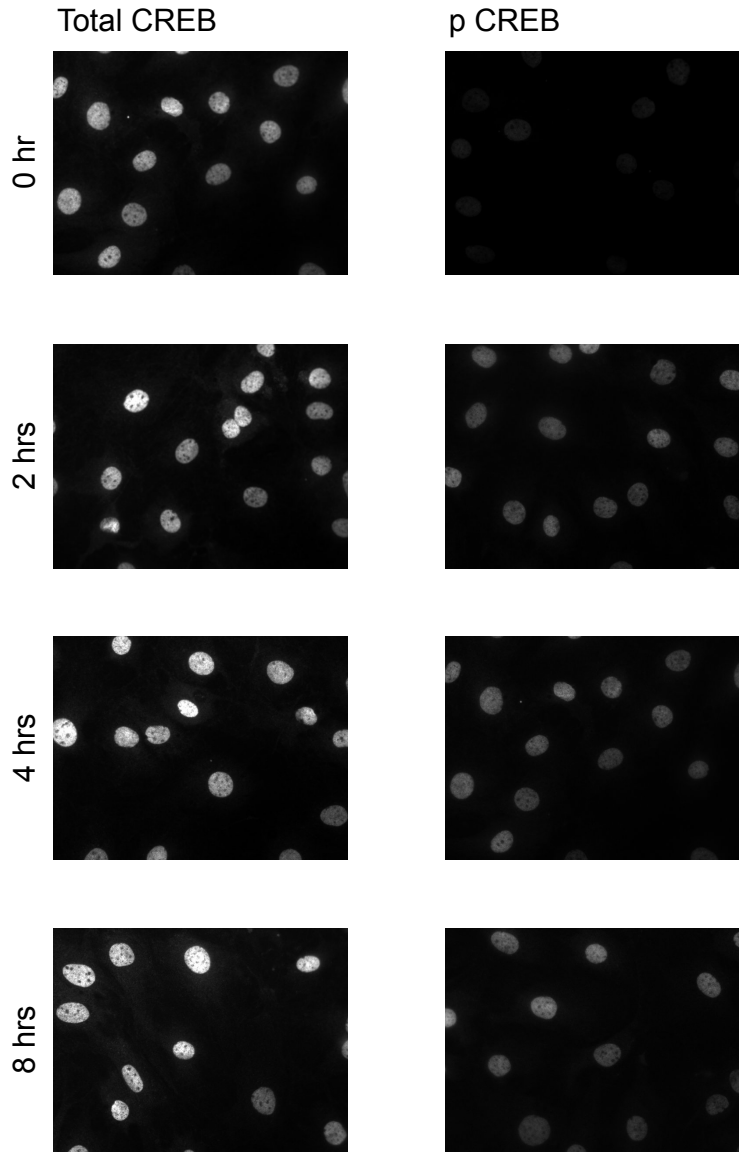

Figure 4.21: Images of anti-CREB and anti-pCREB immunofluorescence in C3H10T1/2 cells expressing total and phosphorylated CREB before and after adipogenesis induction.

4.2.6.2 Sonication optimization

Sonication of chromatin is a pivotal step in chromatin immunoprecipitation (ChIP) and the resulting chromatin fragment sizes are influenced by a number of factors including power of sonication, number of cycles, cross-linking conditions, buffer compositions etc. The ideal fragment sizes are 200 -500 bp for ChIP RT-qPCR. Before the immunoprecipitation experiment, an initial sonication time course experiment was performed to test and optimise the chromatin shearing and fragment sizes. Samples were sheared respectively for 9, 12 and 15 cycles of 20 sec ON/20 sec OFF at power 35. A 1.5% agarose gel was run to check the sonication efficiency and confirm that the target sizes were achieved. A smear from 200-500 bp was seen at 9 cycles (Figure 4.22). (Due to a fault developed with the transilluminator, the image displayed was blurred, so the gel was double-checked using another trasnilluminator, a clear smear located at 200-500 bp was confirmed with others being located below 500 bp). An unsonicated sample was also electrophoresed for comparison. So for all the ChIP experiments conducted below, samples were sonicated for 9 cycles of 20 sec ON/20 sec OFF at power 35.

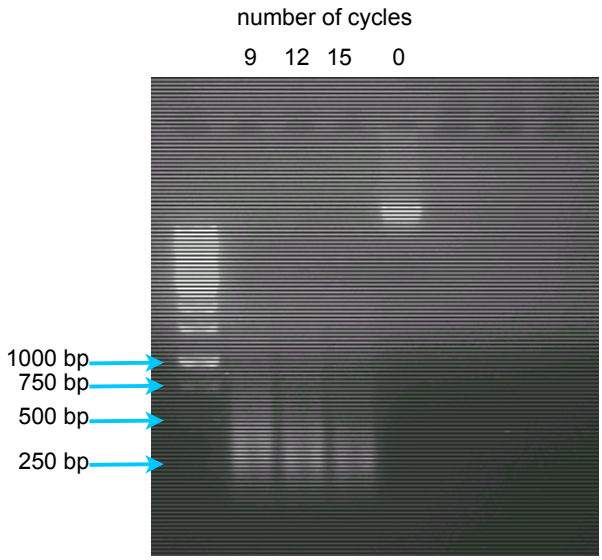

Figure 4.22: Chromatin fragment sizes after sonication for several cycles of 20 sec ON/20 sec OFF

4.2.6.3 Identification of CRE in MmTPC2

The DECODE[1] program revealed the presence of a putative CRE within the 2500 bp region upstream of the transcription start site (detected by the Neural Network Promoter Prediction program provided by M.G. Reese[2]) of *MmTpcn2* promoter (Figure 4.23). Having confirmed a putative binding site for CREB, the next step was to check if DM-induced activation of this transcription factor contributes to *Tpcn2* promoter activity.

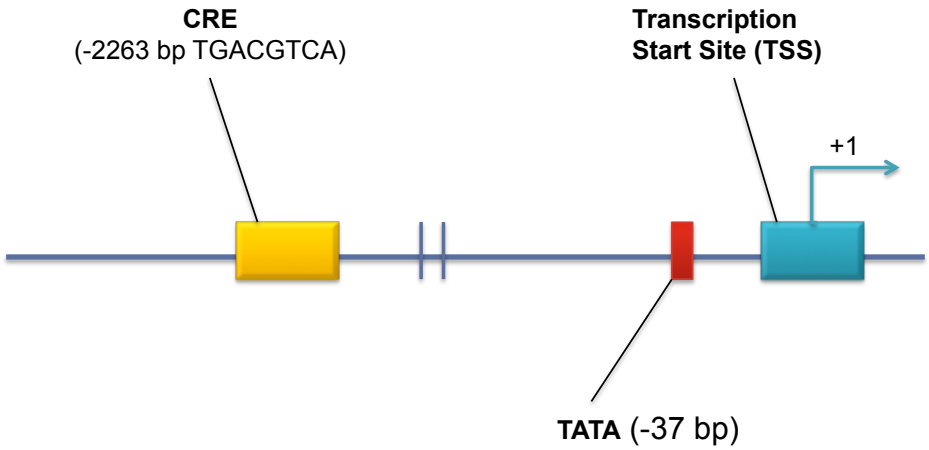

Figure 4.23: Schematic of *MmTpcn2* promoter. Sequence of consensus CRE is depicted with distance relative to the transcriptional start site.

4.2.6.4 Recruitment of pCREB to the *Tpcn2* promoter

C3H10T1/2 cells were induced to differentiate into adipocytes by DM and at 2 hours post-induction nuclear lysates were collected for ChIP assay to detect the binding of pCREB to the *Tpcn2* promoter and *cFos* promoter. The latter served as a positive control as it is well established that CREB binds to and regulates *cFos*. A specific anti-pCREB antibody was used and the ChIP signal was measured by qPCR using primers which amplify the region flanking the CRE of *Tpcn2* and the mouse *cFos* gene. For both pairs of *cFos* primers, an

[1] DECODE: http://www.sabiosciences.com/chipqpcrsearch.php?gene=Tpcn2&factor=Over+200+TF&species_id=1&ninfo=n&ngene=n&nfactor=y
[2] Neural Network Promoter Prediction: http://www.fruitfly.org/seq_tools/promoter.html

approximately 40% and 35% increase was seen respectively with forskolin-stimulated and DM-induced pCREB-*cFos* signal, which were ~2 fold higher than their negative controls (no antibody incubation, signal served as non-specific binding) (Figure 4.24A). On the other hand, the DM-induced pCREB-*Tpcn2* signal displayed a ~20% increase for both pairs of primers, which was ~1.5 fold higher than its negative control (Figure 4.24B). These findings indicated that pCREB was recruited to the CRE in the *Tpcn2* promoter at 2 hours post-induction.

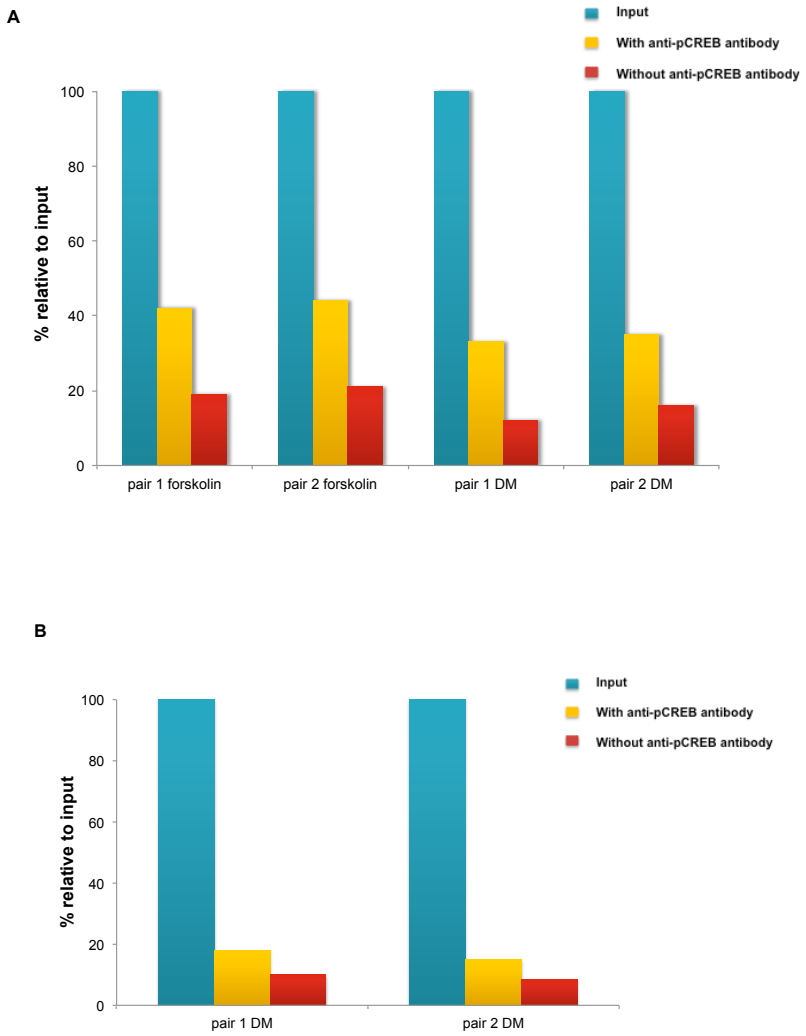

Figure 4.24: ChIP data plotted as percentage ChIP DNA/input. **(A)** At 2 days postconfluence, C3H10T1/2 cells were left untreated or stimulated with forskolin or adipogenic differentiation inducing agent (DM) for 2 hours. Binding of p-CREB to the *cFos* promoter was assessed by ChIP. **(B)** Ay 2 days postconfluence, C3H10T1/2 cells were left untreated or stimulated with DM for 2 hours. Binding of pCREB to the *Tpcn2* promoter was determined by ChIP. In both experiments, two pairs of primers (namely pair 1 and pair 2; primer sequences refer to Materials and Methods) were tested and absence of anti-pCREB antibody was used as negative control. ChIP data obtained was analysed using RT-PCR.

4.3 Discussion

4.3.1 TPC2 – a novel regulator of C3H10T1/2 cell adipogenesis in vitro

Adipogenesis involves significant changes of cell shape and functions. The entire adipocyte differentiation program is strictly governed by defined molecular events, yet the precise mechanisms are only partially elucidated. C3H10T1/2 cell line is one of the commonly employed *in vitro* models for studying adipogenesis regulation. Differentiation of C3H10T1/2 cells into adipocytes occurs under the treatment of hormonal cocktail MDI which includes IBMX, insulin and dexamethasone [208, 343]. Recently, TPCs have been demonstrated to be involved in regulation of MSC differentiation into other cell lineages. Aley and colleagues showed that siRNA-mediated KD of TPC1 and TPC2 produced a moderate and remarkable inhibition respectively in myogenic differentiation of C2C12 cells [133]; whereas Notomi and colleagues demonstrated a dramatic impairment of osteoclastogenesis elicited by miRNA-mediated TPC2 KD in an osteoclast precursor cell line [134].

In my study, I confirmed a transient and substantial upregulation of *Tpcn2* mRNA expression during the early stage of adipogenesis in differentiating C3H10T1/2 cells when stimulated with the standard hormonal cocktail MDI: an initial rise in *Tpcn2* expression occurred between 4 to 8 hours post-induction, expression was then downregulated at 24 hours and remained at nearly the same level at 48 hours (Figure 4.9). The result is consistent with that shown previously by Dr Ruth Tunn (in preparation) except that the peak happened at 4 hours in her study (Appendix section 4.4.1). These data suggest that TPC2 is mainly required during early differentiation events rather than the later stage. Also, shRNA KD of TPC2 in C3H10T1/2 cells resulted in a significant reduction (about 50%) in lipid accumulation compared with cells transfected with empty vector, scrambled shRNA or untransfected cells (WT), all being exposed to DM (Figure 4.10A and B),

suggesting an inhibitory effect on adipogenesis by downregulation of this gene. These findings were further confirmed by a significant reduction seen with mRNA expression of an adipocyte marker gene PPARγ in TPC2KD C3H10T1/2 cells measured at 24 and 48 hours post-induction (Figure 4.11 and 4.12) and also a dramatic attenuation observed with another adipocyte marker gene C/EBPα at 24, 48 and 72 hours post-induction (David Gay; in preparation; Appendix section 4.4.3). All these findings provide preliminary evidence for the involvement of TPC2 in adipogenesis, implicating TPC2 a functional role in adipocyte differentiation in C3H10T1/2 preadipocytes. This compelling evidence of a new role of TPC2 in adipocyte differentiation prompted me to explore further what factors trigger the TPC2 upregulation and how such TPC2-mediated signalling contributes to adipogenesis.

Looking back at the inhibitory effects on both PPARγ and C/EBPα mRNA expression mentioned above, these results also indicate that TPC2 is likely to act upstream of them, as their expressions are abundant from 24 hours post-induction onwards [242]. In fact, this suggestion has been further supported by addition of troglitazone (a well-known PPARγ ligand) that substantially augmented the adipogenic capacity in TPC2KD C3H10T1/2 cells as indicated by lipid accumulation (David Gay; in preparation; Appendix section 4.4.4).

The implication of TPC2 acting upstream of PPARγ and C/EBPα is of particular importance because PPARγ together with C/EBPα are both regarded as important master regulators of adipogenesis activating the entire program of adipogenesis [206, 207, 216, 228]. C/EBPα appears later than PPARγ [242] and expression of C/EBPα and PPARγ are further maintained by reciprocal upregulation [238]. PPARγ and C/EBPα are initially switched on by C/EBPβ and C/EBPδ [238], expression of which happens around 2 hours post-induction in 3T3-L1 preadipocytes [242] and C3H10T1/2 preadipocytes (Dr Ruth

Tunn; in preparation; Appendix section 4.4.2) and are induced directly by adipogenic hormones [242]. With the early expression profile of *Tpcn2*, a potential link between these three genes cannot be ruled out due to their early upregulation pattern in adipogenesis and also the evidence that TPC2 is acting upstream of PPARγ and C/EBPα. Collectively, it is suggested that TPC2 is potentially involved in the regulation of PPARγ and/or C/EBPα expression, and the precise mechanism remains to be investigated.

4.3.2 Intracellular Ca^{2+} regulation in adipogenesis of C3H10T1/2 cells

Ca^{2+} signalling has been shown to play a role in regulating adipogenesis, however, unlike skeletal muscle differentiation in which a clear impact has been identified, the involvement of Ca^{2+} signalling in adipogenesis is less well defined and more complicated; both stimulatory and inhibitory effects have been demonstrated on this process, and the underlying mechanisms remain elusive (detailed description refers to section 4.1.4). NAADP has recently been identified as a novel Ca^{2+}-mobilizing second messenger and its role in adipocyte differentiation was investigated pharmacologically in my studies. Bafilomycin was introduced at 0-4 and 0-8 hours post-induction respectively and a dose-response relationship between adipogenic capacity and bafilomycin was revealed, with the 0-8 hours treatment producing a slightly more potent effect. When introduced at high concentrations (>IC_{50}) bafilomycin also exhibited the ability to completely inhibit the adipogenic response as judged by lipid accumulation (Figure 4.14A-D) and morphological phenotype (Figure 4.14E). However, such dose-dependent inhibition did not occur with the Ned-19 treatment (Figure 4.15A), nor did Ned-19 produce any positive effects on adipocyte differentiation as assessed by lipid accumulation (Figure 4.15B). Even application of a very high dosage, 100 μM, which is the same concentration used in myogenesis inhibition [133] and keratinocyte differentiation inhibition [136] experiments

did not produce any obvious effects in my studies. It may be possible that an even higher concentration is required which is quite unusual as in other systems Ned-19-induced suppression of NAADP signalling responses increases dose-dependently from negligible to maximal spanning a dosage range of several orders of magnitude [94]. An exception is a lipid bilayer study in which a potentiation of TPC2 channel opening probability occurs at 30 to 100 nM Ned-19 treatment but substantial blockade at 1 μM [102]. However, in my case, concentrations higher than 100 μM resulted in obvious cell death so evaluation was deemed impossible for doses higher than 100 μM. Another explanation accounting for the difference seen with bafilomycin and Ned-19 treatment could be the different time frames of drug administration. Bafilomycin treatment was introduced during 0-4 or 0-8 hours post-induction whereas Ned-19 was included during 0-48 hours post-induction. This raises the possibility that the first 8 hours post-induction could be the critical window for blockade of adipogenesis by inhibition mediated by NAADP signalling pathway inhibitors. In fact, previous studies have pharmacologically demonstrated the importance of critical timing and temporal control of Ca^{2+} signalling on regulating adipogenesis. Wang and colleagues showed that CaMKII inhibitors when introduced at either 6-12 or 24-48 hours post-induction markedly impeded adipogenesis in 3T3-L1 preadipocytes [305]; Shi and colleagues showed that in human preadipocytes substantial inhibition of adipogenesis produced by thapsigargin or A23187 only occurred with introduction at 0-1 hour post-induction but not 47-48 hours; sustained and mild stimulation of Ca^{2+} influx with KCl or agouti at 0-48 hours also blocked adipogenesis; whereas stimulatory effects were seen at late stage of adipogenesis, 71-72 or 48-72 hours [304]. The narrow time frame for blockade of adipogenesis by bafilomycin may reflect the transient prominent upregulation of *Tpcn2* during early adipogenesis, which was found to happen at 2-8 hours post-induction (Figure 4.9). Similar reflection can also be found in CaMKII inhibition in

that the identification of two different phases for differentiation attenuation are well corresponded to the biphasic activation of CaM kinase [305]. Thus, whether Ned-19 can effectively alter adipogenesis awaits further investigation to locate the time window during which the differentiation program can be inhibited by Ned-19, with particular focus on those periods during which bafilomycin has been shown to have an inhibitory effect. In addition, testing the effects of bafilomycin at a different period of time can help validate bafilomycin's time window as well. Moreover, investigations involving membrane permeant NAADP-AM, an endogenous modulator of TPC, to activate NAADP in both undifferentiated preadipocytes and differentiated adipocytes could further assist in characterising the spatiotemporal properties of this signalling in adipogenesis and thus elucidation of the contribution of this signalling to adipogenesis, albeit NAADP-AM has the same drawback as Ned-19 – lack of TPC isoform specificity. It would also be interesting to see if increase in NAADP activity is limited to a critical time frame like those described above and whether a typical bell-shaped concentration-response curve will be produced for NAADP treatment. Nevertheless, the perturbation of adipogenic capacity resulting from BAPTA-AM suggested the involvement of intracellular Ca^{2+} signalling during early adipogenesis of C3H10T1/2 cells; the disruption of adipogenesis noted with bafilomycin implicated the involvement of lysosomal stores in early stage of adipogenesis in C3H10T1/2 cells; and since NAADP receptors are found to reside on acidic organelles including lysosomes, a role of NAADP-induced Ca^{2+} signalling in regulation of adipogenesis is highly possible, especially given that the upregulation of *Tpcn2* expression was noted in the same period with the bafilomycin-induced inhibition of adipogenesis. Further work including key Ca^{2+} imaging experiments should provide further evidence for this new and very attractive role of TPC2 in adipogenesis. For example, experiments with NAADP or membrane-permeant NAADP-AM, an endogenous modulator of TPC2, to

activate NAADP in both undifferentiated preadipocytes and differentiated adipocytes could assist in characterising the spatiotemporal properties of this signalling in adipogenesis and thus a better understanding of the differentiation regulation. It would also be interesting to see if increase in NAADP activity is limited to a critical time frame like those described above and whether a typical bell-shaped concentration-response curve will be produced for NAADP treatment. Finally, future work based on primary adipocytes extracted from TPC2$^{-/-}$ mice could also be very valuable to understand the adipogenesis regulation *in vivo*.

4.3.3 Involvement of cAMP effectors – PKA and Epac in Tpcn2 upregulation

Previous studies reported a cAMP-mediated upregulation of *Tpcn2* mRNA levels (this occurred at 4 hours post-induction) in C3H10T1/2 cells with the aid of different pharmacological agents including IBMX, forskolin, rolipram and adenylyl cyclase inhibitor SQ22536 to change the cAMP levels (Appendix section 4.4.5 and 4.4.6). Together with my findings which implicate TPC2 in a role during early adipogenesis in C3H10T1/2 cells treated with DM, this raises the possibility that PKA and/or Epac may have a role in the cAMP-mediated upregulation of *Tpcn2* expression in C3H10T1/2 cells. In the present study, the selective PKA C subunit inhibitor PKI was shown to suppress *Tpcn2* mRNA expression at 2 hours post-induction (Figure 4.16), suggesting that PKA kinase activity is required for upregulation of *Tpcn2* expression at that time point. The use of the selective Epac inhibitor ESI-09 also demonstrated an essential role for Epac in such regulation, as substantial inhibition was noted at 2 and 4 hours post-induction (Figure 4.19). However, both failed to suppress the upregulation of *Tpcn2* expression at 8 hours during which maximal upregulation is observed. This could be because PKA and Epac

may not be responsible for upregulation at 8 hours, as indicated by the substantial abridged Epac1 expression at that time point (Figure 4.17). The low level of Epac1 at this time point may alternatively imply an anti-adipogenic effect of Epac1 and low expression could be to augment this anti-adipogenic effect. On the other hand, both PKA C and R subunits expressions have not been tested here or reported in C3H10T1/2 cells previously, thus it would be important to look into their temporal expression patterns in order to understand more about its correlation with *Tpcn2* expression. Of note, findings have pointed the importance of R subunits in 3T3-L1 and human preadipocyte adipogenesis [268, 273], thus it would be useful to explore whether the R subunits are involved in *Tpcn2* upregulation as well. Intriguingly, C subunits have been shown to be required for MCE of 3T3-L1 preadipocyte adipogenesis [274], and here the upregulation of *Tpcn2* at 2 hours suggested to be mediated by C subunits falls into the time frame (generally 0-48 hours post-induction) when MCE is occurring in C3H10T1/2 cells, therefore does it imply that *Tpcn2* upregulation is associated with MCE as well? Future studies are definitely required to elucidate all these questions so as to provide additional insights into the regulation of *Tpcn2* expression by PKA and Epac. These include mRNA and protein expression studies of R and C subunits, also genetic methods which employ overexpression and sh/siRNA KD of these two subunits and Epac1. Due to the lack of convincing studies about the dominant negative effect of Epac, the use of dominant-negative Epac is deemed not preferable [268].

The finding that *Tpcn2* upregulation at 8 hours failed to be inhibited by PKA or Epac inhibitors may suggest the involvement of non-cAMP effects of IBMX. Previous findings from Dr Ruth Tunn (in preparation; Appendix section 4.4.5 and 4.4.6) showed an upregulation of *Tpcn2* expression by cAMP-elevating agents, and the increase for forskolin and rolipram was slightly lower than that observed with IBMX, indicating the

possibility of a contribution by non-cAMP effects of IBMX, e.g. elevated cGMP levels. Again, future investigations are required to evaluate the participation of cGMP in regulating *Tpcn2* expression.

Since only one concentration of the inhibitors was tested, it would be useful to evaluate the effects using a range of concentrations. Also, since upregulation at 4 hours and 8 hours was only reported in IBMX-induced differentiation, thus it would be interesting to check whether other cAMP-elevating agents are able to upregulate *Tpcn2* expression at these time points. Intriguingly, while Epac is necessary for cAMP-mediated *Tpcn2* upregulation, substitution of IBMX with the Epac specific cAMP analog 8pCPT failed to promote *Tpcn2* upregulation at any time points (Figure 4.18), indicating that Epac alone is not sufficient to promote *Tpcn2* upregulation in C3H10T1/2 cells. Similar observations from recent reports also demonstrated that replacing IBMX or forskolin with 8pCPT could not mimic the adipogenic effect induced by an increase in endogenous cAMP level in 3T3-L1 cells [268, 275]. The observation that ESI-09 failed to mimic such upregulation could be due to the concentration of Epac analog used being insufficient for eliciting an effect; or it may probably be the dual effects of Epac, with high concentrations being stimulatory and promotes *Tpcn2* expression and low concentrations being inhibitory. Epidermal growth factor (EGF) which has been suggested to inhibit adipogenesis via activation of PKA [267], was reported to promote adipogenesis at concentrations <1 nM but blocks differentiation at higher concentrations [344]. Thus a dual effect of Epac is not completely impossible. Future investigations involving a range of concentrations would be necessary to uncover the definitive role of Epac regulation in *Tpcn2* expression. Alternatively, it could be the synergistic activation of both PKA and Epac that is required to upregulate *Tpcn2* expression. Evidence has shown that in both 3T3-L1 preadipocytes and hMSCs, Epac activation failed to promote adipogenesis when the PKA-dependent suppression of

Rho/ROCK activity was absent, while adipogenesis was enhanced with concomitant action of Epac activation and ROCK inhibitor, suggesting that Epac activity stimulated adipogenesis through counteraction of the downregulated IGF-1/insulin signalling [275, 276]. Similar synergism was also reported in PC-12 cell differentiation as assessed by neurite extension [341]. And more importantly, my results have demonstrated that both PKI- and Epac-mediated inhibition of *Tpcn2* expression occurred in a similar time frame, thereby suggesting the possibility that PKA activation could be linked to Epac activation in upregulating *Tpcn2* expression. Additional investigations are needed to look into whether such synergism is required for mediation of *Tpcn2* expression in adipogenesis, or alternative feedback mechanism associated with factors other than PKA are necessary. This could be verified by employing range of doses of specific Epac and PKA analog (e.g. 6-MB-cAMP and 6-Bnz-cAMP), either solely or in combination, or by using specific Epac and PKA inhibitors together. Apart from this, another useful study would be to investigate whether addition of a specific Epac or PKA analog or both combined can augment the loss of adipogenic capacity seen in TPC2KD C3H10T1/2 cells.

4.3.4 CREB

The data presented here demonstrated that CREB is constitutively expressed in C3H10T1/2 cells prior to and after adipogenesis induction by DM treatment (Figure 4.21); in addition, CREB phosphorylation is rapidly activated in C3H10T1/2 cells upon DM treatment. Both findings are consistent with that shown in 3T3-L1 cells and MEFs [251, 252, 282]. That expression of CREB occurs before differentiation induction displays a marked difference from other adipocyte transcription factors (e.g. C/EBPα and β and RXR) which are only detectable after adipogenesis induction [242].

A CRE element within the promoter of *Tpcn2* was identified (Figure 4.23), and that

pCREB binds to this CRE element in C3H10T1/2 cells at 2 hours post-induction was revealed by ChIP (Figure 4.24). Due to time limitations, only this time point has been assessed and thus the ability of pCREB to bind to CRE at other time points awaits further investigation. Certainly the current data obtained by ChIP only provides indirect evidence of CREB's involvement in *Tpcn2* transcription; further investigation will be essential to verify whether direct transactivation by CREB or recruitment of another factor(s) is necessary for *Tpcn2* expression. This could be addressed by cotransfection of a constitutively expressed CREB or sh/siRNA KD/dominant-negative CREB with the CRE-containing portion of *Tpcn2* gene promoter linked to a luciferase reporter gene. A prerequisite is to obtain a promising transfection method for this difficult to transfect cell line.

On the other hand, emerging evidence has shown that AFT1, a closely related factor of CREB, is also necessary for adipogenesis as indicated by the effects of KD of both genes in 3T3-L1 cells *in vitro* and 3T3-F442A cell *in vivo* [281] and that multiple CRE-binding factors are involved in MDI-induced C/EBPβ expression [252, 345, 346]. It will therefore be equally important to analyse other CRE-binding factors, co-activators and co-repressors that bind to the *Tpcn2* gene promoter to better understand the regulation of this gene's expression, although involvement of these components in adipogenesis is not as extensively studied as CREB.

Apart from being activated by cAMP signalling pathway, phosphorylation of CREB is also known to be activated by insulin. Insulin-mediated regulation of CREB transcriptional activity has been shown to act via the Ras/Raf1/MEK/ERK1/2 kinase pathway in 3T3-L1 preadipocytes, causing phosphorylation of CREB [282]. This raises the possibility that *Tpcn2* expression may alternatively be modulated by the insulin/CREB pathway. However, this possibility needs to be tempered with reference to the results from

section 4.2.5.2.2 (Figure 4.18), which clearly showed that C3H10T1/2 cells treated with DM in the absence of IBMX failed to elicit the remarkable *Tpcn2* upregulation as that seen with the complete DM treatment.

Taken together, while the present data are insufficient to conclude that CREB directly regulates the cAMP-mediated upregulation of *Tpcn2* expression in DM-induced differentiating C3H10T1/2 cells, the demonstrated evidence of pCREB binding to CRE element of *Tpcn2* gene promoter however provides tantalizing preliminary evidence that this transcription factor is at least in part involved in regulating *Tpcn2* expression at 2 hours post-induction in C3H10T1/2 cells treated with DM and detailed investigation is absolutely required to uncover the missing link.

4.3.5 How does TPC2 contribute to adipogenesis?

4.3.5.1 Downstream effectors

One of the profound effects induced by IBMX (via cAMP signalling pathway) is the activation of c/EBPβ expression during early adipogenesis which is crucial for activation of the two master transcriptional factors PPARγ and c/EBPα (section 4.1.2.2) [206, 228, 347]. The IBMX-triggered upregulation of c/EBPβ expression is directly stimulated by adipogenic hormones in the absence of prior protein synthesis [242], implying that a direct recruitment of TPC2 for the enhanced c/EBPβ expression is precluded. Nevertheless, c/EBPβ needs be activated to acquire the DNA-binding activity for the subsequent transactivation of c/EBPα [216]. One possibility for c/EBPβ activation may be mediated through the Ca^{2+}-activated protease calpain activity. Since a blockade of IBMX-triggered 3T3-L1 preadipocyte adipogenesis and c/EBPα expression has been observed with suppression of calpain activity during a critical time frame of 6-24 hours post-induction, more compelling is that the ability of c/EBPβ to bind to c/EBPα promoter is impeded

without affecting c/EBPβ expression [309]. Taken together, by comparing the current data presented in my study, TPC2 may potentially be implicated in a role of activating calpain in this proposed model. Future investigations employing sh/siRNA KD of *Tpcn2* in C3H10T1/2 cells could be valuable in understanding the influence of *Tpcn2* downregulation on calpain activity as well as the possible pathways whereby TPC2/caplain may facilitate adipogenesis regulation.

On the other hand, it has been suggested that Ca^{2+} signalling may be implicated in regulating adipogenesis through effects at the post-confluent mitosis stage (detailed description in section 4.1.4). Since upregulation of *Tpcn2* expression occurs during 4-8 hours post-induction which coincides with the MCE stage that generally happens during the first 48 hours post-induction, the possibility that TPC2 may also play a part during cell proliferation cannot be ruled out. And the finding that calpain inhibition prevents p27 degradation and thus reentry of post-confluent cells into the cell cycle [348] suggest another pathway through which TPC2 might mediate calpain activity to regulate adipogenesis. Investigations including cell counting and [^{3}H] thymidine incorporation of *Tpcn2*KD and KO cells would be crucial to further elucidate whether abolition of TPC2-mediated Ca^{2+} signalling would influence the MCE phase of adipogenesis.

Since a biphasic upregulation of CaMKII activity occurs during 0-15 hours post-induction of adipogenesis [305], and in pituitary cells CaMKII-induced enhancement of c/EBPβ transcription has been revealed [349], suggesting that Ca^{2+} signalling could play a similar role in adipogenesis. On the other hand, calcineurin activated by Ca^{2+}/CaM has been shown to promote NFAT nuclear translocation and regulate gene expression in adipogenesis, and repression of adipogenesis resulted from blockade of NFAT nuclear translocation at 1-2 days post-induction has been revealed [307]. Taking into account the findings that TPC2 regulates osteoclastogenesis through influencing NFAT translocation

[134], research of this mechanism in adipogenesis may provide additional insights to our knowledge of TPC2-mediated adipogenesis regulation. KD and KO studies will be useful for determining TPC2/CaMKII and TPC2/NFAT pathways in adipogenesis.

4.3.5.2 Upstream mediators

Upstream mediators must be responsible for transducing the signal from IBMX or other cAMP-elevating agents to transactivate *Tpcn2* expression. As discussed above, the two main effectors of cAMP, PKA and Epac, have been implicated in mediating cAMP signal to promote adipogenesis with an upregulation of PPARγ and C/EBPα expression [275, 277]. In view of the findings that IBMX and cAMP mimetics (Figure 4.9 and 4.18 and Appendix section 4.4.5 and 4.4.6) but not insulin or dexamethasone (Figure 4.18), lead to upregulation of *Tpcn2* expression, and that specific PKA C subunits and Epac inhibitors result in downregulation of *Tpcn2* expression in C3H10T1/2 cells treated with MDI (Fig. 4.16 and 4.19), PKA C subunit and Epac are thus implied to be regulators of *Tpcn2* expression. Since R subunits of PKA have also been implicated to be pro-adipogenic, it is possible that they may contribute in this process which needs to be identified in further studies. On the other hand, non-cAMP effects of IBMX such as cGMP are also suggested to be involved in regulating *Tpcn2* expression.

CREB is the primary transcription factor target for cAMP/PKA signalling and is also activated by the Epac/Rap/PI3K/PKD/PKB signalling pathway in hMSCs [277], suggesting that CREB could be acting downstream of PKA/Epac to regulate the cAMP-mediated *Tpcn2* upregulation. Besides, the evidence showing that CREB together with ATF1, regulates the expression of PPARγ directly and C/EBPα partially in differentiating 3T3-L1 preadipocytes [281] suggests that CREB could be involved in transactivation of *Tpcn2* expression. A preliminary finding in the present study has shown CREB binding to

CRE element of *Tpcn2* gene promoter at 2 hours post-induction in MDI-treated C3H10T1/2 cells; further investigations are required to look into the binding ability of CREB at different time points particularly 4 and 8 hours when significant upregulation of *Tpcn2* expression occurs. Additional studies to identify whether *Tpcn2* transactivation is solely dependent on CREB activation, or through multiple binding factor regulation or by means of other pathways, would also be of particular importance.

4.3.6 Future plan for determining TPC role(s) in adipogenesis

4.3.6.1 Summary of potential future studies

A number of future studies employing various sorts of techniques have been suggested in previous sections, one of the key future work which is immensely valuable for investigating the underlying mechanism(s) mediated by TPC2 and NAADP in adipogenesis regulation is Ca^{2+} imaging experiments. For example, pharmacological experiments using endogenous TPC2 modulator NAADP or NAADP-AM will be very informative for this study; while genetics studies based on primary adipocytes extracted from $TPC2^{-/-}$ mice is equally important because this provides valuable information to understand the adipogenesis regulation *in vivo*. Other *in vitro* work using overexpression, KD or KO techniques could provide further evidence for this new and attractive role of TPC2 in adipogenesis as well. It is noteworthy that genetic studies can directly modulate transcriptional activity without interrupting other signalling pathways and transcription factors which might happen with pharmacological agents, therefore they can provide valuable complementary evidence to help identify and clarify the functional role(s) of TPC2 in adipogenesis regulation, as well as the mediators and effectors that have been tested here. In addition, it would be useful to determine any differences at the molecular level between adipogenesis *in vivo* and *in vitro*.

It should be noted that the observed upregulation of *Tpcn2* mRNA mediated by cAMP and downregulation mediated by PKA and Epac in my current study are elicited pharmacologically, but not induced directly by physiological extracellular stimuli. Future investigations looking into the effects of endogenous stimulus-induced cAMP (precisely PKA and Epac) on *Tpcn2* expression would be important, in order to identify whether the cAMP stimulation describes a general mechanism for regulation of endogenous *Tpcn2* expression.

On the other hand, future studies looking into the participation of IP_3 and cADPR-mediated Ca^{2+} signalling would be crucial for a comprehensive understanding of adipogenesis regulation mediated by distinct Ca^{2+} release mechanisms. Findings have suggested that Ca^{2+}-mediated changes in transcriptional activity is important in adipogenesis regulation (detailed description see section 4.1.4), it is therefore crucial to investigate the spatiotemporal control of intracellular Ca^{2+} signals for identification of physiologically representative effects on adipogenesis. Furthermore, it is known that in other systems NAADP-mediated Ca^{2+} release acts as a 'trigger', sensitizing the IP_3 and RyRs, resulting in further Ca^{2+} release from the ER [55, 57]. Similar mechanism may occur in adipogenesis.

Due to the lack of specific antibodies against mouse TPC2, the present study was limited to a focus on *Tpcn2* mRNA expression; the search for an effective and specific anti-mouse TPC2 antibody which recognises native protein is utterly important in order to detect the expression of TPC2 protein during adipogenesis and to evaluate if protein expression at different time points map with the corresponding mRNA expression.

Compelling evidence showed that calpain played a stimulatory role in 3T3-L1 preadipocyte adipogenesis but was inhibitory in ST-13 preadipocyte adipogenesis [311]. This striking difference is probably due to the distinct adipogenesis mechanism between

ST-13 preadipocytes and 3T3-L1 preadipocytes, as clonal expansion is not required for ST-13 preadipocyte adipogenesis [311]. Intriguingly, C3H10T1/2 cells have also been shown to differentiate well into adipocytes with a lack of MCE [350]. In view of this and evidence about *Tpcn2* mRNA upregulation during MCE, future investigation to examine whether *Tpcn2* expression would be altered under the condition that MCE is prevented during C3H10T1/2 cell adipogenesis should be taken into consideration. Other potential studies including investigations of potential upstream mediators and downstream effectors as mentioned in previous sections are essentially important for thorough understanding of the underlying mechanisms of this newly discovered TPC2-mediated adipogenesis regulation.

4.3.6.2 Preliminary study and future investigation of calpain activity in adipogenesis of C3H10T1/2 cells

In fact, a preliminary study has been conducted on calpain activity in adipogenesis of C3H10T1/2 cells but due to time limitations, only activity of WT cells was studied but not TPC2KD cells.

Here, calpain activity in C3H10T1/2 cells subjected to MDI induction was analysed by fluorescent calpain substrate assays using a cell-permeable calpain substrate BOC. Quenching BOC is separated from the fluorescent coumarin when proteinase activity cleaves the peptide linker (Leu-Met), thus increasing fluorescence intensity. Time course experiments were performed and the average *in vivo* active and total calpain activities were measured in both the cytosol and the nucleus, before (active calpain activity) and after calcium stimulation by ionomycin (total calpain activity). Measurement was conducted at a single cell level in which dead cells or non-differentiating cells (there are always a small population of cells locating near the side of the wells tend not to

differentiate well even they are cultured under the same differentiation condition; the number is insignificant though) can be avoided to obtain more accurate analysis. Attempts have been made to measure the average activity from a population of cells using the SensoLyte® 520 Calpain Activity Assay Kit Fluorimetric but inaccurate and very inconsistent results were generated. Thus, the current method using BOC was employed. Active calpain activity was a measure of the activity of endogenously active calpain after induction of adipogenesis while total calpain activity was an indication of the total calpain protein expression. Representative images showing changes in both active and total calpain activity in C3H10T1/2 cells at different time points post-induction are presented in Appendix section 4.4.10.

In 3T3-L1 cells, both calpain mRNA and protein expression was abundant in preadipocytes and declined gradually during differentiation upon MDI induction [309]. The findings here showed that calpain protein in C3H10T1/2 cells, both cytoplasmic and nuclear, however, displayed a slightly different expression profile, with expression started with low levels from 0 to 8 hours post-induction and a dramatic increase occurred at 24 hours, and declined gradually in the following days but levels remained higher than that before 24 hours (Appendix sections 4.4.7B and 4.4.8B). Another finding is that nuclear expression was higher than the cytoplasmic expression throughout the entire time course (Appendix sections 4.4.9A and B). Although expression patterns before 24 hours appear to be different between 3T3-L1 preadipocytes and C3H10T1/2 preadipocytes, similar expression profiles are observed after 24 hours.

A critical time window for calpain activity in adipogenesis has been shown in 3T3-L1 cells, that calpain was required during the first 24 hours post-induction, as indicated by an effective inhibition of adipogenesis by ALLN during 6-24 hours [310]. Looking at the active calpain activity of C3H10T1/2 cells shown in Appendix sections 4.4.7A and

4.4.8A, a dramatic increase in active calpain activity, both cytoplasmic and nuclear, was noted at 24 hours, activity between 0 to 8 hours was rather low, while activity after 24 hours declined gradually, level was still higher than that before 24 hours though. It appears that 24 hours may be a critical time window for calpain activity in C3H10T1/2 cells as maximal activity was recorded. However, it should be noted that the current data only provides information about the general endogenous calpain activity upon MDI induction, whether this time window (24 hours) is also critical for adipogenesis in C3H10T1/2 cells awaits further investigations. Besides, future studies on whether calpain activity is correlated with *Tpcn2* upregulation are equally important. Since calpain was implicated in transcriptional activation of C/EBPα gene in 3T3-L1 cells [309] and similarly TPC2KD C3H10T1/2 cells also displayed a downregulation of C/EBPα expression (Appendix section 4.4.3), whether a potential link might exist between TPC2 and calpain activity on regulating C/EBPα expression would be worth looking into as well.

4.3.7 Conclusion

In conclusion, the work presented here clearly demonstrates the involvement of TPC2 in adipogenesis as indicated by the perturbation of adipogenic capacity in TPC2KD C3H10T1/2 cells. A transient and significant upregulation of *Tpcn2* expression during early adipogenesis of C3H10T1/2 cells is also confirmed, which is mediated by IBMX and other cAMP mimetics but not insulin or dexamethasone. Besides, the current findings suggest the requirement of PKA and Epac in *Tpcn2* upregulation during 2-4 hours, and other mediators may be responsible for the remarkable upregulation at 8 hours. Conversely, Epac alone is insufficient for eliciting the IBMX-induced upregulation. In addition, the evidence that CREB binds to the CRE element of *Tpcn2* promoter implicates

its involvement in the transactivation of this gene. On the other hand, participation of intracellular Ca^{2+} signalling and lysosomal stores during early adipogenesis of C3H10T1/2 cells is implicated by the findings of BAPTA-AM and bafilomycin treatment. Due to its localisation on acidic stores including lysosomes, a role for NAADP-induced Ca^{2+} signalling in regulating adipogenesis in C310T1/2 cells cannot be ruled out. The preliminary results showing the endogenous calpain expression pattern and activity profile further indicate its potential role as an effector of TPC2 in mediating the adipogenesis program in C3H10T1/2 cells.

Certainly, the present findings are not enough to identify the precise mechanism(s) that underlies the role(s) of TPC2 in adipogenesis and its mechanism of activation during this process, yet the data here demonstrates clearly C3H10T1/2 cell adipocyte differentiation is a Ca^{2+} dependent process, likely mediated in part by TPC2 and NAADP. Thus TPC2 represent a novel and highly potential target and mediator in adipogenesis regulation in C3H10T1/2 cells.

4.4 Appendix

4.4.1 *Tpcn2* mRNA expression profile in differentiating C3H10T1/2 cells (Dr Ruth Tunn; in preparation)

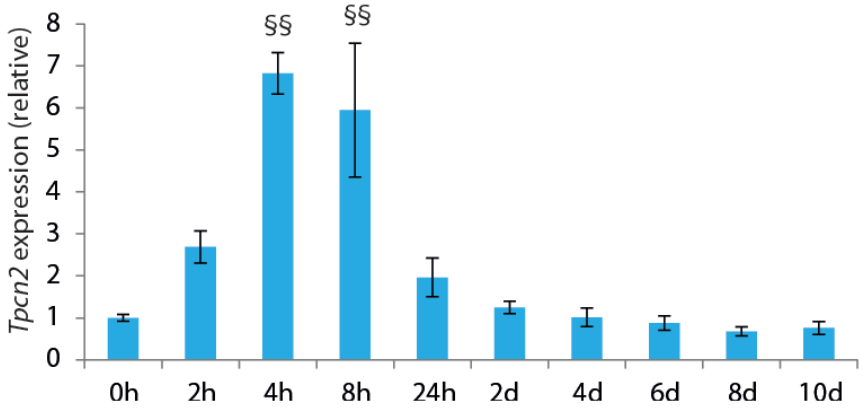

4.4.2 PPARγ mRNA expression profile in differentiating C3H10T1/2 cells (Dr Ruth Tunn; in preparation)

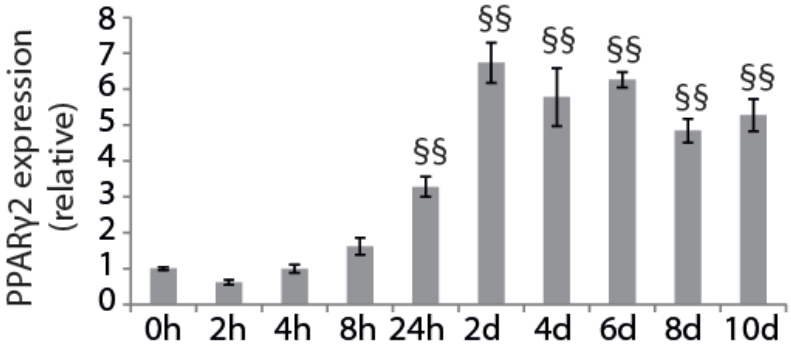

4.4.3 c/EBPα mRNA expression in differentiating C3H10T1/2 cells transfected with empty vector pLK0.1, scrambled shRNA or anti-TPC2 shRNA construct (David Gay; in preparation)

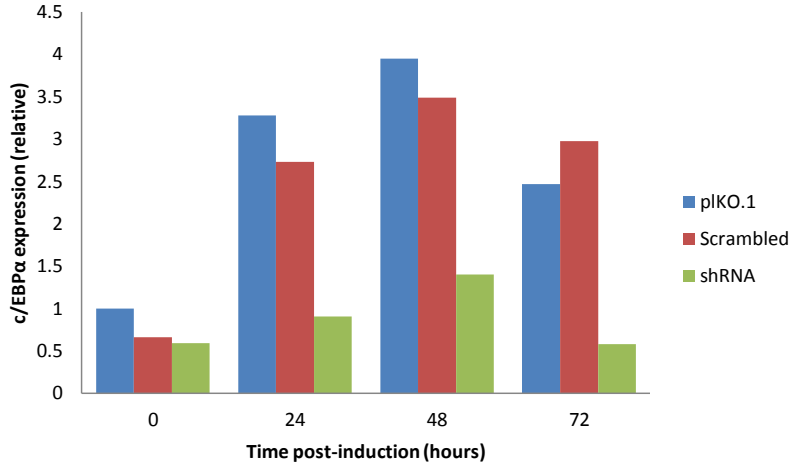

4.4.4 Addition of troglitazone to DM partially augmented the attenuated adipogenic capacity of anti-TPC2 shRNA expressing C3H10T1/2 cells as determined by lipid accumulation (David Gay; in preparation)

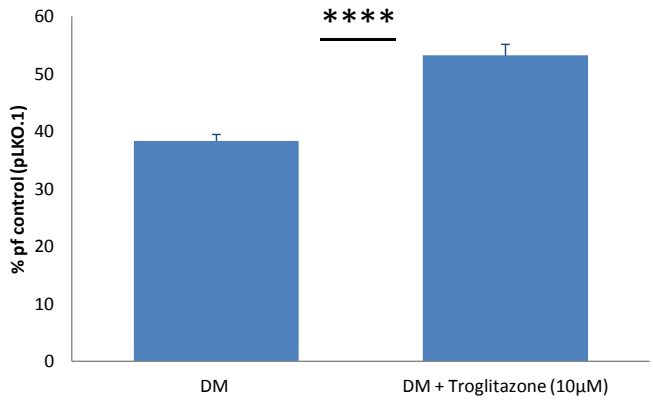

4.4.5 Effect of IBMX on *Tpcn2* mRNA expression in differentiating C3H10T1/2 cells at 4 hours post-induction (Dr Ruth Tunn; in preparation)

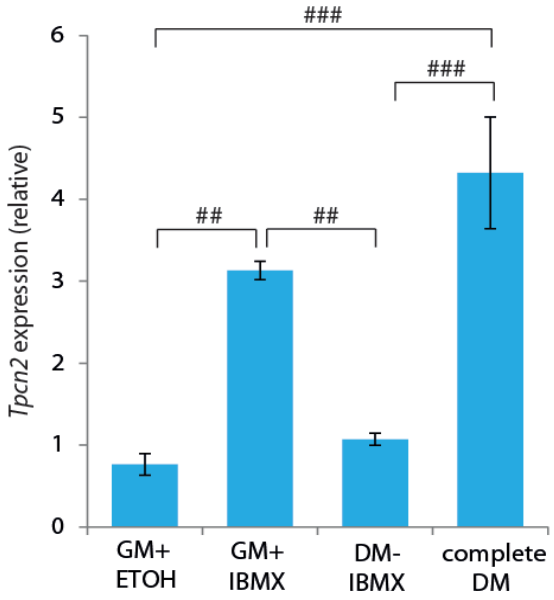

4.4.6 *Tpcn2* mRNA expression in differentiating C3H10T1/2 cells at 4 hours post-induction in response to drugs that alter cAMP levels (Dr Ruth Tunn; in preparation)

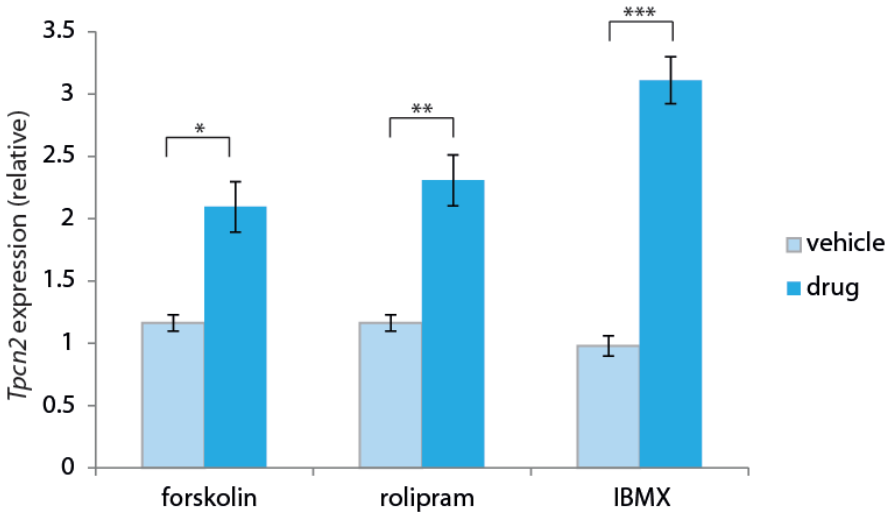

4.4.7 Fluorescent calpain substrate assays determining calpain activity in the nucleus of differentiating C3H10T1/2 cells at different time points post-induction.

Cells were incubated in 20µM of the cell-permeable calpain substrate BOC for 20 minutes. For total calpain activity measurement, cells were treated with 1 M calcium and 5 µM ionomycin for a further 1 minute after the BOC incubation. Graphs demonstrating (A) active calpain activity, (B) total calpain activity, (C) comparison of active and total calpain activity and (D) percentage of active calpain activity/total calpain activity in the nucleus. n = 3. Each experiment measuring BOC fluorescence in ~100 cells. *p<0.05; **p<0.01; ***p<0.001 (student's *t-test*). ##p<0.01; ###p<0.001 (ANOVA *post-hoc* Turkey test, compared between consecutive time points). §§p<0.01 for 2 hrs post-induction and §§§p<0.001 for all other time points (Not shown on graph) (ANOVA *post-hoc* Dunnett test vs 0 hr) Data presented ± SEM.

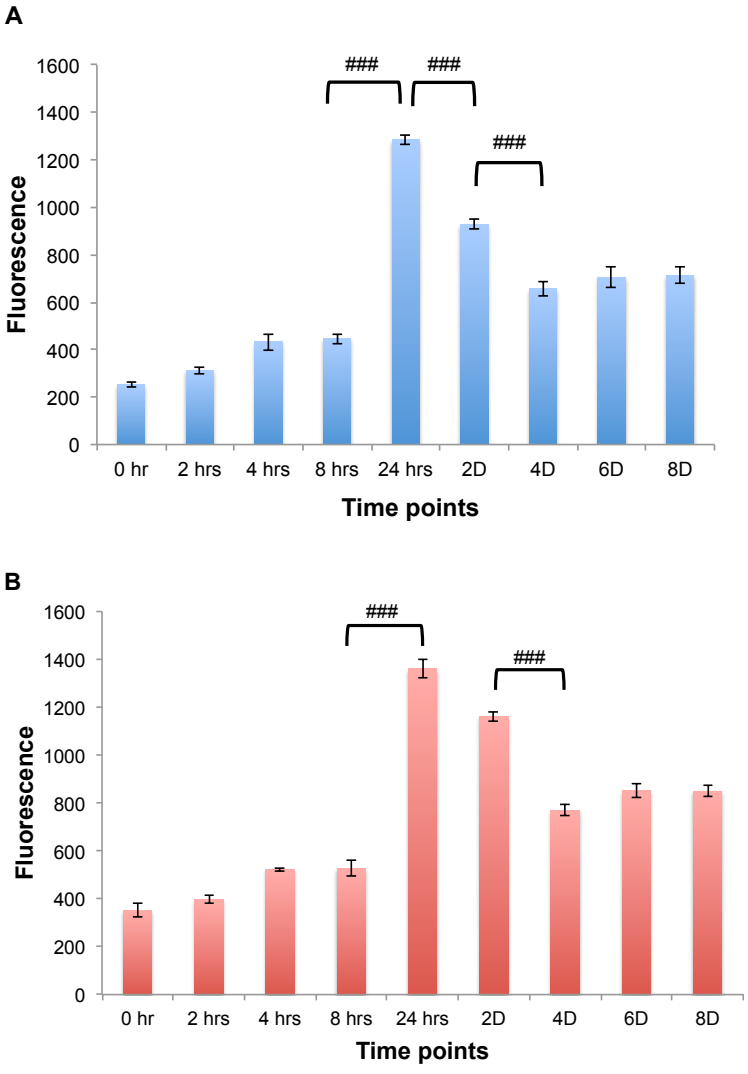

C

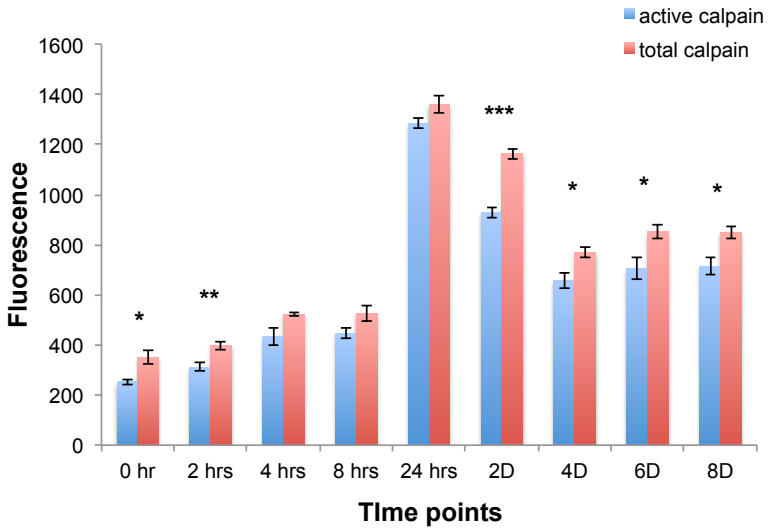
active calpain
total calpain
Fluorescence
1600
1400
1200
1000
800
600
400
200
0
*
**
***
*
*
*
0 hr
2 hrs
4 hrs
8 hrs
24 hrs
2D
4D
6D
8D
TIme points

D

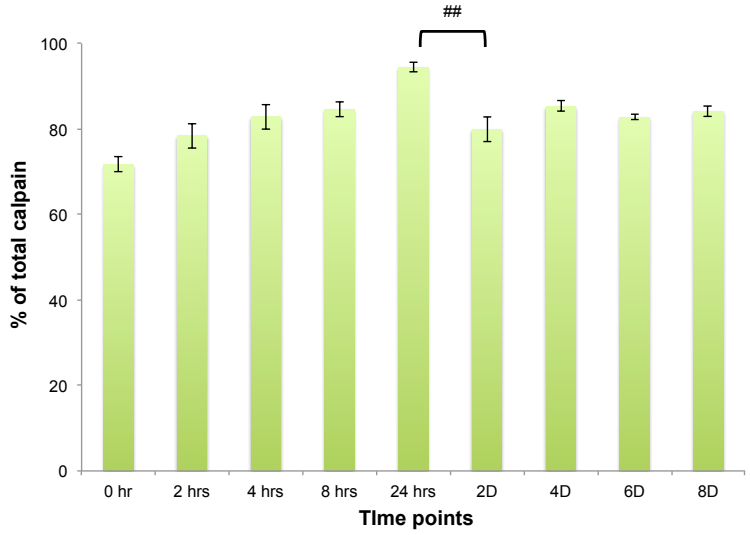
##
% of total calpain
100
80
60
40
20
0
0 hr
2 hrs
4 hrs
8 hrs
24 hrs
2D
4D
6D
8D
TIme points

4.4.8 Fluorescent calpain substrate assays determining calpain activity in the cytoplasm of differentiating C3H10T1/2 cells at different time points post-induction.

Cells were incubated in 20 µM of the cell-permeable calpain substrate BOC for 20 minutes. For total calpain activity measurement, cells were treated with 1 M calcium and 5 µM ionomycin for a further 1 minute after the BOC incubation. Graphs demonstrating (A) active calpain activity, (B) total calpain activity, (C) comparison of active and total calpain activity and (D) percentage of active calpain activity/total calpain activity in the cytoplasm. n = 3. Each experiment measuring BOC fluorescence in ~100 cells. *p<0.05; **p<0.01; ***p<0.001 (student's *t-test*). ##p<0.01; ### p<0.001 (ANOVA *post-hoc* Turkey test, compared between consecutive time points). §§p<0.01 for 2 hrs post-induction and §§§p<0.001 for all other time points (Not shown on graph) (ANOVA *post-hoc* Dunnett test vs 0 hr) Data presented ± SEM.

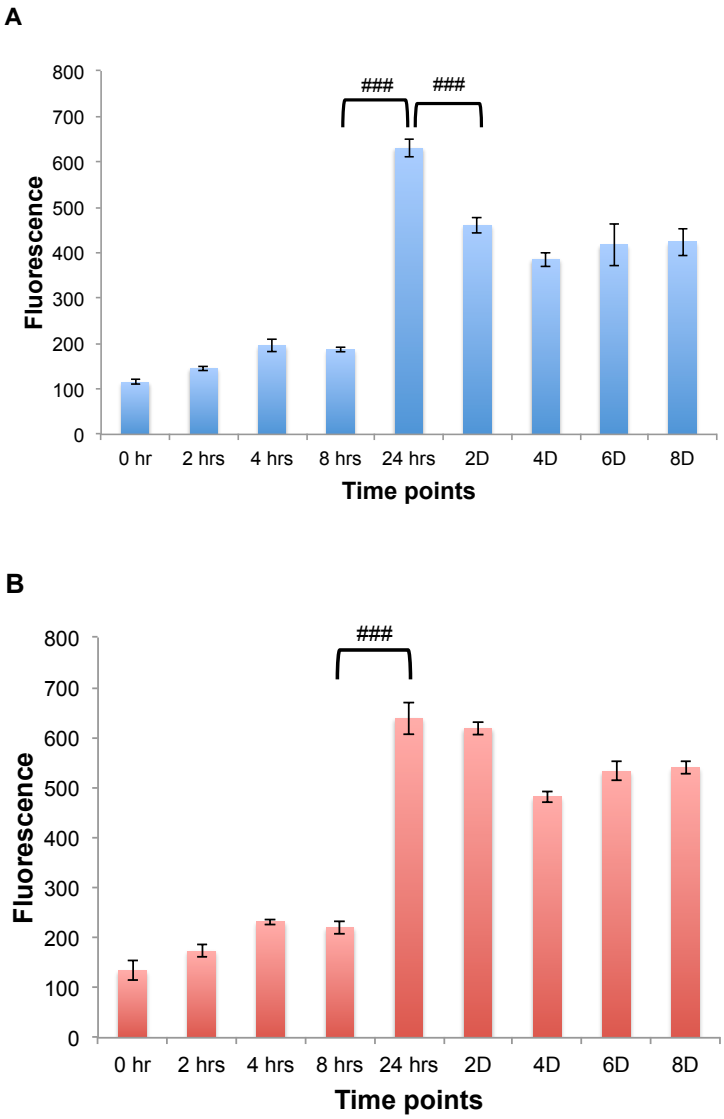

C

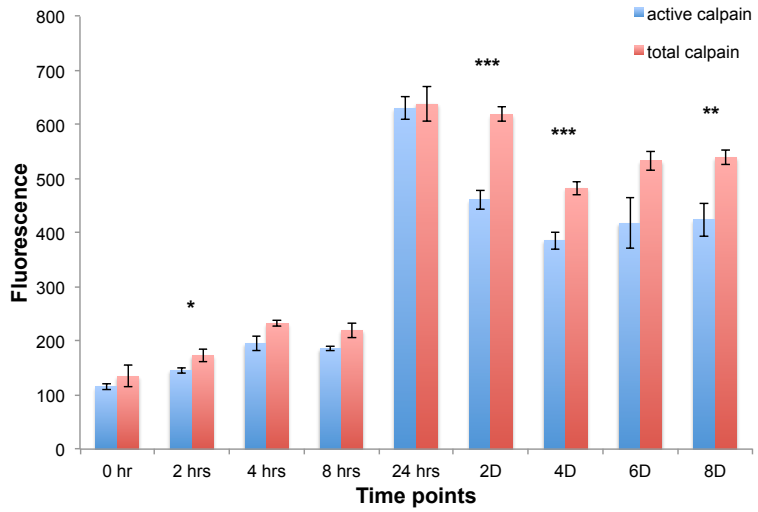
active calpain
total calpain
Fluorescence
800
700
600
500
400
300
200
100
0
*
***
***
**
0 hr
2 hrs
4 hrs
8 hrs
24 hrs
2D
4D
6D
8D
Time points

D

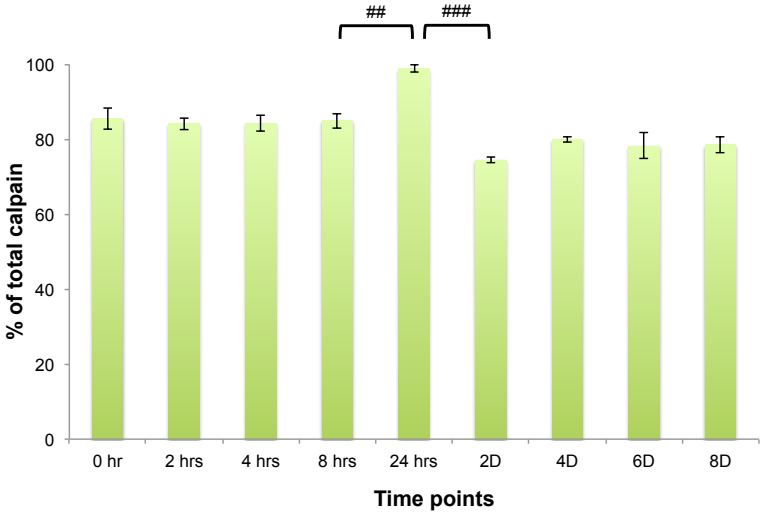
##
###
% of total calpain
100
80
60
40
20
0
0 hr
2 hrs
4 hrs
8 hrs
24 hrs
2D
4D
6D
8D
Time points

4.4.9 Comparison of nuclear and cytoplasmic (A) total and (B) active calpain activity

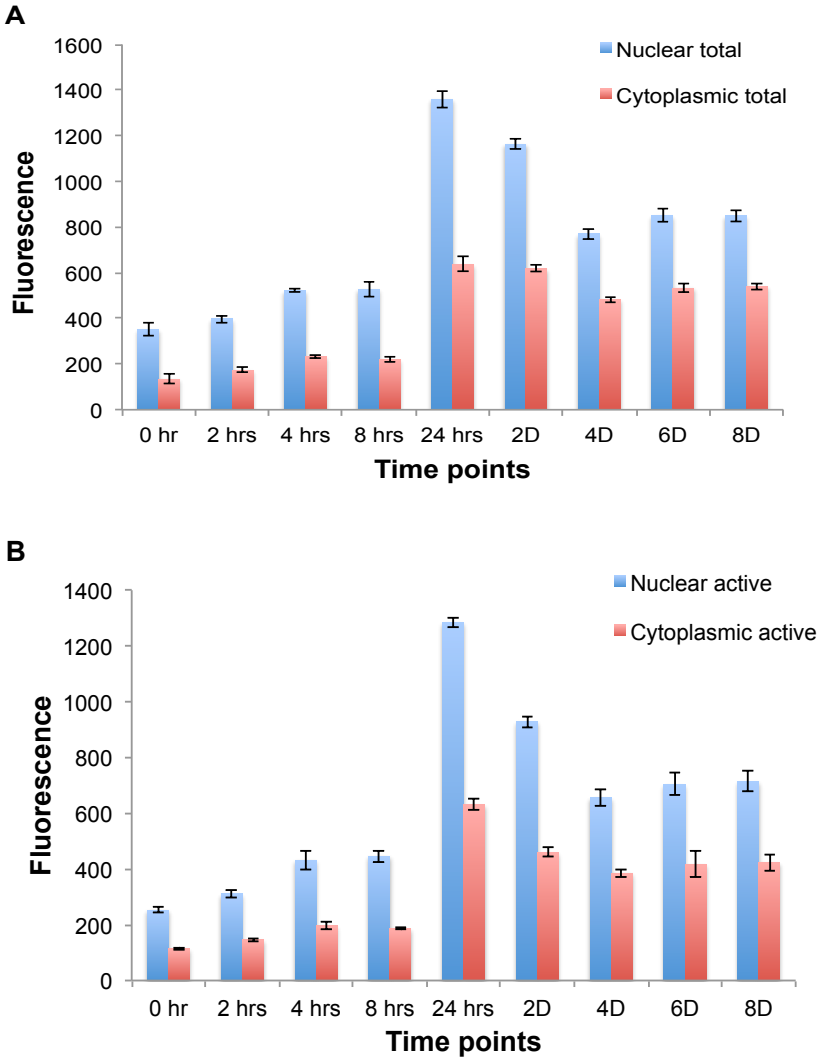

4.4.10 Comparison of calpain activity of C3H10T1/2 cells subjected to MDI adipogenesis induction.

Cells were incubated in 20 μM of the cell-permeable calpain substrate BOC for 20 minutes. For total calpain activity measurement, cells were treated with 1 M calcium and 5 μM ionomycin for a further 1 minute after the BOC incubation. Images were captured (i, iii) before and (ii, iv) after addition of BOC (20 μM) as described under "Materials and Methods".

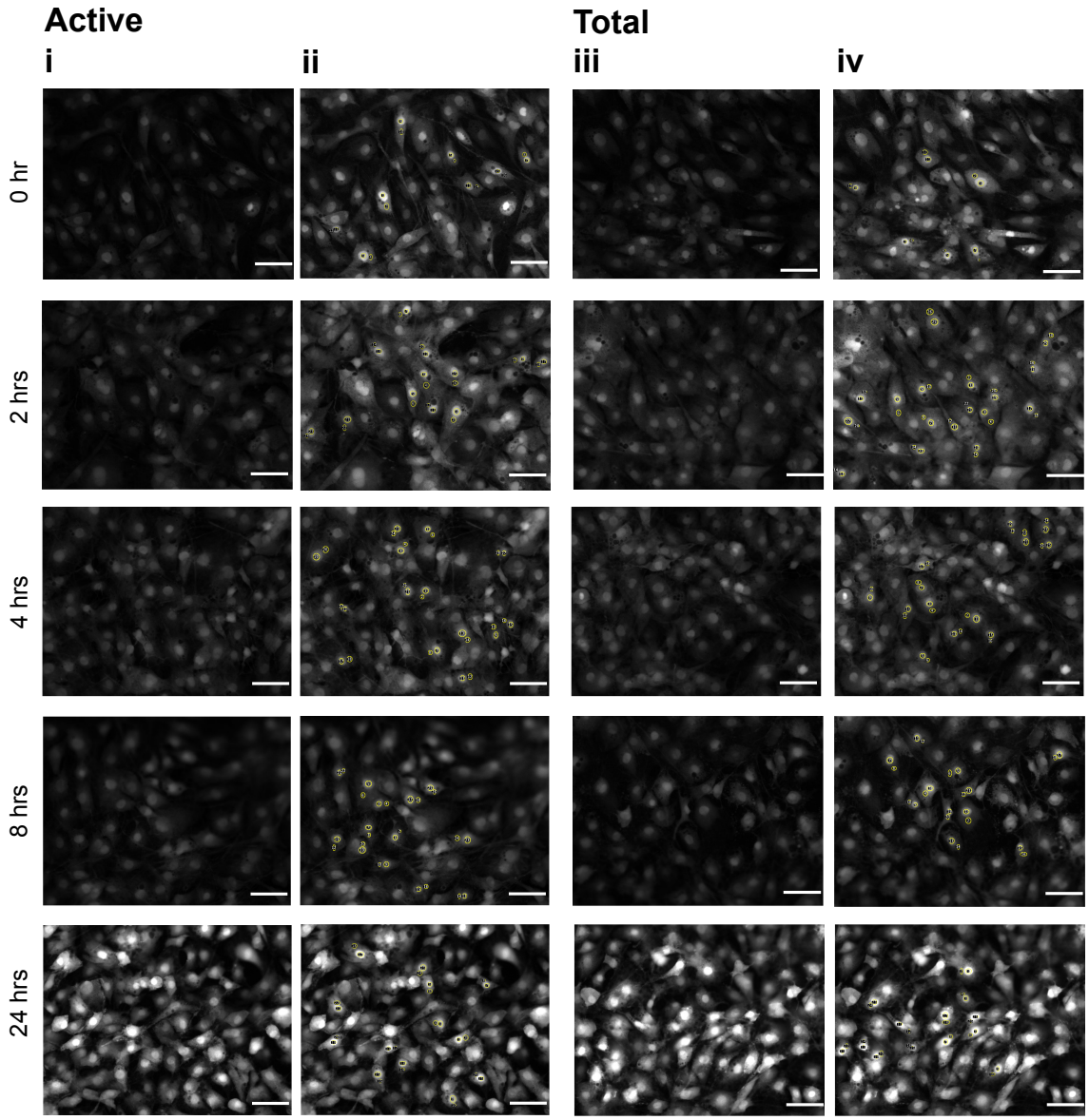

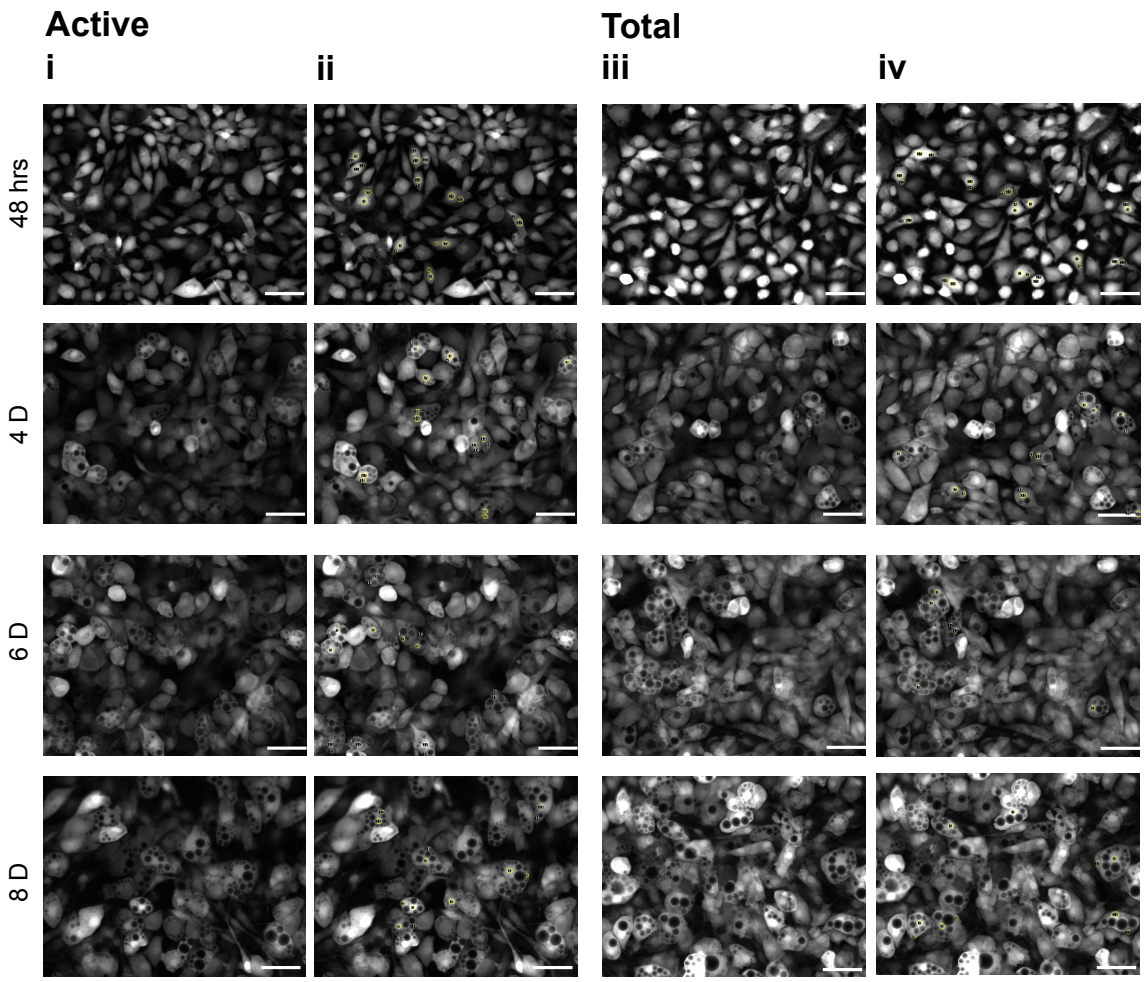
Active
Total
i
ii
iii
iv
48 hrs
4 D
6 D
8 D

Chapter 5

Expression pattern of *Tpcn1* mRNA in the brain

5.1 Introduction

5.1.1 TPCs and NAADP in the nervous system

The NAADP/TPC signalling pathway in the nervous system is less well-established compared with the other two well-known Ca^{2+} releasing channels IP_3Rs and RyRs; however, mounting evidence has suggested important roles of this novel intracellular Ca^{2+} release mechanism in certain aspects of neuronal functions.

NAADP, when added presynaptically at cholinergic synapses, was shown to modulate acetylcholine release in the sea hare *Aplysia*, by means of regulating the presynaptic $[Ca^{2+}]$ in a mechanism distinct from that mediated by IP_3P and RyR [351]. Studies of the frog neuromuscular junction also confirmed a role for NAADP in neurotransmitter release [352, 353]. Thus an enhancement in the frequency of spontaneous excitatory postsynaptic potentials was noted, suggesting that NAADP could mediate Ca^{2+} release from synaptic vesicles [352]. Intriguingly it appears that in non-neuronal cells, NAADP activity is unaffected by thapsigargin [352]. Additionally, the combined influence of NAADP and IP_3/cADPR was greater than additive in terms of neurotransmission [353], in line with the functional coupling of NAADP receptors and CICR channels [354].

For mammalian preparations, NAADP-induced Ca^{2+} release from rat brain microsomes was shown to act via a mechanism similar to that identified in sea urchin eggs [355]. Besides, the capability of rat brain homogenates to synthesize and degrade NAADP was also revealed [79][355]. The characterization of NAADP metabolism in rat brain membranes showed that this event occurred via a pathway involving the removal of 2' phosphate, which was Ca^{2+}-dependent, and was suggested to provide a feedback mechanism for modulation of NAADP responses [356], hence supporting a signalling role for NAADP in the brain [357]. Binding studies using the radioligand [^{32}P]NAADP demonstrated high affinity NAADP binding sites in rat brain membranes and

autoradiography analysis identified a notably heterogeneous distribution of [^{32}P]NAADP binding in the rat brain [348]. Thus a markedly high enrichment in the medulla, midbrain and thalamus and appreciable levels in anterior cortical regions and globus pallidus were shown, but low binding levels in the striatum and hippocampus were found, both areas were abundant with IP_3Rs and RyRs though. Another study confirmed moderate binding levels in the cerebellum which was also enriched with other intracellular Ca^{2+} release channels [358]. More intriguingly, binding appeared in both gray and white matter such as corpus callosum, suggesting that NAADP binding sites likely occur in both neuronal and non-neuronal cells. Notably, this binding study was the first to identify specific binding sites for NAADP in a mammalian tissue and the stark contrast observed in the reversibility of binding between the rat brain and sea urchin eggs suggested distinct regulation in these systems and/or existence of NAADP receptor subtypes. NAADP receptors were also discovered in primary cortical neuronal cultures and the medulla neurons. Using NAADP-AM, NAADP was demonstrated to mediate Ca^{2+} release in primary cortical neuronal cultures [359] and the medulla neurons [360].

In addition to the biochemical findings, functional studies have reported the involvement of NAADP/TPC signalling in mammalian neurons. Thus extracellular introduction of NAADP into mouse and rat astrocytes (both in culture and in acute brain slices) resulted in Ca^{2+} release from endolysosomal stores [361, 362]; similar Ca^{2+} release was also apparent when NAADP was delivered intracellularly into rat astrocytes, with potentiation of Ca^{2+} release in cells overexpressed with TPCs [100]. Furthermore, activation of NAADP receptors was associated with an upregulation of autophagic markers LC3II and beclin-1 whereas interfering TPC2 resulted in an attenuation of LC3II levels. All these point to a regulatory role for TPC-mediated NAADP-induced Ca^{2+} signalling in autophagy in rat astrocytes. In addition, NAADP has been implicated in mobilizing ATP-mediated

Ca^{2+} signalling in cultured astrocytes [363]. Besides, NAADP-induced Ca^{2+} signals were revealed in rat cortical neurons and the PC12 cell line using the liposomal delivery method; and suppression of Ca^{2+} release was seen with bafilomycin treatment, whereas NAADP responses were still observed with thapsigargin treatment [131][364]. Importantly, NAADP was demonstrated to promote neurite outgrowth in cultured rat cortical neurons via an IP_3R- and RyR-mediated mechanism [364] while in PC12 cells, NAADP was sufficient to induce neuronal differentiation [131]. Intriguingly in medullary neurons, coupling of NAADP responses to non-selective cation channels on the cell membrane resulted in depolarization was demonstrated, indicating NAADP could mediate Ca^{2+} signalling both within the cell and on the plasma membrane, offering a novel mechanism for excitation of autonomic neurons [360]. Subsequent studies demonstrated that neurotransmitter glutamate but not ATP was coupled to NAADP signalling, as suggested by the enhanced NAADP levels generated in hippocampal neurons with glutamate treatment [29]. Recently, TPC2 has been shown to regulate neural differentiation of mouse ES cells. Thus TPC2 signalling blocks the entry of ES cells into early neural progenitors, however it is obligatory for late neuronal differentiation [132].

5.1.2 Aims of this chapter

Accumulating evidence has shown the participation of NAADP and TPC in the nervous system and biochemical data has demonstrated the specific binding sites for NAADP and its heterogenous distribution in the mammalian brain [348]. NAADP generation was also confirmed *in vivo* [360] and *in vitro* [359]. However, regarding TPCs, although several reports have implicated them as having a role in neuronal cells, their localization in the nervous system has never been reported apart from an expression study which showed the presence of TPC1 protein in the mouse brain homogenates (Ruth Tunn; in preparation;

Appendix section 5.4.1). Therefore, in an attempt to look into the localization of TPC1 so as to provide spatial evidence for this receptor in the brain, *in situ* hybridisation experiments were performed using oligonucleotide probes to determine the expression of *Tpcn1* mRNA in different regions of the mouse brain.

5.2 Results

5.2.1 Expression of MmTpcn1 mRNA in male mouse brain

To study the expression pattern distribution of *Tpcn1* mRNA in the mouse brain, and to determine the expression levels in particular regions of the brain, oligonucleotide antisense probes were hybridized to coronal brain cryosections obtained from WT and *Tpcn1* KO male mice. Autoradiograms illustrating the abundance of *Tpcn1* mRNA in the frontal cortex (FC), hippocampus (CA1, CA3 and dentate gyrus (DG)), as well as hypothalamus (ventromedial nucleus) are shown in figures 5.2 and 5.3. In WT mice, expression of *Tpcn1* as revealed by an antisense probe was particularly evident in the CA1, CA3 and DG of hippocampus, while fairly faint expression was also seen with the hypothalamus, but not the FC. On the contrary, negligible expression was detected in all of these regions in *Tpcn1* KO mice except for DG of the hippocampus where little signal was still observed; *Tpcn1* KO mice should be absent of *Tpcn1* expression as this provides a control. Quantification of abundance of *Tpcn1* mRNA was also presented in figure 5.6 and expression in the WT and *Tpcn1* KO mice was compared. Significant reduction in expression was revealed with the CA1 and CA3 regions of the KO mice, while the expression in both DG and hypothalamus of the KO mice was only insignificantly attenuated when compared with the WT mice. Moreover, similar *Tpcn1* expression levels were noted in the CA1 and CA3. Thus indicating that *Tpcn1* was significantly expressed in the CA1 and CA3 of the hippocampus. The absence of *Tpcn1* signals in FC and the insignificant expression levels in hypothalamus and DG indicated that *Tpcn1* expression in these regions might be below detection level.

The TPC1 sense probe gave no signal on all coronal sections in the control experiment, indicating that the signal was specific (Figure 5.4 and 5.5).

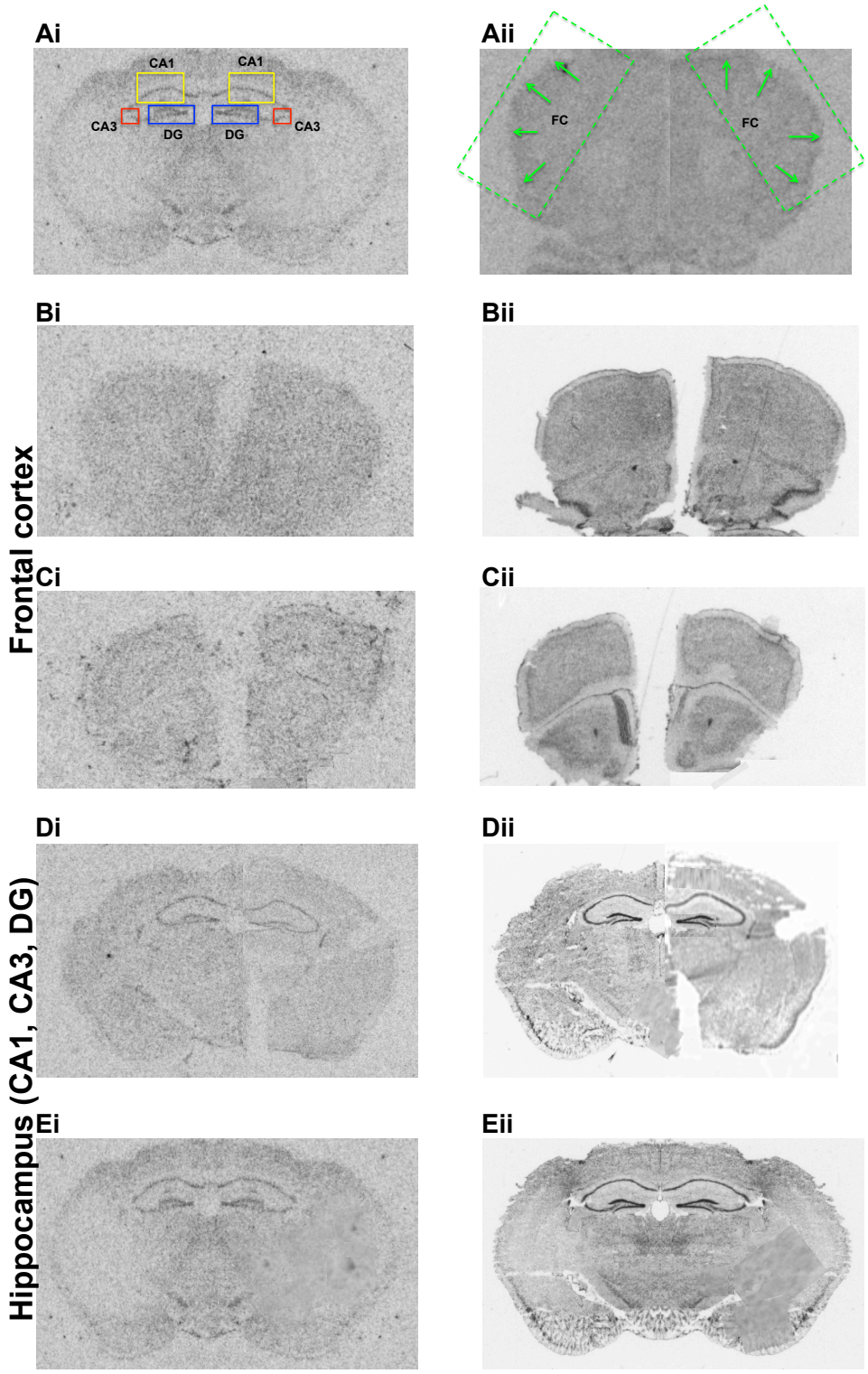
Ai
CA1
CA1
CA3
DG
DG
CA3
Aii
FC
FC
Bi
Bii
Ci
Cii
Frontal cortex
Di
Dii
Ei
Eii
Hippocampus (CA1, CA3, DG)

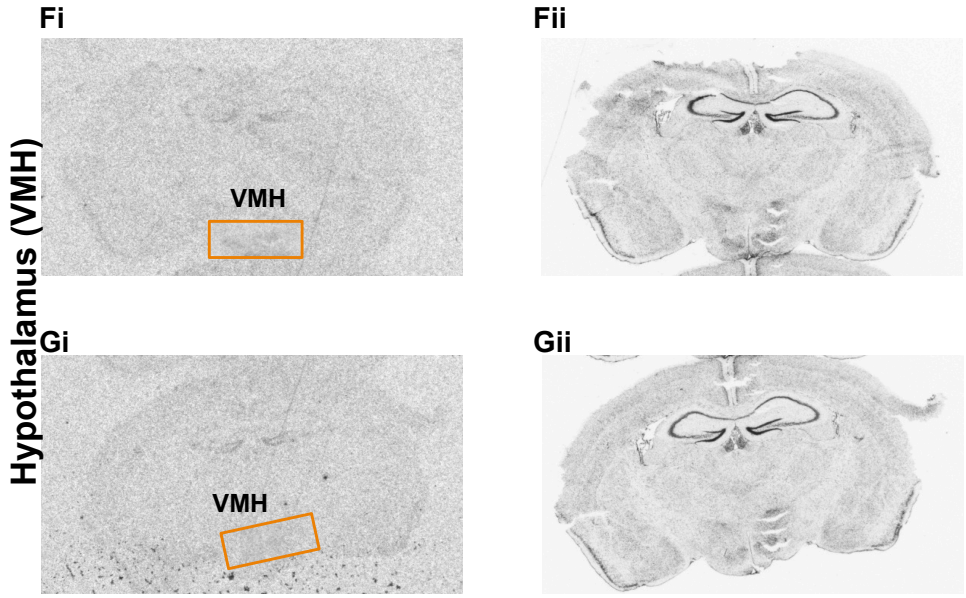

Figure 5.2: Representative autoradiograms showing distribution of *Tpcn1* in **(Bi, Ci)** frontal cortex (FC), **(Di, Ei)** CA1, CA3 and dentate gyrus (DG) of hippocampus, **(Fi, Gi)** ventralmedial nucleus of hypothalamus (VMH) of male WT mouse brain. Antisense probe was hybridized to *Tpcn1* mRNA and expression was shown as dark colour in the autoradiograms. **(Bii-Gii)** show corresponding sections which were counter-stained with Toludine Blue. **(Ai and ii)** are autoradiograms illustrating the locations of FC, CA1, CA3 and DG. Experiments were performed on 9 similar slides per animal and 3 animals were used; only representative autoradiograms were displayed here. n = 3.

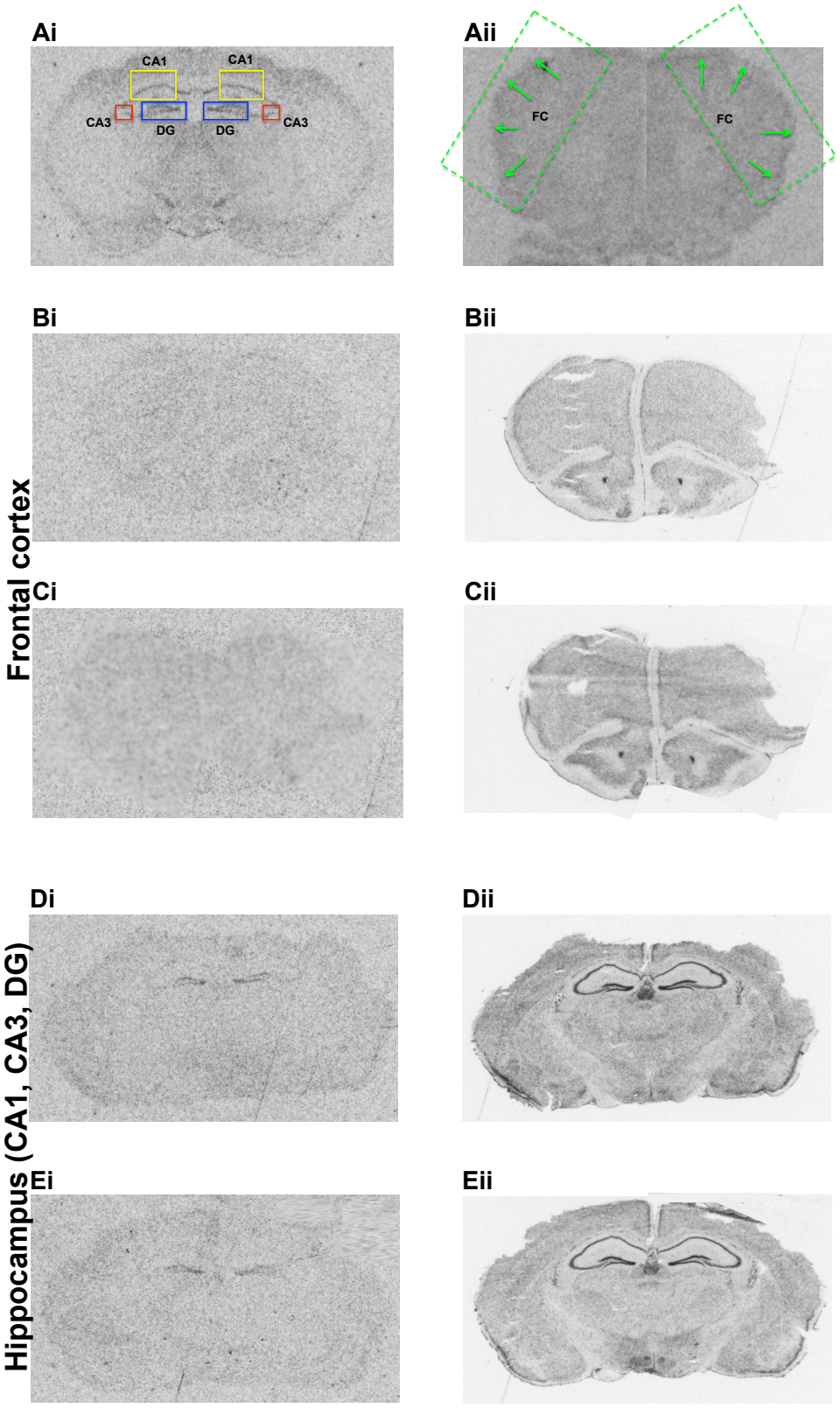
Ai
CA1
CA1
CA3
DG
DG
CA3
Aii
FC
FC
Bi
Bii
Frontal cortex
Ci
Cii
Di
Dii
Hippocampus (CA1, CA3, DG)
Ei
Eii

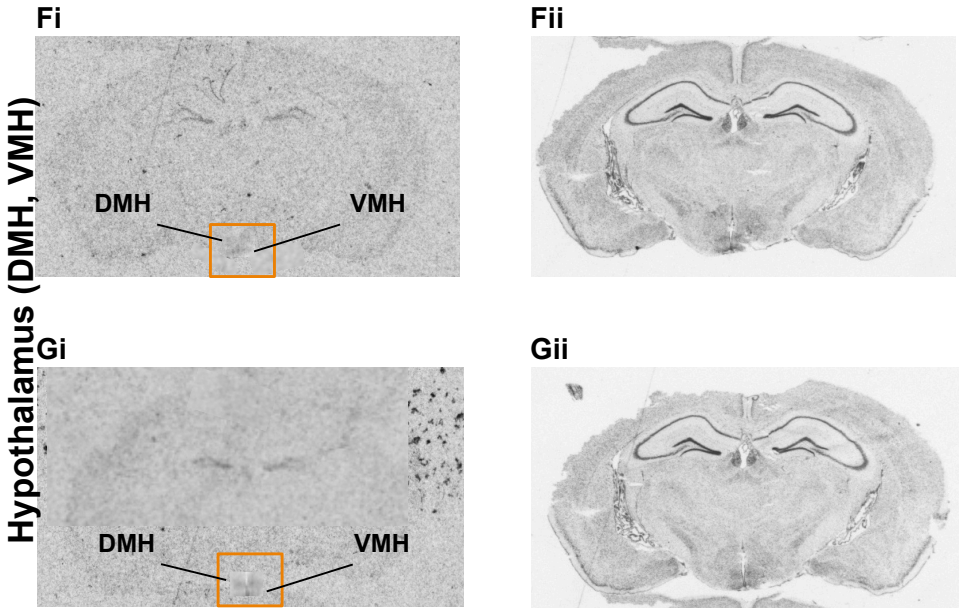

Figure 5.3: Representative autoradiograms showing distribution of *Tpcn1* in **(Bi, Ci)** frontal cortex (FC), **(Di, Ei)** CA1, CA3 and dentate gyrus (DG) of hippocampus, **(Fi, Gi)** dorsalmedial and ventralmedial nucleus of hypothalamus (DMH and VMH) of male *Tpcn1* KO mouse brain. Antisense probe was hybridized to *Tpcn1* mRNA and expression was shown as dark colour in the autoradiograms. **(Bii-Gii)** showing corresponding sections which were counter-stained with Toludine Blue. **(Ai and ii)** are autoradiograms illustrating the locations of FC, CA1, CA3 and DG. Experiments were performed on 9 similar slides per animal and 3 animals were used, only representative autoradiograms were displayed here. n = 3.

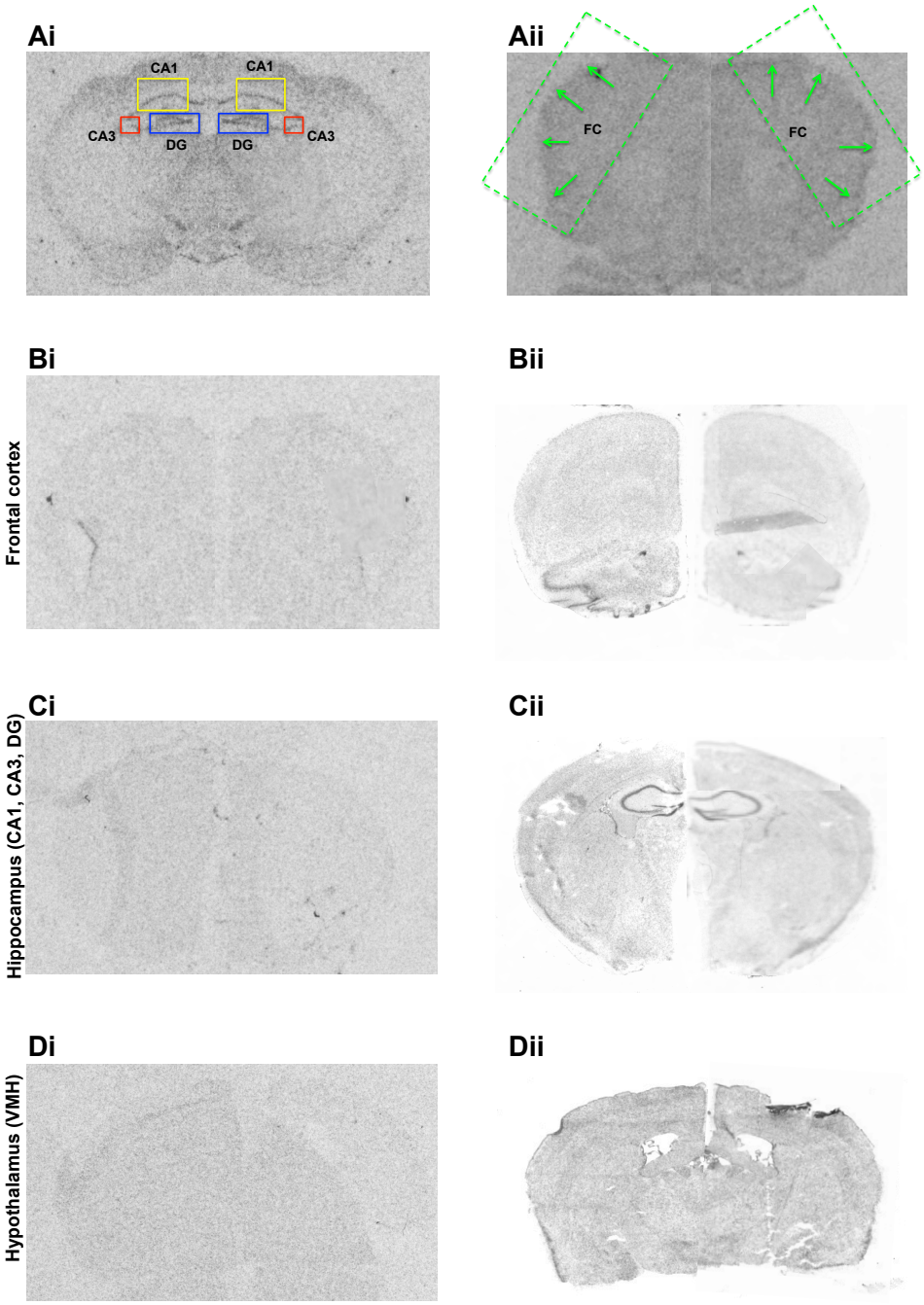

Figure 5.4: Control experiment using sense probe and representative autoradiograms showing distribution of *Tpcn1* in **(Bi, Ci)** frontal cortex (FC), **(Di, Ei)** CA1, CA3 and dentate gyrus (DG) of hippocampus, **(Fi, Gi)** dorsalmedial and ventralmedial nucleus of hypothalamus (DMH and VMH) of male WT mouse brain. Antisense probe was hybridized to *Tpcn1* mRNA and expression was shown as dark colour in the autoradiograms. Claearly no signals were detected when sense probe was used, indicating the *Tpcn1* signal detected using the antisense probe was specific. **(Bii-Gii)** showing corresponding sections which were counter-stained with Toludine Blue. **(Ai and ii)** are autoradiograms illustrating the locations of FC, CA1, CA3 and DG. Experiments were performed on 9 similar slides per animal and 3 animals were used, only representative autoradiograms were displayed here. n = 3.

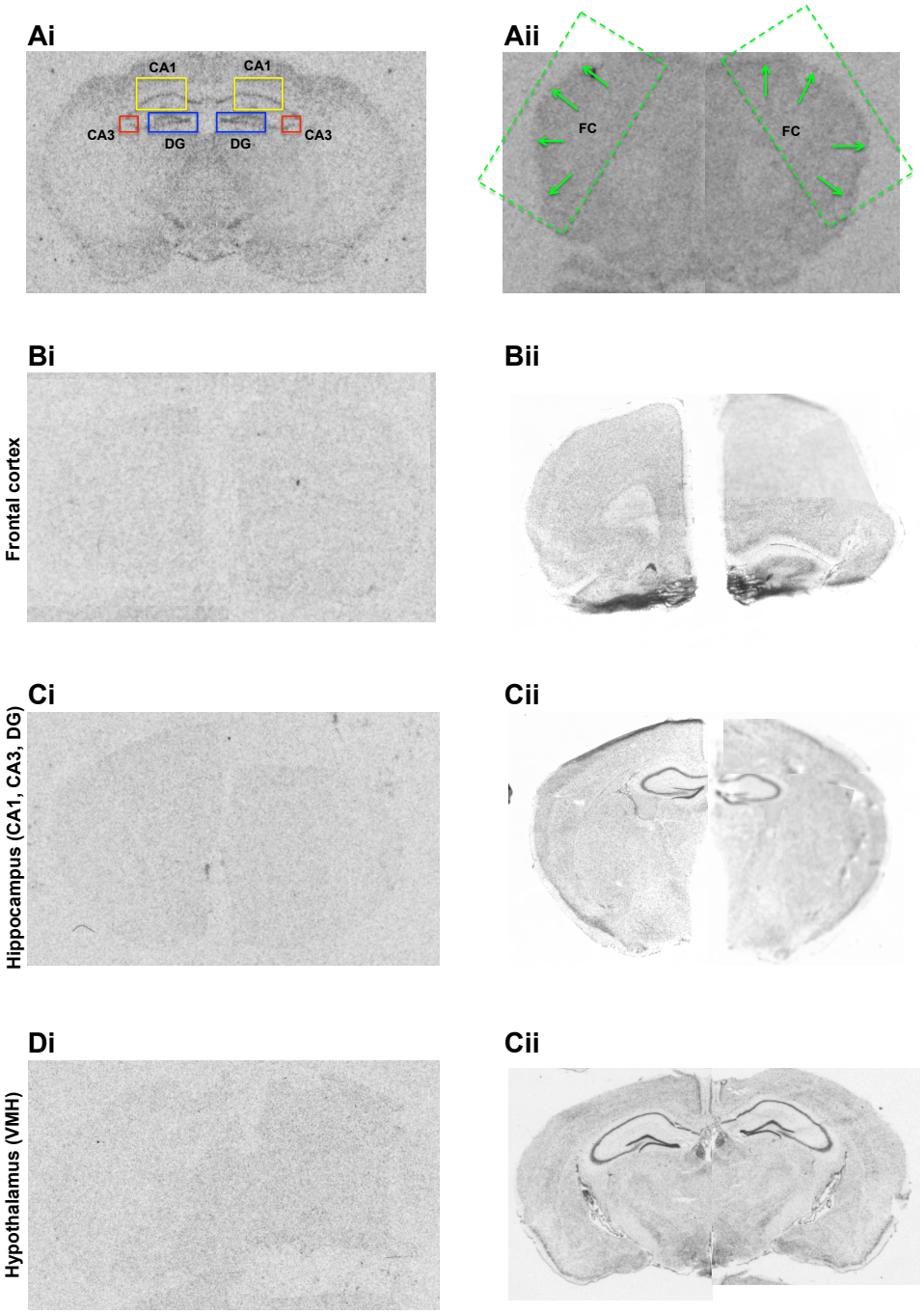

Figure 5.5: Control experiment using the sense probe and representative autoradiograms showing distribution of *Tpcn1* in **(Bi, Ci)** frontal cortex (FC), **(Di, Ei)** CA1, CA3 and dentate gyrus (DG) of hippocampus, **(Fi, Gi)** ventralmedial nucleus of hypothalamus (VMH) of male *Tpcn1* KO mouse brain. Antisense probe was hybridized to *Tpcn1* mRNA and expression was shown as dark colour in the autoradiograms. Clearly no signals were detected when the sense probe was used, indicating that the *Tpcn1* signal detected using the antisense probe was specific. **(Bii-Gii)** show corresponding sections which were counter-stained with Toludine Blue. **(Ai and ii)** are autoradiograms illustrating the locations of FC, CA1, CA3 and DG. Experiments were performed on 9 similar slides per animal and 3 animals were used; only representative autoradiograms were displayed here. n = 3.

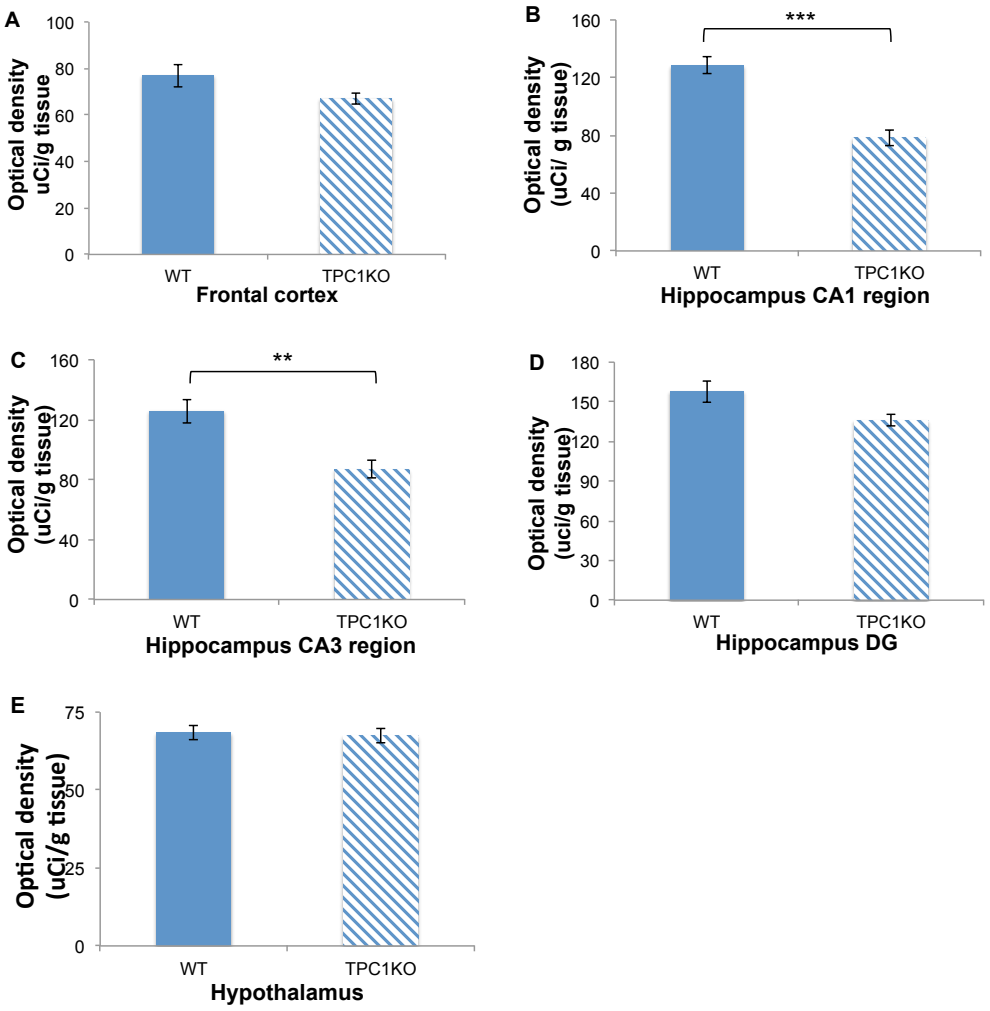

Figure 5.6: Quantification of abundance of *Tpcn1* mRNA expression measured in different regions of the male mouse brain: **(A)** frontal cortex **(B)** CA1 of hippocampus **(C)** CA3 of hippocampus **(D)** dentate gyrus (DG) of hippocampus **(E)** hypothalamus (ventromedial nucleus). Average optical density was calculated as average of three mice, in which three sections of the same region were quantified for each mice. WT density was compared with *Tpcn1* KO density in each region. n=3. $^{**}p<0.01$, $^{**}p<0.001$ (student's *t-test*). Data presented ± SEM.

5.2.2 Expression of MmTpcn1 mRNA in female mice brain

Similarly, *Tpcn1* mRNA distribution and expression level in the female mouse brain was also determined in both WT and *Tpcn1* KO mice. Autoradiograms illustrating the abundance of *Tpcn1* mRNA in the FC, hippocampus (CA1, CA3 and DG), as well as hypothalamus (ventromedial nucleus) were shown in figure 5.7 and 5.8. Interestingly, the WT female mice displayed an analogous expression pattern to that of WT male mice, such that expression of *Tpcn1* in female mice was particularly evident in the CA1, CA3 and DG of hippocampus, while very low expression was observed in the hypothalamus, and no signal was noted in the FC. In *Tpcn1* KO mice, negligible expression was detected in all of these regions except for DG where a very faint signal was still noticeable, which in theory should be absent of *Tpcn1* expression. Quantification of abundance of *Tpcn1* mRNA was also presented in figure 5.11 and expression in the WT and *Tpcn1* KO mice was compared. Significant reduction in *Tpcn1* level was seen in the CA1 and CA3 whereas that of DG and hypothalamus was demonstrated to be insignificantly reduced when compared with the mutant mice, suggesting that *Tpcn1* was only significantly expressed in the CA1 and CA3 of the hippocampus. Moreover, similar *Tpcn1* expression levels were noted in the CA1 and CA3. Thus indicating that *Tpcn1* was significantly expressed in the CA1 and CA3 of the hippocampus. The absence of *Tpcn1* signals in FC and the insignificant expression levels in hypothalamus and DG indicated that *Tpcn1* expression in these regions might be below detection level.

The TPC1 sense probe gave no signal in all coronal sections in the control experiment, indicating that the signal was specific (Figure 5.9 and 5.10).

On the other hand, it was also revealed that both WT male and female mice displayed comparable level of *Tpcn1* mRNA expression in the CA1 and CA3 of the hippocampus (Figure 5.12).

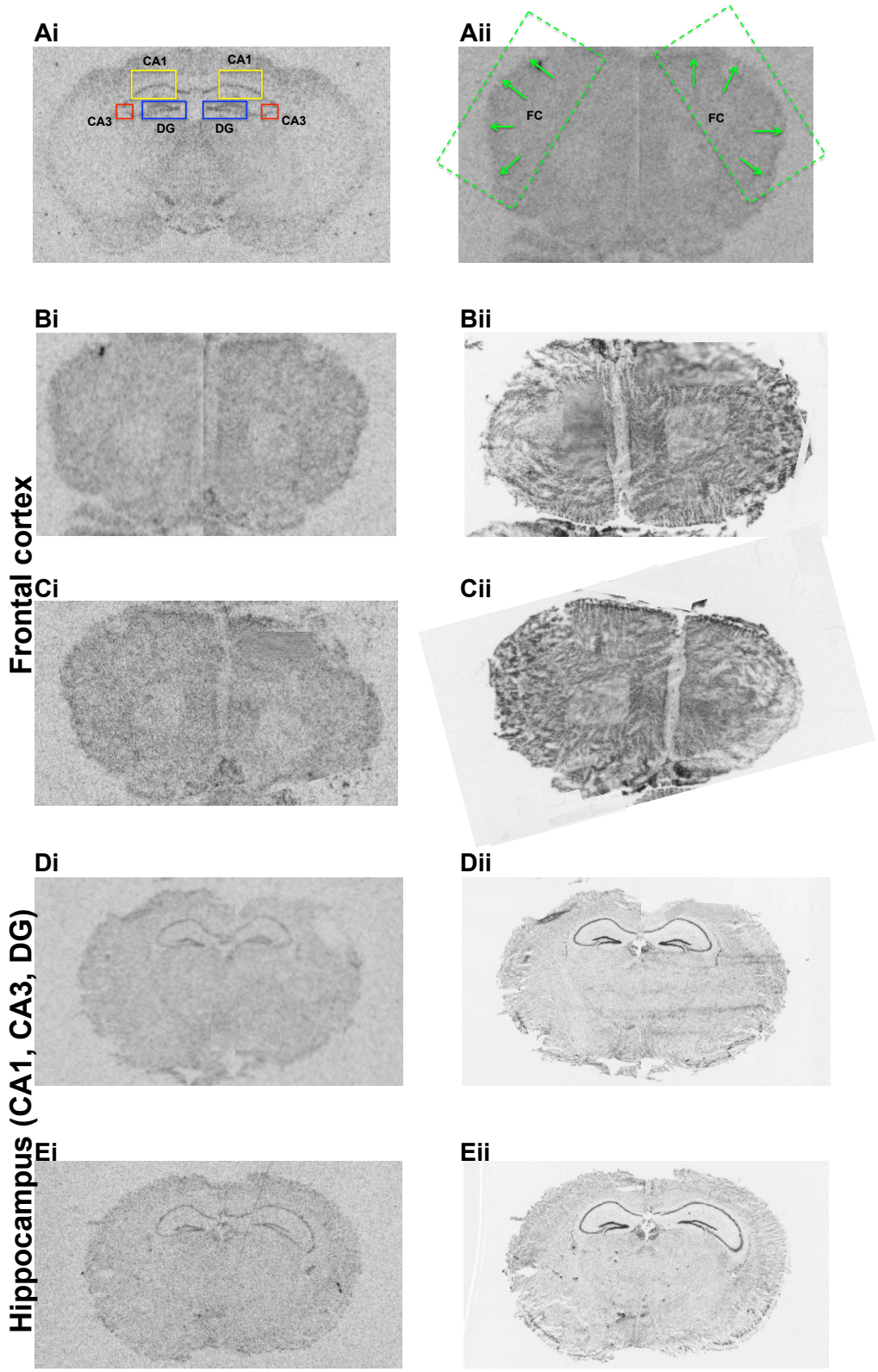
Ai
CA1
CA1
CA3
DG
DG
CA3
Aii
FC
FC
Bi
Bii
Ci
Cii
Di
Dii
Ei
Eii
Frontal cortex
Hippocampus (CA1, CA3, DG)

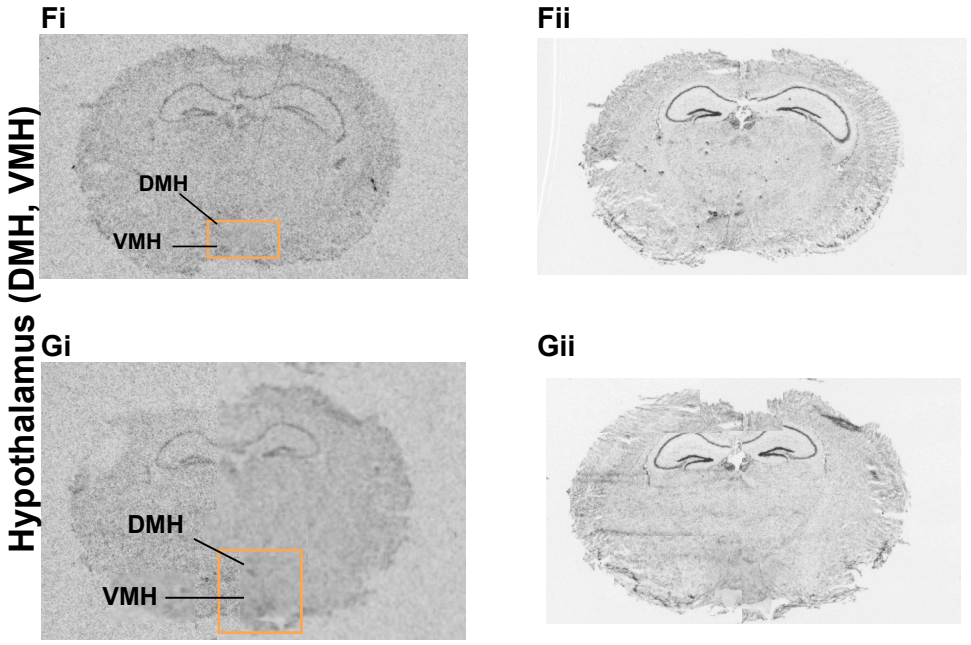

Figure 5.7: Representative autoradiograms showing distribution of *Tpcn1* in **(Bi, Ci)** frontal cortex (FC), **(Di, Ei)** CA1, CA3 and dentate gyrus (DG) of hippocampus, **(Fi, Gi)** dorsalmedial and ventralmedial nucleus of hypothalamus (DMH and VMH) of female WT mouse brain. Antisense probe was hybridized to *Tpcn1* mRNA and expression was shown as dark colour in the autoradiograms. **(Bii-Gii)** showing corresponding sections which were counter-stained with Toludine Blue. **(Ai and ii)** are autoradiograms illustrating the locations of FC, CA1, CA3 and DG. Experiments were performed on 9 similar slides per animal and 3 animals were used, only representative autoradiograms were displayed here. n = 3.

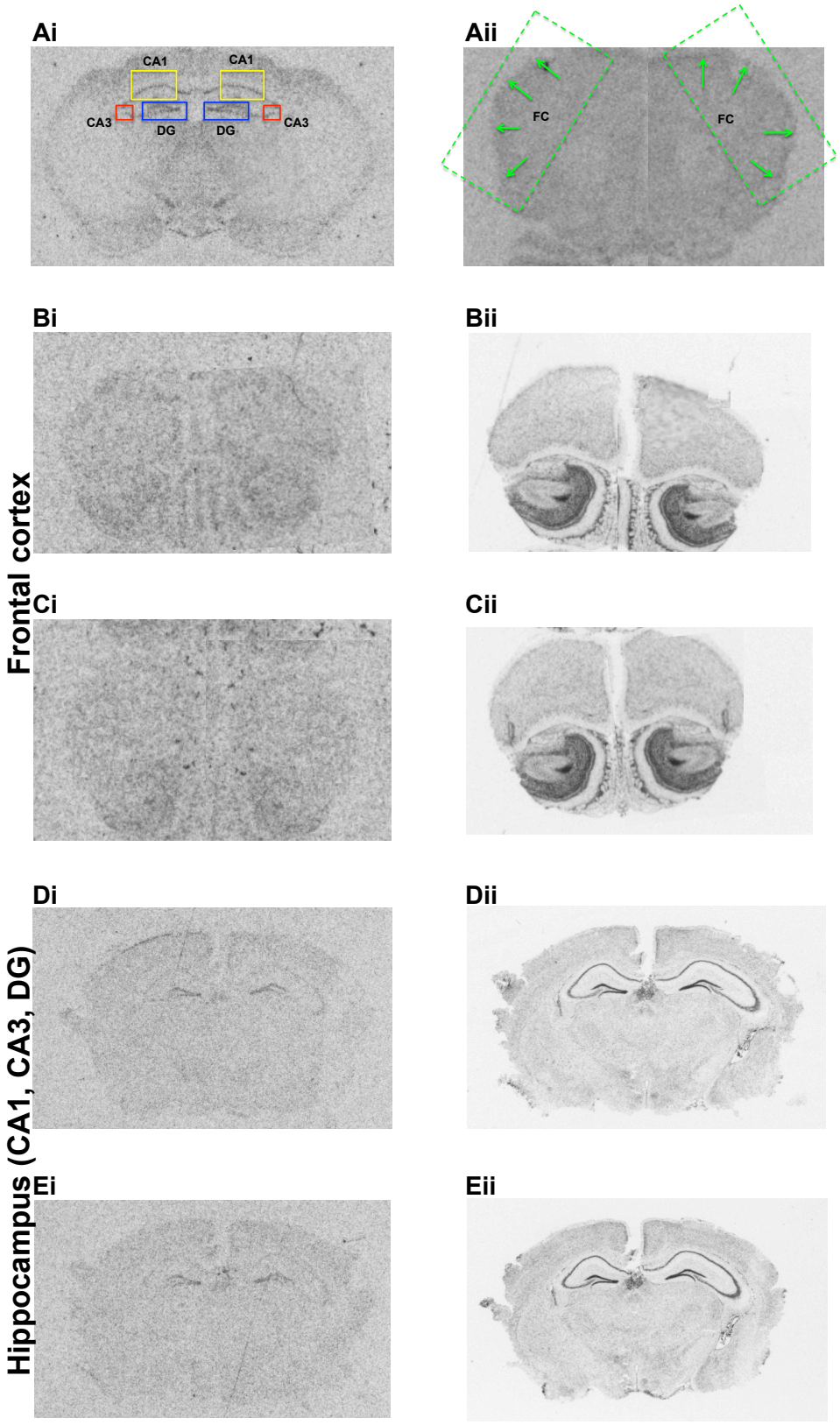
Ai
CA1
CA1
CA3
DG
DG
CA3
Aii
FC
FC
Bi
Bii
Frontal cortex
Ci
Cii
Di
Dii
Hippocampus (CA1, CA3, DG)
Ei
Eii

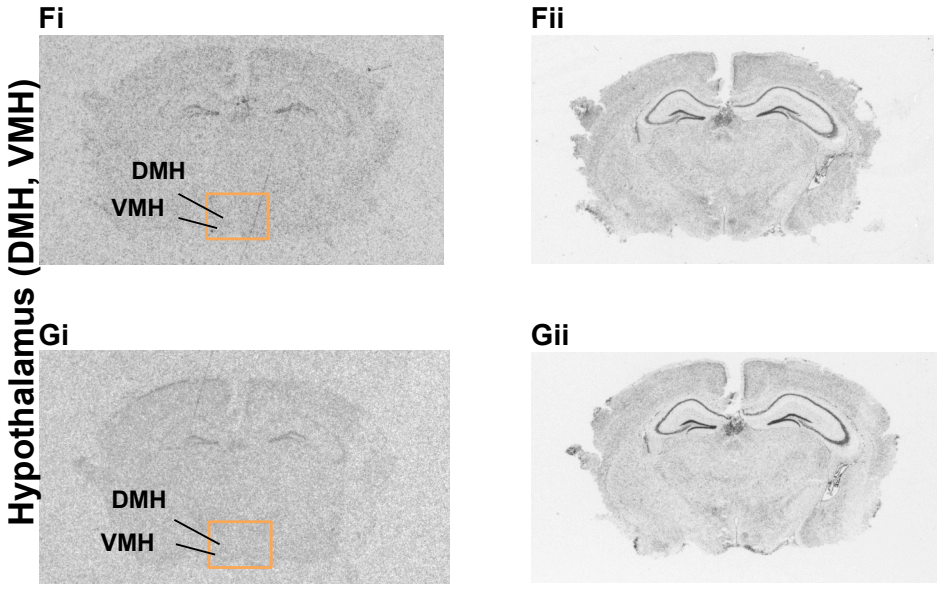

Figure 5.8: Representative autoradiograms showing distribution of *Tpcn1* in **(Bi, Ci)** frontal cortex (FC), **(Di, Ei)** CA1, CA3 and dentate gyrus (DG) of hippocampus, **(Fi, Gi)** dorsalmedial and ventralmedial nucleus of hypothalamus (DMH and VMH) of female *Tpcn1* KO mouse brain. Antisense probe was hybridized to *Tpcn1* mRNA and expression was shown as dark colour in the autoradiograms. **(Bii-Gii)** showing corresponding sections which were counter-stained with Toludine Blue. **(Ai and ii)** are autoradiograms illustrating the locations of FC, CA1, CA3 and DG. Experiments were performed on 9 similar slides per animal and 3 animals were used; only representative autoradiograms were displayed here. n = 3.

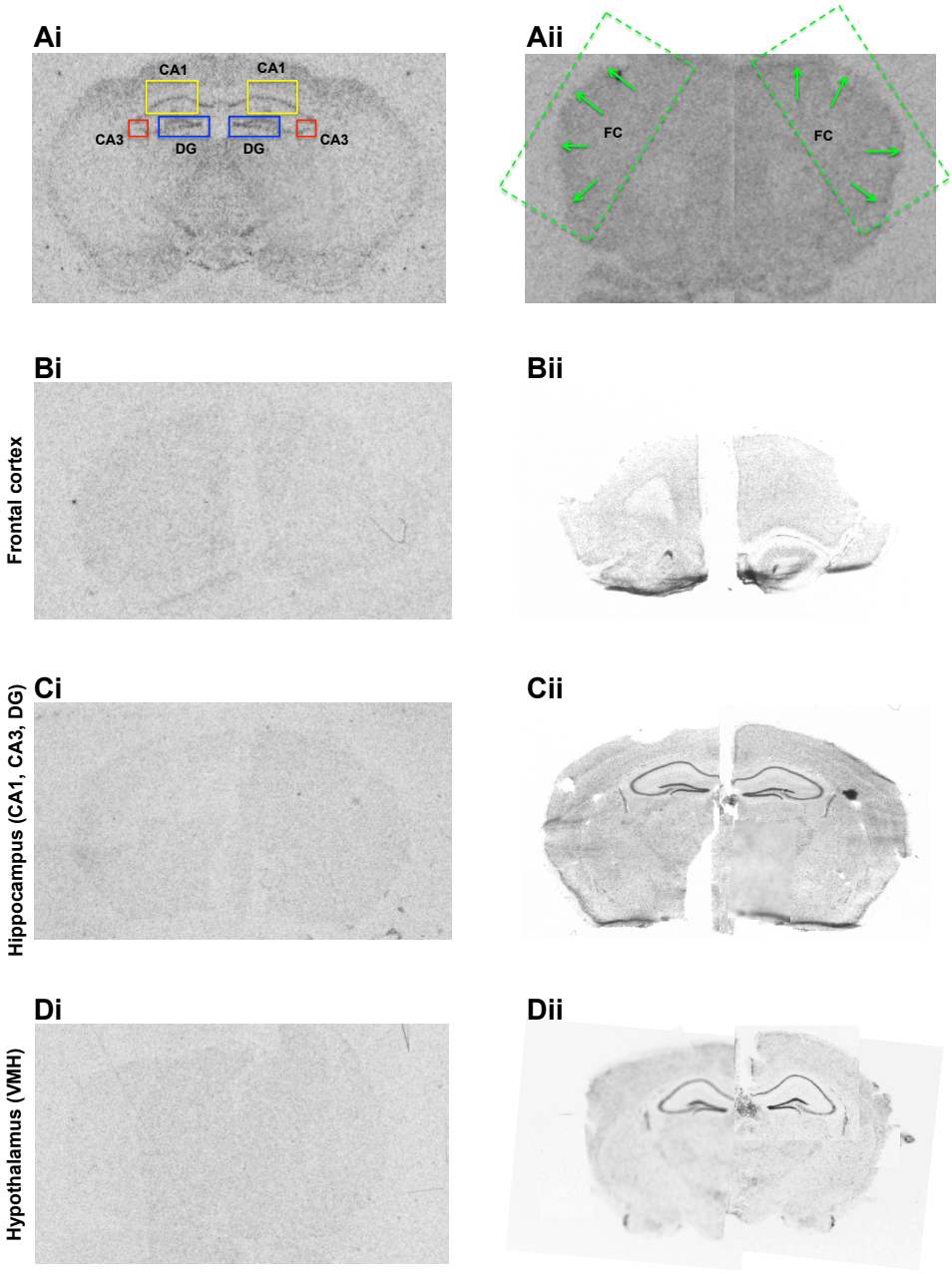

Figure 5.9: Control experiment using sense probe and representative autoradiograms showing distribution of *Tpcn1* mRNA in **(Bi, Ci)** frontal cortex (FC), **(Di, Ei)** CA1, CA3 and dentate gyrus (DG) of hippocampus, **(Fi, Gi)** dorsalmedial nucleus of hypothalamus (DMH) of female WT mouse brain. Antisense probe was hybridized to *Tpcn1* mRNA and expression is shown as dark colour in the autoradiograms. Claearly no signals were detected when sense probe was used, indicating the *Tpcn1* signal detected using the antisense probe was specific. **(Bii-Gii)** showing corresponding sections which were counter-stained with Toludine Blue. **(Ai and ii)** are autoradiograms illustrating the locations of FC, CA1, CA3 and DG. Experiments were performed on 9 similar slides per animal and 3 animals were used; only representative autoradiograms are displayed here. n = 3.

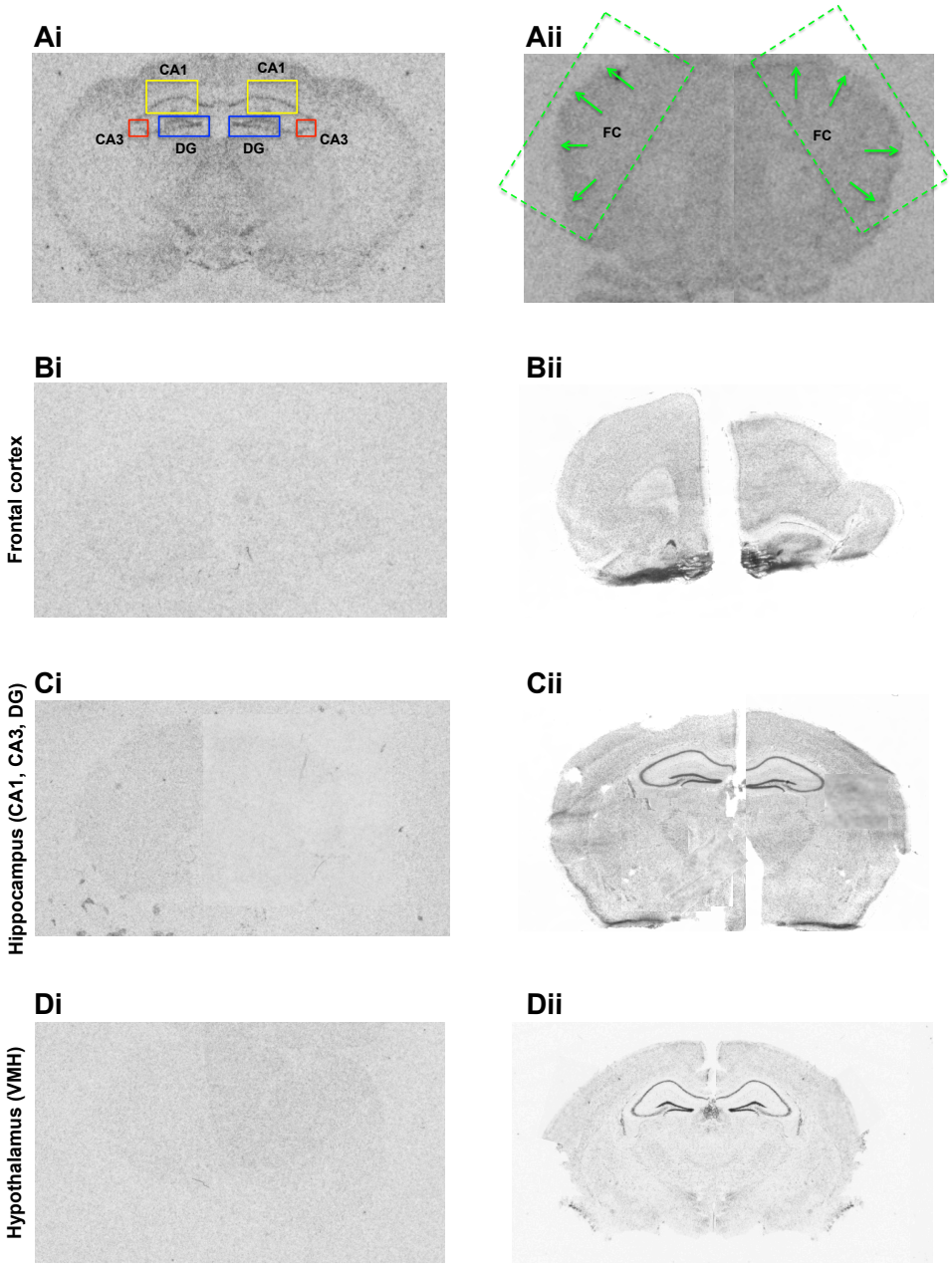

Figure 5.10: Control experiment using sense probe and representative autoradiograms showing distribution of *Tpcn1* in **(Bi, Ci)** frontal cortex (FC), **(Di, Ei)** CA1, CA3 and dentate gyrus (DG) of hippocampus, **(Fi, Gi)** dorsalmedial and ventralmedial nucleus of hypothalamus (DMH and VMH) of female *Tpcn1* KO mouse brain. Antisense probe was hybridized to *Tpcn1* mRNA and expression was shown as dark colour in the autoradiograms. Claearly no signals were detected when sense probe was used, indicating the *Tpcn1* signal detected using the antisense probe was specific. **(Bii-Gii)** showing corresponding sections which were counter-stained with Toludine Blue. **(Ai and ii)** are autoradiograms illustrating the locations of FC, CA1, CA3 and DG. Experiments were performed on 9 similar slides per animal and 3 animals were used, only representative autoradiograms were displayed here. n = 3.

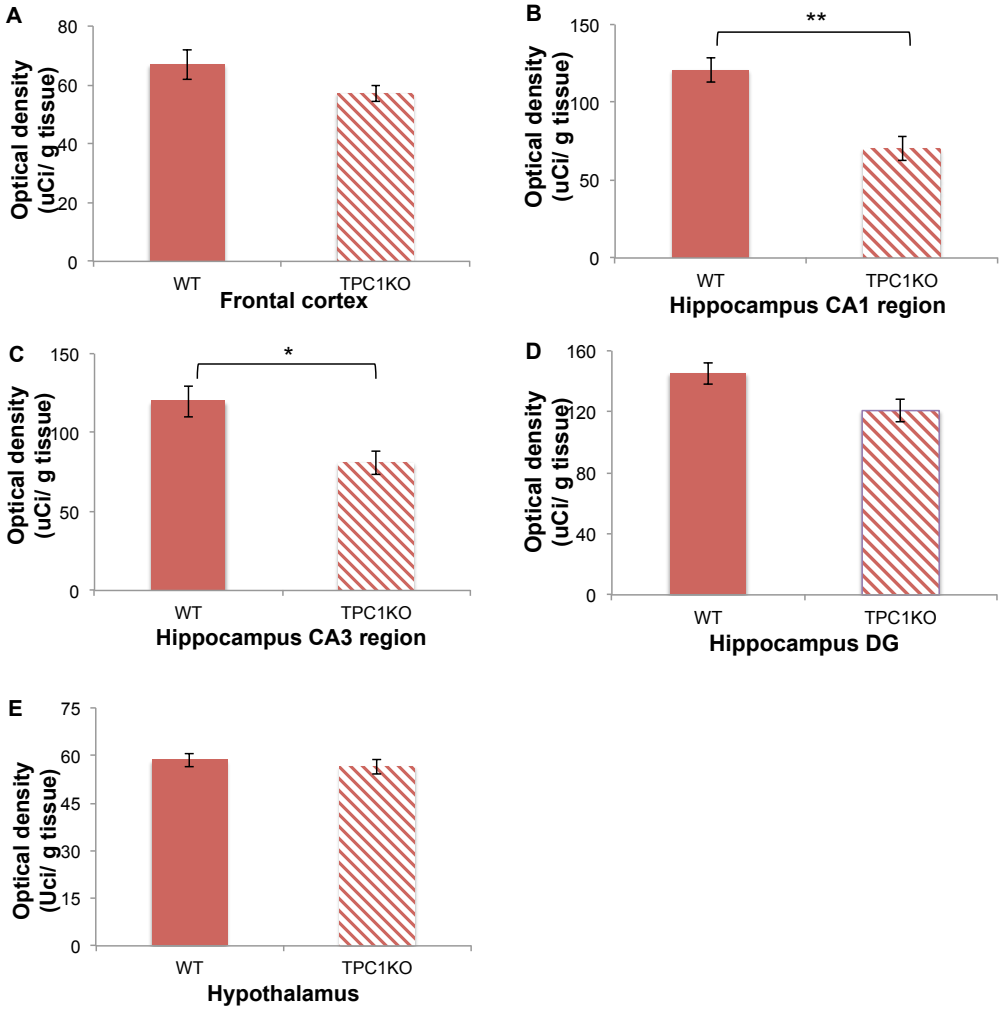

Figure 5.11: Quantification of abundance of *Tpcn1* mRNA expression measured in different regions of the female mouse brain: **(A)** frontal cortex **(B)** CA1 of hippocampus **(C)** CA3 of hippocampus **(D)** dentate gyrus (DG) of hippocampus **(E)** hypothalamus (ventromedial nucleus). Average optical density was calculated as average of three mice, in which three sections of the same region were quantified for each mice. WT density was compared with *Tpcn1* KO density in each region. n=3. **p*<0.05, ***p*<0.01 (student's *t-test*). Data presented ± SEM.

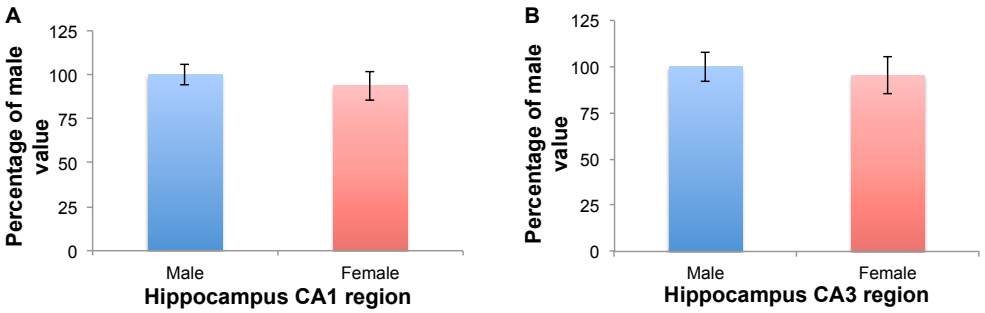

Figure 5.12: Comparison of density between male and female WT mouse brain. **(A)** CA1 of hippocampus **(B)** CA3 of hippocampus. Average optical density was calculated as average of three mice, in which three sections of the same region were quantified for each mice. The male density are presented as 100% and the female density is expressed as percentage of the male density. n=3 (student's *t-test*). Data presented ± SEM.

5.3 Discussion

The present study has delineated the distribution of *Tpcn1* mRNA in mouse brain by *in situ* hybridisation, using both WT and *Tpcn1* KO male and female mice. Results showed that *Tpcn1* was discretely localised in the cerebrum, with a significantly higher expression in CA1 and CA3 of the hippocampus, while only limited expression levels in the hypothalamus and DG of the hippocampus and no signals in the FC. That *Tpcn1* only scarcely expressed in those areas could be real, and the low abundance (or absence in the case of FC) might indicate that the expression of *Tpcn1* in these regions is below the limit of detection. The observations here partially confirmed those reported in the Allen Brain Atlas. Thus a higher expression level was found in the hippocampus compared with other brain areas whereas negligible signals were detected in the hypothalamus, which are in agreement with my results. However, they additionally pointed to a higher expression in the isocortex which is in contrast to my data. The difference could be due to the different methods used to label the target gene. In their case, an RNA antisense probe was used to label *Tpcn1* in sagittal brain sections, compared with the oligonucleotide probe used in my study for labelling the coronal brain sections. That RNA probes have much longer size (~100s of base-pairs) than oligonucleotide probes (40-50 base-pairs long) suggesting that they are generally less specific as non-selective binding to close members of the same gene family might occur even under stringent hybridising conditions. However, the search for *Tpcn2* expression using the Allen Brian Atlas showed negligible *Tpcn2* expression in all brain areas tested. Therefore, the signals should not be due to non-selective binding. In view of this, it is highly likely that the low abundance of *Tpcn1* gene makes the detection more difficult. Hence, modification to the current protocol of my study is important to enhance the signal sensitivity. Additionally, the specificity of binding can be strengthened by utilising multiple oilgonucletide probes complementary to distinct regions within the

target gene.

Taken together with the recent [^{32}P]NAADP binding study demonstrated by another group [348], NAADP receptor and *Tpcn1* mRNA overlapped in certain regions. The hippocampus is the region where strongest concordance occurred between receptor and mRNA expression as a modest signal of [^{32}P]NAADP binding was also detected in this area. Detection of NAADP receptor was also found in the FC, which matches with the mRNA findings of the Allen Brain Atlas, further confirming the expression of *Tpcn1* in this area, and again suggested that the negligible expression revealed in my study could be a result of below-limit detection. Other regions that were not assessed in my study, but have been demonstrated to exhibit both NAADP receptor and *Tpcn1* mRNA expression included medulla, thalamus and cerebellum. Interestingly, dissimilar expression densities were displayed by receptor and mRNA in some regions, for instance thalamus and medulla were significantly evident with receptor but only low mRNA expression was detected, whereas cerebellum was shown to express a modest amount of receptor and mRNA. More striking is that both the midbrain and globus pallidus where significant receptor density was shown, were absent of mRNA signals. It should be noted that in the radioligand assay, the distribution of NAADP binding gives a measure of NAADP receptor protein, and since other proteins like TPC2, TRPML1, TRPML2 and RyRs have been suggested to be potential receptors of NAADP in different cell types [35,90,91][365-367], the presence of these receptors, particularly TPC2 which is one of the isoforms of TPC family [71, 73, 75-77, 102, 130][368], might contribute to NAADP binding as well, and thus accounts for the apparent discrepancies observed in the distribution density of *Tpcn1* and NAADP receptor binding. Recent studies have indicated that instead of directly binding with NAADP, TPCs may require an accessory protein that co-immunoprecipitaed with TPCs [76, 96-98], thus it may explain why the NAADP binding results did not

correlate with the *Tpcn1* mRNA expression because NAADP may bind to the accessory protein instead of TPC1.

On the other hand, if different receptors are involved, then their different binding affinities with NAADP may also account for the observed heterogenous NAADP binding pattern in the brain.

Intriguingly, *in situ* hybridisation of the sagittal section of mouse brain from another group showed expression of *Tpcn1* in the cerebellum and DG of the hippocampus and lower signals in the remaining brain [73]. In my study, however, no significant expression was detected in the DG. One reason may be that *Tpcn1* is only expressed in particular area of the DG which was not present in the coronary section used for my *in situ* study. Alternatively, it may be due to the low *Tpcn1* expression in that area such that it was hardly detectable.

Collectively, a heterogenous expression pattern was demonstrated for *Tpcn1* mRNA in mouse brain, and no sex difference has been revealed. The low expression in certain regions may be due to the low abundance of mRNA that is below detection limit. The partial agreement between the *in situ* hybridisation studies and the radioligand binding assay suggests that the search for the true NAADP receptor is particularly sought after, especially if NAADP regulation of TPC-mediated signalling is conferred by an accessory protein rather than through TPC itself. Studies that delineate the protein expression of TPC1 in mouse brain is also important, as mRNA expression does not necessarily correlate to protein level, and this means a search for a specific anti-TPC1 antibody is equally crucial.

Future investigations including cellular and subcellular localization studies of TPCs and the acidic Ca^{2+} stores are crucial for better understanding the interaction between different types of intracellular Ca^{2+} releasing channels. Since NAADP has also been detected in

several brain regions, and previous functional studies have also identified a role for both NAADP and TPCs a role in certain brain cells such as astrocytes and medulla neurons, thus studies involving the spatial pattern of TPCs could definitely provide deeper insight into how these channels may interact with NAADP. Expression studies can be done by *in situ* hybridization, immunocytochemistry and electron microscopy using specific anti-TPCs antibodies. It would also be useful to co-stain the IP_3Rs and RyRs so as to evaluate for co-localization (if any) between these receptors, as tight association is highly flavourable for CICR. In addition to expression studies, functional studies regarding those regions with prominent TPC expression would be of top priority, in order to identify their roles in key physiological processes regulated by the nervous system. For example, memory deficits associated with hippocampal dysfunction are a key feature of a number of neurodegenerative and psychiatric disorders, and given that biochemical and functional evidence has shown the involvement of TPC1 in the hippocampus, it would be insightful to investigate the molecular mechanisms underlying the TPC1-mediated signalling in this brain area.

5.4 Appendix

5.4.1 Western blot of *Tpcn1/2* DKO (lung, brain, kidney, heart and pancreas) and *Tpcn1* KO (liver and adipose tissue) and strain-matched WT tissue membrane fraction using affinity purified anti-TPC1 antibody (Ruth Tunn's thesis)

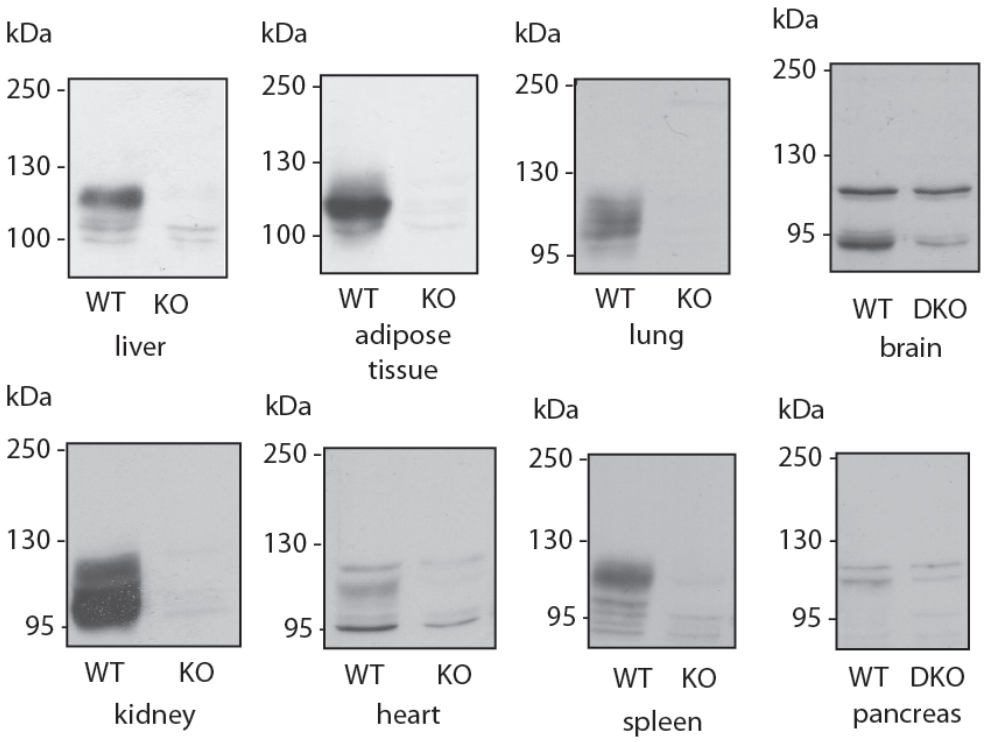

Chapter 6

General Discussion

6.1 *Tpcn* expression – other possible regulations

To date, not much has been reported concerning the factors associated with physiological regulation of *Tpcn* expression. Recently, an upregulation of *Tpcn2* has been revealed in kidneys of rats fed with low-protein diet and vitamin D [369]. On the other hand, a transient upregulation of vitamin D receptor (VDR) mRNA expression induced via cAMP pathway was shown to be maximal during 2-6 hours post induction of 3T3-L1 adipogenesis, while differentiation was disrupted in VDR KD cells [370]. The timeframe of VDR mRNA upregulation during adipogenesis is comparable to that of *Tpcn2*, and similarly, both temporal enhancements are driven by cAMP pathway. Moreover, VDR KO mice displayed a lean phenotype and resistance to HFD [371, 372], which was a consequence of increased energy expenditure [371] due to increased rate of fatty acid β-oxidation in WAT and absence of vitamin D-mediated inhibition of uncoupling protein (UCP) expression in BAT [372]; while previous findings from Dr John Parrington's lab has demonstrated a low-adiposity phenotype with significant reduction of lean mass in male *Tpcn2* KO mice at 9 months old (Dr Ruth Tunn; in preparation). Given the remarkable similarities in the temporal upregulation of VDR and *Tpcn2* expression during adipocyte differentiation and the lean phenotype of the KO mice, as well as the implication of vitamin D-mediated *Tpcn2* upregulation in the rat kidney [369], one might speculate that vitamin D could modulate *Tpcn2* expression during adipogenesis, and if so, what are the functional differences between the observed cAMP-mediated *Tpcn2* upregulation in this study and the VDR-mediated modulation of *Tpcn2* expression in adipogenesis? Hence, future studies would be informative to delineate if other factors, including vitamin D, are physiologically relevant in regulation of TPC2 expression during adipogenesis.

In the same study in which a low-adiposity phenotype was identified in male *Tpcn2* KO

mice, neither fasting hyperglycaemia nor defects in glucose tolerance or obvious hepatic steatosis was observed (Dr Ruth Tunn; in preparation), indicating that the involvement of TPCs in pancreatic β-cell function may be less essential than previously suggested [71][373]. Given the functional implications of TPC2 in adipogenesis (Chapter 4), whether the aforementioned phenotype is caused by an impaired adipogenic capacity awaits further investigations. Interestingly, the same study showed that only male *Tpcn2* KO mice displayed the low-adiposity phenotype; no significant changes were noted with females; while another study showed that only female CD38KO mice displayed an upregulation of RyR2 and only male CD38KO mice developed cardiac hypertrophy [374]. Such gender-dependent differential regulation identified in TPC2KO and CD38KO mice is intriguing and novel in NAADP/TPC-mediated signalling mechanism. It would be useful to compare if there are any sex-specific differences in the effects of adipogenesis between male and female *Tpcn2* KO mice as well.

On the other hand, a recent study on whole-organism metabolism has revealed mature-onset obesity in *Tpcn1/2* DKO mice, which was attributed to impairment in thermogenesis in BAT resulted from decreased lipid availability and use, as well as dysfunctional β-adrenergic receptor signalling [138]. This is the first report to demonstrate that absence of both TPC1 and 2 led to disrupted BAT thermogenesis. All of these findings, together with the data presented in my study, suggested functional roles of TPCs in regulating adipose tissue development and functioning. Adipocytes are essential in maintaining whole body energy homeostasis, with excess accumulation of adipose tissue leading to obesity, which is correlated with a higher risk of insulin resistance, type 2 diabetes, metabolic syndrome, heart disease and stroke etc. and its incidence worldwide is increasing (World Health Organization, 2000). Therefore delineation of the signalling pathways and molecular mechanisms controlling adiposity and lipid metabolism is critical and identification of

new players like TPC2 may provide potential therapeutic targets for the treatment of obesity in humans.

6.2 Alternative functional roles for TPCs?

A significant amount of findings have shown that TPCs are the long-sought-after target of NAADP receptors mediating Ca^{2+} release from the endolysosomal organelles. Recently, this notion has been challenged by the rising number of studies pointing TPCs to be Na^{+} channels gated by other factors (Chapter 1 Section 1.6) [104, 105, 114]. Given the contradictory results of these studies, NAADP- and TPC-mediated signalling is becoming more perplexing. Investigations clarifying the discrepancies are crucial for unveiling any undiscovered signalling pathways, which might require re-assessment of the potential effects and underlying mechanisms of the TPC expressions and knockdown phenotype findings reported in this thesis.

6.3 Final conclusions

This study has presented the first evidence of TPC2-mediated Ca^{2+} signalling being both essential and necessary for the development of SMCs in intact zebrafish embryos. Not only was the characteristic Ca^{2+} signalling signatures generated by IP_3R and RyR mobilisation [128] disrupted by genetic and pharmacological knockdown of TPC2, but also the gross and fine structure of the trunk of zebrafish embryo were impaired, hence TPC2 is implicated functional roles in ET and EC coupling. Together with the localisation data which revealed a close proximity between TPC2 and IP_3Rs and RyRs, a potential functional coupling between TPCs, IP_3R and RyR possibly via the CICR-induced ‘trigger’ mechanism [35] is suggested, implying interplay between these channels in regulating SMC development [129].

In addition, preliminary evidence has shown the expression and distribution pattern of *Tpcn3* during zebrafish embryogenesis, and future investigations are necessary to explore its role and physiological relevance in such process.

My data has also suggested a functional role for TPC2 in adipogenesis. Impaired adipogenic capacity was seen in TPC2KD C3H10T1/2 cells, participation of intracellular Ca^{2+} signalling and lysosomal stores in early adipogenesis was also demonstrated, indicating the involvement of NAADP/TPC-mediated Ca^{2+} signalling in such process. The transient and significant upregulation of *Tpcn2* expression during early adipogenesis was shown to be mediated by IBMX and other cAMP mimetics but not insulin or dexamethasone. Also, evidence has demonstrated a requirement of PKA and Epac in *Tpcn2* upregulation during 2-4 hours post-induction, while other mediators were suggested to be involved in the substantial upregulation at 8 hours. Furthermore, CREB was shown to be associated with the transactivation of *Tpcn2*, at least at 2 hours. Collectively, this work provides a foundation for future investigations of the mechanisms underlying the TPC2-mediated regulation of adipogenesis.

Data from the *in situ* hybridization study has revealed the expression pattern of *Tpcn1* in the CA1 and CA3 regions of the hippocampus, implicating a role of TPC1 in synaptic plasticity. Again, future investigations of TPC1's involvement in this process would be useful given the accumulating evidence showing the differential roles of NAADP signaling in the nervous system but only a few reports concerning the roles of TPCs.

In conclusion, the compelling evidence reported in this thesis has demonstrated novel functional roles of TPCs in key physiological processes, adding new insights into our understanding of the complex Ca^{2+} signalling system in development.

Word count: 46009

References

1. Berridge, M.J., M.D. Bootman, and H.L. Roderick, *Calcium signalling: dynamics, homeostasis and remodelling.* Nat Rev Mol Cell Biol, 2003. **4**(7): p. 517-29.
2. Rizzuto, R. and T. Pozzan, *When calcium goes wrong: genetic alterations of a ubiquitous signaling route.* Nat Genet, 2003. **34**(2): p. 135-41.
3. Stricker, S.A., *Comparative biology of calcium signaling during fertilization and egg activation in animals.* Dev Biol, 1999. **211**(2): p. 157-76.
4. Berridge, M.J., P. Lipp, and M.D. Bootman, *The versatility and universality of calcium signalling.* Nat Rev Mol Cell Biol, 2000. **1**(1): p. 11-21.
5. Clapham, D.E., *Calcium signaling.* Cell, 2007. **131**(6): p. 1047-58.
6. Patel, S., S.K. Joseph, and A.P. Thomas, *Molecular properties of inositol 1,4,5-trisphosphate receptors.* Cell Calcium, 1999. **25**(3): p. 247-64.
7. Taylor, C.W., A.A. Genazzani, and S.A. Morris, *Expression of inositol trisphosphate receptors.* Cell Calcium, 1999. **26**(6): p. 237-51.
8. Foskett, J.K., et al., *Inositol trisphosphate receptor Ca2+ release channels.* Physiol Rev, 2007. **87**(2): p. 593-658.
9. Lee, H.C., *Mechanisms of calcium signaling by cyclic ADP-ribose and NAADP.* Physiol Rev, 1997. **77**(4): p. 1133-64.
10. Fill, M. and J.A. Copello, *Ryanodine receptor calcium release channels.* Physiol Rev, 2002. **82**(4): p. 893-922.
11. Lee, H.C., *Calcium signaling: NAADP ascends as a new messenger.* Curr Biol, 2003. **13**(5): p. R186-8.
12. Patel, S., *NAADP-induced Ca2+ release -- a new signalling pathway.* Biol Cell, 2004. **96**(1): p. 19-28.
13. Churchill, G.C., et al., *NAADP mobilizes Ca(2+) from reserve granules, lysosome-related organelles, in sea urchin eggs.* Cell, 2002. **111**(5): p. 703-8.
14. Morgan, A.J., *Sea urchin eggs in the acid reign.* Cell Calcium, 2011. **50**(2): p. 147-56.
15. Morgan, A.J., et al., *Molecular mechanisms of endolysosomal Ca2+ signalling in health and disease.* Biochem J, 2011. **439**(3): p. 349-74.
16. Patel, S., et al., *The endo-lysosomal system as an NAADP-sensitive acidic Ca(2+) store: role for the two-pore channels.* Cell Calcium, 2011. **50**(2): p. 157-67.
17. Guse, A.H., *Linking NAADP to ion channel activity: a unifying hypothesis.* Sci Signal, 2012. **5**(221): p. pe18.
18. Zhu, M.X., et al., *Calcium signaling via two-pore channels: local or global, that is the question.* Am J Physiol Cell Physiol, 2010. **298**(3): p. C430-41.
19. Ogunbayo, O.A., et al., *Cyclic adenosine diphosphate ribose activates ryanodine receptors, whereas NAADP activates two-pore domain channels.* J Biol Chem, 2011. **286**(11): p. 9136-40.
20. Yamaguchi, S., et al., *Transient receptor potential mucolipin 1 (TRPML1) and two-pore channels are functionally independent organellar ion channels.* J Biol Chem, 2011. **286**(26): p. 22934-42.
21. Zhang, F., et al., *Reconstitution of lysosomal NAADP-TRP-ML1 signaling pathway and its function in TRP-ML1(-/-) cells.* Am J Physiol Cell Physiol, 2011. **301**(2): p. C421-30.

22. Patel, S. and R. Docampo, *Acidic calcium stores open for business: expanding the potential for intracellular Ca2+ signaling.* Trends Cell Biol, 2010. **20**(5): p. 277-86.
23. Patel, S. and S. Muallem, *Acidic Ca(2+) stores come to the fore.* Cell Calcium, 2011. **50**(2): p. 109-12.
24. Christensen, K.A., J.T. Myers, and J.A. Swanson, *pH-dependent regulation of lysosomal calcium in macrophages.* J Cell Sci, 2002. **115**(Pt 3): p. 599-607.
25. Gerasimenko, J.V., et al., *Calcium uptake via endocytosis with rapid release from acidifying endosomes.* Curr Biol, 1998. **8**(24): p. 1335-8.
26. Haller, T., et al., *The lysosomal compartment as intracellular calcium store in MDCK cells: a possible involvement in InsP3-mediated Ca2+ release.* Cell Calcium, 1996. **19**(2): p. 157-65.
27. Lloyd-Evans, E., et al., *Niemann-Pick disease type C1 is a sphingosine storage disease that causes deregulation of lysosomal calcium.* Nat Med, 2008. **14**(11): p. 1247-55.
28. Miyawaki, A., et al., *Fluorescent indicators for Ca2+ based on green fluorescent proteins and calmodulin.* Nature, 1997. **388**(6645): p. 882-7.
29. Pandey, V., et al., *Recruitment of NAADP-sensitive acidic Ca2+ stores by glutamate.* Biochem J, 2009. **422**(3): p. 503-12.
30. Sherwood, M.W., et al., *Activation of trypsinogen in large endocytic vacuoles of pancreatic acinar cells.* Proc Natl Acad Sci U S A, 2007. **104**(13): p. 5674-9.
31. Lee, H.C. and R. Aarhus, *A derivative of NADP mobilizes calcium stores insensitive to inositol trisphosphate and cyclic ADP-ribose.* J Biol Chem, 1995. **270**(5): p. 2152-7.
32. Galione, A. and O.H. Petersen, *The NAADP receptor: new receptors or new regulation?* Mol Interv, 2005. **5**(2): p. 73-9.
33. Guse, A.H. and H.C. Lee, *NAADP: a universal Ca2+ trigger.* Sci Signal, 2008. **1**(44): p. re10.
34. Galione, A., et al., *NAADP as an intracellular messenger regulating lysosomal calcium-release channels.* Biochem Soc Trans, 2010. **38**(6): p. 1424-31.
35. Galione, A., *NAADP receptors.* Cold Spring Harb Perspect Biol, 2011. **3**(1): p. a004036.
36. Lee, H.C., *Cyclic ADP-ribose and nicotinic acid adenine dinucleotide phosphate (NAADP) as messengers for calcium mobilization.* J Biol Chem, 2012. **287**(38): p. 31633-40.
37. Gerasimenko, J.V., et al., *NAADP mobilizes Ca2+ from a thapsigargin-sensitive store in the nuclear envelope by activating ryanodine receptors.* J Cell Biol, 2003. **163**(2): p. 271-82.
38. Churchill, G.C., et al., *Sperm deliver a new second messenger: NAADP.* Curr Biol, 2003. **13**(2): p. 125-8.
39. Cancela, J.M., G.C. Churchill, and A. Galione, *Coordination of agonist-induced Ca2+-signalling patterns by NAADP in pancreatic acinar cells.* Nature, 1999. **398**(6722): p. 74-6.
40. Yamasaki, M., et al., *Organelle selection determines agonist-specific Ca2+ signals in pancreatic acinar and beta cells.* J Biol Chem, 2004. **279**(8): p. 7234-40.
41. Yamasaki, M., et al., *Role of NAADP and cADPR in the induction and maintenance of agonist-evoked Ca2+ spiking in mouse pancreatic acinar cells.* Curr Biol, 2005. **15**(9): p. 874-8.

42. Boittin, F.X., A. Galione, and A.M. Evans, *Nicotinic acid adenine dinucleotide phosphate mediates Ca2+ signals and contraction in arterial smooth muscle via a two-pool mechanism.* Circ Res, 2002. **91**(12): p. 1168-75.
43. Kinnear, N.P., et al., *Lysosome-sarcoplasmic reticulum junctions. A trigger zone for calcium signaling by nicotinic acid adenine dinucleotide phosphate and endothelin-1.* J Biol Chem, 2004. **279**(52): p. 54319-26.
44. Kim, B.J., et al., *Generation of nicotinic acid adenine dinucleotide phosphate and cyclic ADP-ribose by glucagon-like peptide-1 evokes Ca2+ signal that is essential for insulin secretion in mouse pancreatic islets.* Diabetes, 2008. **57**(4): p. 868-78.
45. Cancela, J.M., et al., *Transformation of local Ca2+ spikes to global Ca2+ transients: the combinatorial roles of multiple Ca2+ releasing messengers.* Embo j, 2002. **21**(5): p. 909-19.
46. Aley, P.K., et al., *A functional role for nicotinic acid adenine dinucleotide phosphate in oxytocin-mediated contraction of uterine smooth muscle from rat.* J Pharmacol Exp Ther, 2010. **333**(3): p. 726-35.
47. Galione, A., *NAADP, a new intracellular messenger that mobilizes Ca2+ from acidic stores.* Biochem Soc Trans, 2006. **34**(Pt 5): p. 922-6.
48. Aarhus, R., et al., *ADP-ribosyl cyclase and CD38 catalyze the synthesis of a calcium-mobilizing metabolite from NADP.* J Biol Chem, 1995. **270**(51): p. 30327-33.
49. Cosker, F., et al., *The ecto-enzyme CD38 is a nicotinic acid adenine dinucleotide phosphate (NAADP) synthase that couples receptor activation to Ca2+ mobilization from lysosomes in pancreatic acinar cells.* J Biol Chem, 2010. **285**(49): p. 38251-9.
50. Kim, S.Y., B.H. Cho, and U.H. Kim, *CD38-mediated Ca2+ signaling contributes to angiotensin II-induced activation of hepatic stellate cells: attenuation of hepatic fibrosis by CD38 ablation.* J Biol Chem, 2010. **285**(1): p. 576-82.
51. Davis, L.C., et al., *Ca(2+) signaling occurs via second messenger release from intraorganelle synthesis sites.* Curr Biol, 2008. **18**(20): p. 1612-8.
52. Rah, S.Y., et al., *Generation of cyclic ADP-ribose and nicotinic acid adenine dinucleotide phosphate by CD38 for Ca2+ signaling in interleukin-8-treated lymphokine-activated killer cells.* J Biol Chem, 2010. **285**(28): p. 21877-87.
53. Zhang, F., M. Xia, and P.L. Li, *Lysosome-dependent Ca(2+) release response to Fas activation in coronary arterial myocytes through NAADP: evidence from CD38 gene knockouts.* Am J Physiol Cell Physiol, 2010. **298**(5): p. C1209-16.
54. Churchill, G.C. and A. Galione, *Spatial control of Ca2+ signaling by nicotinic acid adenine dinucleotide phosphate diffusion and gradients.* J Biol Chem, 2000. **275**(49): p. 38687-92.
55. Churchill, G.C. and A. Galione, *NAADP induces Ca2+ oscillations via a two-pool mechanism by priming IP3- and cADPR-sensitive Ca2+ stores.* Embo j, 2001. **20**(11): p. 2666-71.
56. Churchill, G.C. and A. Galione, *Prolonged inactivation of nicotinic acid adenine dinucleotide phosphate-induced Ca2+ release mediates a spatiotemporal Ca2+ memory.* J Biol Chem, 2001. **276**(14): p. 11223-5.
57. Patel, S., G.C. Churchill, and A. Galione, *Coordination of Ca2+ signalling by NAADP.* Trends Biochem Sci, 2001. **26**(8): p. 482-9.
58. Kilpatrick, B.S., et al., *Direct mobilisation of lysosomal Ca2+ triggers complex Ca2+ signals.* J Cell Sci, 2013. **126**(Pt 1): p. 60-6.

59. Lopez-Sanjurjo, C.I., et al., *Lysosomes shape Ins(1,4,5)P3-evoked Ca2+ signals by selectively sequestering Ca2+ released from the endoplasmic reticulum.* J Cell Sci, 2013. **126**(Pt 1): p. 289-300.
60. Morgan, A.J., et al., *Bidirectional Ca(2)(+) signaling occurs between the endoplasmic reticulum and acidic organelles.* J Cell Biol, 2013. **200**(6): p. 789-805.
61. Penny, C.J., et al., *A computational model of lysosome-ER Ca2+ microdomains.* J Cell Sci, 2014. **127**(Pt 13): p. 2934-43.
62. Penny, C.J., et al., *A "mix-and-match" approach to designing Ca(2+) microdomains at membrane-contact sites.* Commun Integr Biol, 2014. **7**: p. e29586.
63. Morgan, A.J. and A. Galione, *Two-pore channels (TPCs): current controversies.* Bioessays, 2014. **36**(2): p. 173-83.
64. Ishibashi, K., M. Suzuki, and M. Imai, *Molecular cloning of a novel form (two-repeat) protein related to voltage-gated sodium and calcium channels.* Biochem Biophys Res Commun, 2000. **270**(2): p. 370-6.
65. Furuichi, T., K.W. Cunningham, and S. Muto, *A putative two pore channel AtTPC1 mediates Ca(2+) flux in Arabidopsis leaf cells.* Plant Cell Physiol, 2001. **42**(9): p. 900-5.
66. Peiter, E., et al., *The vacuolar Ca2+-activated channel TPC1 regulates germination and stomatal movement.* Nature, 2005. **434**(7031): p. 404-8.
67. Choi, W.G., et al., *Salt stress-induced Ca2+ waves are associated with rapid, long-distance root-to-shoot signaling in plants.* Proc Natl Acad Sci U S A, 2014. **111**(17): p. 6497-502.
68. Brailoiu, E., et al., *Essential requirement for two-pore channel 1 in NAADP-mediated calcium signaling.* J Cell Biol, 2009. **186**(2): p. 201-9.
69. Brailoiu, E., et al., *An ancestral deuterostome family of two-pore channels mediates nicotinic acid adenine dinucleotide phosphate-dependent calcium release from acidic organelles.* J Biol Chem, 2010. **285**(5): p. 2897-901.
70. Brailoiu, E., et al., *An NAADP-gated two-pore channel targeted to the plasma membrane uncouples triggering from amplifying Ca2+ signals.* J Biol Chem, 2010. **285**(49): p. 38511-6.
71. Calcraft, P.J., et al., *NAADP mobilizes calcium from acidic organelles through two-pore channels.* Nature, 2009. **459**(7246): p. 596-600.
72. Schrlau, M.G., et al., *Carbon nanopipettes characterize calcium release pathways in breast cancer cells.* Nanotechnology, 2008. **19**(32): p. 325102.
73. Zong, X., et al., *The two-pore channel TPCN2 mediates NAADP-dependent Ca(2+)-release from lysosomal stores.* Pflugers Arch, 2009. **458**(5): p. 891-9.
74. Strong, M., K.G. Chandy, and G.A. Gutman, *Molecular evolution of voltage-sensitive ion channel genes: on the origins of electrical excitability.* Mol Biol Evol, 1993. **10**(1): p. 221-42.
75. Rietdorf, K., et al., *Two-pore channels form homo- and heterodimers.* J Biol Chem, 2011. **286**(43): p. 37058-62.
76. Ruas, M., et al., *Purified TPC isoforms form NAADP receptors with distinct roles for Ca(2+) signaling and endolysosomal trafficking.* Curr Biol, 2010. **20**(8): p. 703-9.
77. Hooper, R., et al., *Membrane topology of NAADP-sensitive two-pore channels and their regulation by N-linked glycosylation.* J Biol Chem, 2011. **286**(11): p. 9141-9.
78. Zhu, M.X., et al., *TPCs: Endolysosomal channels for Ca2+ mobilization from acidic organelles triggered by NAADP.* FEBS Lett, 2010. **584**(10): p. 1966-74.

79. Chini, E.N. and T.P. Dousa, *Nicotinate-adenine dinucleotide phosphate-induced Ca(2+)-release does not behave as a Ca(2+)-induced Ca(2+)-release system.* Biochem J, 1996. **316 (Pt 3)**: p. 709-11.
80. Morgan, A.J., et al., *TPC: the NAADP discovery channel?* Biochem Soc Trans, 2015. **43**(3): p. 384-9.
81. Kurusu, T., et al., *Identification of a putative voltage-gated Ca2+ -permeable channel (OsTPC1) involved in Ca2+ influx and regulation of growth and development in rice.* Plant Cell Physiol, 2004. **45**(6): p. 693-702.
82. Wang, Y.J., et al., *Functional analysis of a putative Ca2+ channel gene TaTPC1 from wheat.* J Exp Bot, 2005. **56**(422): p. 3051-60.
83. Kadota, Y., et al., *Identification of putative voltage-dependent Ca2+-permeable channels involved in cryptogein-induced Ca2+ transients and defense responses in tobacco BY-2 cells.* Biochem Biophys Res Commun, 2004. **317**(3): p. 823-30.
84. Patel, S., J.S. Marchant, and E. Brailoiu, *Two-pore channels: Regulation by NAADP and customized roles in triggering calcium signals.* Cell Calcium, 2010. **47**(6): p. 480-90.
85. Cai, X. and S. Patel, *Degeneration of an intracellular ion channel in the primate lineage by relaxation of selective constraints.* Mol Biol Evol, 2010. **27**(10): p. 2352-9.
86. Ruas, M., et al., *TPC1 has two variant isoforms, and their removal has different effects on endo-lysosomal functions compared to loss of TPC2.* Mol Cell Biol, 2014. **34**(21): p. 3981-92.
87. Berridge, G., et al., *Solubilization of receptors for the novel Ca2+-mobilizing messenger, nicotinic acid adenine dinucleotide phosphate.* J Biol Chem, 2002. **277**(46): p. 43717-23.
88. Genazzani, A.A., et al., *Pharmacological properties of the Ca2+-release mechanism sensitive to NAADP in the sea urchin egg.* Br J Pharmacol, 1997. **121**(7): p. 1489-95.
89. Mandi, M., et al., *Ca2+ release triggered by NAADP in hepatocyte microsomes.* Biochem J, 2006. **395**(2): p. 233-8.
90. Zhang, F., et al., *TRP-ML1 functions as a lysosomal NAADP-sensitive Ca2+ release channel in coronary arterial myocytes.* J Cell Mol Med, 2009. **13**(9b): p. 3174-85.
91. Zhang, F. and P.L. Li, *Reconstitution and characterization of a nicotinic acid adenine dinucleotide phosphate (NAADP)-sensitive Ca2+ release channel from liver lysosomes of rats.* J Biol Chem, 2007. **282**(35): p. 25259-69.
92. Ruas, M., et al., *Expression of Ca(2)(+)-permeable two-pore channels rescues NAADP signalling in TPC-deficient cells.* Embo j, 2015. **34**(13): p. 1743-58.
93. Santella, L., et al., *Nicotinic acid adenine dinucleotide phosphate-induced Ca(2+) release. Interactions among distinct Ca(2+) mobilizing mechanisms in starfish oocytes.* J Biol Chem, 2000. **275**(12): p. 8301-6.
94. Naylor, E., et al., *Identification of a chemical probe for NAADP by virtual screening.* Nat Chem Biol, 2009. **5**(4): p. 220-6.
95. Dickinson, G.D. and S. Patel, *Modulation of NAADP (nicotinic acid-adenine dinucleotide phosphate) receptors by K+ ions: evidence for multiple NAADP receptor conformations.* Biochem J, 2003. **375**(Pt 3): p. 805-12.
96. Walseth, T.F., et al., *Photoaffinity labeling of high affinity nicotinic acid adenine dinucleotide phosphate (NAADP)-binding proteins in sea urchin egg.* J Biol Chem, 2012. **287**(4): p. 2308-15.

97. Lin-Moshier, Y., et al., *Photoaffinity labeling of nicotinic acid adenine dinucleotide phosphate (NAADP) targets in mammalian cells.* J Biol Chem, 2012. **287**(4): p. 2296-307.
98. Walseth, T.F., et al., *Nicotinic Acid Adenine Dinucleotide 2'-Phosphate (NAADP) Binding Proteins in T-Lymphocytes.* Messenger (Los Angel), 2012. **1**(1): p. 86-94.
99. Genazzani, A.A., et al., *Kinetic properties of nicotinic acid adenine dinucleotide phosphate-induced Ca2+ release.* J Biol Chem, 1997. **272**(12): p. 7669-75.
100. Pereira, G.J., et al., *Nicotinic acid adenine dinucleotide phosphate (NAADP) regulates autophagy in cultured astrocytes.* J Biol Chem, 2011. **286**(32): p. 27875-81.
101. Lu, Y., et al., *Two pore channel 2 (TPC2) inhibits autophagosomal-lysosomal fusion by alkalinizing lysosomal pH.* J Biol Chem, 2013. **288**(33): p. 24247-63.
102. Pitt, S.J., et al., *TPC2 is a novel NAADP-sensitive Ca2+ release channel, operating as a dual sensor of luminal pH and Ca2+.* J Biol Chem, 2010. **285**(45): p. 35039-46.
103. Rosen, D., et al., *Analogues of the nicotinic acid adenine dinucleotide phosphate (NAADP) antagonist Ned-19 indicate two binding sites on the NAADP receptor.* J Biol Chem, 2009. **284**(50): p. 34930-4.
104. Wang, X., et al., *TPC proteins are phosphoinositide- activated sodium-selective ion channels in endosomes and lysosomes.* Cell, 2012. **151**(2): p. 372-83.
105. Cang, C., et al., *mTOR regulates lysosomal ATP-sensitive two-pore Na(+) channels to adapt to metabolic state.* Cell, 2013. **152**(4): p. 778-90.
106. Dong, X.P., et al., *PI(3,5)P(2) controls membrane trafficking by direct activation of mucolipin Ca(2+) release channels in the endolysosome.* Nat Commun, 2010. **1**: p. 38.
107. Churamani, D., et al., *The N-terminal region of two-pore channel 1 regulates trafficking and activation by NAADP.* Biochem J, 2013. **453**(1): p. 147-51.
108. Marchant, J.S. and S. Patel, *Questioning regulation of two-pore channels by NAADP.* Messenger (Los Angel), 2013. **2**(2): p. 113-119.
109. Jha, A., et al., *Convergent regulation of the lysosomal two-pore channel-2 by Mg(2)(+), NAADP, PI(3,5)P(2) and multiple protein kinases.* Embo j, 2014. **33**(5): p. 501-11.
110. Grimm, C., et al., *High susceptibility to fatty liver disease in two-pore channel 2-deficient mice.* Nat Commun, 2014. **5**: p. 4699.
111. Pitt, S.J., et al., *Reconstituted human TPC1 is a proton-permeable ion channel and is activated by NAADP or Ca2+.* Sci Signal, 2014. **7**(326): p. ra46.
112. Rybalchenko, V., et al., *Membrane potential regulates nicotinic acid adenine dinucleotide phosphate (NAADP) dependence of the pH- and Ca2+-sensitive organellar two-pore channel TPC1.* J Biol Chem, 2012. **287**(24): p. 20407-16.
113. Schieder, M., et al., *Characterization of two-pore channel 2 (TPCN2)-mediated Ca2+ currents in isolated lysosomes.* J Biol Chem, 2010. **285**(28): p. 21219-22.
114. Cang, C., B. Bekele, and D. Ren, *The voltage-gated sodium channel TPC1 confers endolysosomal excitability.* Nat Chem Biol, 2014. **10**(6): p. 463-9.
115. Cang, C., K. Aranda, and D. Ren, *A non-inactivating high-voltage-activated two-pore Na(+) channel that supports ultra-long action potentials and membrane bistability.* Nat Commun, 2014. **5**: p. 5015.
116. Gillespie, D. and M. Fill, *Intracellular calcium release channels mediate their own countercurrent: the ryanodine receptor case study.* Biophys J, 2008. **95**(8): p. 3706-14.

117. Vais, H., et al., *Permeant calcium ion feed-through regulation of single inositol 1,4,5-trisphosphate receptor channel gating.* J Gen Physiol, 2012. **140**(6): p. 697-716.
118. Mayer, M.L. and G.L. Westbrook, *Permeation and block of N-methyl-D-aspartic acid receptor channels by divalent cations in mouse cultured central neurones.* J Physiol, 1987. **394**: p. 501-27.
119. Morgan, A.J. and A. Galione, *NAADP induces pH changes in the lumen of acidic Ca2+ stores.* Biochem J, 2007. **402**(2): p. 301-10.
120. Collins, T.P., et al., *NAADP influences excitation-contraction coupling by releasing calcium from lysosomes in atrial myocytes.* Cell Calcium, 2011. **50**(5): p. 449-58.
121. Morgan, A.J., J. Parrington, and A. Galione, *The luminal Ca(2+) chelator, TPEN, inhibits NAADP-induced Ca(2+) release.* Cell Calcium, 2012. **52**(6): p. 481-7.
122. Boccaccio, A., et al., *The phosphoinositide PI(3,5)P(2) mediates activation of mammalian but not plant TPC proteins: functional expression of endolysosomal channels in yeast and plant cells.* Cell Mol Life Sci, 2014. **71**(21): p. 4275-83.
123. Lin-Moshier, Y., et al., *The Two-pore channel (TPC) interactome unmasks isoform-specific roles for TPCs in endolysosomal morphology and cell pigmentation.* Proc Natl Acad Sci U S A, 2014. **111**(36): p. 13087-92.
124. Lam, A.K., et al., *Hax-1 identified as a two-pore channel (TPC)-binding protein.* FEBS Lett, 2013. **587**(23): p. 3782-6.
125. Lopez, J., et al., *Two-pore channel 2 (TPC2) modulates store-operated Ca(2+) entry.* Biochim Biophys Acta, 2012. **1823**(10): p. 1976-83.
126. Ramos, I., A. Reich, and G.M. Wessel, *Two-pore channels function in calcium regulation in sea star oocytes and embryos.* Development, 2014. **141**(23): p. 4598-609.
127. Arndt, L., et al., *NAADP and the two-pore channel protein 1 participate in the acrosome reaction in mammalian spermatozoa.* Mol Biol Cell, 2014. **25**(6): p. 948-64.
128. Cheung, C.Y., et al., *Visualization, characterization and modulation of calcium signaling during the development of slow muscle cells in intact zebrafish embryos.* Int J Dev Biol, 2011. **55**(2): p. 153-74.
129. Kelu, J.J., et al., *Two-Pore Channel 2 activity is required for slow muscle cell-generated Ca (2+)signaling during myogenesis in intact zebrafish.* Int J Dev Biol, 2015. **59**(7-9): p. 313-25.
130. Tugba Durlu-Kandilci, N., et al., *TPC2 proteins mediate nicotinic acid adenine dinucleotide phosphate (NAADP)- and agonist-evoked contractions of smooth muscle.* J Biol Chem, 2010. **285**(32): p. 24925-32.
131. Brailoiu, E., et al., *Messenger-specific role for nicotinic acid adenine dinucleotide phosphate in neuronal differentiation.* J Biol Chem, 2006. **281**(23): p. 15923-8.
132. Zhang, Z.H., Y.Y. Lu, and J. Yue, *Two pore channel 2 differentially modulates neural differentiation of mouse embryonic stem cells.* PLoS One, 2013. **8**(6): p. e66077.
133. Aley, P.K., et al., *Nicotinic acid adenine dinucleotide phosphate regulates skeletal muscle differentiation via action at two-pore channels.* Proc Natl Acad Sci U S A, 2010. **107**(46): p. 19927-32.
134. Notomi, T., Y. Ezura, and M. Noda, *Identification of two-pore channel 2 as a novel regulator of osteoclastogenesis.* J Biol Chem, 2012. **287**(42): p. 35057-64.

135. Cheng, X., et al., *The role of calcium and nicotinic acid adenine dinucleotide phosphate (NAADP) in human osteoclast formation and resorption.* Calcif Tissue Int, 2015. **96**(1): p. 73-9.
136. Park, K.H., et al., *Role of Nicotinic Acid Adenine Dinucleotide Phosphate (NAADP) in Keratinocyte Differentiation.* J Invest Dermatol, 2015. **135**(6): p. 1692-4.
137. Favia, A., et al., *VEGF-induced neoangiogenesis is mediated by NAADP and two-pore channel-2-dependent Ca2+ signaling.* Proc Natl Acad Sci U S A, 2014. **111**(44): p. E4706-15.
138. Lear, P.V., et al., *Absence of intracellular ion channels TPC1 and TPC2 leads to mature-onset obesity in male mice, due to impaired lipid availability for thermogenesis in brown adipose tissue.* Endocrinology, 2015. **156**(3): p. 975-86.
139. Xu, M., et al., *Regulation of autophagic flux by dynein-mediated autophagosomes trafficking in mouse coronary arterial myocytes.* Biochim Biophys Acta, 2013. **1833**(12): p. 3228-36.
140. Xu, M., et al., *Enhancement of dynein-mediated autophagosome trafficking and autophagy maturation by ROS in mouse coronary arterial myocytes.* J Cell Mol Med, 2014. **18**(11): p. 2165-75.
141. Dickinson, G.D., et al., *Deviant nicotinic acid adenine dinucleotide phosphate (NAADP)-mediated Ca2+ signaling upon lysosome proliferation.* J Biol Chem, 2010. **285**(18): p. 13321-5.
142. Neely Kayala, K.M., et al., *Presenilin-null cells have altered two-pore calcium channel expression and lysosomal calcium: implications for lysosomal function.* Brain Res, 2012. **1489**: p. 8-16.
143. Lin, P.H., et al., *Lysosomal two-pore channel subtype 2 (TPC2) regulates skeletal muscle autophagic signaling.* J Biol Chem, 2015. **290**(6): p. 3377-89.
144. Sulem, P., et al., *Two newly identified genetic determinants of pigmentation in Europeans.* Nat Genet, 2008. **40**(7): p. 835-7.
145. Huang, X. and A. Madan, *CAP3: A DNA sequence assembly program.* Genome Res, 1999. **9**(9): p. 868-77.
146. Westerfield, M., *The zebrafish book. A guide for the laboratory use of zebrafish (Brachydanio rerio).* 1994: Univ. of Oregon Press, Eugene.
147. Bill, B.R., et al., *A primer for morpholino use in zebrafish.* Zebrafish, 2009. **6**(1): p. 69-77.
148. Robu, M.E., et al., *p53 activation by knockdown technologies.* PLoS Genet, 2007. **3**(5): p. e78.
149. Guan, H. and K. Yang, *RNA isolation and real-time quantitative RT-PCR.* Methods Mol Biol, 2008. **456**: p. 259-70.
150. Buckingham, M., et al., *The formation of skeletal muscle: from somite to limb.* J Anat, 2003. **202**(1): p. 59-68.
151. Grefte, S., et al., *Skeletal muscle development and regeneration.* Stem Cells Dev, 2007. **16**(5): p. 857-68.
152. Zhao, P. and E.P. Hoffman, *Embryonic myogenesis pathways in muscle regeneration.* Dev Dyn, 2004. **229**(2): p. 380-92.
153. Le Grand, F. and M.A. Rudnicki, *Skeletal muscle satellite cells and adult myogenesis.* Curr Opin Cell Biol, 2007. **19**(6): p. 628-33.
154. Tajbakhsh, S., *Skeletal muscle stem cells in developmental versus regenerative myogenesis.* J Intern Med, 2009. **266**(4): p. 372-89.
155. Ringer, S., *Concerning the Influence exerted by each of the Constituents of the Blood on the Contraction of the Ventricle.* J Physiol, 1882. **3**(5-6): p. 380-93.

156. Ferrari, M.B., J. Rohrbough, and N.C. Spitzer, *Spontaneous calcium transients regulate myofibrillogenesis in embryonic Xenopus myocytes.* Dev Biol, 1996. **178**(2): p. 484-97.
157. Ferrari, M.B., et al., *A calcium signaling cascade essential for myosin thick filament assembly in Xenopus myocytes.* J Cell Biol, 1998. **141**(6): p. 1349-56.
158. Lorenzon, P., et al., *Spontaneous and repetitive calcium transients in C2C12 mouse myotubes during in vitro myogenesis.* Eur J Neurosci, 1997. **9**(4): p. 800-8.
159. Jaimovich, E., et al., *IP(3) receptors, IP(3) transients, and nucleus-associated Ca(2+) signals in cultured skeletal muscle.* Am J Physiol Cell Physiol, 2000. **278**(5): p. C998-c1010.
160. Powell, J.A., et al., *IP(3) receptor function and localization in myotubes: an unexplored Ca(2+) signaling pathway in skeletal muscle.* J Cell Sci, 2001. **114**(Pt 20): p. 3673-83.
161. Li, H., et al., *Calcium transients regulate patterned actin assembly during myofibrillogenesis.* Dev Dyn, 2004. **229**(2): p. 231-42.
162. Harris, B.N., et al., *Calcium transients regulate titin organization during myofibrillogenesis.* Cell Motil Cytoskeleton, 2005. **60**(3): p. 129-39.
163. Fujita, H., T. Nedachi, and M. Kanzaki, *Accelerated de novo sarcomere assembly by electric pulse stimulation in C2C12 myotubes.* Exp Cell Res, 2007. **313**(9): p. 1853-65.
164. Ferrari, M.B. and N.C. Spitzer, *Calcium signaling in the developing Xenopus myotome.* Dev Biol, 1999. **213**(2): p. 269-82.
165. Brennan, C., et al., *Acetylcholine and calcium signalling regulates muscle fibre formation in the zebrafish embryo.* J Cell Sci, 2005. **118**(Pt 22): p. 5181-90.
166. David, J.D. and C.A. Higginbotham, *Fusion of chick embryo skeletal myoblasts: interactions of prostaglandin E1, adenosine 3':5' monophosphate, and calcium influx.* Dev Biol, 1981. **82**(2): p. 308-16.
167. David, J.D., W.M. See, and C.A. Higginbotham, *Fusion of chick embryo skeletal myoblasts: role of calcium influx preceding membrane union.* Dev Biol, 1981. **82**(2): p. 297-307.
168. Campbell, N.R., S.P. Podugu, and M.B. Ferrari, *Spatiotemporal characterization of short versus long duration calcium transients in embryonic muscle and their role in myofibrillogenesis.* Dev Biol, 2006. **292**(1): p. 253-64.
169. Jaimovich, E. and E. Rojas, *Intracellular Ca2+ transients induced by high external K+ and tetracaine in cultured rat myotubes.* Cell Calcium, 1994. **15**(5): p. 356-68.
170. Cardenas, C., et al., *Nuclear inositol 1,4,5-trisphosphate receptors regulate local Ca2+ transients and modulate cAMP response element binding protein phosphorylation.* J Cell Sci, 2005. **118**(Pt 14): p. 3131-40.
171. Hohenegger, M., et al., *Nicotinic acid-adenine dinucleotide phosphate activates the skeletal muscle ryanodine receptor.* Biochem J, 2002. **367**(Pt 2): p. 423-31.
172. Rennie, M.J., et al., *Control of the size of the human muscle mass.* Annu Rev Physiol, 2004. **66**: p. 799-828.
173. Schiaffino, S., et al., *Mechanisms regulating skeletal muscle growth and atrophy.* Febs j, 2013. **280**(17): p. 4294-314.
174. Hamasaki, M., S.T. Shibutani, and T. Yoshimori, *Up-to-date membrane biogenesis in the autophagosome formation.* Curr Opin Cell Biol, 2013. **25**(4): p. 455-60.
175. Choi, A.M., S.W. Ryter, and B. Levine, *Autophagy in human health and disease.* N Engl J Med, 2013. **368**(7): p. 651-62.
176. Sandri, M., *Autophagy in skeletal muscle.* FEBS Lett, 2010. **584**(7): p. 1411-6.

177. Malicdan, M.C. and I. Nishino, *Autophagy in lysosomal myopathies.* Brain Pathol, 2012. **22**(1): p. 82-8.
178. Medina, D.L., et al., *Lysosomal calcium signalling regulates autophagy through calcineurin and TFEB.* Nat Cell Biol, 2015. **17**(3): p. 288-99.
179. Yang, Z. and D.J. Klionsky, *Mammalian autophagy: core molecular machinery and signaling regulation.* Curr Opin Cell Biol, 2010. **22**(2): p. 124-31.
180. Kraus, M., B. Wolf, and B. Wolf, *Crosstalk between cellular morphology and calcium oscillation patterns. Insights from a stochastic computer model.* Cell Calcium, 1996. **19**(6): p. 461-72.
181. Perc, M., et al., *Establishing the stochastic nature of intracellular calcium oscillations from experimental data.* Biophys Chem, 2008. **132**(1): p. 33-8.
182. Ekker, S.C. and J.D. Larson, *Morphant technology in model developmental systems.* Genesis, 2001. **30**(3): p. 89-93.
183. Nasevicius, A. and S.C. Ekker, *Effective targeted gene 'knockdown' in zebrafish.* Nat Genet, 2000. **26**(2): p. 216-20.
184. Kimmel, C.B., et al., *Stages of embryonic development of the zebrafish.* Dev Dyn, 1995. **203**(3): p. 253-310.
185. Eisen, J.S. and J.C. Smith, *Controlling morpholino experiments: don't stop making antisense.* Development, 2008. **135**(10): p. 1735-43.
186. Lawson, N.D. and S.A. Wolfe, *Forward and reverse genetic approaches for the analysis of vertebrate development in the zebrafish.* Dev Cell, 2011. **21**(1): p. 48-64.
187. Devoto, S.H., et al., *Identification of separate slow and fast muscle precursor cells in vivo, prior to somite formation.* Development, 1996. **122**(11): p. 3371-80.
188. Horikawa, K., et al., *Spontaneous network activity visualized by ultrasensitive Ca(2+) indicators, yellow Cameleon-Nano.* Nat Methods, 2010. **7**(9): p. 729-32.
189. Saint-Amant, L. and P. Drapeau, *Time course of the development of motor behaviors in the zebrafish embryo.* J Neurobiol, 1998. **37**(4): p. 622-32.
190. Naganawa, Y. and H. Hirata, *Developmental transition of touch response from slow muscle-mediated coilings to fast muscle-mediated burst swimming in zebrafish.* Dev Biol, 2011. **355**(2): p. 194-204.
191. Blagden, C.S., et al., *Notochord induction of zebrafish slow muscle mediated by Sonic hedgehog.* Genes Dev, 1997. **11**(17): p. 2163-75.
192. Frank, D., et al., *The sarcomeric Z-disc: a nodal point in signalling and disease.* J Mol Med (Berl), 2006. **84**(6): p. 446-68.
193. Knoll, R., et al., *The cardiac mechanical stretch sensor machinery involves a Z disc complex that is defective in a subset of human dilated cardiomyopathy.* Cell, 2002. **111**(7): p. 943-55.
194. Arber, S., G. Halder, and P. Caroni, *Muscle LIM protein, a novel essential regulator of myogenesis, promotes myogenic differentiation.* Cell, 1994. **79**(2): p. 221-31.
195. Krolenko, S.A., et al., *Acridine orange accumulation in acid organelles of normal and vacuolated frog skeletal muscle fibres.* Cell Biol Int, 2006. **30**(11): p. 933-9.
196. Davis, A.K. and S.S. Carlson, *Proteoglycans are present in the transverse tubule system of skeletal muscle.* Matrix Biol, 1995. **14**(8): p. 607-21.
197. Bezin, S., et al., *Regulation of nuclear Ca2+ signaling by translocation of the Ca2+ messenger synthesizing enzyme ADP-ribosyl cyclase during neuronal depolarization.* J Biol Chem, 2008. **283**(41): p. 27859-70.
198. Detrich, H.W., 3rd, et al., *Intraembryonic hematopoietic cell migration during vertebrate development.* Proc Natl Acad Sci U S A, 1995. **92**(23): p. 10713-7.

199. Davidson, A.J., et al., *cdx4 mutants fail to specify blood progenitors and can be rescued by multiple hox genes.* Nature, 2003. **425**(6955): p. 300-6.
200. Davidson, A.J. and L.I. Zon, *The 'definitive' (and 'primitive') guide to zebrafish hematopoiesis.* Oncogene, 2004. **23**(43): p. 7233-46.
201. Thompson, M.A., et al., *The cloche and spadetail genes differentially affect hematopoiesis and vasculogenesis.* Dev Biol, 1998. **197**(2): p. 248-69.
202. Hsia, N. and L.I. Zon, *Transcriptional regulation of hematopoietic stem cell development in zebrafish.* Exp Hematol, 2005. **33**(9): p. 1007-14.
203. Bertrand, J.Y., et al., *Definitive hematopoiesis initiates through a committed erythromyeloid progenitor in the zebrafish embryo.* Development, 2007. **134**(23): p. 4147-56.
204. Auer, T.O. and F. Del Bene, *CRISPR/Cas9 and TALEN-mediated knock-in approaches in zebrafish.* Methods, 2014. **69**(2): p. 142-50.
205. Nebel, M., et al., *Nicotinic acid adenine dinucleotide phosphate (NAADP)-mediated calcium signaling and arrhythmias in the heart evoked by beta-adrenergic stimulation.* J Biol Chem, 2013. **288**(22): p. 16017-30.
206. MacDougald, O.A. and M.D. Lane, *Transcriptional regulation of gene expression during adipocyte differentiation.* Annu Rev Biochem, 1995. **64**: p. 345-73.
207. Rosen, E.D. and O.A. MacDougald, *Adipocyte differentiation from the inside out.* Nat Rev Mol Cell Biol, 2006. **7**(12): p. 885-96.
208. Gregoire, F.M., C.M. Smas, and H.S. Sul, *Understanding adipocyte differentiation.* Physiol Rev, 1998. **78**(3): p. 783-809.
209. Covas, D.T., et al., *Multipotent mesenchymal stromal cells obtained from diverse human tissues share functional properties and gene-expression profile with CD146+ perivascular cells and fibroblasts.* Exp Hematol, 2008. **36**(5): p. 642-54.
210. Lin, C.S., et al., *Defining adipose tissue-derived stem cells in tissue and in culture.* Histol Histopathol, 2010. **25**(6): p. 807-15.
211. Huang, H., et al., *BMP signaling pathway is required for commitment of C3H10T1/2 pluripotent stem cells to the adipocyte lineage.* Proc Natl Acad Sci U S A, 2009. **106**(31): p. 12670-5.
212. Berry, D.C., et al., *The developmental origins of adipose tissue.* Development, 2013. **140**(19): p. 3939-49.
213. Unger, R.H., et al., *Lipid homeostasis, lipotoxicity and the metabolic syndrome.* Biochim Biophys Acta, 2010. **1801**(3): p. 209-14.
214. Farmer, S.R., *Regulation of PPARgamma activity during adipogenesis.* Int J Obes (Lond), 2005. **29 Suppl 1**: p. S13-6.
215. Rosen, E.D. and B.M. Spiegelman, *Molecular regulation of adipogenesis.* Annu Rev Cell Dev Biol, 2000. **16**: p. 145-71.
216. Tang, Q.Q. and M.D. Lane, *Adipogenesis: from stem cell to adipocyte.* Annu Rev Biochem, 2012. **81**: p. 715-36.
217. McGregor, R.A. and M.S. Choi, *microRNAs in the regulation of adipogenesis and obesity.* Curr Mol Med, 2011. **11**(4): p. 304-16.
218. Bowers, R.R., et al., *Stable stem cell commitment to the adipocyte lineage by inhibition of DNA methylation: role of the BMP-4 gene.* Proc Natl Acad Sci U S A, 2006. **103**(35): p. 13022-7.
219. Tang, Q.Q., T.C. Otto, and M.D. Lane, *Commitment of C3H10T1/2 pluripotent stem cells to the adipocyte lineage.* Proc Natl Acad Sci U S A, 2004. **101**(26): p. 9607-11.
220. Bowers, R.R. and M.D. Lane, *Wnt signaling and adipocyte lineage commitment.* Cell Cycle, 2008. **7**(9): p. 1191-6.

221. Kang, S., et al., *Wnt signaling stimulates osteoblastogenesis of mesenchymal precursors by suppressing CCAAT/enhancer-binding protein alpha and peroxisome proliferator-activated receptor gamma.* J Biol Chem, 2007. **282**(19): p. 14515-24.
222. Ross, S.E., et al., *Inhibition of adipogenesis by Wnt signaling.* Science, 2000. **289**(5481): p. 950-3.
223. Spinella-Jaegle, S., et al., *Sonic hedgehog increases the commitment of pluripotent mesenchymal cells into the osteoblastic lineage and abolishes adipocytic differentiation.* J Cell Sci, 2001. **114**(Pt 11): p. 2085-94.
224. van der Horst, G., et al., *Hedgehog stimulates only osteoblastic differentiation of undifferentiated KS483 cells.* Bone, 2003. **33**(6): p. 899-910.
225. Zehentner, B.K., U. Leser, and H. Burtscher, *BMP-2 and sonic hedgehog have contrary effects on adipocyte-like differentiation of C3H10T1/2 cells.* DNA Cell Biol, 2000. **19**(5): p. 275-81.
226. Lowe, C.E., S. O'Rahilly, and J.J. Rochford, *Adipogenesis at a glance.* J Cell Sci, 2011. **124**(Pt 16): p. 2681-6.
227. Lefterova, M.I. and M.A. Lazar, *New developments in adipogenesis.* Trends Endocrinol Metab, 2009. **20**(3): p. 107-14.
228. Rosen, E.D., et al., *Transcriptional regulation of adipogenesis.* Genes Dev, 2000. **14**(11): p. 1293-307.
229. Savage, D.B., *PPAR gamma as a metabolic regulator: insights from genomics and pharmacology.* Expert Rev Mol Med, 2005. **7**(1): p. 1-16.
230. Lefterova, M.I., et al., *PPARgamma and C/EBP factors orchestrate adipocyte biology via adjacent binding on a genome-wide scale.* Genes Dev, 2008. **22**(21): p. 2941-52.
231. MacDougald, O.A. and S. Mandrup, *Adipogenesis: forces that tip the scales.* Trends Endocrinol Metab, 2002. **13**(1): p. 5-11.
232. Rosen, E.D., et al., *PPAR gamma is required for the differentiation of adipose tissue in vivo and in vitro.* Mol Cell, 1999. **4**(4): p. 611-7.
233. Rosen, E.D., et al., *C/EBPalpha induces adipogenesis through PPARgamma: a unified pathway.* Genes Dev, 2002. **16**(1): p. 22-6.
234. Sarjeant, K. and J.M. Stephens, *Adipogenesis.* Cold Spring Harb Perspect Biol, 2012. **4**(9): p. a008417.
235. Tontonoz, P., E. Hu, and B.M. Spiegelman, *Stimulation of adipogenesis in fibroblasts by PPAR gamma 2, a lipid-activated transcription factor.* Cell, 1994b. **79**(7): p. 1147-56.
236. Tontonoz, P. and B.M. Spiegelman, *Fat and beyond: the diverse biology of PPARgamma.* Annu Rev Biochem, 2008. **77**: p. 289-312.
237. Kubota, N., et al., *PPAR gamma mediates high-fat diet-induced adipocyte hypertrophy and insulin resistance.* Mol Cell, 1999. **4**(4): p. 597-609.
238. Wu, Z., et al., *Cross-regulation of C/EBP alpha and PPAR gamma controls the transcriptional pathway of adipogenesis and insulin sensitivity.* Mol Cell, 1999. **3**(2): p. 151-8.
239. Parsons, W.J., V. Ramkumar, and G.L. Stiles, *Isobutylmethylxanthine stimulates adenylate cyclase by blocking the inhibitory regulatory protein, Gi.* Mol Pharmacol, 1988. **34**(1): p. 37-41.
240. Bennett, C.N., et al., *Regulation of Wnt signaling during adipogenesis.* J Biol Chem, 2002. **277**(34): p. 30998-1004.

241. Tang, Q.Q., M.S. Jiang, and M.D. Lane, *Repressive effect of Sp1 on the C/EBPalpha gene promoter: role in adipocyte differentiation.* Mol Cell Biol, 1999. **19**(7): p. 4855-65.
242. Cao, Z., R.M. Umek, and S.L. McKnight, *Regulated expression of three C/EBP isoforms during adipose conversion of 3T3-L1 cells.* Genes Dev, 1991. **5**(9): p. 1538-52.
243. Hamm, J.K., B.H. Park, and S.R. Farmer, *A role for C/EBPbeta in regulating peroxisome proliferator-activated receptor gamma activity during adipogenesis in 3T3-L1 preadipocytes.* J Biol Chem, 2001. **276**(21): p. 18464-71.
244. Yeh, W.C., et al., *Cascade regulation of terminal adipocyte differentiation by three members of the C/EBP family of leucine zipper proteins.* Genes Dev, 1995. **9**(2): p. 168-81.
245. Hansen, J.B., et al., *Peroxisome proliferator-activated receptor delta (PPARdelta)-mediated regulation of preadipocyte proliferation and gene expression is dependent on cAMP signaling.* J Biol Chem, 2001. **276**(5): p. 3175-82.
246. Hallenborg, P., et al., *Epidermis-type lipoxygenase 3 regulates adipocyte differentiation and peroxisome proliferator-activated receptor gamma activity.* Mol Cell Biol, 2010. **30**(16): p. 4077-91.
247. Madsen, L., et al., *Adipocyte differentiation of 3T3-L1 preadipocytes is dependent on lipoxygenase activity during the initial stages of the differentiation process.* Biochem J, 2003. **375**(Pt 3): p. 539-49.
248. Mayr, B.M., G. Canettieri, and M.R. Montminy, *Distinct effects of cAMP and mitogenic signals on CREB-binding protein recruitment impart specificity to target gene activation via CREB.* Proc Natl Acad Sci U S A, 2001. **98**(19): p. 10936-41.
249. Petersen, R.K., et al., *Arachidonic acid-dependent inhibition of adipocyte differentiation requires PKA activity and is associated with sustained expression of cyclooxygenases.* J Lipid Res, 2003. **44**(12): p. 2320-30.
250. Tzameli, I., et al., *Regulated production of a peroxisome proliferator-activated receptor-gamma ligand during an early phase of adipocyte differentiation in 3T3-L1 adipocytes.* J Biol Chem, 2004. **279**(34): p. 36093-102.
251. Reusch, J.E., L.A. Colton, and D.J. Klemm, *CREB activation induces adipogenesis in 3T3-L1 cells.* Mol Cell Biol, 2000. **20**(3): p. 1008-20.
252. Zhang, J.W., et al., *Role of CREB in transcriptional regulation of CCAAT/enhancer-binding protein beta gene during adipogenesis.* J Biol Chem, 2004. **279**(6): p. 4471-8.
253. Cheng, X., et al., *Epac and PKA: a tale of two intracellular cAMP receptors.* Acta Biochim Biophys Sin (Shanghai), 2008. **40**(7): p. 651-62.
254. Bos, J.L., *Epac proteins: multi-purpose cAMP targets.* Trends Biochem Sci, 2006. **31**(12): p. 680-6.
255. Kiermayer, S., et al., *Epac activation converts cAMP from a proliferative into a differentiation signal in PC12 cells.* Mol Biol Cell, 2005. **16**(12): p. 5639-48.
256. Rangarajan, S., et al., *Cyclic AMP induces integrin-mediated cell adhesion through Epac and Rap1 upon stimulation of the beta 2-adrenergic receptor.* J Cell Biol, 2003. **160**(4): p. 487-93.
257. Ster, J., et al., *Exchange protein activated by cAMP (Epac) mediates cAMP activation of p38 MAPK and modulation of Ca2+-dependent K+ channels in cerebellar neurons.* Proc Natl Acad Sci U S A, 2007. **104**(7): p. 2519-24.
258. Boularan, C. and C. Gales, *Cardiac cAMP: production, hydrolysis, modulation and detection.* Front Pharmacol, 2015. **6**: p. 203.

259. Taylor, S.S., et al., *PKA: a portrait of protein kinase dynamics.* Biochim Biophys Acta, 2004. **1697**(1-2): p. 259-69.
260. Cho-Chung, Y.S., *Role of cyclic AMP receptor proteins in growth, differentiation, and suppression of malignancy: new approaches to therapy.* Cancer Res, 1990. **50**(22): p. 7093-100.
261. Tortora, G., T. Clair, and Y.S. Cho-Chung, *An antisense oligodeoxynucleotide targeted against the type II beta regulatory subunit mRNA of protein kinase inhibits cAMP-induced differentiation in HL-60 leukemia cells without affecting phorbol ester effects.* Proc Natl Acad Sci U S A, 1990. **87**(2): p. 705-8.
262. Van Harmelen, V., et al., *Noradrenaline-induced lipolysis in isolated mesenteric, omental and subcutaneous adipocytes from obese subjects.* Int J Obes Relat Metab Disord, 1997. **21**(11): p. 972-9.
263. Skalhegg, B.S. and K. Tasken, *Specificity in the cAMP/PKA signaling pathway. Differential expression,regulation, and subcellular localization of subunits of PKA.* Front Biosci, 2000. **5**: p. D678-93.
264. Lania, A.G., et al., *Proliferation of transformed somatotroph cells related to low or absent expression of protein kinase a regulatory subunit 1A protein.* Cancer Res, 2004. **64**(24): p. 9193-8.
265. Mantovani, G., et al., *Different expression of protein kinase A (PKA) regulatory subunits in cortisol-secreting adrenocortical tumors: relationship with cell proliferation.* Exp Cell Res, 2008. **314**(1): p. 123-30.
266. Mantovani, G., et al., *High expression of PKA regulatory subunit 1A protein is related to proliferation of human melanoma cells.* Oncogene, 2008. **27**(13): p. 1834-43.
267. Li, F., et al., *Protein kinase A suppresses the differentiation of 3T3-L1 preadipocytes.* Cell Res, 2008. **18**(2): p. 311-23.
268. Ji, Z., F.C. Mei, and X. Cheng, *Epac, not PKA catalytic subunit, is required for 3T3-L1 preadipocyte differentiation.* Front Biosci (Elite Ed), 2010. **2**: p. 392-8.
269. Madsen, L., et al., *cAMP-dependent signaling regulates the adipogenic effect of n-6 polyunsaturated fatty acids.* J Biol Chem, 2008. **283**(11): p. 7196-205.
270. Cummings, D.E., et al., *Genetically lean mice result from targeted disruption of the RII beta subunit of protein kinase A.* Nature, 1996. **382**(6592): p. 622-6.
271. Mantovani, G., et al., *Protein kinase A regulatory subunits in human adipose tissue: decreased R2B expression and activity in adipocytes from obese subjects.* Diabetes, 2009. **58**(3): p. 620-6.
272. McKnight, G.S., et al., *Cyclic AMP, PKA, and the physiological regulation of adiposity.* Recent Prog Horm Res, 1998. **53**: p. 139-59; discussion 160-1.
273. Peverelli, E., et al., *PKA regulatory subunit R2B is required for murine and human adipocyte differentiation.* Endocr Connect, 2013. **2**(4): p. 196-207.
274. Martini, C.N., M.V. Plaza, and C. Vila Mdel, *PKA-dependent and independent cAMP signaling in 3T3-L1 fibroblasts differentiation.* Mol Cell Endocrinol, 2009. **298**(1-2): p. 42-7.
275. Petersen, R.K., et al., *Cyclic AMP (cAMP)-mediated stimulation of adipocyte differentiation requires the synergistic action of Epac- and cAMP-dependent protein kinase-dependent processes.* Mol Cell Biol, 2008. **28**(11): p. 3804-16.
276. Jia, B., et al., *Activation of protein kinase A and exchange protein directly activated by cAMP promotes adipocyte differentiation of human mesenchymal stem cells.* PLoS One, 2012. **7**(3): p. e34114.
277. Tang, Z., et al., *Exchange protein activated by cyclic adenosine monophosphate regulates the switch between adipogenesis and osteogenesis of human*

mesenchymal stem cells through increasing the activation of phosphatidylinositol 3-kinase. Int J Biochem Cell Biol, 2012. **44**(7): p. 1106-20.
278. Gonzalez, G.A. and M.R. Montminy, *Cyclic AMP stimulates somatostatin gene transcription by phosphorylation of CREB at serine 133.* Cell, 1989. **59**(4): p. 675-80.
279. Shaywitz, A.J. and M.E. Greenberg, *CREB: a stimulus-induced transcription factor activated by a diverse array of extracellular signals.* Annu Rev Biochem, 1999. **68**: p. 821-61.
280. Christy, R.J., et al., *CCAAT/enhancer binding protein gene promoter: binding of nuclear factors during differentiation of 3T3-L1 preadipocytes.* Proc Natl Acad Sci U S A, 1991. **88**(6): p. 2593-7.
281. Fox, K.E., et al., *Depletion of cAMP-response element-binding protein/ATF1 inhibits adipogenic conversion of 3T3-L1 cells ectopically expressing CCAAT/enhancer-binding protein (C/EBP) alpha, C/EBP beta, or PPAR gamma 2.* J Biol Chem, 2006. **281**(52): p. 40341-53.
282. Klemm, D.J., et al., *Insulin stimulates cAMP-response element binding protein activity in HepG2 and 3T3-L1 cell lines.* J Biol Chem, 1998. **273**(2): p. 917-23.
283. Casimir, D.A. and J.M. Ntambi, *cAMP activates the expression of stearoyl-CoA desaturase gene 1 during early preadipocyte differentiation.* J Biol Chem, 1996. **271**(47): p. 29847-53.
284. Liu, H., et al., *Importance of cAMP-response element-binding protein in regulation of expression of the murine cyclic nucleotide phosphodiesterase 3B (Pde3b) gene in differentiating 3T3-L1 preadipocytes.* J Biol Chem, 2006. **281**(30): p. 21096-113.
285. Fox, K.E., et al., *Regulation of cyclin D1 and Wnt10b gene expression by cAMP-responsive element-binding protein during early adipogenesis involves differential promoter methylation.* J Biol Chem, 2008. **283**(50): p. 35096-105.
286. Berridge, M.J., *Calcium signalling and cell proliferation.* Bioessays, 1995. **17**(6): p. 491-500.
287. Kahl, C.R. and A.R. Means, *Regulation of cell cycle progression by calcium/calmodulin-dependent pathways.* Endocr Rev, 2003. **24**(6): p. 719-36.
288. Santella, L., *The role of calcium in the cell cycle: facts and hypotheses.* Biochem Biophys Res Commun, 1998. **244**(2): p. 317-24.
289. Whitaker, M. and M.G. Larman, *Calcium and mitosis.* Semin Cell Dev Biol, 2001. **12**(1): p. 53-8.
290. Whitfield, J.F., et al., *Calcium-cell cycle regulator, differentiator, killer, chemopreventor, and maybe, tumor promoter.* J Cell Biochem Suppl, 1995. **22**: p. 74-91.
291. Greber, U.F. and L. Gerace, *Depletion of calcium from the lumen of endoplasmic reticulum reversibly inhibits passive diffusion and signal-mediated transport into the nucleus.* J Cell Biol, 1995. **128**(1-2): p. 5-14.
292. Hussain, A., et al., *Direct involvement of intracellular Ca2+ transport ATPase in the development of thapsigargin resistance by Chinese hamster lung fibroblasts.* J Biol Chem, 1995. **270**(20): p. 12140-6.
293. Short, A.D., et al., *Intracellular Ca2+ pool content is linked to control of cell growth.* Proc Natl Acad Sci U S A, 1993. **90**(11): p. 4986-90.
294. Rasmussen, C.D. and A.R. Means, *Calmodulin is involved in regulation of cell proliferation.* Embo j, 1987. **6**(13): p. 3961-8.
295. Rasmussen, C.D. and A.R. Means, *Calmodulin, cell growth and gene expression.* Trends Neurosci, 1989. **12**(11): p. 433-8.

296. Chafouleas, J.G., et al., *Changes in calmodulin and its mRNA accompany reentry of quiescent (G0) cells into the cell cycle.* Cell, 1984. **36**(1): p. 73-81.
297. Hidaka, H., et al., *N-(6-aminohexyl)-5-chloro-1-naphthalenesulfonamide, a calmodulin antagonist, inhibits cell proliferation.* Proc Natl Acad Sci U S A, 1981. **78**(7): p. 4354-7.
298. Lopez-Girona, A., et al., *Calmodulin regulates DNA polymerase alpha activity during proliferative activation of NRK cells.* Biochem Biophys Res Commun, 1992. **184**(3): p. 1517-23.
299. Reddy, G.P., et al., *Calmodulin-specific monoclonal antibodies inhibit DNA replication in mammalian cells.* Biochemistry, 1992. **31**(43): p. 10426-30.
300. Takuwa, N., et al., *Ca2+/calmodulin is involved in growth factor-induced retinoblastoma gene product phosphorylation in human vascular endothelial cells.* FEBS Lett, 1992. **306**(2-3): p. 173-5.
301. Taules, M., et al., *Calmodulin is essential for cyclin-dependent kinase 4 (Cdk4) activity and nuclear accumulation of cyclin D1-Cdk4 during G1.* J Biol Chem, 1998. **273**(50): p. 33279-86.
302. Wei, J.W., R.A. Hickie, and D.J. Klaassen, *Inhibition of human breast cancer colony formation by anticalmodulin agents: trifluoperazine, W-7, and W-13.* Cancer Chemother Pharmacol, 1983. **11**(2): p. 86-90.
303. Ntambi, J.M. and T. Takova, *Role of Ca2+ in the early stages of murine adipocyte differentiation as evidenced by calcium mobilizing agents.* Differentiation, 1996. **60**(3): p. 151-8.
304. Shi, H., et al., *Role of intracellular calcium in human adipocyte differentiation.* Physiol Genomics, 2000. **3**(2): p. 75-82.
305. Wang, H., M.S. Goligorsky, and C.C. Malbon, *Temporal activation of Ca2+-calmodulin-sensitive protein kinase type II is obligate for adipogenesis.* J Biol Chem, 1997. **272**(3): p. 1817-21.
306. Hogan, P.G., et al., *Transcriptional regulation by calcium, calcineurin, and NFAT.* Genes Dev, 2003. **17**(18): p. 2205-32.
307. Ho, I.C., et al., *A potential role for the nuclear factor of activated T cells family of transcriptional regulatory proteins in adipogenesis.* Proc Natl Acad Sci U S A, 1998. **95**(26): p. 15537-41.
308. Neal, J.W. and N.A. Clipstone, *Calcineurin mediates the calcium-dependent inhibition of adipocyte differentiation in 3T3-L1 cells.* J Biol Chem, 2002. **277**(51): p. 49776-81.
309. Patel, Y.M. and M.D. Lane, *Role of calpain in adipocyte differentiation.* Proc Natl Acad Sci U S A, 1999. **96**(4): p. 1279-84.
310. Patel, Y.M. and M.D. Lane, *Mitotic clonal expansion during preadipocyte differentiation: calpain-mediated turnover of p27.* J Biol Chem, 2000. **275**(23): p. 17653-60.
311. Yajima, Y., et al., *Calpain system regulates the differentiation of adult primitive mesenchymal ST-13 adipocytes.* Endocrinology, 2006. **147**(10): p. 4811-9.
312. Tang, Q.Q. and M.D. Lane, *Role of C/EBP homologous protein (CHOP-10) in the programmed activation of CCAAT/enhancer-binding protein-beta during adipogenesis.* Proc Natl Acad Sci U S A, 2000. **97**(23): p. 12446-50.
313. Watt, F. and P.L. Molloy, *Specific cleavage of transcription factors by the thiol protease, m-calpain.* Nucleic Acids Res, 1993. **21**(22): p. 5092-100.
314. Jiang, M.S., et al., *Derepression of the C/EBPalpha gene during adipogenesis: identification of AP-2alpha as a repressor.* Proc Natl Acad Sci U S A, 1998. **95**(7): p. 3467-71.

315. Yajima, Y. and S. Kawashima, *Calpain function in the differentiation of mesenchymal stem cells.* Biol Chem, 2002. **383**(5): p. 757-64.
316. Song, E.K., et al., *NAADP mediates insulin-stimulated glucose uptake and insulin sensitization by PPARgamma in adipocytes.* Cell Rep, 2012. **2**(6): p. 1607-19.
317. Park, K.H., et al., *Autocrine/paracrine function of nicotinic acid adenine dinucleotide phosphate (NAADP) for glucose homeostasis in pancreatic beta-cells and adipocytes.* J Biol Chem, 2013. **288**(49): p. 35548-58.
318. Singh, R., et al., *Autophagy regulates adipose mass and differentiation in mice.* J Clin Invest, 2009. **119**(11): p. 3329-39.
319. Meyre, D., et al., *Genome-wide association study for early-onset and morbid adult obesity identifies three new risk loci in European populations.* Nat Genet, 2009. **41**(2): p. 157-9.
320. Dupuis, J., et al., *New genetic loci implicated in fasting glucose homeostasis and their impact on type 2 diabetes risk.* Nat Genet, 2010. **42**(2): p. 105-16.
321. Al-Daghri, N.M., et al., *Mammalian NPC1 genes may undergo positive selection and human polymorphisms associate with type 2 diabetes.* BMC Med, 2012. **10**: p. 140.
322. Robiou-du-Pont, S., et al., *Contribution of 24 obesity-associated genetic variants to insulin resistance, pancreatic beta-cell function and type 2 diabetes risk in the French population.* Int J Obes (Lond), 2013. **37**(7): p. 980-5.
323. Garver, W.S., et al., *Localization of the murine Niemann-Pick C1 protein to two distinct intracellular compartments.* J Lipid Res, 2000. **41**(5): p. 673-87.
324. Higgins, M.E., et al., *Niemann-Pick C1 is a late endosome-resident protein that transiently associates with lysosomes and the trans-Golgi network.* Mol Genet Metab, 1999. **68**(1): p. 1-13.
325. Neufeld, E.B., et al., *The Niemann-Pick C1 protein resides in a vesicular compartment linked to retrograde transport of multiple lysosomal cargo.* J Biol Chem, 1999. **274**(14): p. 9627-35.
326. Vanier, M.T., *Niemann-Pick disease type C.* Orphanet J Rare Dis, 2010. **5**: p. 16.
327. Jelinek, D., et al., *Decreased Npc1 gene dosage in mice is associated with weight gain.* Obesity (Silver Spring), 2010. **18**(7): p. 1457-9.
328. Jelinek, D., et al., *Npc1 haploinsufficiency promotes weight gain and metabolic features associated with insulin resistance.* Hum Mol Genet, 2011. **20**(2): p. 312-21.
329. Kulyte, A., et al., *MTCH2 in human white adipose tissue and obesity.* J Clin Endocrinol Metab, 2011. **96**(10): p. E1661-5.
330. Bambace, C., et al., *NPC1 in human white adipose tissue and obesity.* BMC Endocr Disord, 2013. **13**: p. 5.
331. Fletcher, R., et al., *The role of the Niemann-Pick disease, type C1 protein in adipocyte insulin action.* PLoS One, 2014. **9**(4): p. e95598.
332. Tsien, R.Y., *New calcium indicators and buffers with high selectivity against magnesium and protons: design, synthesis, and properties of prototype structures.* Biochemistry, 1980. **19**(11): p. 2396-404.
333. Macgregor, A., et al., *NAADP controls cross-talk between distinct Ca2+ stores in the heart.* J Biol Chem, 2007. **282**(20): p. 15302-11.
334. Rodrigues, C.O., D.A. Scott, and R. Docampo, *Characterization of a vacuolar pyrophosphatase in Trypanosoma brucei and its localization to acidocalcisomes.* Mol Cell Biol, 1999. **19**(11): p. 7712-23.

335. Rosen, D., et al., *Analogues of the nicotinic acid adenine dinucleotide phosphate (NAADP) antagonist Ned-19 indicate two binding sites on the NAADP receptor.* J Biol Chem, 2009. **284**(50): p. 34930-4.
336. Thai, T.L., G.C. Churchill, and W.J. Arendshorst, *NAADP receptors mediate calcium signaling stimulated by endothelin-1 and norepinephrine in renal afferent arterioles.* Am J Physiol Renal Physiol, 2009. **297**(2): p. F510-6.
337. de Souza, N.J., A.N. Dohadwalla, and J. Reden, *Forskolin: a labdane diterpenoid with antihypertensive, positive inotropic, platelet aggregation inhibitory, and adenylate cyclase activating properties.* Med Res Rev, 1983. **3**(2): p. 201-19.
338. de Rooij, J., et al., *Epac is a Rap1 guanine-nucleotide-exchange factor directly activated by cyclic AMP.* Nature, 1998. **396**(6710): p. 474-7.
339. Glass, D.B., et al., *Primary structural determinants essential for potent inhibition of cAMP-dependent protein kinase by inhibitory peptides corresponding to the active portion of the heat-stable inhibitor protein.* J Biol Chem, 1989. **264**(15): p. 8802-10.
340. Davies, S.P., et al., *Specificity and mechanism of action of some commonly used protein kinase inhibitors.* Biochem J, 2000. **351**(Pt 1): p. 95-105.
341. Christensen, A.E., et al., *cAMP analog mapping of Epac1 and cAMP kinase. Discriminating analogs demonstrate that Epac and cAMP kinase act synergistically to promote PC-12 cell neurite extension.* J Biol Chem, 2003. **278**(37): p. 35394-402.
342. Enserink, J.M., et al., *A novel Epac-specific cAMP analogue demonstrates independent regulation of Rap1 and ERK.* Nat Cell Biol, 2002. **4**(11): p. 901-6.
343. Student, A.K., R.Y. Hsu, and M.D. Lane, *Induction of fatty acid synthetase synthesis in differentiating 3T3-L1 preadipocytes.* J Biol Chem, 1980. **255**(10): p. 4745-50.
344. Harrington, M., S. Pond-Tor, and C.M. Boney, *Role of epidermal growth factor and ErbB2 receptors in 3T3-L1 adipogenesis.* Obesity (Silver Spring), 2007. **15**(3): p. 563-71.
345. Lin, W.C., et al., *Transcriptional activation of C/EBPbeta gene by c-Jun and ATF2.* DNA Cell Biol, 2002. **21**(8): p. 551-60.
346. Niehof, M., M.P. Manns, and C. Trautwein, *CREB controls LAP/C/EBP beta transcription.* Mol Cell Biol, 1997. **17**(7): p. 3600-13.
347. Hwang, C.S., et al., *Adipocyte differentiation and leptin expression.* Annu Rev Cell Dev Biol, 1997. **13**: p. 231-59.
348. Patel, S., et al., *Widespread distribution of binding sites for the novel Ca2+-mobilizing messenger, nicotinic acid adenine dinucleotide phosphate, in the brain.* J Biol Chem, 2000. **275**(47): p. 36495-7.
349. Wegner, M., Z. Cao, and M.G. Rosenfeld, *Calcium-regulated phosphorylation within the leucine zipper of C/EBP beta.* Science, 1992. **256**(5055): p. 370-3.
350. Cho, Y.C. and C.R. Jefcoate, *PPARgamma1 synthesis and adipogenesis in C3H10T1/2 cells depends on S-phase progression, but does not require mitotic clonal expansion.* J Cell Biochem, 2004. **91**(2): p. 336-53.
351. Chameau, P., et al., *Ryanodine-, IP3- and NAADP-dependent calcium stores control acetylcholine release.* Pflugers Arch, 2001. **443**(2): p. 289-96.
352. Brailoiu, E., M.D. Miyamoto, and N.J. Dun, *Nicotinic acid adenine dinucleotide phosphate enhances quantal neurosecretion at the frog neuromuscular junction: possible action on synaptic vesicles in the releasable pool.* Mol Pharmacol, 2001. **60**(4): p. 718-24.

353. Brailoiu, E., S. Patel, and N.J. Dun, *Modulation of spontaneous transmitter release from the frog neuromuscular junction by interacting intracellular Ca(2+) stores: critical role for nicotinic acid-adenine dinucleotide phosphate (NAADP).* Biochem J, 2003. **373**(Pt 2): p. 313-8.
354. Rutter, G.A., *Calcium signalling: NAADP comes out of the shadows.* Biochem J, 2003. **373**(Pt 2): p. e3-4.
355. Bak, J., et al., *Nicotinic acid adenine dinucleotide phosphate triggers Ca2+ release from brain microsomes.* Curr Biol, 1999. **9**(14): p. 751-4.
356. Berridge, G., et al., *Metabolism of the novel Ca2+-mobilizing messenger nicotinic acid-adenine dinucleotide phosphate via a 2'-specific Ca2+-dependent phosphatase.* Biochem J, 2002. **365**(Pt 1): p. 295-301.
357. Petersen, O.H. and J.M. Cancela, *New Ca2+-releasing messengers: are they important in the nervous system?* Trends Neurosci, 1999. **22**(11): p. 488-95.
358. Sharp, A.H., et al., *Differential immunohistochemical localization of inositol 1,4,5-trisphosphate- and ryanodine-sensitive Ca2+ release channels in rat brain.* J Neurosci, 1993. **13**(7): p. 3051-63.
359. Parkesh, R., et al., *Cell-permeant NAADP: a novel chemical tool enabling the study of Ca2+ signalling in intact cells.* Cell Calcium, 2008. **43**(6): p. 531-8.
360. Brailoiu, G.C., et al., *NAADP-mediated channel 'chatter' in neurons of the rat medulla oblongata.* Biochem J, 2009. **419**(1): p. 91-7, 2 p following 97.
361. Heidemann, A.C., C.G. Schipke, and H. Kettenmann, *Extracellular application of nicotinic acid adenine dinucleotide phosphate induces Ca2+ signaling in astrocytes in situ.* J Biol Chem, 2005. **280**(42): p. 35630-40.
362. Singaravelu, K. and J.W. Deitmer, *Calcium mobilization by nicotinic acid adenine dinucleotide phosphate (NAADP) in rat astrocytes.* Cell Calcium, 2006. **39**(2): p. 143-53.
363. Barcelo-Torns, M., et al., *NAADP mediates ATP-induced Ca2+ signals in astrocytes.* FEBS Lett, 2011. **585**(14): p. 2300-6.
364. Brailoiu, E., et al., *Nicotinic acid adenine dinucleotide phosphate potentiates neurite outgrowth.* J Biol Chem, 2005. **280**(7): p. 5646-50.
365. Beck, A., et al., *Nicotinic acid adenine dinucleotide phosphate and cyclic ADP-ribose regulate TRPM2 channels in T lymphocytes.* Faseb j, 2006. **20**(7): p. 962-4.
366. Churamani, D., et al., *Domain assembly of NAADP-gated two-pore channels.* Biochem J, 2012. **441**(1): p. 317-23.
367. Dammermann, W., et al., *NAADP-mediated Ca2+ signaling via type 1 ryanodine receptor in T cells revealed by a synthetic NAADP antagonist.* Proc Natl Acad Sci U S A, 2009. **106**(26): p. 10678-83.
368. Davis, L.C., et al., *NAADP activates two-pore channels on T cell cytolytic granules to stimulate exocytosis and killing.* Curr Biol, 2012. **22**(24): p. 2331-7.
369. Chen, G., et al., *Suppression subtractive hybridization analysis of low-protein diet- and vitamin D-induced gene expression from rat kidney inner medullary base.* Physiol Genomics, 2010. **41**(3): p. 203-11.
370. Blumberg, J.M., et al., *Complex role of the vitamin D receptor and its ligand in adipogenesis in 3T3-L1 cells.* J Biol Chem, 2006. **281**(16): p. 11205-13.
371. Narvaez, C.J., et al., *Lean phenotype and resistance to diet-induced obesity in vitamin D receptor knockout mice correlates with induction of uncoupling protein-1 in white adipose tissue.* Endocrinology, 2009. **150**(2): p. 651-61.
372. Wong, K.E., et al., *Involvement of the vitamin D receptor in energy metabolism: regulation of uncoupling proteins.* Am J Physiol Endocrinol Metab, 2009. **296**(4): p. E820-8.

373. Arredouani, A., et al., *An emerging role for NAADP-mediated Ca2+ signaling in the pancreatic beta-cell.* Islets, 2010. **2**(5): p. 323-30.
374. Takahashi, J., et al., *Deficit of CD38/cyclic ADP-ribose is differentially compensated in hearts by gender.* Biochem Biophys Res Commun, 2003. **312**(2): p. 434-40.